

ELECTRON SPIN RESONANCE STUDIES OF
SURFACE STABILIZED METHYL RADICALS

A Thesis Submitted to the
Faculty of Graduate Studies and Research,
The University of Manitoba.

In Partial Fulfillment of the Requirements
for the Degree
Doctor of Philosophy

by
G. Barry Garbutt
June, 1968.



ACKNOWLEDGMENTS

I would like to express my heartfelt thanks to Dr. H.D. Gesser for his wise direction and thoughtfulness. I would also like to acknowledge the interest and assistance of Dr. M. Fujimoto. Many thanks are extended to every graduate student under the direction of Dr. H.D. Gesser and all staff members of the Chemistry Department. Financial assistance provided by the University of Manitoba, Canadian Industries Limited and the United States Air Force has been greatly appreciated. I would also like to thank all members of my immediate family for their understanding and support.

TO MY WIFE, LORNA

ABSTRACT

Electron spin Resonance studies have been carried out on methyl radicals stabilized on the surface of porous Vycor glass. These methyl radicals were produced by U.V. photolysis, at 77°K, of adsorbed methyl iodide. Two very different methyl radicals, denoted Me and Me', have been observed. Me is believed to be a methyl radical which is very weakly bonded to surface "free" hydroxyl groups while Me' has been assigned to a more strongly bound methyl radical, probably chemisorbed to the Lewis acid site, $\equiv B$, which is prominent on the surface of high temperature (700°-900°C) degassed porous Vycor glass. Satellites about Me have been observed when the surface was degassed at lower temperatures (400°-500°C). These satellites have been assigned to methyl radicals trapped at particular sites where interactions with the surface hydroxyl protons is possible. Four of the six satellites have been assigned to forbidden "spin-flip" transitions while the other two have been assigned to direct interaction (strong hydrogen bond) between methyl radicals and surface hydroxyl protons. During the course of this work it was shown that dehydroxylation of porous Vycor glass at high temperatures is irreversible. The second order splitting of the methyl radical has been observed and measured. It was shown that multiple trapping sites and unresolved proton splittings contribute to the E.S.R. linewidth. There is evidence for radical diffusion at 77°K even though there is no measurable decay.

The proton, deuterium, and carbon-13 hyperfine splittings were measured as a function of temperature in order to make comparisons with the dependences calculated by D.M. Schrader. In addition, the line widths, line asymmetries, and relative line intensities in the methyl radical E.S.R. spectrum were measured as a function of temperature. The absolute values of the temperature coefficients of the proton and deuterium splittings were found to be slightly larger than those predicted by theory. The carbon-13 hyperfine splittings were found to agree with theory above 200°K but a large deviation was observed below 200°K. Below 275°K the proton lines became increasingly asymmetric. The relative line intensities approach but do not attain the binomial values as the temperature is increased. The proton linewidths were found to have different temperature dependences below 200°K, while having similar dependences above 200°K. The observed results may be explained by a physical model based on increased surface interaction at low temperatures. Similar studies were carried out on chlorinated porous Vycor glass surfaces. Marginal results indicate smaller interactions between the radical and this surface.

The proton and deuteron linewidths have been measured carefully as a function of temperature and surface characteristics. The linewidths were then fitted to the expression $(T_2)^{-1} = a_0 + a_1M + a_2M^2$. From the constants a_0 , a_1 and a_2 one is able to calculate correlation times and "Tumbling Frequencies". The methyl radical

lineshapes are not Lorentzian or Gaussian. On increasing the temperature the linewidths decrease due to the disappearance of unresolved splittings and/or increased motion of the radicals. At higher temperatures the linewidths broaden possibly due to diffusion of the radicals between potential wells. Each proton and deuteron line has a different linewidth temperature dependence. These studies revealed an unresolved proton splitting linewidth contribution, which was dependent on the nuclear spin quantum number, for methyl radicals on low temperature degassed surfaces. As the number of hydroxyl groups on the surface increases the "tumbling frequency" decreases. The "tumbling frequency" of the methyl radical on a chlorinated surface is less than on a high temperature degassed surface while the reverse is true for the deuteromethyl radical. The "tumbling frequency" of the deuteromethyl radical is less than the "tumbling frequency" of the methyl radical. A small value for the hyperfine anisotropy indicates rapid reorientations even at 77°K. The resulting activation energies for "tumbling" are very small (about 300 cal/mole) and may be associated with oscillations of the adsorbed molecules between different available surface sites. The line asymmetry and non-binomial relative amplitudes are due to incomplete motional averaging of the g-tensor and hyperfine tensor or to radicals taking up particular orientations with respect to the applied magnetic field. Since there

are many indications for radical motion, even at 77°K, the first explanation is believed to be more reasonable. The "tumbling frequencies" are small for rotation but are of the right order of magnitude for diffusion.

Methyl radical decay has been studied. This decay may be best fitted to second order kinetics. The decay is very sensitive to small changes in temperature indicating a continuum of trapping sites. A critical temperature at which decay begins was noticed. A curvature in the Arrhenius plot was observed. Below 173°K the activation energy is small or zero. Above 173°K the activation energy is 2.0-3.2 kcal/mole indicating a diffusion controlled decay. Three possible reasons for the curvature in the Arrhenius plot have been suggested.

TABLE OF CONTENTS

	PAGE
Chapter I	
INTRODUCTION	
1. Theory of Electron Spin Resonance	1
A. Orbital and Spin Magnetic Moments	2
B. The Resonance Condition	4
C. The Hydrogen Atom	9
1. Development of The Spin Hamiltonian	9
2. Perturbation Theory	11
3. Solving the Hydrogen Atom Problem Using Perturbation Theory	11
4. First-Order E.S.R. Spectrum	15
5. Second-Order E.S.R. Spectrum	19
6. Zero-Field Levels of Hydrogen Atom	20
D. Hyperfine Splittings in Polynuclear Free Radicals	20
1. The Interaction of an Electron with two non-equivalent protons	21
2. Radicals with two Equivalent Protons	22
3. Radicals with three Equivalent Protons (CH ₃)	24
4. Radicals with n Equivalent Protons	25
5. Radicals with Several Sets of Equivalent Protons	25
6. Radicals with Several Sets of Equivalent Nuclei	27
7. Hyperfine Splittings Due to C ¹³ in the Methyl Radical	28
8. Hyperfine Splittings in the Deuterated Methyl Radical	28
E. Brief Description of the Mechanisms of Hyperfine Coupling	30
1. Unpaired Spin Density	30
2. Indirect Coupling Through a C-H Bond	31
3. β Proton Splittings	34

	PAGE
F. Relaxation Processes and Linewidths	36
1. General Introduction	36
2. Origin of Magnetic Relaxation	39
3. Linewidths in Liquids	41
4. Spin Relaxation of Radicals in Solution	41
2. Silica and Porous Vycor Glass Surfaces	45
A. Introduction	45
B. Silica Surfaces	49
1. Hydration-Dehydration Studies	49
2. Adsorbent Perturbation on Adsorption	53
3. Adsorbate Perturbations on Adsorption	56
C. Adsorption Studies on Porous Glass	58
1. Introduction	58
2. Hydration-Dehydration Studies	59
3. Surface Heterogeneity	62
4. Length Changes upon Adsorption	65
5. Restricted Rotation of Adsorbed Molecules	65
D. Reactions of Surface Silanol Groups	67
1. Esterification	67
2. Fluorination	68
3. Chlorination	69
4. Grignard Reactions	69
5. Carboxylic Acid Derivatives	70
6. Reactions with Organosilicon Compounds	70
7. Reaction with Diborane	71
8. Reaction with Silicon Tetrachloride	71
9. Reaction with Boron Trichloride	72
3. Previous E.S.R. Studies of Methyl Radicals	73
Chapter II GENERAL CHARACTERISTICS OF THE E.S.R. SPECTRA OF METHYL RADICALS STABILIZED ON POROUS VYCOR GLASS	
1. Introduction	80
2. Experimental	87
3. Results	88

	PAGE
A. Radical Build-Up Studies	89
B. A Second Kind of Methyl Radical (denoted Me')	93
C. Satellites of the Four Main Proton Lines of the Methyl Radical	97
D. Resolving Proton Lines 3 and 3a	109
E. A Study of the Splitting of the Proton Line 3a and of the Linewidths of 3 and 3a on Warming and Cooling	111
4. Discussion	114
A. Radical Build-Up Studies	114
B. The Radical Me'	115
C. Satellites of the Four Main Proton Lines of the Methyl Radical	118
D. Resolving Proton Lines 3 and 3a	125
E. Second-Order Splitting of Line 3a and Linewidths of Lines 3 and 3a on Warming and Cooling	125
5. Conclusions	126
Chapter III TEMPERATURE DEPENDENCES OF STABILIZED METHYL RADICALS	
1. Introduction	127
A. Proton Hyperfine Splittings in Aromatic Systems	128
B. Hyperfine Splittings From Nuclei Other Than Protons	136
1. Isotropic Hyperfine Splitting from Atoms with a Net π -Electron Spin Density	136
2. Anisotropic Hyperfine Splitting from Atoms with a Net π -Electron Spin Density	138

	PAGE
C. Theoretical Interpretations of the E.S.R. Spectrum of the Methyl Radical	140
D. Theoretical Temperature Dependences of the Methyl Radical	145
2. Experimental	159
3. Methods of Measurement of E.S.R. Parameters	161
4. Results	167
A. Proton Hyperfine Splittings	167
B. Deuterium Hyperfine Splittings	173
C. Carbon-13 Splittings	173
D. Linewidth, Asymmetry, and Intensity Studies of the Proton Lines	178
E. Methyl Radicals on a Chlorinated Surface	181
5. Discussion of Results	186
6. Conclusions	194
Chapter IV FURTHER STUDIES OF LINEWIDTHS	
1. Introduction	196
2. Experimental	205
A. Nature of the Samples Studied	205
B. Linewidths	207
C. Linewidth Studies Performed	208

	PAGE
3. Results	209
4. Discussion	226
5. Conclusions	233
Chapter V	DECAY KINETICS
1. Introduction	236
2. Experimental	239
3. Results and Discussion	240
4. Conclusions	247
Appendix I	249
Bibliography	251

LIST OF TABLES

TABLE		PAGE
1.1	Comparison of $\rho\pi$, a_H and Q for Several Cyclic Polyene Radicals	32
1.2	Effect of Different Matrices on Some Methyl Radical E.S.R. Parameters ⁵⁸	74
1.3	Methyl Radical Hyperfine Splittings Measured in Solution and in a Krypton Matrix ⁷³	78
2.1	Characteristics of Methyl and Deuteromethyl Radicals ⁷⁹	86
2.2	Relative Amplitudes as a Function of Irradiation Time for Methyl Radicals Stabilized on a Dehydrated Surface	89
2.3	Relative Amplitudes vs. Irradiation Time for Methyl Radicals Stabilized on a Chlorinated Surface (77°K)	92
2.4	Average Splittings of Satellites from Main Proton Lines at 77°K	107
2.5	Average Linewidths _{p.p.} and Relative Amplitudes of B and B' at 77°K	107
2.6	Splittings and Linewidths of Satellites B and B' as a Function of Temperature	108
2.7	Linewidth of Line 3a as a Function of Modulation	109
2.8	Splitting and Linewidth of Line 3a on Warming and Cooling Cycles	112
2.9	Linewidth of Line 3 on Warming and Cooling Cycles.	113

	PAGE
3.1 Empirical Values of ρ^{π} , $Q_{\text{CH}^{\cdot}}$, $Q_{\text{CCH}_3^{\cdot}}$ For Some Neutral Radicals ⁷¹	130
3.2 $Q_{\text{CH}^{\cdot}}$ Values For a Series of Radicals $\text{CH}_3\text{-CH-X}$ ¹⁰⁶	131
3.3 Comparison of Experimental and Theoretical Values ($\rho=1$) of $ a^{\text{H}} $ and $ a^{\text{C}} $ for Methyl Radicals ¹⁰²	141
3.4 Proton and Carbon-13 Splittings for the Methyl Radical as a Function of θ ($\rho=1$) ¹⁰²	142
3.5 $\langle a^{\text{H}} \rangle$, $\langle a^{\text{C}} \rangle$ and R_1 for Various Values of $\rho(0)$ and $\rho(90)$ ¹⁰²	143
3.6 How $\langle a^{\text{H}} \rangle$, $\langle a^{\text{C}} \rangle$, and R_1 Change With Simultaneous Variations in ρ and Δ Values ¹⁰²	144
3.7 Splittings and Orbital Spin Populations as Functions of θ (DMS)	156
3.8 Contributions of Each Orbital to the Total Splitting for Several Nuclei in Methyl Radicals (DMS)	158
3.9 Temperature Coefficients of Proton and Carbon-13 Splittings	170
3.10 Comparisons of Temperature Coefficients	172
4.1 Measured Peak-to-Peak and One-Half Intensity Linewidths at 77°K	213
4.2 Linewidths as a Function of Temperature	214

	PAGE
4.3 Parameters Derived from Curvilinear Regression Analysis Applied to Measured Linewidths at 77°K	215
4.4 Parameters Derived from Curvilinear Regression Analysis as a Function of Temperature	216
4.5 Relative Amplitudes for Some Samples and for One Temperature Run	217

LIST OF FIGURES

FIGURE		PAGE
1.1	Energy of Electron Spin States in a Magnetic Field	6
1.2	Vector Diagram for the Precession of a Magnetic Dipole Under the Influence of a Static Magnetic Field H_0 and a Rotating Magnetic Field H_1	8
1.3	First-order Spin Energy Levels of the Hydrogen Atom and the Allowed E.S.R. Transitions	13
1.4	Second-order Hyperfine Energy Levels of the Hydrogen Atom	16
1.5	Exact Energy Levels of the Hydrogen Atom as a Function of the Applied Field H	17
1.6	Hyperfine Energy Levels and Transitions for Two Non-Equivalent Protons	23
1.7	Hyperfine Energy Levels and Spectra for Three Equivalent Protons	26
1.8	Carbon-13 Splitting in the Methyl Radical	29
1.9	Structures Considered when Treating Indirect Coupling Through a C-H Bond	33
1.10	Hyperconjugation in the Ethyl Radical	35
1.11	Lorentzian and Gaussian Line Shapes	40
1.12	Hydration and Dehydration of a Silica Surface	54
1.13	Contraction of Porous Glass on Methanol Adsorption	66

FIGURE	PAGE
2.1 E.S.R. Spectra of the Methyl Radical at 77°K	90a,b
2.2 Build-Up Study of Methyl Radicals Stabilized on a Regular p.V.g. Surface	91
2.3 Spectrum of Me and Me' at 77°K	94
2.4 Spectrum of Radical X ^{80,81}	98
2.5 A More Recent Spectrum of Radical X	100
2.6 "Stick" Diagram of the Satellites Around one of the Four Proton Lines P	101
2.7 Comparison of Satellites Observed for High Temperature Degassed Surfaces Followed by Treatment with H ₂ O and D ₂ O at 400°C	103
2.8 Comparison of Satellites Observed About Proton Lines 3 and 3a for Low Temperature Degassed Surfaces Followed by Treatment with H ₂ O and D ₂ O at 400°C	104
2.9 Spectrum Exhibiting the Satellites C and C' About Proton Line 3	106
2.10 Spectrum of Unresolved Second-Order Splittings of Lines 3 and 3a	110
3.1 The Difference Between θ and θ^I (DMS)	149
3.2 Useful Following Parameters [$\rho(90)$ and $\rho(0)$] (DMS)	150
3.3 Calculated Values of $ a^H $ and $6.51437 a^D $ for C ¹² H ₃ and C ¹² D ₃ , respectively, using Following Models C and D (DMS)	152

FIGURE		PAGE
3.4	Calculated Values of a^C for $C^{13}H_3$ and $C^{13}D_3$ Using Following Models C and D (DMS)	153
3.5	Temperature Coefficients of $ a^H $ and $ a^D $ for $C^{12}H_3$ and $C^{12}D_3$ as a Function of Temperature (Following Model C) [DMS]	154
3.6	Temperature Coefficients of a^C for $C^{13}H_3$ and $C^{13}D_3$ as a Function of Temperature (Following Model C) [DMS]	155
3.7	"Stick" Diagram of $C^{12}H_3$ (a), $C^{12}D_3$ (b) and $C^{12}H_3 - C^{13}H_3$ (c) Indicating Measurements Made	162
3.8	Spectrum of the Deuteromethyl Radical at 98.7°K	164
3.9	Spectrum of a mixture of $C^{12}H_3$ and $C^{13}H_3$ Radicals at 192°K	166
3.10	Temperature Dependence of the Proton Hyperfine Splitting (Average Values)	168
3.11	Temperature Dependence of the Proton Hyperfine Splitting (Three Individual Temperature Runs)	169
3.12	Temperature Dependence of the Temperature Coefficients of the Proton Splitting	171
3.13	Temperature Dependence of the Deuterium Hyperfine Splitting	174
3.14	Temperature Dependence of Carbon-13 Splitting	175
3.15	Temperature Dependence of Carbon-13 Temperature Coefficients	177

FIGURE		PAGE
3.16	Temperature Dependence of Linewidths of Proton Lines 3 and 3a	179
3.17	Asymmetry of Lines 3 and 3a as a Function of Temperature	180
3.18	Area of Line 3 Divided by Total Area of Lines 3 and 3a as a Function of Temperature	182
3.19	Relative Intensities of the Four Methyl Radical Lines as a Function of Temperature	183
3.20	Area of Proton Lines Below Baseline Divided by Total Area of Lines as a Function of Temperature	184
3.21	Temperature Dependence of the Proton Splitting of Methyl Radicals Stabilized on Chlorinated p.V.g.	185
3.22	Asymmetry of Proton Line 3 of Methyl Radicals Stabilized on Chlorinated p.V.g.	187
4.1	Measured and Calculated Linewidths as a Function of Nuclear Quantum Number M	210
4.2	Measured Linewidths as a Function of M at Various Temperatures (Sample 4)	218
4.3	Tumbling Frequencies (from measured Linewidths) as a Function of Temperature (Sample 4)	219
4.4	Logarithms of the Tumbling Frequencies vs. $T(^{\circ}\text{K})^{-1}$	221
4.5	Measured Linewidths vs. M. at Various Temperatures (Sample 8)	222

FIGURE		PAGE
4.6	Measured Linewidths vs. M at Various Temperatures (Sample 3)	223
4.7	Measured Linewidths as a Function of M for Different Samples at 77°K	224
4.8	Measured Linewidths (Lines 1 and 3) as a Function of Temperature	225
5.1	Proton Line Amplitude vs. Decay Time at Various Temperatures ⁸⁰	237
5.2	First-order Decay Plot of the Methyl Radical at -170°C ⁸⁰	238
5.3	Decay of Line 3a at 152°K	241
5.4	Log $\frac{dc}{dt}$ as a Function of Log C (Sample at 110°K)	244
5.5	The Arrhenius Plot (Log k vs. T ⁻¹) Applied to Methyl Radical Decay	246

CHAPTER I
INTRODUCTION

1. THEORY OF ELECTRON SPIN RESONANCE

This thesis is primarily concerned with Electron Spin Resonance or Electron Paramagnetic Resonance spectroscopy and its application to the study of free radicals on surfaces. It therefore seems desirable to begin with a brief introduction to Electron Spin Resonance.

This branch of spectroscopy, which is little more than twenty years old, is now known colloquially as E.P.R. or, more commonly, E.S.R. The treatment of E.S.R. will not be mathematically rigorous and will be slanted towards predominately isotropic systems. Theories pertaining to studies which have been performed by the candidate will be discussed at greater length in the introductory sections of the appropriate chapters.

E.S.R. may be applied to systems which are paramagnetic, that is, the individual sites of interest must exhibit a net magnetic moment and these sites must be sufficiently separated as to behave as independent sites, interacting at most very weakly. Such systems are odd molecules and free radicals, biradicals, triplet electronic states, transition metal ions, and materials with unfilled conduction bands. The experimental work which will be discussed in the following chapters deals specifically with free radicals (in particular, methyl radicals and isotopically substituted methyl radicals). A "free radical" may be defined as a molecular fragment with an unsatisfied valence electron.

Many very different chemical problems such as the study of reactions of atoms and ions in flames, electron exchange reactions in solutions, the behaviour of catalysts, the structure of

semiconductors and the interpretation of metabolic processes in biological systems can be studied by E.S.R. Many introductions to the theory and to the applications of E.S.R. to Chemistry, Chemical Physics and Biology are available.¹⁻⁶ For this reason, nothing more will be said about the applications of E.S.R.

A. ORBITAL AND SPIN MAGNETIC MOMENTS

Classically, the electron may be shown to have an orbital magnetic moment of the form

$$\underline{\mu}_L = \frac{-e}{2mc} \cdot \underline{P}_L \quad (1-1)$$

where $\underline{\mu}_L$ is the orbital magnetic moment vector and \underline{P}_L is the orbital angular momentum vector. The magnetic moment vector, for the electron, is opposite in direction to the angular momentum vector. The maximum observable value of \underline{P}_L is $\underline{l} \hbar$ where \underline{l} is the azimuthal quantum number which can have any integral positive value, or zero. The actual magnitude of the orbital angular momentum vector is $\sqrt{[\underline{l}(\underline{l}+1)]} \hbar$. The unit of the magnetic moment is the Bohr magneton (β) which equals $\frac{e\hbar}{2mc}$ ($9.2732 \times 10^{-21} \frac{\text{ergs}}{\text{gauss}}$). For systems with more than one electron, angular momenta are combined vectorially to give a resultant designated by the quantum number L. Unidentified splittings seen in the atomic spectra of samples in magnetic fields (Zeeman Effect) led to the postulated existence of an additional angular momentum term attributable to the rotation of the electron about its own axis.

Uhlenbeck and Goudsmit⁷ suggested each electron possessed an intrinsic or spin angular momentum of magnitude $\underline{P}_S = 1/2 \hbar$. The magnitude of the spin angular momentum vector for a system containing

n electrons is $\sqrt{S(S+1)} \hbar$ where $S = n/2, n/2 - 1, n/2 - 2, \dots, 1/2$ or 0 . The maximum observable value is $S \hbar$. The total angular momentum of the system is then defined by a quantum number J which for light atoms takes the positive values $J = L + S, L + S - 1, L + S - 2, \dots, L - S$ (Russell-Saunders coupling). For $L = 0$, Goudsmit found it necessary to assume that the spin magnetic moment had twice the value that follows from the classical relation between angular momentum and magnetic moment.

$$\underline{\mu}_S = 2 \left(\frac{-e}{2mc} \cdot \underline{P}_S \right) \quad (1-2)$$

where $\underline{P}_S = 1/2 \hbar$ for a single electron.

The Landé splitting factor is given by

$$g_J = 1 + \frac{S(S+1) + J(J+1) - L(L+1)}{2 J (J+1)} \quad (1-3)$$

This factor may be evaluated for $J = 1/2$ ($S = 1/2, L = 0$)

$$g_{J=1/2} = 2$$

Therefore equation (1-2) becomes:

$$\underline{\mu}_S = g \frac{-e}{2mc} \cdot \underline{P}_S \quad (1-4)$$

The Landé g - factor may be calculated accurately for light atoms using Russell-Sanders coupling. The general spectroscopic splitting factor (g -factor or g -value) in equation (1-4) can only be determined experimentally. For free radicals where there is very little orbital angular momentum, if any at all, the value of g is close to the free electron value which is 2.00232 (the deviation from the integral number is a relativistic correction for the orbital velocity of the electron). The orbital angular momentum in organic free radicals has been quenched by crystal fields.

B. THE RESONANCE CONDITION

Let us assume there are N independent elements in a magnetic field, each of spin angular momentum $\sqrt{1/2(1/2+1)} \hbar$. These elements align themselves either along or opposed to the direction of the applied field H_0 . Each of these elements, due to the fact that they are charged, has a magnetic moment which points along or opposed to the direction of the spin angular momentum. Since $\underline{P}_S = \underline{S} \hbar$, equation (1-4) becomes

$$\underline{\mu}_S = g \frac{e\hbar}{2mc} \underline{S} \quad (1-5)$$

The energy of a magnetic moment in a magnetic field depends on the orientation of that magnetic moment with respect to the field.

$$E = - \underline{\mu}_S \cdot \underline{H}_0 \quad (1-6)$$

Substituting (1-5) into (1-6)

$$E = g \frac{e\hbar}{2mc} \underline{S} \cdot \underline{H}_0 \quad (1-7)$$

Since $\frac{e\hbar}{2mc} = \beta$ (Bohr magneton) and since M_Z is the component of the spin angular momentum along the direction of the applied field H_0 (Z-axis)

$$E = g \beta M_Z H_0 \quad (1-8)$$

Because $M_Z = \pm 1/2$, the energies of the two spin states are

$$\begin{aligned} E_{+1/2} &= 1/2 g \beta H_0 \\ E_{-1/2} &= -1/2 g \beta H_0 \end{aligned} \quad (1-9)$$

The difference in energy between the two spin states is

$$\Delta E = E_{+1/2} - E_{-1/2} = g \beta H_0 \quad (1-10)$$

The energies of the two spin states as a function of the applied field H_0 can be seen in Fig. 1.1. An energy of $h\nu$ must be absorbed

in order to induce a transition between the two spin states. The relationship governing transitions is:

$$h\nu = g \beta H_0 \quad (1-11)$$

$h\nu \cong 2.8 \text{ MHz}$ per gauss of applied field H_0 for a radical where $g = 2.0$.

Considering N elements (or spin systems), one is able to say that N_+ are in the $m_z = +1/2$ state and N_- are in the $m_z = -1/2$ state at any instant. Thermal processes modulate the interactions which these spins experience with their surroundings. These fluctuations in the interactions induce transitions between the two levels and, at thermal equilibrium, establish a Boltzmann distribution.

$$\frac{N_+}{N_-} = e^{-\frac{h\nu}{kT}} = e^{-\frac{g\beta H_0}{kT}} \quad (1-12)$$

$$\frac{N_+}{N_-} = 1 - \frac{g\beta H_0}{kT} \quad (1-12a)$$

Equation (1-12a) is valid above a few degrees absolute since $g\beta H_0 \ll kT$. When $T = 300^\circ\text{K}$, $g = 2.0$, and $H_0 = 3000$ gauss, $\frac{N_+}{N_-} = 0.9986$.

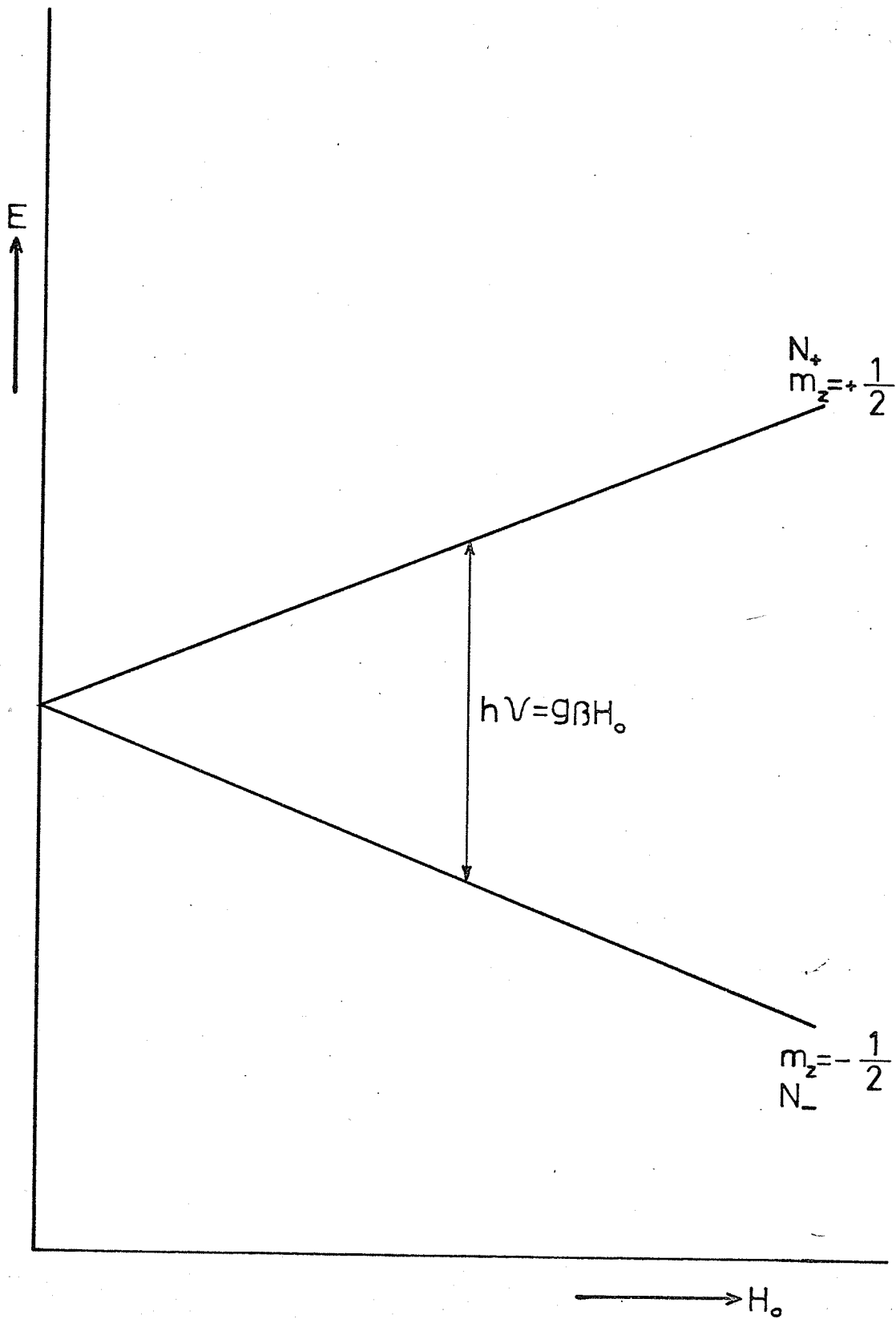
The excess population in the lower state on which the whole phenomenon of E.S.R. depends is only about 0.14%.

What conditions are necessary for inducing the resonance transitions? Laboratory magnets are limited to fields between zero and 50,000 gauss. Therefore, from equation (1-11), absorption frequencies applicable range between zero and 150,000 MHz. In the normal E.S.R. experiment one leaves the source frequency fixed and adjusts the energy levels to the resonant condition by sweeping the magnetic field. Optimum signal to noise ratios are obtained by

Fig. 1.1

Energy of Electron Spin States in a Magnetic Field

6.



using x-band (8-12 GHz) and K-band (27-35 GHz) spectrometers. A Varian E-3 spectrometer (x-band) was used for the majority of the work to be reported in the following chapters. Transitions between the two energy levels in Fig. 1.1 may be induced by the interaction between the magnetic dipole of the electron and the oscillating magnetic field accompanying the x-band electromagnetic irradiation. The Larmor frequency of precession of a magnetic dipole $\underline{\mu}$ in a field H_0 is given by

$$\omega_0 = \gamma H_0 \quad (1-13)$$

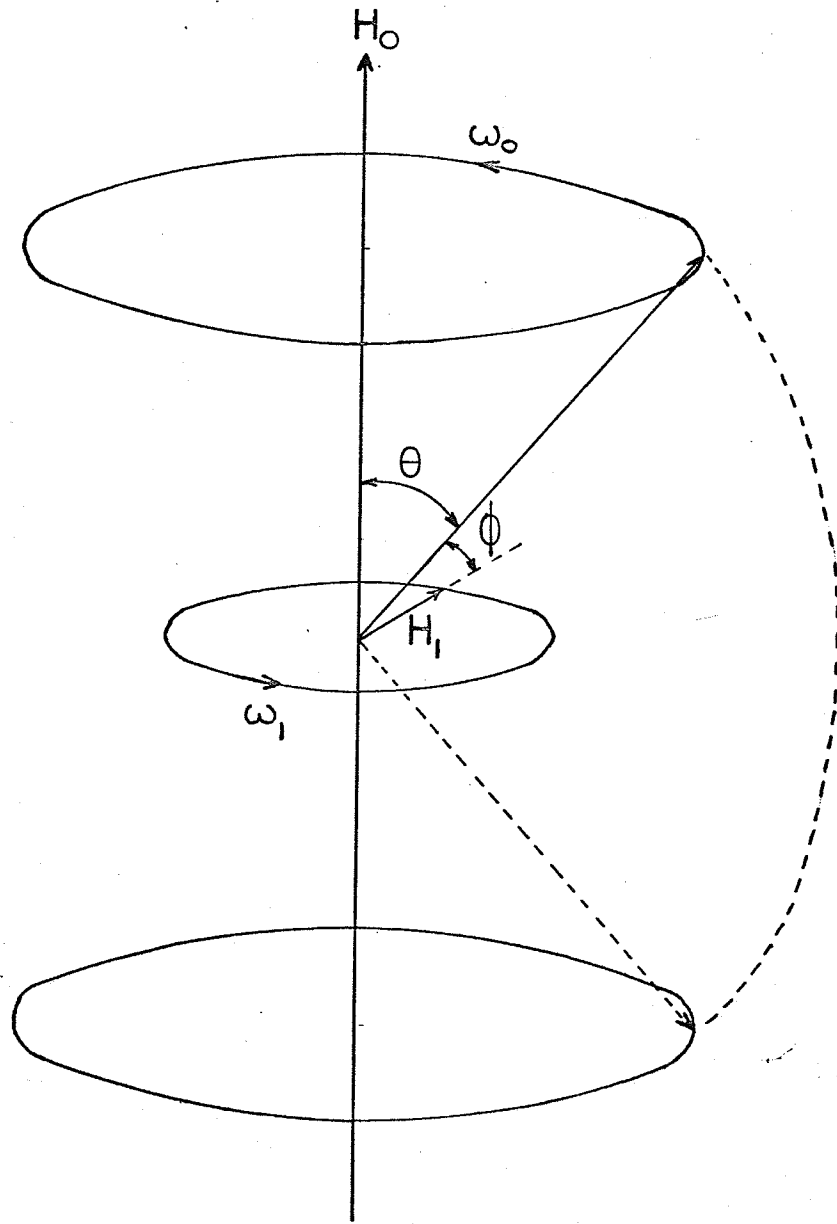
where $\gamma (= \frac{g\beta}{\hbar})$ is the magnetogyric ratio which is the ratio of the magnetic moment to the angular momentum. For free electrons, γ has the value $17.6 \times 10^6 \text{ sec}^{-1} \text{ gauss}^{-1}$. The energy of the dipole in the field H_0 is

$$E_M = -\underline{\mu} \cdot \underline{H}_0 = -\mu H_0 \cos \theta \quad (1-14)$$

where E_M is quantized, corresponding to discrete values of θ . On applying a field \underline{H}_1 perpendicular to the plane containing $\underline{\mu}$ and \underline{H}_0 , the dipole $\underline{\mu}$ will experience an additional couple $\underline{\mu} \underline{H}_1 \cos \phi$, tending to cause precession about \underline{H}_1 . (See Fig. 1.2). Let us now allow H_1 to rotate about H_0 at a frequency ω_1 . When $\omega_1 = \omega_0$ the dipole $\underline{\mu}$ will execute a motion in which θ will change continuously. Since a change in θ corresponds to a change in the energy of the system, it is concluded that transitions between magnetic energy levels are induced by the applied field H_1 rotating at the Larmor frequency. This is the resonance condition. An excellent comparison between the classical and quantum mechanical descriptions of E.S.R. has been given by Anderson⁸

Fig. 1.2

Vector Diagram for the Precession of a
Magnetic Dipole Under the Influence of
a Static Magnetic Field H_0 and a Rotating
Magnetic Field H_1 .



C. THE HYDROGEN ATOM

1. Development of the Spin Hamiltonian.

Up until now we have been dealing with the isolated electron in a magnetic field. The hydrogen atom will be treated in detail because it is the simplest system involving most of the principles of E.S.R. Four combinations may arise since the electron and proton spins can assume two possible orientations each. The spin Hamiltonian for the hydrogen atom is somewhat simpler than most since the atom is spherical. The total Hamiltonian for the hydrogen atom is

$$\mathcal{H} = \mathcal{H}_0 + \mathcal{H}_1. \quad (1-15)$$

\mathcal{H}_0 represents the interaction of the nucleus and the electron with the applied field H_0 (Zeeman Splitting), while \mathcal{H}_1 represents the isotropic hyperfine coupling and the dipolar interaction. In more detail,

$$\mathcal{H}_0 = g \beta H S_Z - g_N \beta_N H I_Z \quad (1-16)$$

where the subscript N denotes nuclear terms. The nuclear Zeeman interaction term in equation (1-16) may be neglected in many cases because it is very small in comparison to the electronic Zeeman interaction term. \mathcal{H}_1 may be written as:

$$\begin{aligned} \mathcal{H}_1 &= a \underline{I} \cdot \underline{S} - g \beta g_N \beta_N \left(\frac{\underline{I} \cdot \underline{S}}{r^3} - \frac{3(\underline{I} \cdot \underline{r})(\underline{S} \cdot \underline{r})}{r^5} \right) \quad (1-17) \\ &= \mathcal{H}_{1a} + \mathcal{H}_{1b} \end{aligned}$$

\mathcal{H}_{1a} represents the coupling of the magnetic moments of the electrons and nuclei via the "Fermi Contact Interaction".

$$\mathcal{H}_{1a} = a \underline{I} \cdot \underline{S} = a(I_x S_x + I_y S_y + I_z S_z) \quad (1-18)$$

where a_N (equals a in all equations) is the coupling constant which is proportional to the unpaired spin density at the nucleus.

$$a = \frac{8\pi}{3} g\beta g_N \beta_N |\psi(0)|^2 \quad (1-19)$$

\mathcal{H}_{1a} may be expressed as a function of the Dirac δ function $\delta(\underline{r})$

$$\mathcal{H}_{1a} = \frac{8\pi}{3} g\beta g_N \beta_N \delta(\underline{r}) \underline{I} \cdot \underline{S} \quad (1-20)$$

Therefore contact interaction may only occur when the electron has a finite probability density at the nucleus. (i.e. the electron must have some S-orbital character).

In the hydrogen atom the unpaired electron occupies a 1S orbital which can be expressed by the wave function

$$\psi_{1S} = \frac{1}{\sqrt{\pi} a_0^3} e^{-\frac{r}{a_0}} \quad (1-21)$$

where $a_0 = \frac{\hbar^2}{me^2} = 0.52918 \text{ \AA}$ (Bohr radius). Substitution of (1-21)

into (1-19) and solving for a_N (in units of energy) one obtains $\frac{a}{\hbar} = 1422.74 \text{ Mc/S}$. This value is close to the experimental values which are generally about 1420 Mc/S.

\mathcal{H}_{1b} represents the dipolar interaction between the electron and the nucleus which is analogous to the classical dipolar coupling between two bar magnets. Averaging \mathcal{H}_{1b} over the entire probability distribution $|\psi(r)|^2$ for the odd electron leads to a value of zero whenever the electron cloud is spherical. Therefore the magnetic interactions in the hydrogen atom are isotropic and the total spin Hamiltonian is

$$\mathcal{H} = g\beta H S_Z - g_N \beta_N H I_Z + a \underline{S} \cdot \underline{I} \quad (1-22)$$

2. Perturbation Theory

\mathcal{H}_0 is the main term of the spin Hamiltonian while \mathcal{H}_{1a} may be classed as a small perturbation of \mathcal{H}_0 . Spin wave functions, which are linear combinations of the four basis functions ϕ_1, ϕ_2, ϕ_3 , and ϕ_4 , are chosen to be eigenfunctions of \mathcal{H}_0 with "zero-order" unperturbed energy values e_1, e_2, e_3 , and e_4 .

The perturbation \mathcal{H}_{1a} yields modified wave functions and energies of the form

$$\psi_n = \phi_n - \sum_{m \neq n} \frac{\langle m | \mathcal{H}_{1a} | n \rangle}{e_m - e_n} \phi_m \quad (1-23)$$

$$E_n = e_n + \langle n | \mathcal{H}_{1a} | n \rangle - \sum_{m \neq n} \frac{\langle m | \mathcal{H}_{1a} | n \rangle \langle n | \mathcal{H}_{1a} | m \rangle}{e_m - e_n} \quad (1-24)$$

The two extra terms on the right hand side of (1-24) represent first and second order corrections to the energy. $\langle n | \mathcal{H}_{1a} | n \rangle$ and $\langle m | \mathcal{H}_{1a} | n \rangle$ are matrix elements of \mathcal{H}_{1a} . $\langle n | \mathcal{H}_{1a} | n \rangle$ represents the fact that \mathcal{H}_{1a} shifts the energy of ϕ_n without changing its form and $\langle m | \mathcal{H}_{1a} | n \rangle$ indicates that \mathcal{H}_{1a} also mixes ϕ_n with other functions ϕ_m .

3. Solving the Hydrogen Atom Problem using Perturbation Theory.

Can perturbation theory be applied? At a field of 10,000 gauss \mathcal{H}_{1a} leads to a hyperfine frequency of 1420 Mc/s which is considerably smaller than the electronic part of \mathcal{H}_0 which is 28,026 Mc/s. Therefore perturbation theory is applicable.

(a) Zero Order Energies

For the electron there are two possible spin functions $|\alpha_e\rangle$ and $|\beta_e\rangle$ with spin quantum numbers $m_s = +1/2$ and $-1/2$. Similarly the proton has two possible spin functions $|\alpha_N\rangle$ and $|\beta_N\rangle$.

Therefore the four basis functions are:

$$\begin{aligned}
 \phi_1 &= |\alpha_e \alpha_N \rangle \\
 \phi_2 &= |\alpha_e \beta_N \rangle \\
 \phi_3 &= |\beta_e \alpha_N \rangle \\
 \phi_4 &= |\beta_e \beta_N \rangle
 \end{aligned}
 \tag{1-25}$$

Neglecting \mathcal{H}_{1a} , these four states are degenerate until H_0 is applied. Equations (1-25) are all eigenfunctions of \mathcal{H}_0 and the matrix of \mathcal{H}_0 is diagonal. Operating on equations (1-25) with \mathcal{H}_0 yields four zero-order energies. (See Fig. 1.3).

$$\begin{aligned}
 e_1 &= 1/2 g\beta H - 1/2 g_N \beta_N H \\
 e_2 &= 1/2 g\beta H + 1/2 g_N \beta_N H \\
 e_3 &= -1/2 g\beta H - 1/2 g_N \beta_N H \\
 e_4 &= -1/2 g\beta H + 1/2 g_N \beta_N H
 \end{aligned}
 \tag{1-26}$$

(b) First Order Energies

Here we will consider the effect of \mathcal{H}_{1a} on the zero-order wave functions (1-25).

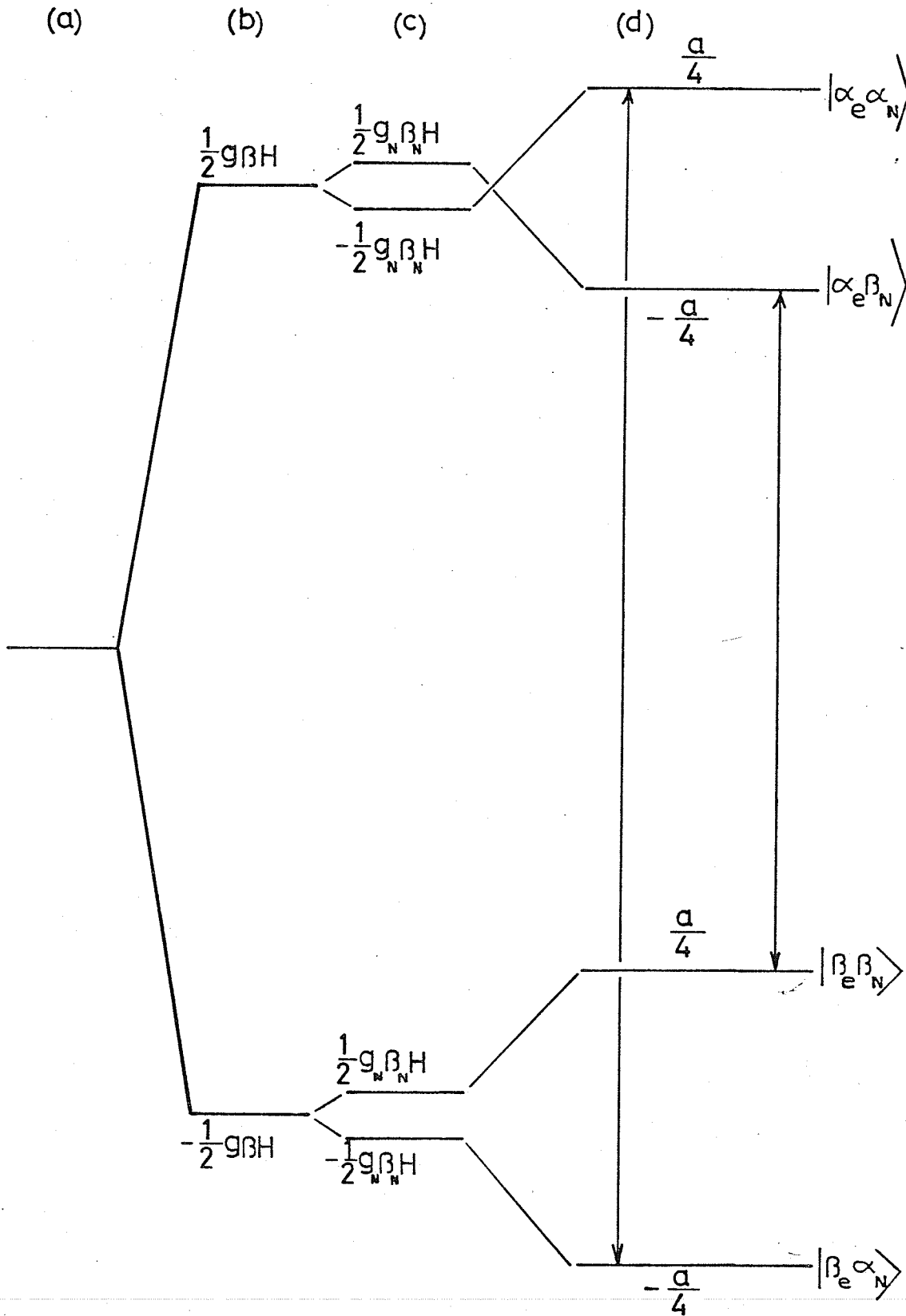
$$\mathcal{H}_{1a} = a \underline{S} \cdot \underline{I} = a [S_Z I_Z + S_X I_X + S_Y I_Y]
 \tag{1-27}$$

The operators S_X , S_Y , I_X , I_Y do not effect the energies of ϕ_1 and ϕ_4 but do mix ϕ_2 and ϕ_3 . Therefore the term $a[S_X I_X + S_Y I_Y]$ leads to second order effects. Let us operate on ϕ_1 to ϕ_4 with the operator $aS_Z I_Z$.

$$\begin{aligned}
 \langle \alpha_e \alpha_N | aS_Z I_Z | \alpha_e \alpha_N \rangle &= \frac{a}{4} \\
 \langle \beta_e \beta_N | aS_Z I_Z | \beta_e \beta_N \rangle &= \frac{a}{4} \\
 \langle \alpha_e \beta_N | aS_Z I_Z | \alpha_e \beta_N \rangle &= -\frac{a}{4} \\
 \langle \beta_e \alpha_N | aS_Z I_Z | \beta_e \alpha_N \rangle &= -\frac{a}{4}
 \end{aligned}
 \tag{1-28}$$

Fig. 1.3

First-order Spin Energy Levels of the Hydrogen Atom and the Allowed E.S.R. Transitions. (a) is the Zero Field contribution, (b) is the Electron Zeeman Contribution, (c) is the Nuclear Zeeman Contribution and (d) is the Hyperfine Coupling Contribution.



Assuming a_N to be positive these first order energy shifts may be seen in Fig. 1.3.

(c) Second-Order Hyperfine Interactions

Two new operators must be defined in order to look at the effect of $a_N(S_x I_x + S_y I_y)$ on the spin states. These two operators are known as "shift" or "ladder" operators

$$\begin{aligned} S^+ &= S_x + i S_y \\ S^- &= S_x - i S_y \end{aligned} \quad (1-29)$$

Similar operators may be defined for the nuclear spins.

$$\begin{aligned} I^+ &= I_x + i I_y \\ I^- &= I_x - i I_y \end{aligned} \quad (1-30)$$

It may be shown that

$$S_x I_x + S_y I_y = 1/2 (S^+ I^- + S^- I^+) \quad (1-31)$$

The operator (1-31) does not effect ϕ_1 and ϕ_4 but mixes ϕ_2 and ϕ_3 . The complete matrix of operator \mathcal{H}_{1a} is

$$a \underline{I} \cdot \underline{S} = 1/4 a \begin{vmatrix} 1 & 0 & 0 & 0 \\ 0 & -1 & 2 & 0 \\ 0 & 2 & -1 & 0 \\ 0 & 0 & 0 & 1 \end{vmatrix} \begin{matrix} \alpha_e \alpha_N \\ \alpha_e \beta_N \\ \beta_e \alpha_N \\ \beta_e \beta_N \end{matrix} \quad (1-32)$$

$$\begin{aligned} \text{since } & \langle \alpha_e \beta_N | S^+ I^- | \beta_e \alpha_N \rangle = 1 \\ & \langle \beta_e \alpha_N | S^- I^+ | \alpha_e \beta_N \rangle = 1 \end{aligned}$$

The two modified wave function, obtained by using equation (1-23) are

$$\begin{aligned} \psi_2 &= | \alpha_e \beta_N \rangle + \frac{a}{2(g\beta_H + g_N \beta_N H)} | \beta_e \alpha_N \rangle \\ \psi_3 &= | \beta_e \alpha_N \rangle - \frac{a}{2(g\beta_H + g_N \beta_N H)} | \alpha_e \beta_N \rangle \end{aligned} \quad (1-33)$$

Their energies, shown in Fig. 1.4, are:

$$\begin{aligned}
 E_2 &= (1/2g\beta H + 1/2g_N\beta_N H) - 1/4 a + \frac{a^2}{4(g\beta H + g_N\beta_N H)} \\
 E_3 &= -(1/2g\beta H + 1/2g_N\beta_N H) - 1/4 a - \frac{a^2}{4(g\beta H + g_N\beta_N H)} \quad (1-34)
 \end{aligned}$$

Setting $\Delta_e = g\beta H$ and $\Delta_n = g_N\beta_N H$, the complete secular determinant may be written:

	$ \alpha\alpha\rangle$	$ \alpha\beta\rangle$	$ \beta\alpha\rangle$	$ \beta\beta\rangle$	
$\langle\alpha\alpha $	$1/2(\Delta_e - \Delta_n) + \frac{a}{4} - E$	0	0	0	(1-35)
$\langle\alpha\beta $	0	$1/2(\Delta_e + \Delta_n) - \frac{a}{4} - E$	$\frac{a}{2}$	0	
$\langle\beta\alpha $	0	$\frac{a}{2}$	$-1/2(\Delta_e + \Delta_n) - \frac{a}{4} - E$	0	
$\langle\beta\beta $	0	0	0	$-1/2(\Delta_e - \Delta_n) + \frac{a}{4} - E$	

Fig. 1.5 shows the behaviour of the exact energy levels as a function of H_0 .

4. First-Order E.S.R. Spectrum

The first-order spin states and energies for the hydrogen atom may be seen in Fig. 1.3. If an oscillating magnetic field of strength $2H_1 \cos \omega t$ acts on the atom several kinds of spin transitions may occur (if $\omega = \omega_0$). There are three types of spin transitions possible:

- 1) E.S.R. transitions $\alpha_e \alpha_N \rightarrow \beta_e \alpha_N$
- 2) N.M.R. transitions $\alpha_e \alpha_N \rightarrow \alpha_e \beta_N$
- 3) Forbidden transitions $\alpha_e \beta_N \rightarrow \beta_e \alpha_N$

If H_1 is applied parallel to H_0 only modulations in the energy levels occur. H_1 must be applied perpendicular to H_0 for transitions to occur. The resulting time-dependent perturbation on the atom is:

$$\begin{aligned}
 V(t) &= 2(g\beta H_1 S_x - g_N\beta_N H_1 I_x) \cos \omega t \\
 &= 2 V \cos \omega t \quad (1-36)
 \end{aligned}$$

Fig. 1.4

(a) represents the first-order hyperfine energy levels of the hydrogen atom while (b) is the second-order hyperfine energy levels of the hydrogen atom. The "dashed" transitions are "forbidden" and $\lambda = \frac{a^2}{4(g\beta_H + g_N\beta_N H)}$

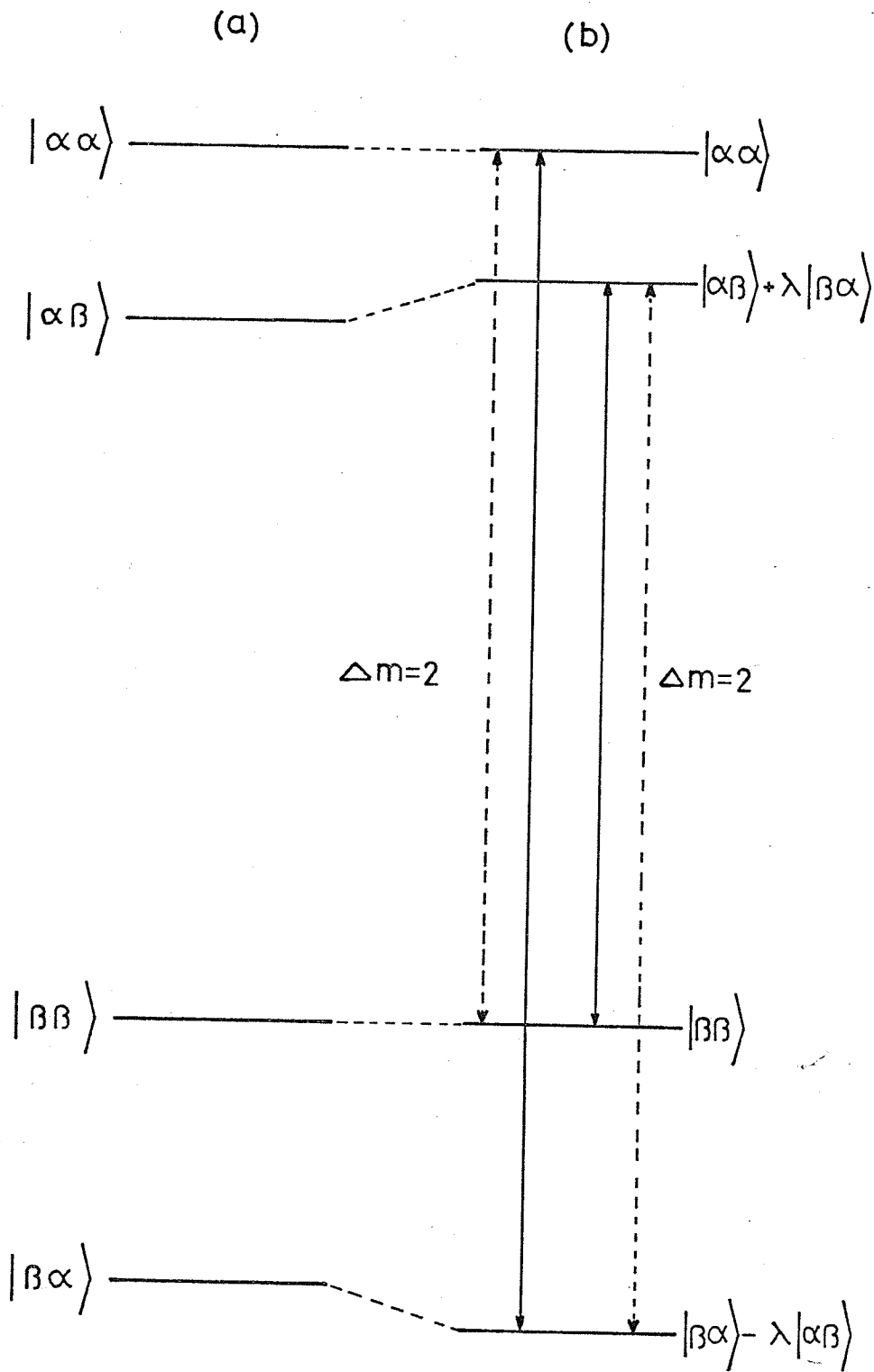
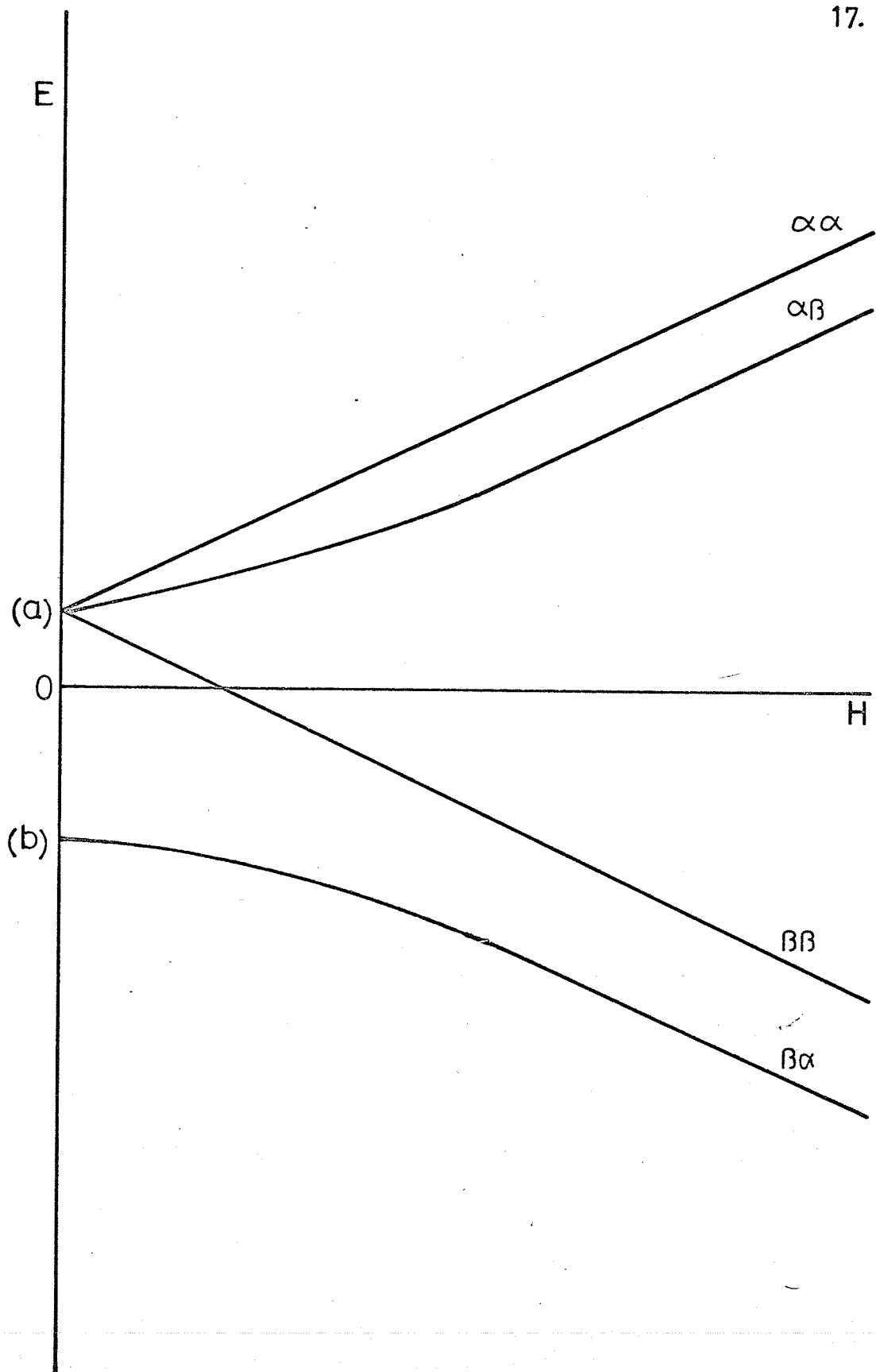


Fig. 1.5

Exact Energy Levels of the Hydrogen Atom as a Function of the Applied Field H. (a) represents the functions $\alpha\alpha$, $\frac{1}{\sqrt{2}} (\alpha\beta+\beta\alpha)$ and $\beta\beta$ while (b) represents the Function $\frac{1}{\sqrt{2}} (\alpha\beta-\beta\alpha)$.



From (1-36) one can see that H_1 is being applied in the x-direction while H_0 is being applied in the Z direction. The transition probability between states n and m is

$$P_{nm} = \frac{2\pi}{\hbar^2} |\langle n|V|m\rangle|^2 \delta(\omega_{mn} - \omega) \quad (1-37)$$

The term involving I_x in equation (1-36) may be omitted since we are dealing with E.S.R. transitions only. Equation (1-37) may be written

$$P_{nm} = \frac{2\pi}{\hbar^2} g^2 \beta^2 H_1^2 |\langle n|S_x|m\rangle|^2 \delta(\omega_{mn} - \omega) \quad (1-38)$$

Considering the transition $\beta_e \alpha_N \leftrightarrow \alpha_e \alpha_N$ (Fig. 1.3) and keeping in mind that $S_x = 1/2 (S^+ + S^-)$ equation (1-38) becomes

$$P_{nm} = \frac{2\pi}{\hbar^2} g^2 \beta^2 H_1^2 |\langle \alpha_e \alpha_N | 1/2 (S^+ + S^-) | \beta_e \alpha_N \rangle|^2 \delta(\omega_{mn} - \omega) \quad (1-39)$$

Factoring out the nuclear spin parts from (1-39)

$$P_{nm} = \frac{2\pi}{\hbar^2} g^2 \beta^2 H_1^2 |\langle \alpha_e | 1/2 (S^+ + S^-) | \beta_e \rangle|^2 |\langle \alpha_N | \alpha_N \rangle|^2 \delta(\omega_{mn} - \omega) \quad (1-40)$$

Since $|\langle \alpha_N | \alpha_N \rangle|^2 = 1$ and $\gamma = \frac{g\beta}{\hbar}$

$$\begin{aligned} P_{nm} &= 2\pi \gamma^2 H_1^2 |\langle \alpha_e | 1/2 (S^+ + S^-) | \beta_e \rangle|^2 \delta(\omega_{mn} - \omega) \\ &= 1/2 \pi \gamma^2 H_1^2 \delta(\omega_{mn} - \omega) \end{aligned} \quad (1-41)$$

Substitutions of the general line shape function $g(\omega)$ for the δ function gives

$$P_{nm} = 1/2 \pi \gamma^2 H_1^2 g(\omega) \quad (1-42)$$

The transition probability of the other allowed E.S.R. transition (Fig. 1.3) can be shown to be equal to the one just calculated.

Allowed E.S.R. transitions obey the following selection rules:

$$\Delta m_S = \pm 1 \quad \Delta m_I = 0 \quad (1-43)$$

If two transitions have equal probabilities they must have equal intensities (neglecting thermal population differences). By subtracting the energies of the lower states from the energies of the upper states, for the allowed transitions in the hydrogen atom, one obtains the frequencies of the two transitions.

$$\begin{aligned} h\nu_1 &= g\beta H + 1/2 a \\ h\nu_2 &= g\beta H - 1/2 a \end{aligned} \quad (1-44)$$

The first order E.S.R. spectrum of the hydrogen atom consists, therefore, of two equally intense lines separated by a_N (the hyperfine coupling constant).

5. Second-Order E.S.R. Spectrum

Figure 1.4 illustrates that the two allowed transitions are shifted slightly but are still separated by a_N . The changes in the spin wave functions lead to a slight decrease in line intensity. The transition $\alpha_e\beta_N \leftrightarrow \beta_e\alpha_N$, strictly forbidden by first-order treatment, becomes weakly allowed in second order treatment provided H_1 is polarized parallel to H_0 . To compute the transition probabilities we use wave functions (1-33) and set λ equal to the mixing coefficient $\frac{a}{2(g\beta H + g_N\beta_N H)}$. The perturbation $2H_1 g\beta S_z \cos \omega\tau$ has a matrix element

$$\langle \psi_2 | S_z | \psi_3 \rangle = \langle \alpha_e\beta_N + \lambda\beta_e\alpha_N | S_z | \beta_e\alpha_N - \lambda\alpha_e\beta_N \rangle = -\lambda \quad (1-45)$$

The transition probability is

$$P = 2\lambda^2 \pi \gamma^2 H_1^2 g(\omega) \quad (1-46)$$

This transition would be seen only at low fields since at high fields λ^2 would be negligible. Equation (1-45) is only valid for small λ since each wave function (1-33) should contain a normalization factor of $(1+\lambda^2)^{-1/2}$. This transition is allowed only because m_s and m_I values of the exact wave function are not sharply defined due to mixing.

6. Zero-Field Levels of Hydrogen Atom

When H_0 is zero the only term in the Hamiltonian is the isotropic interaction term, a $\underline{I} \cdot \underline{S}$, which couples the spin vectors \underline{I} and \underline{S} into a resultant angular momentum \underline{F} .

$$\underline{F} = (\underline{I} + \underline{S}) \quad (1-47)$$

\underline{F} may be 0 (singlet) or 1 (triplet). See Figure 1.5. There are three triplet functions which may be differentiated from one another by their F_z values, or $(m_I + m_S)$ values, which may be 1, 0, and -1. The E.S.R. spectrum consists of a single line at 1420 Mc/S which is due to singlet-triplet transitions.

D. HYPERFINE SPLITTINGS IN POLYNUCLEAR FREE RADICALS

The electron-nuclear hyperfine interaction is, in general, represented by the term

$$\mathcal{H}_1 = \underline{S} \cdot \underline{T} \cdot \underline{I} \quad (1-48)$$

where \underline{T} is the hyperfine Tensor. \mathcal{H}_1 may be split into two terms by decomposing the tensor \underline{T} .

$$\mathcal{H}_1 = a \underline{S} \cdot \underline{I} + \underline{S} \cdot \underline{T}' \cdot \underline{I} \quad (1-49)$$

where $a_N (=a)$ is the isotropic contact part, and \underline{T}' is the magnetic dipolar tensor. For radicals in the liquid phase or in any physical

environment where rapid tumbling or reorientation is allowed the average value of \underline{T}^1 is zero and the observed hyperfine splitting (h.f.s.) gives the isotropic coupling constant a_N directly. In the following discussion the average value of \underline{T}^1 is assumed to be zero.

1. THE INTERACTION OF AN ELECTRON WITH TWO NON-EQUIVALENT PROTONS.

In this free radical we have two coupling constants a_1 and a_2 . The total spin Hamiltonian is given by

$$\mathcal{H} = g\beta HS_Z - g_N\beta_N H(I_{1Z} + I_{2Z}) + a_1 \underline{S} \cdot \underline{I}_1 + a_2 \underline{S} \cdot \underline{I}_2 \quad (1-50)$$

Dropping the nuclear Zeeman terms since they do not effect the positions of the absorption lines (Fig. 1.3).

$$\mathcal{H} = g\beta HS_Z + a_1 \underline{S} \cdot \underline{I}_1 + a_2 \underline{S} \cdot \underline{I}_2 \quad (1-51)$$

Most free radical spectra may be treated adequately using first-order perturbation theory. Therefore equation (1-51) becomes

$$\mathcal{H} = g\beta HS_Z + S_Z(a_1 I_{1Z} + a_2 I_{2Z}) \quad (1-52)$$

The eight basis functions for the system are found by multiplying the four possible nuclear states ($\alpha_1\alpha_2, \alpha_1\beta_2, \beta_1\alpha_2, \beta_1\beta_2$) by the two possible electron states (α_e, β_e). These basis functions are, in a first-order approximation, the correct eigenfunctions of \mathcal{H} . Let us calculate the energy for the eigenfunction $|\alpha_e\alpha_1\alpha_2\rangle$.

$$\begin{aligned} E &= g\beta H \langle \alpha_e\alpha_1\alpha_2 | S_Z | \alpha_e\alpha_1\alpha_2 \rangle + a_1 \langle \alpha_e\alpha_1\alpha_2 | S_Z I_{1Z} | \alpha_e\alpha_1\alpha_2 \rangle + a_2 \langle \alpha_e\alpha_1\alpha_2 | S_Z I_{2Z} | \alpha_e\alpha_1\alpha_2 \rangle \\ &= 1/2 g\beta H + \frac{a_1}{4} + \frac{a_2}{4} \\ E &= 1/2 (g\beta H + \frac{a_1}{2} + \frac{a_2}{2}) \quad (1-53) \end{aligned}$$

Making appropriate substitutions:

$$E = m_s (g\beta H + a_1 m_1 + a_2 m_2) \quad (1-54)$$

Equation (1-54) may be verified by performing the same operations on the other seven basis functions. The energy levels and allowed transitions may be seen in Fig. 1.6. Since $\Delta m_s = \pm 1$ and $\Delta m_n = 0$ for allowed transitions, the corresponding resonance frequency is

$$h\nu = g\beta H + a_1 m_1 + a_2 m_2 \quad (1-55)$$

The isolated electron resonates at $H = H^*$

$$h\nu = g\beta H^* \quad (1-56)$$

Substituting (1-56) into (1-55) and changing a_1 and a_2 into gauss (1 gauss = 2.803 Mc/s),

$$H = H^* - a_1 m_1 - a_2 m_2 \quad (1-57)$$

$$H = H^* - \sum_i a_i m_i \quad (1-58)$$

For the system under consideration one obtains four equally intense lines (see Fig. 1.6). Proton 1 splits the original single line due to the electron spin into a doublet, each line being split into a further two lines due to the interaction with proton 2.

2. RADICALS WITH TWO EQUIVALENT PROTONS

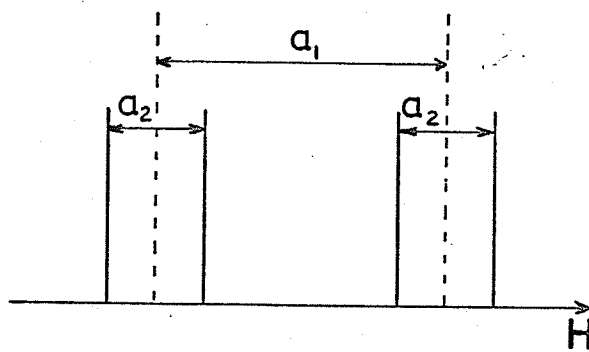
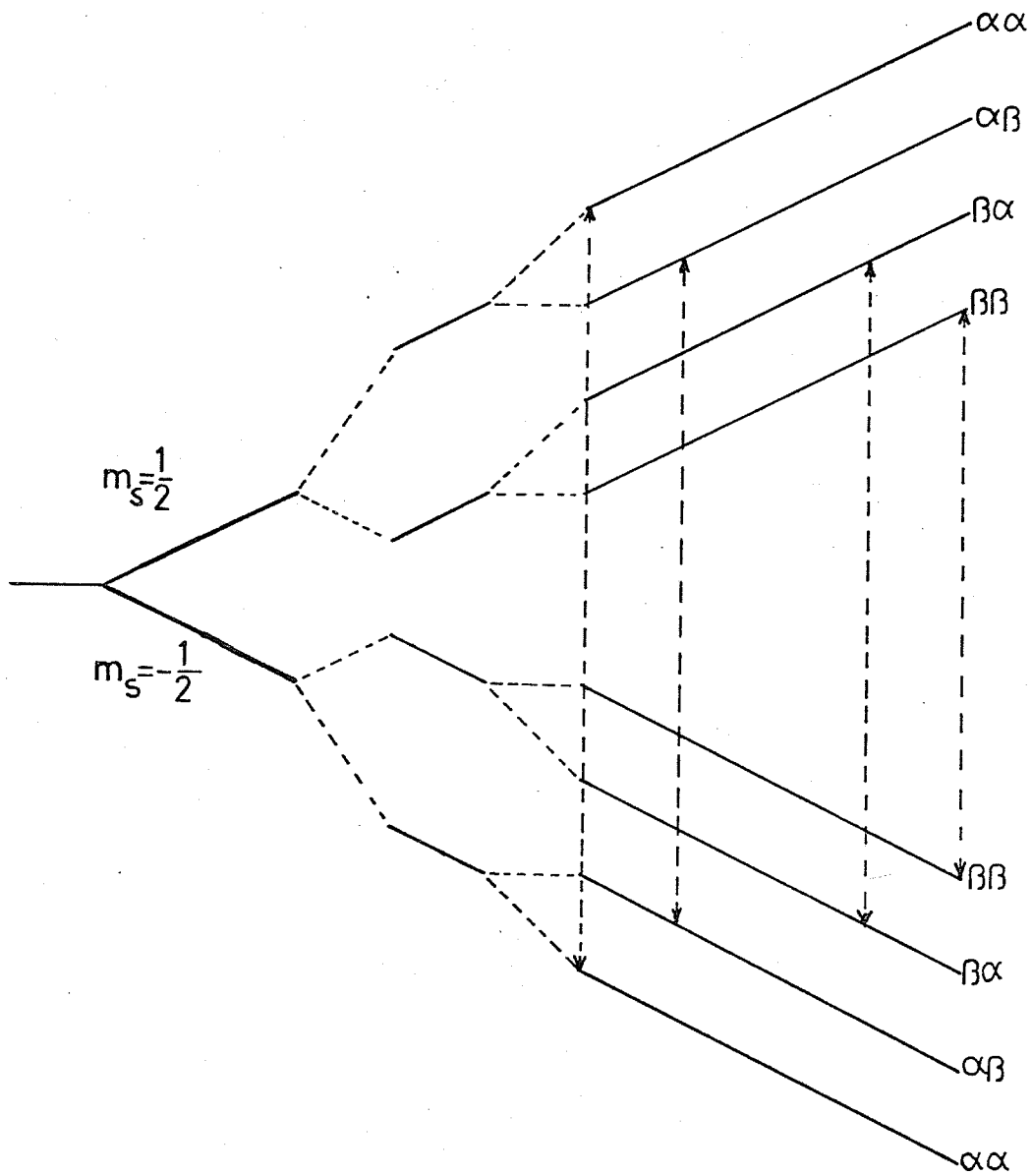
Equivalent protons occupy equivalent positions in the molecular fragment and their coupling constants are equal. Applying equation (1-58)

$$\begin{aligned} H &= H^* - \sum_i a_i m_i \\ &= H^* - a \sum_i m_i \end{aligned} \quad (1-59)$$

where $\sum_i m_i = m_1 + m_2 = M$

Fig. 1.6

Hyperfine Energy Levels and Transitions for Two
Non-equivalent Protons (a_1 and a_2 are assumed to
be positive)



Therefore

<u>Field</u>	<u>m_1+m_2</u>	<u>Nuclear Spin States</u>
$H^* - a$	1	$\alpha\alpha$
H^*	0	$\alpha\beta, \beta\alpha$
$H^* + a$	-1	$\beta\beta$

For two equivalent protons there are three E.S.R. lines with relative intensities equal to 1:2:1 due to the degeneracy of the $M = 0$ level.

3. RADICALS WITH THREE EQUIVALENT PROTONS (CH_3)

Employing equation (1-59) we obtain

<u>Field</u>	<u>$m_1+m_2+m_3$</u>	<u>Nuclear Spin States</u>
$H^* - \frac{3a}{2}$	$\frac{3}{2}$	$\alpha_1\alpha_2\alpha_3$
$H^* - \frac{a}{2}$	1/2	$\alpha_1\alpha_2\beta_3$
		$\alpha_1\beta_2\alpha_3$
		$\beta_1\alpha_2\alpha_3$
		$\alpha_1\beta_2\beta_3$
$H^* + \frac{a}{2}$	-1/2	$\beta_1\alpha_2\beta_3$
		$\beta_1\beta_2\alpha_3$
		$\beta_1\beta_2\beta_3$
$H^* + \frac{3a}{2}$	-3/2	$\beta_1\beta_2\beta_3$

The resulting first-order hyperfine splitting pattern is shown in Fig. 1.7. From the eight allowed transitions one obtains four lines with the intensity ratio 1:3:3:1.

4. RADICALS WITH n EQUIVALENT PROTONS

The interaction of n equivalent protons with an electron spin results in n+1 lines whose relative intensities are proportional to the coefficients of the binomial expansion $(1 + x)^n$. The relative intensities for n = 0 to n = 6 are shown below.

n = 0				1											
n = 1			1		1										
n = 2			1		2		1								
n = 3			1		3		3		1						
n = 4			1		4		6		4		1				
n = 5			1		5		10		10		5		1		
n = 6			1		6		15		20		15		6		1

The separation between any two adjacent lines yields the coupling constant a.

5. RADICALS WITH SEVERAL SETS OF EQUIVALENT PROTONS

Let us assume we have several distinct sets A, B, C of equivalent protons. The spin Hamiltonian is

$$\mathcal{H} = g\beta H S_Z + S_Z (a_A F_{ZA} + a_B F_{ZB} + \dots) \quad (1-60)$$

where $F_{ZA} = I_{1ZA} + I_{2ZA} + \dots$

where 1,2..... indicates the number of the proton in the equivalent set A. Each equivalent set is characterized by a coupling constant different in value from those of the other equivalent sets. Let us consider the naphthalene anion.

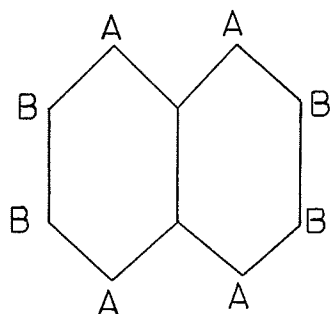
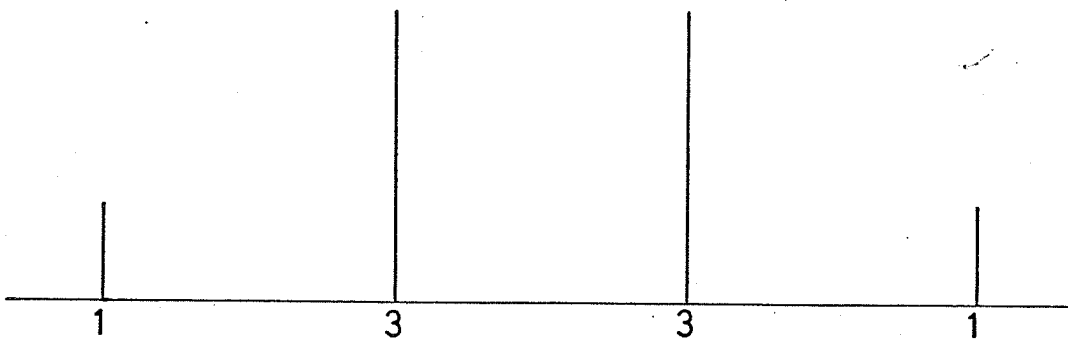
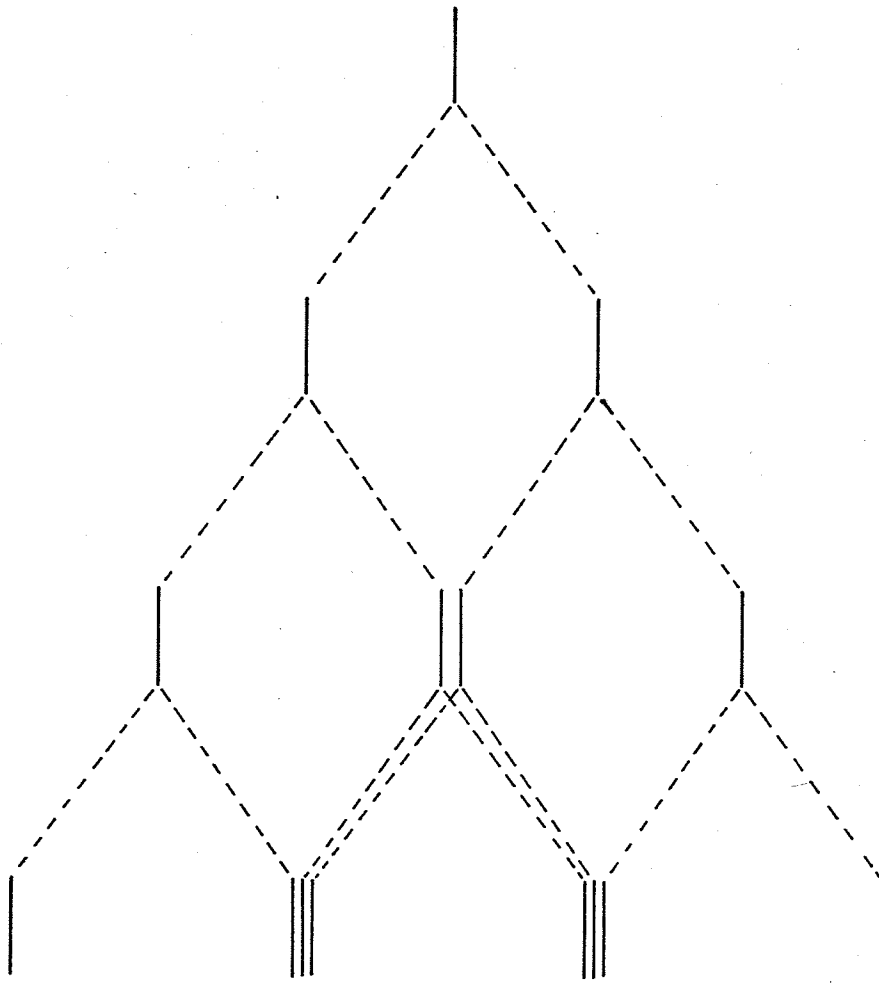


Fig. 1.7

Hyperfine Energy Levels and Spectra for Three Equivalent Protons. Relative Intensities of the pattern is indicated.

26.



The unpaired electron spin interacts with four A and four B type protons. The interaction with the four A type protons gives a five line pattern with relative intensities 1:4:6:4:1 and a coupling constant a_A (4.9g). Each of these lines is further split into quintets by the interaction with the B type protons. The coupling constant $a_B = 1.83$ gauss. If $a_A \gg a_B$ one would see five completely resolved quintets but in this case, as in most other radicals, one obtains an overlapped spectrum. The relative intensities of the five quintets are determined by the following procedure.

$$\begin{aligned}
 1 \times (1:4:6:4:1) &= 1:4:6:4:1 \\
 4 \times (1:4:6:4:1) &= 4:16:24:16:4 \\
 6 \times (1:4:6:4:1) &= 6:24:36:24:6 \\
 4 \times (1:4:6:4:1) &= 4:16:24:16:4 \\
 1 \times (1:4:6:4:1) &= 1:4:6:4:1
 \end{aligned}
 \tag{1-61}$$

The coupling constants may be converted from gauss to M_C/s by multiplication by 2.803 (only for $g = 2$ radicals). The hyperfine structure is independent of the signs of the coupling constants. The coupling constant signs may be determined by second order effects on line widths and hyperfine splittings.

6. RADICALS WITH SEVERAL SETS OF EQUIVALENT NUCLEI

In order to determine, using the first order approach, the total number of h.f. lines observable for an electron interacting with n equivalent nuclei of spin I_Z the following relation may be used.

$$2nI_Z + 1 \tag{1-62}$$

For n protons this relation reduces to $n+1$ as seen before. The total number of h.f. lines for an electron interacting with several sets A, B, C, of n_A, n_B, n_C, \dots equivalent nuclei is

$$(2n_A I_A + 1) (2n_B I_B + 1) (2n_C I_C + 1) \dots \dots \dots \quad (1-63)$$

7. HYPERFINE SPLITTINGS DUE TO C^{13} IN THE METHYL RADICAL

The natural abundance of C^{13} ($I = 1/2$) is 1.1%. Therefore 98.9% of the methyl radicals present will exhibit the normal four line spectra with relative intensities 1:3:3:1 and $|a_H| = 23$ gauss. [See Fig. 1.8 (A)]. The remaining 1.1% of the methyl radicals have an additional coupling of approximately 40 gauss which splits each of the four lines into doublets [See Fig. 1.8 (B)]. The superposition of the two spectra lead to the presence of very weak satellite lines [Fig. 1.8 (C)]. These satellite lines may be enhanced by enriching the methyl radicals in C^{13} .

8. HYPERFINE SPLITTINGS IN THE DEUTERATED METHYL RADICAL

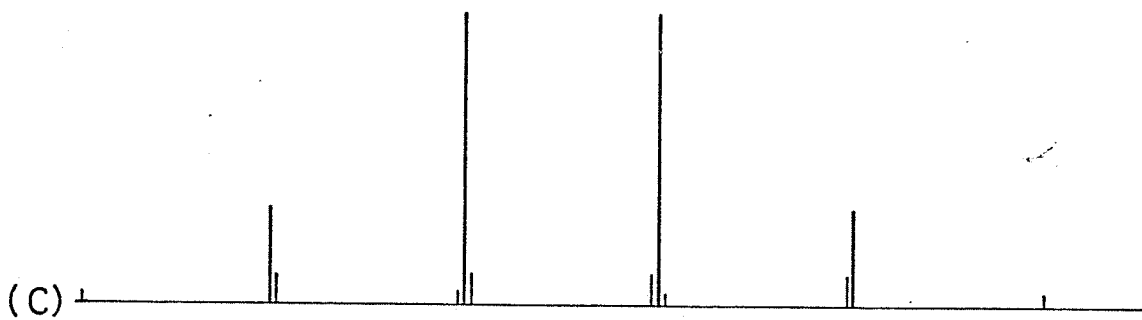
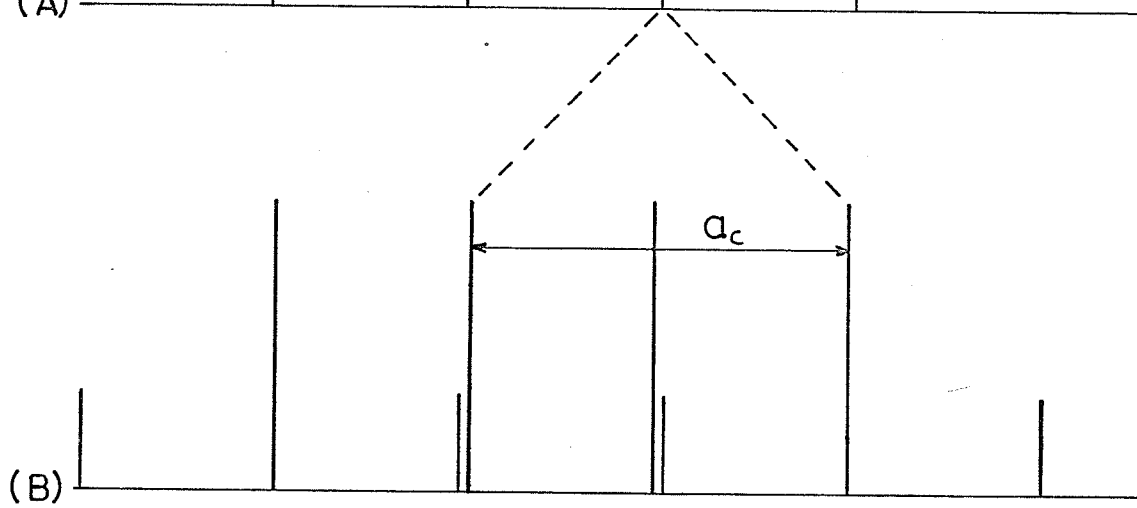
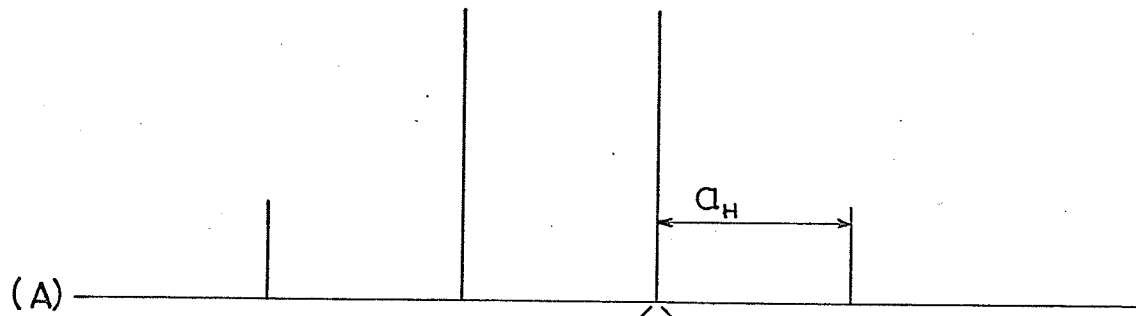
The hyperfine lines observed are due to the interaction of the unpaired electron with three equivalent deuterons ($I=1$). A nucleus with $I=1$ has three allowed spin orientations with components in the Z- direction corresponding to m_I values of $+1(\alpha)$, $0(\beta)$, and $-1(\gamma)$. Making use of equation (1-59)

<u>Field</u>	<u>Σm</u>	<u>Nuclear Spin States</u>
$H^* - 3a$	3	$\alpha\alpha\alpha$
$H^* - 2a$	2	$\alpha\alpha\beta, \alpha\beta\alpha, \beta\alpha\alpha$
$H^* - a$	1	$\alpha\beta\beta, \beta\alpha\beta, \beta\beta\alpha, \alpha\alpha\gamma, \alpha\gamma\alpha, \gamma\alpha\alpha$
H^*	0	$\beta\beta\beta, \alpha\beta\gamma, \alpha\gamma\beta, \gamma\beta\alpha, \gamma\alpha\beta, \beta\alpha\gamma, \beta\gamma\alpha$

etc.

Fig. 1.8

Carbon-13 Splitting in the Methyl Radical. (A) Protons in $C^{12}H_3$; (B) Spectrum of $C^{13}H_3$; (C) Natural Mixture of C^{12} and C^{13}



The E.S.R. spectra of CD_3 consists of seven lines separated by a_N with relative intensities 1:3:6:7:6:3:1. It may be shown that $a^D(\text{CD}_3)$ is approximately equal to $0.1531 a^H(\text{CH}_3)$ since $\frac{g^D}{g^H} = 0.1531$.

E. BRIEF DESCRIPTION OF THE MECHANISMS OF HYPERFINE COUPLING.

1. UNPAIRED SPIN DENSITY

The isotropic hyperfine interaction in the hydrogen atom is represented by a term proportional to $|\psi(o)|^2$, the probability of finding the electron at the nucleus. The splitting constant for the hydrogen 1s orbital has been calculated and confirmed to be 506.8 gauss. The unpaired electron in molecular radicals (non-aromatic) occupies a σ orbital (symmetrical on reflection through the molecular plane) which extends over the entire bonding system. Therefore, the probability of finding it on any particular hydrogen atom is dramatically smaller than for the hydrogen atom. This concept leads to much smaller hyperfine coupling constants for each hydrogen atom in the system. If the molecular radical contains i hydrogen atoms

$$\rho_H = \frac{a_i}{506.8} = \text{unpaired spin density (in the 1s orbital of } i) \quad (1-64)$$

There is a direct proportionality between the spin density in the 1s (or other s) orbitals and the hyperfine splittings.

In actual fact a molecule contains many electrons whose spins are coupled together. Therefore, one is unable to say that there is just one "unpaired electron" in a certain orbital, while all others are perfectly paired.

The correct contact Hamiltonian for a molecule is represented by the operator

$$\mathcal{H}_C = \frac{8\pi}{3} g\beta g_N \beta_N \sum_k \delta(\underline{r}_k - \underline{r}_N) \underline{S}_k \cdot \underline{I} \quad (1-65)$$

The sum runs over all electrons, and the value of a_N is found by averaging over the complete set of many-electron wave functions.

The resulting a_N is

$$a = \frac{4\pi}{3} g\beta g_N \beta_N \rho(\underline{r}_N), \quad (1-66)$$

where $\rho(\underline{r}_N)$ [the unpaired electron density at the nucleus] is written

$$\rho(\underline{r}_N) = \int \psi^* \sum_k 2 S_{Zk} \delta(\underline{r}_k - \underline{r}_N) \psi d\tau. \quad (1-67)$$

$\rho(\underline{r}_N)$ is the number of electrons at the nucleus with spin α minus the number with spin β . The operator $2S_{Zk}$ gives a factor ± 1 depending on the spin. The δ function ensures that the electron is at the nucleus.

$\rho(\underline{r}_N)$ is the unpaired electron density or spin density at the nucleus (a probability density measured in electrons / \AA^3) while ρ_H is the spin density in an orbital (a number representing the fractional population of unpaired electrons on the atom). For example: if the electrons on a hydrogen atom are mainly in the $1s$ orbital

$$\rho(\underline{r}_H) = \rho_H |\psi_{1s}(\underline{r}_H)|^2 \quad (1-68)$$

2. INDIRECT COUPLING THROUGH A C-H BOND

In aromatic radicals, the unpaired electron occupies a π molecular orbital which has a node in the plane of the molecule. How does the electron couple with the ring protons which are found at the node? In order to answer this it might be simpler to consider an isolated \dot{C} -H fragment (Fig. 1.9) where the unpaired electron occupies the $2P_Z$ carbon orbital. The other electron on the carbon under consideration occupies an SP^2 hybrid orbital while the electron

on the hydrogen atom occupies its 1s orbital. Two possible structures of this fragment may be drawn [Fig. 1.9(a), 1.9(b)]. Structure (a) is preferred due to a more favourable exchange interaction between the π electron and the carbon σ electron, whose spins are parallel. Structures (a) and (b) would be of equal importance if only perfect pairing is considered. Due to the exchange interaction, the electrons in the C-H σ bond are slightly polarized. If the odd electron has spin α , there is a slight excess α spin in the carbon σ orbital and a corresponding excess β spin in the hydrogen 1s orbital. This gives rise to an isotropic proton splitting. An α spin in the carbon P_z orbital leads to an excess β spin in the hydrogen 1s orbital. For this reason, ρ_H and a_H are considered to be negative. The extent to which the C-H σ electrons are polarized in aromatic radicals is directly proportional to the net unpaired electron population, or " π -electron spin density (ρ_π)" on the carbon atom.

$$a_H = Q \rho_\pi \quad (\text{McConnell's Relation}) \quad (1-69)$$

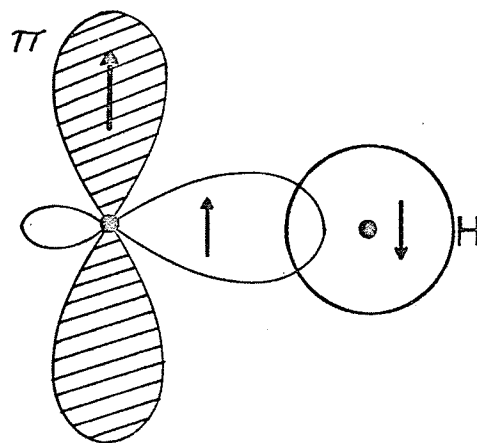
For the benzene anion, the spin density is 1/6 and $a_H = -3.75$ gauss. Therefore, $Q = \frac{-3.75}{1/6} = -22.5$ gauss which is the total splitting for the benzene anion. Table 1.1 gives the values of ρ_π , a_H and Q for different cyclic polyene radicals C_nH_n compared to CH_3 .

TABLE 1.1
COMPARISON OF ρ_π , a_H and Q FOR SEVERAL CYCLIC
POLYENE RADICALS

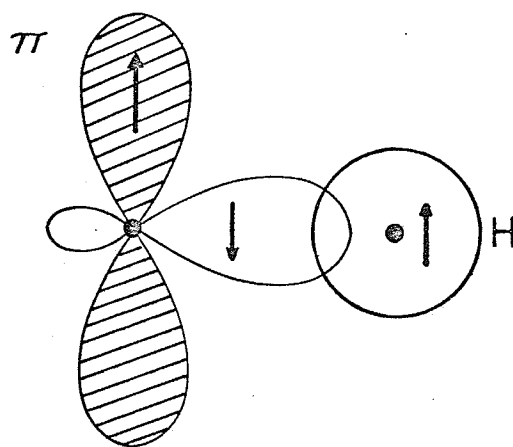
RADICAL	ρ_π	a_H	Q
CH_3	1	-23.04	-23.04
C_5H_5	1/5	- 5.98	-29.9
$C_6H_6^-$	1/6	- 3.75	-22.5
C_7H_7	1/7	- 3.91	-27.4
$C_8H_8^-$	1/8	- 3.21	-25.7

Fig. 1.9

Structures Considered when Treating Indirect Coupling
Through a C-H Bond.



(a)



(b)

3. β PROTON SPLITTINGS

In most cases the β -proton coupling is larger or equal to the α -proton coupling. For example, let us examine the α and β couplings for the ethyl radical in solution.

$$\begin{aligned} a^{\alpha} &= 22.38 \text{ g.} \\ a^{\beta} &= 26.87 \text{ g.} \end{aligned}$$

The mechanism of β -proton coupling probably involves hyperconjugation as well as spin polarization. The three β hydrogen 1s orbitals may be combined to form three new orthogonal group orbitals shown in Fig. 1.10. One of the SP_x orbitals on the β carbon overlaps with ψ_1 (Fig. 1.10) while the other forms the C-C bond. The β -carbon's remaining P_y and P_z orbitals overlap with ψ_2 and ψ_3 respectively. The β carbon P_z orbital also overlaps with the P_z orbital on the α -carbon. Therefore, the odd electron may be thought of as occupying a molecular π orbital compounded of P_z orbitals on both carbon atoms and the group orbital ψ_3 . By this method the odd electron may penetrate directly into the hydrogen 1s orbitals giving the verified positive coupling.

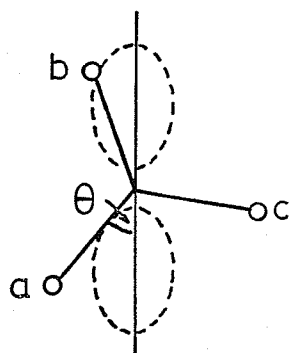
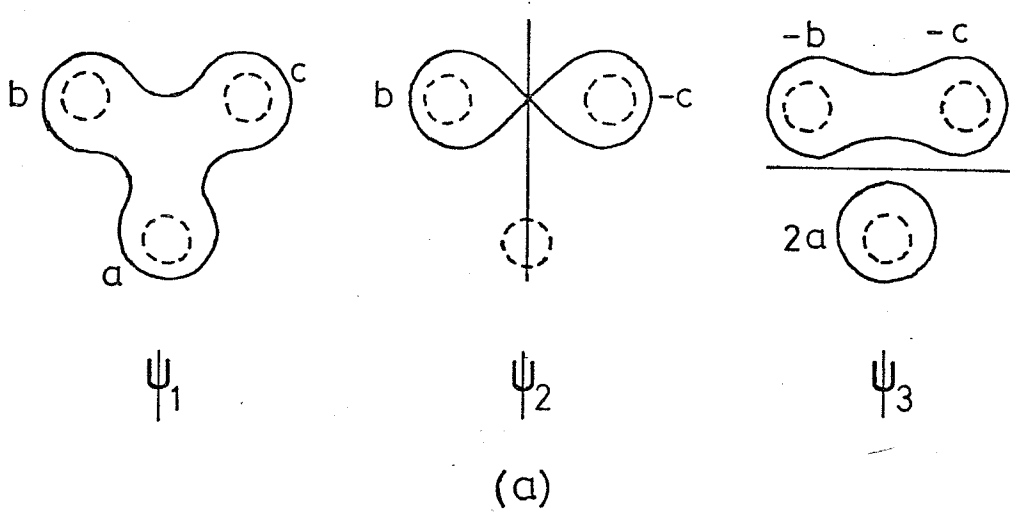
Normally the methyl group is free to rotate and an average isotropic splitting is observed. It is found experimentally that

$$a_{\beta}^H = B_0 + B_2 \cos^2 \theta \quad (1-70)$$

where θ is the angle of twist between the α -carbon's $2P_z$ orbital and the plane containing the β -proton C-H bond [See Fig. 1.10(b)]. From experiment, $B_0 \sim 4\text{g.}$ and $B_2 \sim 50\text{g.}$ B_0 may be interpreted as a spin polarization term which is present even when the β -proton is in the

Fig. 1.10

Hyperconjugation in the Ethyl Radical. (a) Group Orbitals for the β -Hydrogen Atoms. (b) Rotation about the C-C Bond.



(b)

nodal plane of the carbon $2P_z$ orbital and incapable of interacting by a hyperconjugative mechanism. The $B_2 \cos^2\theta$ may be due to hyperconjugation which averages to $\frac{B_2}{2}$ with rapid rotation.

$$a_{\beta}^H = B_0 + 1/2 B_2 \quad (1-71)$$

F. RELAXATION PROCESSES AND LINE WIDTHS

1. General Introduction

Line broadening may be caused by

(a) The interaction of each electronic dipole with all other electronic and nuclear dipoles in the sample and with the surrounding diamagnetic molecules (spin-spin and spin-lattice interactions).

(b) The effect of vibrational, rotational and translational motion of these species and of electron exchange between them (motional and exchange modulation).

(c) Chemical reactions of the paramagnetic species.

(d) Unresolved nuclear hyperfine structure.

(e) Inhomogeneous magnetic fields (H_0).

(f) Variations in the frequency of H_1 .

Interactions (a) \rightarrow (c) increase the line width by decreasing the lifetime of the spin state undergoing the observed transition, or by changing the magnetic field experienced by the spin at the instant of the transition.

Let us assume that we have N spins of which N_+ are in the upper state and N_- are in the lower state. Let us now apply a time-dependent perturbation $V(t)$ to the system in order to stimulate transitions from the - to the + state.

$$P_{-+} = \frac{2\pi}{\hbar} |\langle + | V | - \rangle|^2 \delta(E_+ - E_- - h\nu) \quad (1-72)$$

where P_{-+} is the transition probability in transitions per sec. The perturbation V must couple states $+$ and $-$ in order to stimulate a transition. The δ function imposes the condition that $P_{-+} = 0$ unless $h\nu = E_+ - E_-$. The δ function represents a line shape of perfect sharpness and infinite height with total area of unity.

$$\begin{aligned} \delta(E_+ - E_- - h\nu) &= \infty \text{ if } h\nu = E_+ - E_- \\ &= 0 \text{ if } h\nu \neq E_+ - E_- \end{aligned}$$

$V(t)$ is the applied microwave field. It may be shown that

$$|\langle + | V | - \rangle|^2 = |\langle - | V | + \rangle|^2 \quad (1-73)$$

which means that the probability of transitions upward equals the probability of transitions downward. If we let $n = N_+ - N_-$ the following equations may be derived

$$\frac{dn}{dt} = -2Pn \quad (1-74)$$

$$n = n(0)e^{-2P_{+-}t} \quad (1-75)$$

where $n(0)$ is the population difference at $t = 0$. It can be shown that

$$\frac{dE}{dt} = n P_{+-} \Delta E \quad (1-76)$$

where $\frac{dE}{dt}$ is the rate of absorption of energy from the radiation field H_1 . Equations (1-74) and (1-75) mean that on applying H_1 an exponential decay of the population difference results and eventually the upper and lower levels will be equally populated (saturation). Equation (1-76) implies that when saturation occurs the rate of absorption of energy goes to zero. This argument leads to the conclusion that the spin systems cannot be isolated but must interact with environmental

degrees of freedom (Lattice) in such a way as to discharge excess energy and therefore maintain an excess spin population in the lower state. [Spin-Lattice or Longitudinal Relaxation $-T_1$]. This environmental interaction makes the probabilities of spontaneous spin transitions up and down not equal. It may be shown that

$$\frac{dn}{dt} = - \frac{(n - n_0)}{T_1(\text{sec.})} \quad (1-77)$$

where n_0 is the population difference at thermal equilibrium, and T_1 is a measure of the time taken for the spin system to approach thermal equilibrium. Combining (1-74) and (1-77)

$$\frac{dn}{dt} = - 2Pn - \frac{(n - n_0)}{T_1} \quad (1-78)$$

At equilibrium ($\frac{dn}{dt} = 0$) in the presence of a microwave field

$$n = \frac{n_0}{(1+2PT_1)} \quad (1-79)$$

Substituting (1-79) into (1-76)

$$\frac{dE}{dt} = nP\Delta E = n_0 \Delta E \frac{P}{(1 + 2 PT_1)} \quad (1-80)$$

Equation (1-80) shows that if $2PT_1 \ll 1$ saturation may be avoided. Since P is proportional to the square of the amplitude of H_1 , one normally operates at low power values to avoid saturation.

Because of T_1 the spin states have a finite lifetime, and the line width due to T_1 will be of the order of $\frac{1}{T_1}$. Line broadening may also be caused by processes which vary the relative energies of the spin levels. These processes are called spin-spin (or transverse) relaxation processes and are characterized by the symbol T_2 .

T_1 and T_2 are interrelated because interactions that lead to finite lifetimes may also modulate energy levels.

$$\text{TOTAL LINE WIDTH} = \frac{1}{2T_1} + \frac{1}{T_2} = \frac{1}{T_2} \quad (1-81)$$

where $\frac{1}{T_2}$ is the energy fluctuation term.

Since E.S.R. absorptions have finite linewidths and line shapes the probability of stimulated transitions (1-72) may be rewritten in terms of line shape functions $g(\nu)$ or $g(\omega) = \frac{g(\nu)}{2\pi}$.

$$P_{-+} = \frac{2\pi}{\hbar} | \langle + | V | - \rangle |^2 g(\omega) \quad (1-82)$$

$$\text{where } g(\omega) = \frac{T_2}{\pi} \frac{1}{1 + T_2^2 (\omega - \omega_0)^2} \quad (1-83)$$

for an unsaturated Lorentzian line shape and where

$$g(\omega) = \frac{T_2}{\sqrt{2\pi}} e^{-\frac{1}{2} T_2^2 (\omega - \omega_0)^2} \quad (1-84)$$

for an unsaturated Gaussian line shape.

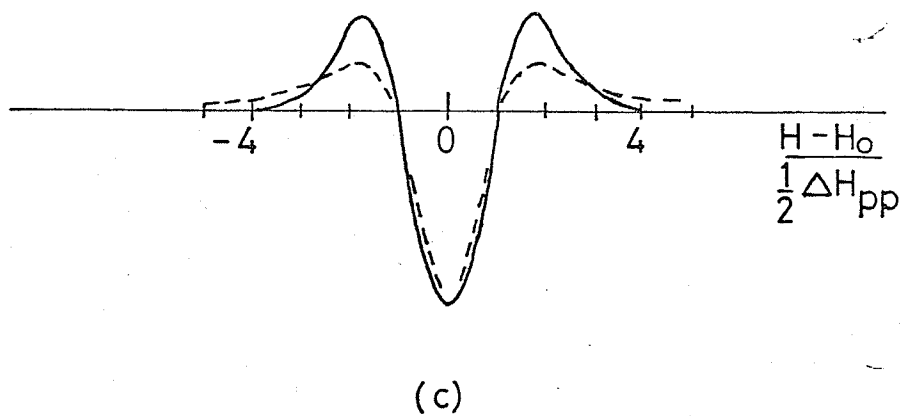
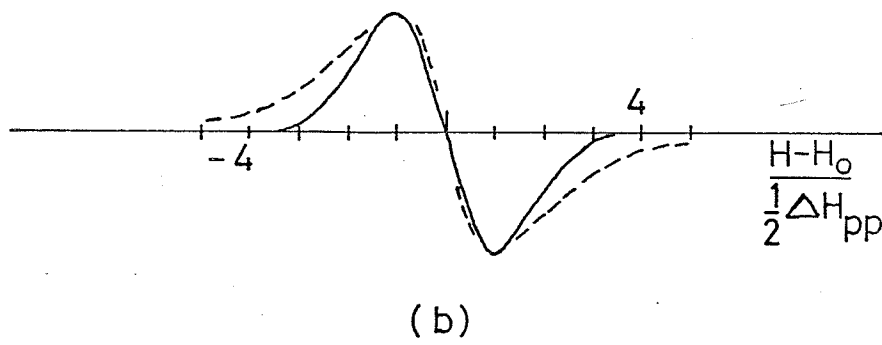
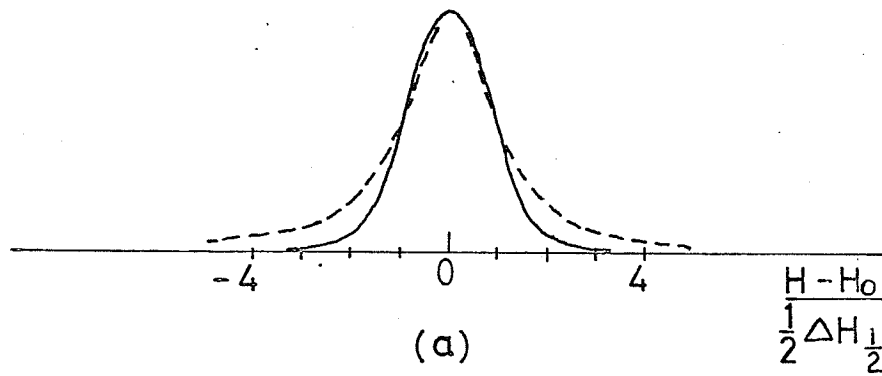
E.S.R. equipment is designed to display the first derivatives $\left(\frac{dg}{d\omega}\right)$ of these absorption line shapes. The differences between the Lorentzian and Gaussian line shapes are seen in Fig. 1.11. More detailed descriptions of these line shapes have been reported.^{9,10}

2. Origin of Magnetic Relaxation

It may be summarized that T_1 determines the degree of saturation and T_2 determines the unsaturated line width. Both T_1 and T_2 are caused by time-dependent magnetic or electric fields at the electron. These fields are generated by random thermal motion present in all matter. Radicals with an anisotropic g tensor experience fluctuating Zeeman interactions with the external magnetic field, which leads to relaxation. For a successful relaxation mechanism there must be a time-dependent interaction acting directly on the spins.

Fig. 1.11

- (a) Lorentzian (dashed) and Gaussian (solid) absorption curves with the same half amplitude linewidth.
- (b) Lorentzian (dashed) and Gaussian (solid) absorption first derivative curves with the same peak-to-peak linewidth.
- (c) Lorentzian (dashed) and Gaussian (solid) absorption second derivative curves with the same peak-to-peak linewidth.



Interactions which change sign at a rate faster than the resonance frequency have little effect. This eliminates electronic motions and molecular vibrations as important mechanisms. Any interaction in the H_1 plane causing transitions between spin states and fluctuating at the resonance frequency leads to powerful spin-lattice relaxation and line broadening. Random forces modulating the energy levels (in H_0 direction) at low frequencies without causing transitions affect T_2 (line width) but not T_1 . Since the time scale of magnetic resonance is slow, rotation and diffusion motions are good sources of relaxation in liquids as are lattice vibrations in solids, collisions in gases, rotational or torsional motions within molecules, and some chemical exchange processes.

3. Line Widths in Liquids

When determining relaxation times and line widths in solution one must consider the Brownian motion of the solute and solvent molecules. How much local order is maintained during the random fluctuations in the liquid and how does the frequency of these environmental changes compare with the frequencies corresponding to the various interaction energies of the system? If the rate of tumbling of radicals in solution is fast enough only the isotropic parts of g and a_N will remain and the line width will be small. The averaging, in general, is not complete and line widths are found to vary with temperature, viscosity, and concentration.

4. Spin Relaxation of Radicals in Solution

For a radical with an electron spin of $1/2$ in solution there are two important anisotropic magnetic interactions within the molecule.

One is the anisotropy of the g tensor (due to spin-orbit interactions) while the other is the dipolar hyperfine coupling with magnetic nuclei. Both these weak anisotropies fluctuate due to tumbling and do not produce much broadening. Electron spin-rotational couplings sometimes contribute to spin relaxation. The isotropic hyperfine interaction does not produce any relaxation unless the coupling constant varies with time as a result of molecular motion. For high concentrations of paramagnetic species, adjacent electron spins interact and lines are broadened. The interaction between these electron spins takes two main forms of which one is a direct dipolar coupling between the electron spin magnetic moments and the other is exchange forces of the type $hJ S_1 \cdot S_2$ between radicals whose electronic wave functions overlap. Paramagnetic ions with $S > 1/2$ normally have large zero-field splittings which lead to broad E.S.R. spectra.

Let us consider a rapidly tumbling (about 10^{11} sec^{-1}) free radical of spin $1/2$ with an anisotropic g -tensor.

$$\mathcal{H}_0 = g\beta H_0 S_Z + \beta \underline{H}_0 \cdot \underline{g}^1(t) \cdot \underline{S} \quad (1-85)$$

where the second term which includes the anisotropic part of the g -tensor is time dependent due to Brownian motions. The perturbation V responsible for relaxation is

$$V(t) = \beta H_0 (g_{ZX}^1 S_X + g_{Zy}^1 S_y + g_{ZZ}^1 S_Z) \quad (1-86)$$

It may be shown that¹¹

$$\overline{(g_{ZZ}^1)^2} = \frac{2}{15} (g^1 : g^1) \quad \text{and} \quad \overline{(g_{ZX}^1)^2} = \overline{(g_{Zy}^1)^2} = \frac{1}{10} (g^1 : g^1)$$

where $(g^1 : g^1)$ is the inner product of the tensor with itself.

Substitution of these values into general perturbation formula for T_1 and T_2 yields

$$\frac{1}{T_1} = \frac{(g^1: g^1) \beta^2 H_o^2}{60 \hbar^2} \left(\frac{12 \tau_c}{1 + \omega_o^2 \tau_o^2} \right) \quad (1-87)$$

$$\left(\frac{1}{T_2} \right) = \frac{(g^1: g^1) \beta^2 H_o^2}{60 \hbar^2} \left(\varepsilon \tau_c + \frac{6 \tau_c}{1 + \omega_o^2 \tau_c^2} \right) \quad (1-88)$$

where τ_c is the correlation time which is the time taken for a typical random fluctuation in solution to die away or τ_c may be defined as the time during which a particular molecular orientation persists. $\frac{1}{\tau_c}$ is approximately equal to the tumbling frequency. For fast tumbling $\frac{T_1}{T_2} = 7/6$ and the effects of g-tensor anisotropy become smaller with increased tumbling rates.

Let us now examine the effects on relaxation time by anisotropic hyperfine interactions

$$\mathcal{H}_o = g \beta H_o S_z + a I_z S_z \quad (1-89)$$

where the time dependent terms are:

$$V(t) = \beta H_o \cdot \underline{g^1}(t) \cdot \underline{S} + \underline{S} \cdot \underline{T^1}(t) \cdot \underline{I} \quad (1-90)$$

$T^1(t)$ is the tensor responsible for the anisotropic hyperfine interactions. The nuclear Zeeman levels as well as the off-diagonal elements of $\underline{I} \cdot \underline{S}$ are being ignored. The electron spin sees fluctuating random local fields from the variations of $\underline{g^1}$ and $\underline{T^1}$ which are correlated since both tensors vary accordingly with the same molecular motions. The line width, therefore, depends on the relative orientations of the g and hyperfine tensors. Let us define three time-dependent operators.

$$\begin{aligned} f_x(t) &= (\beta H_o g_{ZX}^1 + m_I T_{ZX}^1) \\ f_y(t) &= (\beta H_o g_{ZY}^1 + m_I T_{ZY}^1) \\ f_z(t) &= (\beta H_o g_{ZZ}^1 + m_I T_{ZZ}^1) \end{aligned} \quad (1-91)$$

The relaxation rate depends on the mean squared values of f_x , f_y and f_z . Therefore one contribution to $\frac{1}{T_2}$ is:

$$|f_z(t)|^2 = \beta^2 H_o^2 (\overline{g_{ZZ}^2}) + 2\beta H_o (\overline{g_{ZZ}^1 T_{ZZ}^1}) m_I + \overline{(T_{ZZ}^1)^2} m_I^2 \quad (1-92)$$

The combined effects lead to

$$\frac{1}{T_2} = a + B m_I + C m_I^2 \quad (1-93)$$

where $B m_I$ causes asymmetric broadening (outer lines being broader on one side of the spectrum than the other) and $C m_I^2$ makes the outer lines broader than the inner lines. For fast tumbling

$$B = \frac{7\beta H_o \tau_c}{15h^2} (g^1 : T^1) \quad (1-94)$$

$$C = \frac{\tau_c}{15h^2} (T^1 : T^1) \quad (1-95)$$

As the concentration of electron spins becomes larger, radical-radical collisions occur more frequently, and there is more chance for the electronic wave functions to overlap. Interchange of spins between two radicals may cause broadening or narrowing of the spectrum depending on the circumstances. "Exchange narrowing" occurs due to the averaging out of electron dipole-dipole forces which would normally give a broad line. The rate of exchange depends on solution viscosity, radical concentration and temperature. Slow exchange rates normally lead to line broadening. When the exchange rate equals the hyperfine splitting, the hyperfine structure will collapse. At higher exchange rates one sharp line will remain.

2. SILICA AND POROUS VYCOR GLASS SURFACES

A. Introduction.

The free radicals studied by E.S.R. were stabilized on Corning #7930 porous Vycor glass. In the following discussion an attempt will be made to illustrate the chemical entities which are believed to exist on the surface of silica and porous Vycor glass. Adsorption studies will be described in order to illustrate the sites on which molecules adsorb. Much of the discussion will be concerned with studies on high surface area silicas because there are many correspondences between these surfaces and the surface of porous Vycor glass. Much of the information available about surface groups has come as the result of infrared studies although nuclear magnetic resonance and laser raman studies have also contributed. The differences between pure silica and porous Vycor glass surfaces will be pointed out as the discussion progresses. As the discussion of E.S.R. was based on the book by Carrington and McLachlan¹, this discussion will be based on two recent books on the application of infrared spectroscopy to surface chemistry.^{12,13}

A surface may be defined as a "two-dimensional" plane separating two phases. It is obvious that the term "two-dimensional" does not exactly apply since there is no sharply defined plane at which one goes from surface to bulk properties. Surfaces do have a third-dimension which may only be a few molecular layers thick. Surface atoms are subject to asymmetric force fields and are therefore more chemically reactive than bulk atoms. This instability at a surface may be

removed by the rearrangement of surface atoms so that they occupy positions which are displaced from their regular crystallographic positions or by the phenomenon known as adsorption. In this process molecules of a foreign substance distribute themselves on the surface in such a way as to minimize asymmetric force fields. Adsorption processes are nearly always exothermic. Physical adsorption is a process in which the bond between the adsorbent and the adsorbate is of the van der Waals type (2-5 kcal/mole). Chemical adsorption occurs when the adsorbate undergoes a strong chemical interaction with the surface (15-20 kcal/mole). This process may be dissociative, non dissociative, or reactive in nature. Physically adsorbed species may be removed from the surface without decomposition by evacuation at room temperature or by heating to 120°C. This is a possible working definition of physical adsorption. Physical adsorption may also be defined as an adsorption which leads to perturbation of the electronic or stereochemical states of the molecule but otherwise leaves the molecule and its entire electron complement intact while chemisorption produces a new species by fragmentation of the molecule or of its electron complement.

At this point a few simple aspects of infrared spectroscopy will be mentioned. The frequency of the simple harmonic vibration is given by:

$$\nu = \frac{1}{2\pi} \left(\frac{k}{\mu_m} \right)^{1/2} \quad (1-96)$$

where μ_m is the reduced mass of the system and k is the force constant $\left(-\frac{F}{r} \right)$ characteristic of the bond strength. Since $\lambda\nu = c$

equation (1-96) becomes

$$\frac{1}{\lambda} = \frac{1}{2\pi C} \left(\frac{k}{\mu_m} \right)^{1/2} = \bar{\nu} \quad (1-97)$$

The chemical bond is equated with the "spring" concept of the harmonic oscillator. The strength of the spring is considered analogous to the strength of the chemical bond, and thus a determination of k gives a measure of the strength of a chemical bond. If a particular peak shifts to lower wave numbers ($\bar{\nu}$), the bond responsible for the peak is said to have been weakened (smaller force constant). Shifts to higher wave numbers indicates bond strengthening. It also follows that if the force constant remains the same as in isotopic substitution, the frequency of the vibration is dependent upon the mass of the atoms.

$$\frac{\bar{\nu}_1}{\bar{\nu}_2} = \left(\frac{\mu_2}{\mu_1} \right)^{1/2} \quad (1-98)$$

For a free hydroxyl group on the surface of silica $\bar{\nu}_1 = 3750 \text{ cm}^{-1}$. Substitution of this hydroxyl group by deuterium shifts the hydroxyl frequency to 2750 cm^{-1} . Equation (1-98) would predict the OD peak to occur at 2740 cm^{-1} . The measured ratio of $\frac{\bar{\nu}_{\text{OH}}}{\bar{\nu}_{\text{OD}}}$ is 1.37. From equation (1-98) it also may be shown that

$$\frac{\bar{\nu}_{\text{SiO}^{16}\text{H}}}{\bar{\nu}_{\text{SiO}^{18}\text{H}}} = 1.003 \text{ and } \frac{\bar{\nu}_{\text{BO}^{16}\text{H}}}{\bar{\nu}_{\text{BO}^{18}\text{H}}} = 1.006.$$

When a molecule is adsorbed on a surface, its rotational movements will be restricted. If chemisorption occurs the vibrational modes will also be affected. To illustrate this let us look at CO adsorbed on a metal surface. The infrared spectra of CO consists of one band due to a single vibrational mode.

On adsorption to a surface, three processes may occur: 1) physical adsorption, 2) chemisorption, 3) dissociative chemisorption or reaction. In the first case the infrared spectra resembles that of the gas with one band at 2140 cm^{-1} . In the second case, the symmetry of the CO species is changed to that of an x-y-z molecule (x-C-O) where x is considered to have a large mass. There are three possible vibrational modes and therefore three bands would be predicted. Two of these have been observed and the other is inaccessible experimentally. If oxygen is present on the surface a new species with the structure x-y-z₂ is formed (x-C⁰₂). Carbon monoxide has been oxidized to a "-C₀" type of molecule which has two bands (symmetric and asymmetric C-O stretches). On adsorption many other occurrences are possible. For instance, an infrared inactive mode may be seen on adsorption due to loss of symmetry in the molecule.

The following discussion on sample preparation for surface infrared studies will be restricted to a few important aspects. Further information about this as well as other technical aspects can be found in the recent books on the subject^{12,13}. One major disadvantage in using infrared spectrometers to study surface species and adsorbed species is the fact that most silica adsorbents do not transmit over a large enough frequency range. Many people have used pressed discs which alters, in some cases, the surface structure. High pressure produces localized increased temperatures which causes annealing. McDonald¹⁴ noticed that on compressing silica particles at $100,000 \text{ lb/in}^2$ the number of free hydroxyls decreased and the

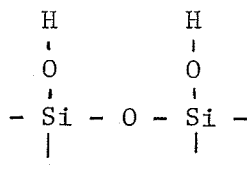
number of hydrogen bonded hydroxyls increased. Hambleton, et al,¹⁵ noticed that after using the pressing process some hydroxyl groups were made inaccessible to deuterium exchange with D₂O. An increase in pressure resulted in a smaller number of hydroxyls available for deuterium exchange. Porous glass, which has reasonable transmission characteristics, lacks homogeneity of surface properties. To gain homogeneity of surface properties and avoid pressure effects, Peri¹⁶ devised a technique for producing a series of silica, alumina, and silica-alumina aerogels in a "glassy" form (transparent plates). Another interesting aspect which must be considered when studying weakly adsorbed molecules is that the infrared radiation absorbed by the sample causes heating which in turn causes desorption. This effect has been studied by McDonald¹⁴ for water adsorbed on silica. Cant and Little¹⁷ estimated a sample temperature increase of 20°C when studying the adsorption isotherms of ammonia on porous silica glass.

B. Silica Surfaces

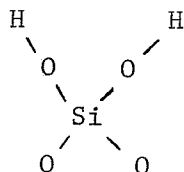
1. Hydration - Dehydration Studies

It is likely that amorphous silica gels and glasses possess the same structure as the crystalline forms of silica. The noncrystalline materials will be characterized by a random packing of the (SiO₄) tetrahedra which gives rise to a nonperiodic structure. These amorphous silicas have surface areas ranging from 100 m²/gm to 500 m²/gm. They are manufactured by: 1) precipitation from aqueous sodium silicate solutions and by 2) high-temperature oxidation or hydrolysis of silicon tetrachloride. Type (2) silicas

are characterized by a rather sharp band at 3747 cm^{-1} and a very broad band centered at about 3500 cm^{-1} . Type (1) silicas exhibit only a very broad asymmetric absorption between 3700 and 3000 cm^{-1} . After degassing type (2) for two hours at 27°C two new peaks at 3520 cm^{-1} and 3660 cm^{-1} appear in addition to the band at 3747 cm^{-1} . Similar treatment of type (1) leaves a peak at 3700 cm^{-1} , a broad band at 3500 cm^{-1} and a shoulder at 3740 cm^{-1} . Heating types (1) and (2) at 500°C in vacuum for 1/2 hour leads to a disappearance of the peak at 3500 cm^{-1} in both cases. This treatment leaves the 3747 cm^{-1} peak very sharp for type (2) but the same peak for type (1) is broader particularly on the low-frequency side. Further heating of types (1) and (2) at 940°C for 8 hours in vacuum results in identical spectra consisting of one sharp symmetric peak at 3748 cm^{-1} . These results were obtained by McDonald¹⁴ in 1958. Previous to 1958 Russian workers had examined the dehydration of silicas and had assigned the 3748 cm^{-1} absorption to the fundamental stretching vibration of a free or isolated hydroxyl group attached to a silicon atom (i.e. hydroxyl groups separated by more than 3 \AA). Vicinal hydroxyl groups are those which are adjacent on the surface.



Geminal groups are attached to the same silicon atom.



Triplet hydroxyl groups have been postulated as existing on the surface as well.¹⁸ The strong and broad absorption band at 3500 cm^{-1} is attributed to molecular water physically adsorbed. This molecular water may be removed at room temperature leaving a peak at 3400 cm^{-1} which is also assigned to molecular water which is more strongly attached to the surface. Rapid replacement of H by D (using D_2O) confirmed the above assignments ($\frac{\nu_{\text{OH}}}{\nu_{\text{OD}}} = 1.35$) as well as suggesting that all hydroxyls were substituted and therefore are surface groups.¹⁹ Other workers^{20,21} found that complete deuteration of the hydroxyl groups contributing to a broad absorption at 3650 cm^{-1} was not possible and therefore postulated the existence of some internal inaccessible hydroxyl groups. Deuteration of surface silanol groups using D_2O is very efficient at temperatures between 100°C and 200°C .

On the rehydration process, Young²² observed that the amount of water physically adsorbed on the silica was directly related to the number of hydroxyl groups existing on the surface, and therefore concluded that the adsorption of water occurred on these groups.

It has been concluded in many studies that water adsorption on a silica surface occurs preferentially on adjacent (or vicinal) hydroxyl groups although it has been shown, by looking at the overtone region, that single hydroxyl groups will interact with adsorbed water. Heating a fully hydroxylated silica gel to 400°C causes a fundamental change in the nature of the surface. Summing up:

1. Physically adsorbed water is completely removed with pumping at room temperature up to 150°C.
2. Surface silanol groups (hydrogen bonded) start to condense and eliminate water at about 170°C.
3. The dehydration is completely reversible up to approximately 400°C.
4. Above 400°C the dehydration is not reversible and the amount of chemisorption is an inverse function of the dehydration temperature. This is due to the elimination of vicinal hydroxyl groups.
5. Above 850°C no chemisorption of water can occur and the surface is hydrophobic since only isolated hydroxyl groups remain.
6. Sintering begins at about 900°C and the loss in surface area is linearly related to the time of heat treatment. The sintering process is one of viscous flow. Impurities lower the sintering temperatures by increasing the fluidity.

It is believed that the surface of silicas, prepared at room temperature in gelatinous forms, has a structure in which every surface silicon atom terminates in an hydroxyl group and

some silicon atoms terminate with two hydroxyl groups (geminal). Figure 1.12 shows the most widely believed dehydration and hydration reactions. When the silica has been completely dehydrated, the reverse of reaction (a) [Figure 1.12] is very slow. The 3520 cm^{-1} band seen by McDonald¹⁴ and mentioned before has been assigned to single hydroxyl groups that are perturbed by strong hydrogen bonding to water molecules. The band at 3660 cm^{-1} noticed by McDonald¹⁴ has been assigned to hydrogen bonded silanol groups. The ratio of free to hydrogen bonded surface hydroxyls depends on the origin of the sample and the temperature and time of dehydration.

Peri¹⁸ obtained evidence for the existence of weak P and R branches for both surface OH and surface OD groups. If the surface hydroxyl group is linear only a Q branch should appear but the discovery of the P and R branches shows that the Si-OH group is non-linear. From the separations of the P and R branches (200 and 140 cm^{-1} , respectively), the Si-OH bond angle has been calculated to be 113° .

2. Adsorbent Perturbation on Adsorption

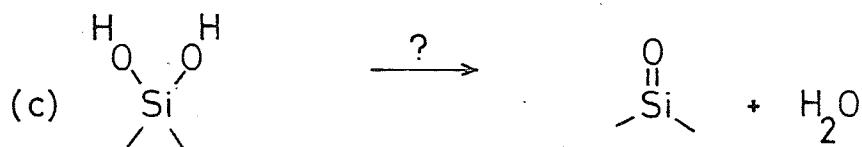
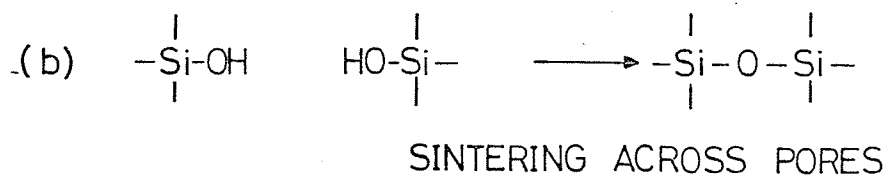
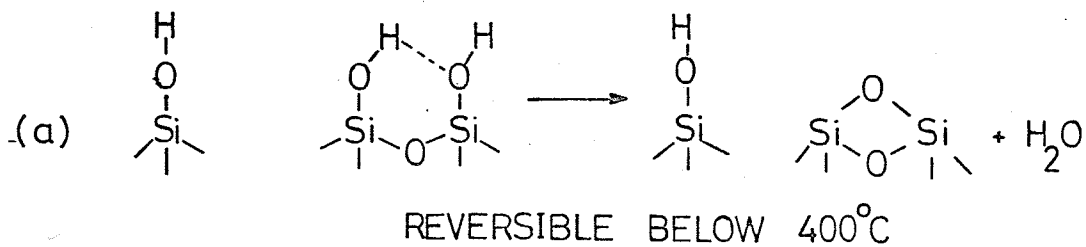
McDonald²³ has shown that on adsorption of argon, krypton, xenon, nitrogen, oxygen, methane, and perfluoromethane at -190°C and -170°C the free hydroxyl peak at 3749 cm^{-1} shifted to lower frequencies. The same effect was seen on adsorbing water, methanol, benzene and cyclohexane at 30°C .¹⁴ This frequency shift is proof positive that the 3749 cm^{-1} absorption is due to a surface group. The shift in the 3749 cm^{-1} absorption is a function of the partial pressure of the adsorbate (surface coverage) and of the temperature

Fig. 1.12

Hydration and Dehydration of a Silica Surface

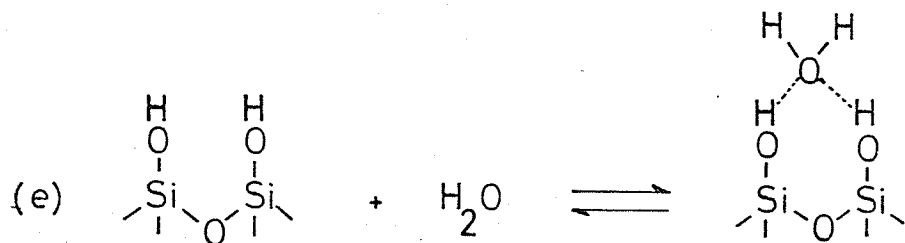
DEHYDRATION

54.



HYDRATION

(d) REVERSE OF a, b, and c



at which the gas is adsorbed. On adsorption the 3749 cm^{-1} absorption peak suffers not only a frequency shift but also an increase in line width accompanied by an overall gain in intensity. At low pressures some OH groups remain unaffected but at increasingly higher pressures complete disappearance of the 3749 cm^{-1} band occurs indicating that all the free hydroxyls are interacting with the adsorbed species. By inspecting the shifts as a function of pressure it may be concluded that nitrogen adsorbs preferentially on the surface free hydroxyls while oxygen and argon are not preferentially adsorbed on the free hydroxyl group. Frohnsdorff and Kingston²⁴ have attempted to correlate the difference in frequency shifts of the 3749 cm^{-1} band for nitrogen and oxygen in terms of differences in their quadrupole moments. Basila²⁵ decided that, since the physical adsorption must be of the hydrogen bonding variety, the strength of the interaction of the surface hydroxyl groups ($\Delta\bar{\nu}$) should be a function of the ionization potential of the donor molecules. Basila showed that, for monolayer coverages of substituted benzenes, $\Delta\bar{\nu}_{\text{OH}}$ (cm^{-1}) increased with decreasing ionization potential (ev) in a smooth fashion. It has been shown that for nonpolar molecules such as carbon tetrachloride and hexane the heat of adsorption is essentially independent of the degree of hydroxylation of the surface whereas the heat of adsorption of a more polarizable molecule such as benzene was shown to be dependent on surface hydroxyl concentration. Polar molecules also cause much larger frequency shifts ($\Delta\bar{\nu}_{\text{OH}}$) than non-polar ones. Therefore frequency shifts

should be and are a linear function of the heat of physical adsorption of the adsorbate on the free hydroxyl group. Therefore the reaction between the hydroxyl groups and the adsorbate is one of charge transfer (hydrogen bonding). Basila²⁵ was able to show, using an incompletely dehydroxylated silica sample, that diethylamine preferentially adsorbs to the isolated or free hydroxyl group ($\Delta\nu_{\text{OH}}=990 \text{ cm}^{-1}$). This behaviour is typical of lone-pair donor adsorbates.

3. Adsorbate Perturbations on Adsorption

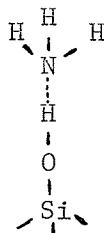
The infrared spectrum of benzene adsorbed on a silica surface is much like the liquid spectra and thus must be only physically adsorbed. Some infrared bands that are typical of the gas-phase spectra appear with multilayer coverages. At monolayer coverages one band that is present in the liquid spectrum but absent in the gas spectrum appears for the adsorbed species. Therefore, the properties of adsorbed benzene lie somewhere in between the liquid and gaseous states. It has been shown that the specific interaction of the surface proton is with the aromatic nucleus by studying those vibrations, the out-of-plane C-H deformation and the C-C stretch, which are associated with the aromaticity of the compound, as a function of surface coverage and hydroxyl group concentrations. The greatest perturbations in the intensity of the two above mentioned modes occur at low coverage and with samples that have high concentrations of surface hydroxyl groups. Woessner²⁶ has looked at benzene adsorbed on silica gel outgassed at 210°C using nuclear spin relaxation phenomena. The results indicate that the

benzene molecules are situated over surface OH groups and rotating rapidly about a molecular axis, likely the hexagonal axis, even at 77°K. There is a broad distribution of temperature dependent correlation times for this motion.

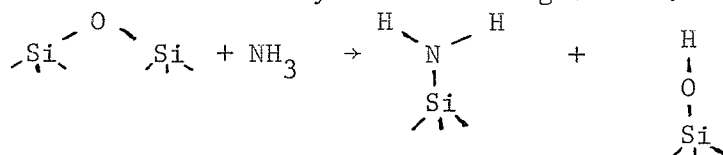
It has now been demonstrated that both aromatic and lone-pair electron compounds interact specifically with the free hydroxyls on the surface while water (with two lone pairs) interacts predominately with hydrogen bonded vicinal hydroxyl groups.^{12,13} Since molecular rotation is restricted upon adsorption, it might be expected that, in the case of molecules that can exist in isomeric forms, one of the isomers would be either more strongly adsorbed or more restricted in its rotations on adsorption on a surface. The relative proportions of the isomeric species existing on a surface might therefore be considerably different from those existing in solution. This effect has been observed for dichloroethane (rotational isomers) and acetylacetone (keto-enol tautomerism).²⁷ On adsorption the ratio $\left(\frac{\text{keto}}{\text{enol}}\right)$ for acetylacetone is much larger than in solution. The ratio (cis/trans) for dichloroethane is larger in the adsorbed state than in solution.

The infrared spectrum of ammonia adsorbed on silica gel has been studied often.^{18,28,29} The adsorption occurs at room temperature via the interaction of the lone pair on the nitrogen atom with, primarily, the free hydroxyls on the surface. Some interaction has been observed between ammonia and the adjacent hydroxyl groups (at 3666 cm^{-1}). It has been observed that $\Delta\bar{\nu}_{\text{OH}}$ is about 900 cm^{-1} to lower frequencies. The physically adsorbed

species is thought to be



Peri¹⁸ reports that a small amount of chemisorption occurs as well at room temperature on a very dry silica surface. This chemisorption is believed to occur by the following scheme.



The maximum number of these strained siloxane sites is 1.4 per 100 Å².

It might be worth mentioning that Hendra and Loader³⁰ have looked at the laser raman spectra of physically adsorbed species on silica gel outgassed at 150°C. They looked at adsorbed CCl₄, Br₂, CS₂ and trans-dichloroethylene over the spectral range 150 to 3400 cm⁻¹ which is a much larger range than is available in infrared studies. The spectra indicated very weak interactions with the surface for all four compounds.

C. ADSORPTION STUDIES ON POROUS GLASS

1. Introduction

Porous glasses scatter much less light than either powders or pressed discs. These glasses may be ground and polished or fabricated into sheets as thin as 0.1 mm. The porous glass being

used by research workers in the Western Hemisphere is normally supplied by Corning (Code Number 7930-porous VYCOR glass). Briefly, this glass is produced as follows. A glass in the sodium borosilicate system is melted and fabricated at quite low temperatures. After fabrication, this glass is subjected to heat treatment which causes it to separate into a boron-rich phase and a silica-rich phase. The boron-rich phase is leached out by weak acid. The final product is a glass that contains 96% silica and yet has not been subjected to the high temperatures that are necessary to melt and form silica products. The material that is left after leaching and before consolidation is known as porous glass. The bulk analysis shows 96% SiO_2 , 3% B_2O_3 , 1% Na_2O , Al_2O_3 , etc. The surface area is usually about $200 \text{ m}^2/\text{gm} \pm 100 \text{ m}^2/\text{gm}$. with an average pore diameter of 40 \AA . The porous glass surface has been shown to have some Lewis acid sites which silica gels do not. (See Part 2 Section (C-3) of this chapter). The B/Si ratio on the surface has been shown, by quantitative ammonia adsorption, to be $1/3$ rather than $1/18$ as indicated by bulk analysis.³¹

2. Hydration - Dehydration Studies

Publications by Sidorov³², Cant and Little^{28,17} and Chapman and Hair²⁹ discuss the similarities and differences between porous glass and silica gel surfaces. The dehydration-hydration stages are exactly as those described for silicas with a few exceptions which will be mentioned. High temperature dehydration of porous Vycor glass leaves not only a sharp band at 3749 cm^{-1} attributable to free hydroxyls attached to silicon atoms but also a small sharp

band at 3700 cm^{-1} .³² Low and Ramasubramanian³³ have reported the presence of a band at 3703 cm^{-1} on all samples which have been dehydrated rigorously. From deuteration experiments and from boric acid impregnation of silica gels, they assigned this band to a free hydroxyl attached to a boron atom. It is believed by many workers that high temperature treatment leads to the diffusion of boron atoms to the surface resulting in a higher concentration of boron hydroxyl groups on the surface. This high surface concentration of boron atoms may also be a result of the leaching process. Low and Ramamurthy³⁴ after impregnation of highly degassed silica and porous glass samples with P_2O_5 , observed a sharp peak at 3665 cm^{-1} which they have assigned to a free POH group on the surface.

Exposure of a completely dehydrated porous glass sample to water vapor causes the reappearance of the band at 3665 cm^{-1} which implies that the first step in rehydration is the reformation of adjacent surface hydroxyl groups. The simultaneous appearance of the 3450 cm^{-1} band shows the presence of physically adsorbed molecular water. These aspects of rehydration are the same as those reported for silica surfaces.

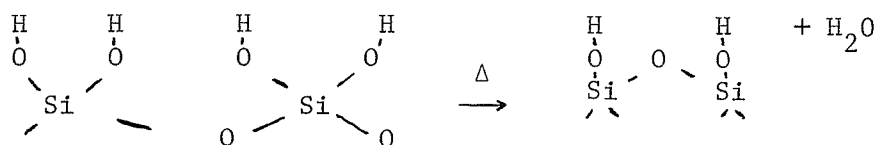
A recent study of the dehydration of porous glass shows:³⁵

1. physically adsorbed water is completely removed by room temperature evacuation
2. significant decreases in surface area occurred only after heat treatment above 500°C
3. fully hydroxylated surfaces exist below 600°C
4. above 600°C free hydroxyls begin to appear

5. dehydration at room temperature to 200°C removed more tightly bound species (not physically adsorbed water)

6. degassing at 300°C left much of the surface covered with geminal hydroxyl groups.

7. degassing above 300°C may go by the mechanism



8. above 600°C boron migrates to the surface.

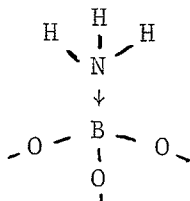
Further work by Ramasubramanian and Low³⁶ on the role of surface boron as the adsorption center for the sorption of water has yielded much information. Water sorption on well dehydroxylated samples showed that the main interaction is with the 3703 cm⁻¹ band which increased in intensity and shifted to lower frequencies. The intensity increase of the free silanol band is much less pronounced than that of the BOH band. This shows that porous glass is not a substitute for silica. Water adsorption at low pressures causes a new band at 3600 cm⁻¹ which is ascribed to molecular water adsorbed on boron atoms. Their results indicate that the spectra of water adsorbed on fluorinated and untreated porous glass is the same. Therefore the same adsorption sites exist in both cases (not the silanol groups). The adsorption of water on well dehydroxylated porous glass occurs predominantly at surface boron atoms with the

formation of BOH and BOH₂ structures. The silica network is hydrophobic. There is a slight reaction of water at room temperature with the silica portion of the glass to form silanol groups which is different than for pure silica. Therefore the siloxane bridges on porous glass are more readily attacked than those of pure silica. The substitution of boron for silicon in the silica network of porous glass could create strained siloxane bridges in the vicinity of the surface boron which would react with water and/or the siloxane-water reaction may be enhanced due to the fact that the BOH groups are centers for water adsorption. Therefore the water would be held to an otherwise hydrophobic surface close to adjacent siloxane bridges. The reaction could then occur on migration of the adsorbed water. However, all boron in the glass is believed to be in three-fold coordination. Therefore, substitution induced strain would be minimal. Possibly small B₂O₃ aggregates, as islands, are formed on diffusion of boron to the surface. The water adsorption may occur on these islands and silanol formation may occur in the vicinity of these islands.

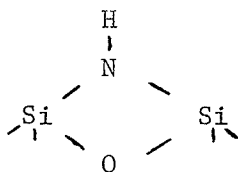
3. Surface Heterogeneity

The adsorption of ammonia on porous glass has been studied by Chapman and Hair²⁹ and by Cant and Little.¹⁷ Besides the physically adsorbed ammonia (attached to surface free hydroxyl groups) another species occurs which can only be removed by heating to 200°C. This species has been identified as being due to ammonia

molecules coordinately bonded to Lewis-acid-type sites on the glass surface.

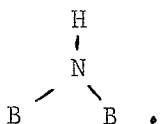


The ammonia molecule preferentially hydrogen bonds to the free hydroxyl groups on the porous glass surface. Folman and Yates,³⁷ prior to the two publications mentioned above, noticed that after adsorbing ammonia on porous glass, approximately 4 cc. of ammonia per gram could not be removed by evacuation at 150°C. No trace of this type of adsorption (Lewis-acid-type) has been found in adsorption studies using larger lone-pair molecules. At higher temperatures ammonia reacts with the surface hydroxyl groups of porous glass to produce a single N-H infrared band at 3373 cm⁻¹ attributable to the structure.



A recent infrared study³⁸ on the reaction of ammonia with high temperature dehydroxylated porous glass has revealed the existence of the expected SiOH...NH₃ and B-OH...NH₃ species.

Cant and Little²⁹ did show that the ammonia protons exchanged rapidly with surface OD groups. This work³⁸ showed that B-OD groups are more reactive to exchange with ammonia than the SiOD groups are. Low, et al,³⁸ also noticed infrared bands ascribable to the $\equiv\text{B}:\text{NH}_3$ group. This complex may be a precursor of dissociation and a more tightly bound species. Infrared bands of the $=\text{B}-\text{NH}_2$ and $\equiv\text{Si}-\text{NH}_2$ groups were also noticed. A band, near one previously assigned to the NH_4^+ group on a fluorinated surface, has been seen on both normal and fluorinated porous glass surfaces. Therefore a more reasonable assignment of this band may be to the group



Reuben, Fiat and Folman³⁹ have studied the N.M.R. relaxation times of adsorbed ammonia. A distribution of correlation times was attributed to surface heterogeneity. Some evidence for two major adsorption sites was encountered. These two sites are believed to be the isolated hydroxyl group and the boron Lewis acid site. Fiat, Reuben and Folman⁴⁰ have also studied the N.M.R. relaxation mechanisms of CH_3OH , CD_3OH and CH_3OD adsorbed on porous glass. The longitudinal relaxation time was found to be one to three orders of magnitude longer than the transverse relaxation time and both strongly depend on surface coverage. This is explained by postulating a distribution of correlation times characteristic of molecular motions. Dipolar interactions between the adsorbed

molecules and the surface hydroxyls contribute significantly to longitudinal relaxation. Correlation times for CD_3OH (as for ammonia) decrease on increasing surface coverage.

4. Length Changes upon Adsorption

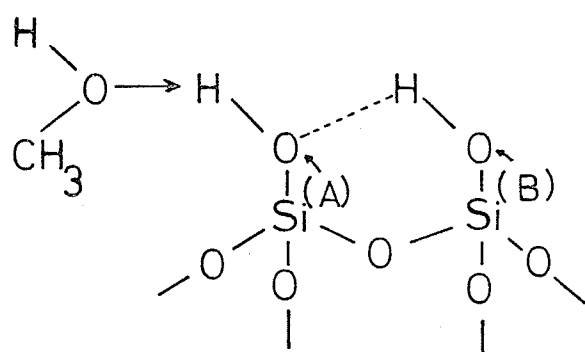
Folman and Yates³⁷ found that adsorption of gases upon porous glass caused a momentary expansion followed by a contraction which continued until 25% of a monolayer was adsorbed. The glass then expanded linearly with increasing coverage. The expansion-contraction pattern was found to be the same for all gases except argon and krypton. The amount of contraction decreased when the adsorption temperatures were increased and when the surface hydroxyl concentration was decreased. A good correlation can be drawn between the strength of the hydrogen bond between the adsorbate and the surface hydroxyls (i.e. $\Delta\bar{\nu}_{\text{OH}}$) and the amount of contraction. As $\Delta\bar{\nu}_{\text{OH}}$ increases the amount of contraction increases. Methylation of the glass surface completely eliminated the contraction stage. Folman and Yates assumed the contraction to be due to hydrogen bonding of the type shown in Fig. 1.13(a). The oxygen atom $\text{O}_{(A)}$ becomes more negative which would strengthen the hydrogen bonding between silanol groups and result in a decrease in the distance between $\text{O}_{(A)}$ and $\text{O}_{(B)}$. Figure 1.13 (b) shows why water hydrogen bonded to vicinal hydroxyls does not show the contraction effect.

5. Restricted Rotation of Adsorbed Molecules

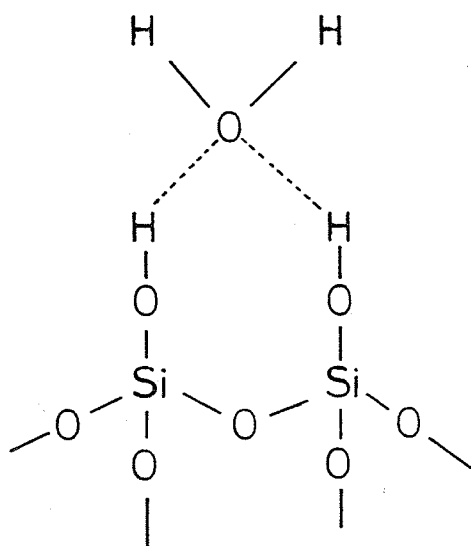
Sheppard, et al,^{41, 42} have looked at the infrared spectra of methane and methyl bromide physically adsorbed on porous glass.

Fig. 1.13

- (a) Contraction of Porous Glass on Methanol Adsorption
- (b) No Measurable Contraction on Water Adsorption



(a)



(b)

The reaction is:



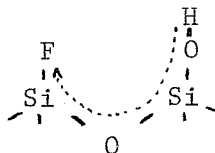
This reaction must be carried out in the absence of water.

Recently, Morterra and Low,⁴⁴ on degassing a methylated aerosil at 750°C, noticed the appearance of a band at 2280 cm⁻¹ which they assigned to a surface SiH group. On degassing an aerosil with Si-OC₂H₅ surface groups at 750°C, a band at 1650 cm⁻¹ appeared. The ratio of these two frequencies (1.38) agrees with the expected value of 1.35 ($\frac{\sqrt{\text{SiH}}}{\sqrt{\text{SiD}}}$).

2. Fluorination

The treatment of a porous glass surface with 30% ammonium fluoride solution followed by heating to 700°C completely replaces the surface silanol groups with fluorine and also reduces the surface area. The result is a hydrophobic surface. The reaction, as well as the regeneration of the original surface by adding water, has been followed spectroscopically.⁴⁵

Chapman and Hair,⁴⁶ using a 12.5% ammonium fluoride solution, have shown that only about one-half of the surface hydroxyl groups on porous glass were replaced by fluorine atoms. The resulting surface exhibited high catalytic activity. This activity results from an inductive effect on the silanol groups by neighbouring fluorine atoms analogous to the increase in acidity of acetic acid on fluorination.

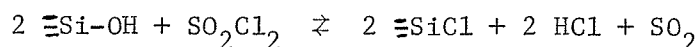


When ammonia is adsorbed on this surface a species identified as the NH_4^+ group was observed.²⁹

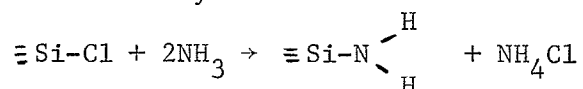
On adsorbing ammonia on a fully fluorinated surface only the infrared bands due to ammonia chemisorbed on Lewis acid sites appeared. Fully fluorinated surfaces tended to react with ammonia at 200°C whereas the partially fluorinated surfaces did not. The surface species produced on reaction are not fully understood.

3. Chlorination

The reaction of the silanol groups with sulfuryl chloride under refluxing conditions or in the gas phase leads to up to 90% replacement of surface silanol groups with chlorine atoms.⁴⁷



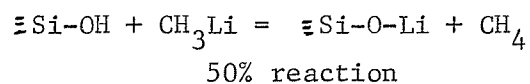
Complete dehydroxylation may be obtained by reaction with chlorine gas at 700°-900°C or by reaction with carbon tetrachloride at 350°-600°C.¹⁸ The chlorinated surface may be reacted with ammonia.¹⁸



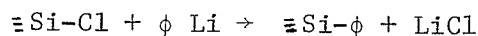
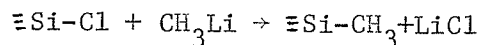
The aminated surface is stable to water but the surface may be regenerated by heating in oxygen at 600°C.

4. Grignard Reactions

Many of these reactions may be carried out using such Grignard reagents as CH_3MgI and " CH_3Li ". The silanol groups may be removed as follows:

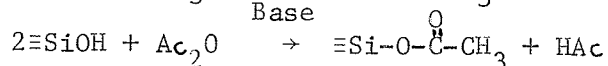
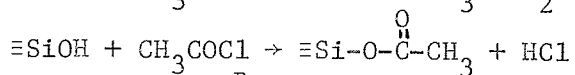
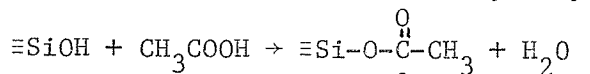


Chlorinated surfaces may undergo many reactions; two of which are:



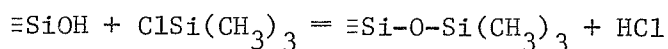
5. Carboxylic Acid Derivatives

These reactions, which are shown below, do not occur with pure silica surfaces. They require the presence of other ions on the surface, an increase in the acidity of the surface hydroxyl groups, or both.

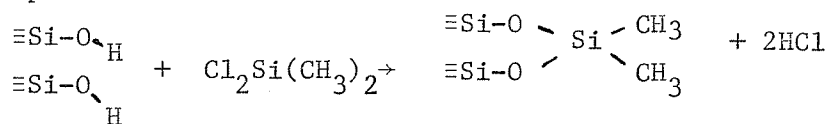


6. Reactions with Organosilicon Compounds

Methylated chlorosilanes are used to efficiently dehydroxylate silica and porous glass surfaces. The resulting surface is nonreactive and reasonably homogeneous which makes it useful as a support in gas chromatography. A typical reaction is:

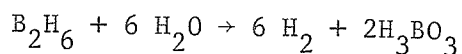


Complete replacement of the surface silanol groups is not attained. Monochlorosilanes are believed to react preferentially with the free silanol groups and dichlorosilanes react preferentially with adjacent hydroxyl groups.



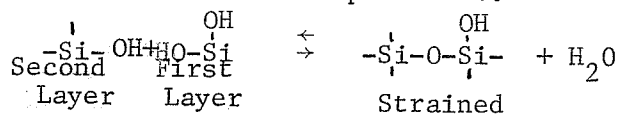
7. Reaction with Diborane

The reaction of diborane with surface silanol groups is not understood due to conflicting results.^{48, 49, 50} After reaction B-H and B-O stretching vibrations have been identified. Probably many step wise reactions occur, accounting for the conflicting results. Even the reaction of diborane with water involves six water molecules.



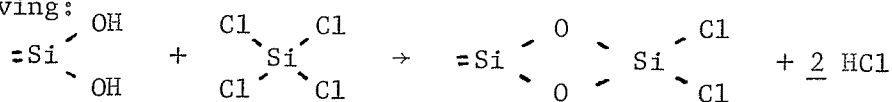
8. Reaction with Silicon Tetrachloride

Peri¹⁸ has studied quantitatively the reaction between silicon tetrachloride and surface hydroxyl groups. Hockey^{51,52} and others believe that freshly formed silica gel has a surface that is fully hydroxylated and on which geminal hydroxyl groups exist. Geminal hydroxyl groups would not be hydrogen bonded with each other. Hockey has suggested that the band at 3500 cm^{-1} in the spectra of some silica surfaces is due to this species. Hockey⁵¹ suggested that the geminal groups remaining on freshly prepared silica surfaces originate from lattice imperfections caused by incomplete polycondensation. He also suggested that the following reaction could occur at low temperatures.



Above $400^{\circ}\text{--}450^{\circ}\text{C}$ the strain is removed and the reaction becomes irreversible.

Silicon tetrachloride would react with geminal hydroxyl groups giving:

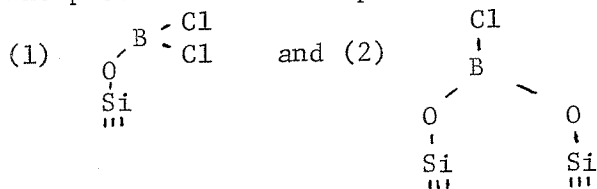


Peri¹⁸ found that a silicon tetrachloride molecule reacted with two hydroxyls on a freshly prepared aerogel (calcined and dehydrated at 600°C). Even after heating to 800°C, over 40% of the silicon tetrachloride molecules reacted with two hydroxyl groups. When virgin silica was first heated in vacuum at 800°C, calcined in oxygen at 600°C, or exposed to air for a year each silicon tetrachloride molecule reacted with one hydroxyl group. These surfaces exhibit no evidence of hydrogen bonding. Therefore, it has been shown that adjacent silanol groups do not necessarily hydrogen bond to give the 3650 cm⁻¹ band and that freshly prepared gels almost certainly contain geminal silanol groups. Peri speculates that surface annealing takes place over a period of time, possibly by the migration of Si(OH)₄ species, leaving the more stable free hydroxyls as the predominate surface species.

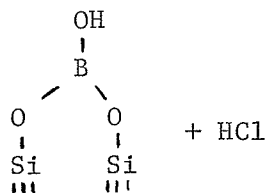
Snyder and Ward,⁵³ by selective silanization and infrared spectroscopy, have shown that "reactive hydroxyls" constitute the strongest site for the adsorption of aromatic hydrocarbons and react most rapidly with trimethylchlorosilane and dimethyl-dichlorosilane. "Reactive hydroxyls", according to them, are adjacent pairs of strongly hydrogen bonded surface hydroxyls which are predominant on fine pore silicas.

9. Reaction with Boron Trichloride⁵⁴

The possible reaction products are:



Product (1) occurs due to reaction of BCl_3 with free hydroxyls and product (2) occurs on reaction of the hydrogen bonded surface hydroxyls. On hydrolysis (1) gives $\text{SiOH} + \text{B(OH)}_3$ and (2) gives:



3. PREVIOUS E.S.R. STUDIES OF METHYL RADICALS

A brief introduction to some previous E.S.R. studies of methyl radicals is appropriate. Some of the studies mentioned below are of historical significance only while others will be referred to and discussed more fully at a later time.

The earliest E.S.R. study of the methyl radical was carried out by Gordy and McCormick.⁵⁵ They investigated x-irradiated methyl and ethyl compounds of zinc, mercury and tin at 77°K. Irradiated $\text{Zn}(\text{CH}_3)_2$ gave a quartet, having a total spread of 70 to 80 gauss, which decayed over a period of ten days at liquid nitrogen temperatures. This quartet was assigned to the methyl radical trapped in a symmetrical cage and rapidly inverting (non-planar) at 77°K. Rexroad and Gordy⁵⁶ irradiated toluene with U.V. in E.P.A. glass (ether, isopentane, and alcohol) at 77°K. They observed the methyl radical which had a h.f. splitting of about 27 gauss.

Smaller and Matheson⁵⁷ γ -irradiated methane at liquid helium temperatures. The methyl radical was not observable until the temperature was raised to 20°K (liq. H_2). The spectrum had a total

spread of 80 gauss and the relative intensities were 1.01:2.84:3.00:1.16. The line width was 3.5 gauss. In order to confirm the above assignment (methyl radical) they then γ -irradiated mercury dimethyl at 77°K. The observed four line spectrum had a total spread of 76 gauss, relative intensities of 1.30:3.00:2.74:0.73, and line width of 10.8 gauss. Jen, et al,⁵⁸ discharged methane at 4.2°K and subsequently observed the methyl radical spectrum. The h.f.s. was 64.39 Mc/s and the g-value was 2.00242. The relative intensities at 4.2°K were 1:2.2:2.2:1. At 4.2°K the spectrum was considered to be partially saturated since on warming the relative intensities approached 1:3:3:1. A similar spectrum was observed for the U.V. irradiation of 1% CH₃I in an argon matrix. Jen, et al,⁵⁸ also discharged a partially deuterated methane at liquid helium temperatures. The resulting spectrum was analyzed and the following species were reported: CD₃, CD₂H, CHD₂ and CH₃. Jen, et al, studied the methyl radical in different matrices. (Table 1.2).

TABLE 1.2
EFFECT OF DIFFERENT MATRICES ON SOME METHYL RADICAL
E.S.R. PARAMETERS⁵⁸

MATRIX	g_J	a(Mc/s)	L.W. _{1/2} Max.Ht. (gauss)
H ₂	2.00266	65.07	1.4
A	2.00203	64.64	3.7
CH ₄	2.00242	64.39	4.5

The binding energy of the matrices increases from H_2 through CH_4 . The g-value is unaffected while the h.f. splitting decreases slightly on increasing binding energy. The linewidths increase on increasing binding energies. Jen, et al, decided that the linewidths are more dependent on the nature of the matrices than on the properties of the radicals. T. Cole, et al,⁵⁹ looked at C^{13} enriched methyl radicals at 77°K produced by x-irradiation of methyl iodide. The C^{13} h.f.s. was measured to be 41 ± 3 gauss which was taken as strong evidence for a planar structure for the methyl radical.

Wall, et al,⁶⁰ γ -irradiated methane at 4.2°K which resulted in the production of hydrogen atoms and methyl radicals. The h.f.s. of the methyl radical was measured to be 23 gauss, the line width at half intensity was 11 gauss and the relative intensities were 1:2.4:2.8:1.1. On warming and then recooling the sample the hydrogen atoms disappeared while the methyl radical spectrum sharpened up. Karplus,⁶¹ using valence-bond theory, calculated the proton h.f.s. for a planar methyl radical to be 27 ± 5 gauss. The method used was insensitive to angles of 10-15° from planarity. Cochran⁶² photolyzed both methane and deuteromethane using vacuum U.V. at 4°K. He identified both the CH_3 and CD_3 spectra. The ratio of the hyperfine splitting constants (a^{CH_3}/a^{CD_3}) was in the ratio of the nuclear g-factors ($g^H/g^D = 6.514$).

Ayscough and Thomson⁶³ looked at the E.S.R. spectra of radicals trapped in γ -irradiated polycrystalline alkyl halides at 77°K. The spectra obtained from γ -irradiated methyl bromide and methyl chloride

were complex. The four line methyl radical spectrum was poorly resolved with average line separation of 70 ± 5 Mc/s. Ayscough, et al,⁶⁴ γ -irradiated (77°K) both dimethyl sulphone and methylisopropyl sulphone. In both cases methyl radical spectra were observed with h.f. splittings of 23 gauss and relative intensities of 1:3:3:1. Ayscough, et al,⁶⁵ on irradiating azomethane at 77°K with U.V. light, observed a broad, asymmetric methyl radical spectrum. Ayscough, et al,⁶⁶ have also looked at the E.S.R. spectra of species, trapped in glassy matrices, produced by γ or U.V. irradiation at 77°K. They γ -irradiated an 8N sodium hydroxide glass (77°K) containing 3×10^{-2} M methyl chloride. The irradiation produced methyl radicals, trapped electrons, and O^- species.

Bouldin, Patten and Gordy⁶⁷ have shown that large concentrations of methyl radicals and hydrogen atoms may be produced by γ -irradiation at 4.2°K of inert gas matrices containing impurity concentrations of methane (less than one part in 10^4). The same amount of methane in the pure form, given the same γ -ray dosage at 4.2°K, would not give a detectable signal. Therefore, for dilute solutions, the matrix must absorb the energy, and then transfer it to the impurity (CH_4 or CD_4) by some mechanism. Further work has been done on this problem.⁶⁸ Here, further experimental work is discussed, possible mechanisms for energy migration are postulated, isotope effects and theories for the observed isotope effects are presented, and satellite lines of unknown origin are spoken of. Gordy and Morehouse,⁶⁹ on γ -irradiating solid methane at 4.2°K, noticed, in addition to the hydrogen atom and methyl radical spectra, a weaker quartet of quartets.

They theoretically interpreted these lines as due to exchange-coupled hydrogen atoms and methyl radicals. Analysis of this interaction indicated the separation of the coupled H and CH_3 to be 6.76\AA . Similar effects were observed on γ -irradiation of methane in a krypton matrix at 4.2°K , but was not observed for γ -irradiation of methane in an argon matrix at 4.2°K . Morehouse, et al,⁷⁰ have produced CH_3 , SiH_3 , GeH_3 and SnH_3 in a krypton matrix at 4.2°K by γ -irradiation of the matrix containing dilute concentrations of CH_4 , SiH_4 , GeH_4 and SnH_4 . The results indicate free rotation for the methyl radical and restricted rotation for the others about an axis perpendicular to the symmetry axis. For SiH_3 the isotropic silicon-29 h.f. splitting is 266 gauss and the anisotropic coupling is 24 gauss. The methyl radical is planar while the others are not.

Fessenden and Schuler⁷¹ developed a technique for looking at alkyl radicals in liquid hydrocarbon systems during irradiation with 2.8 MeV electrons. They studied the methyl radical and deuteromethyl radical over a narrow temperature range (m.p. -183°C , b.p. -161°C). The results obtained for the methyl radical are as follows: Relative intensities 1:3:3:1; $a^{\text{H}} = 23.04 \text{ g.}$; L.W.=0.29 g; only partial resolution of the second-order splitting (0.23g) of each of the central pair of lines was possible; $g = 2.00255$. The results obtained for the deuteromethyl radical are as follows: relative intensities 1:3:6:7:6:3:1; $a^{\text{D}}=3.576(\pm 0.002)\text{g.}$; $g=2.00256$. Fessenden and Schuler⁷² studied the methyl radical in rare-gas matrices in conjunction with studies of fluorinated methyl radicals. They

found that for the methyl radical in a krypton matrix: $a^H=23.0g$; $a^C=38.5g$; $g = 2.0026$; L.W. = 0.5g. In a xenon matrix the L.W. was 4.0 gauss. This increased linewidth was attributed to unresolved splittings due to Xe^{129} and Xe^{131} or due to a decreased tumbling frequency in the xenon matrix. Fessenden⁷³ studied $C^{13}H_3$, $C^{13}H_2D$, $C^{13}HD_2$ and $C^{13}D_3$ in the liquid phase (at $-177^\circ C$) by in situ electron irradiation of the corresponding hydrocarbons. These radicals were also studied in a krypton matrix at $-188^\circ C$. The results may be seen in Table 1.3 below.

Table 1.3
METHYL RADICAL HYPERFINE SPLITTINGS MEASURED IN
SOLUTION AND IN A KRYPTON MATRIX⁷³

RADICAL	$ a^H $	$ a^D $	$ a^C $
$C^{12}H_3^{bd}$	23.03g	-	-
$C^{13}H_3^{bd}$	23.04	-	38.34 ^b (38.53) ^c
$C^{12}H_2D^{cd}$	23.10	3.531	-
$C^{13}H_2D^{ce}$	23.10	3.54	37.82
$C^{12}HD_2^{cd}$	23.21	3.552	-
$C^{13}HD_2^{ce}$	23.19	3.55	37.06
$C^{12}D_3^{bd}$	-	3.576	-
$C^{13}D_3^{bd}$	-	3.578	35.98 ^b (36.18) ^c

b = observed in liquid methane at -177° .

c = observed in krypton matrix at -188° .

d = estimated accuracy $\pm 0.01g$.

e = estimated accuracy $\pm 0.025g$.

A study of the methyl radical in aqueous solution has been done over the temperature range 273°K to 333°K.⁷⁴ The peak-to-peak linewidths decreased from 1.1g at low temperatures to 0.8g. at room temperature. A straight line was fitted to the results of $|a^H|$ versus $T(^{\circ}\text{C})$ over the above temperature range [$-\frac{d|a^H|}{dT} = -2.1 \text{ mg}/^{\circ}\text{C}$].

The methyl radical has also been studied in irradiated single crystals of sodium acetate trihydrate⁷⁵ where the resulting methyl radicals were reported to have the following parameters: relative intensities 1:3:3:1; $a^H = 22.5 \pm 0.5\text{g}$; two sets of satellite lines assigned to "forbidden spin-flip" transitions of the protons on neighbouring water molecules; $a^{C^{13}} = 37.7 \pm 0.5 \text{ g}$. Methyl radicals have been observed in a study of the solute-sensitized photodecomposition of polydimethylsiloxane.⁷⁶ Here, the photolysis of solutions of naphthalene in polymeric dimethylsiloxane has been examined at 77°K. The naphthalene solute sensitizes the decomposition of the solvent by a stepwise two-photon absorption process involving the first triplet state of naphthalene as an intermediate. $\text{CH}_3\cdot$, $-\text{CH}_2\cdot$ and $\equiv\text{Si}\cdot$ radicals were observed by E.S.R.

Several papers have been published on methyl radicals stabilized on surfaces such as silica gel, porous Vycor glass, and zeolites.⁷⁷⁻⁸⁴ These publications will be discussed in the next chapter.

CHAPTER II

GENERAL CHARACTERISTICS OF THE E.S.R.
SPECTRA OF METHYL RADICALS STABILIZED
ON POROUS VYCOR GLASS

1. INTRODUCTION

A very brief description of some of the varied E.S.R. studies that have been carried out on surfaces will be presented. Some of the earliest E.S.R. studies of surface stabilized radicals were performed by Russian workers. Pariiskii, et al,⁷⁷ have studied methyl radicals adsorbed on silicagel at low temperatures. The silicagel, having a specific surface area of $700 \text{ m}^2/\text{gm}$, was outgassed in a vacuum for 6 hours at 300°C before methyl iodide adsorption at room temperature. The silicagel samples were then irradiated at 77°K for 4-6 hr. with a U.V. source. The E.S.R. spectra, recorded at 77°K , consisted of four lines of 1-2 gauss width, spaced 24.2 ± 0.5 gauss apart, and the g-factor was 2.001 ± 0.001 . The relative amplitudes of the four lines were 1:8.5:13:2.5 instead of the binomial values 1:3:3:1. The spectrum described above was assigned to the methyl radical. The unusual relative amplitudes were ascribed to incomplete neutralization of the anisotropic hyperfine spin-orbital interactions. Pariiskii, et al, thought of the methyl radical as being bound to the surface by a one-electron bond due to the attraction of the unpaired electron to the adsorbent. In this situation only the rotation about the three-fold symmetry axis would remain. The small linewidths (1-2 gauss), however, indicates that other motions

of the stabilized methyl radical are still important. The methyl radical was found to be very stable on the silicagel surface (temperature studies). Kazanskii and Pariiskii⁸⁵ observed the E.S.R. spectra of ethyl radicals after γ -irradiating ethane adsorbed on silicagel at 77°K. The reported proton hyperfine splittings were: $|a^\alpha| = 20.5\text{g}$ and $|a^\beta| = 27\text{ gauss}$. The ethyl radical was pictured as being bound to the surface at one end only. The ethyl radicals were found to be quite stable on increasing the temperature but no measurements of $|a^\alpha|$ and $|a^\beta|$ were reported at increased temperatures. The adsorbed radical resembled an entirely free one very closely; its unpaired electron taking no appreciable part in the bond to the surface. Pariiskii and Kazanskii⁸⁶ have also used the E.P.R. technique in studying the recombination of hydrogen atoms, formed on a silicagel surface by the radiolysis of its hydroxyl groups, and their reactions at low temperatures (-170 to -100°C) with oxygen and ethylene. Much of the work done by Kazanskii and Pariiskii on the E.S.R. of free radicals adsorbed on catalysts has been presented in summary.⁷⁸ They concluded, on comparing the h.f.s. in the spectra of radicals adsorbed on silicagel with the h.f.s. for the corresponding free radicals, that the disturbing action of the surface on the unpaired electron cloud of the adsorbed radicals is very small. They have estimated the strength of the one-electron bond to the surface to be 3-5 kcal/mole. Analysis of the amplitude ratios of components in the E.S.R.

spectra of adsorbed alkyl radicals gives some information about the geometry of these radicals and about their motion in the adsorbed state. The conclusion reached, for the methyl radical, was that there is a loss of two rotational degrees of freedom and there remains only one axis of rotation which is the three-fold symmetry axis. Interpretation of the adsorbed ethyl radical spectrum showed that the radical "lies on the adsorbent surface on its side", and there is rotation of its CH_3 and CH_2 groups relative to each other. The ethyl radical was postulated to "roll" along the surface as well. Adsorbed alkyl polymer radicals also "lie on their sides".

The E.S.R. spectra of perylene and anthracene adsorbed on silica-alumina has been studied.⁸⁷ The larger proton h.f. coupling constants of the perylene radical cation, generated on a silica-alumina catalyst surface, are shifted by 4% from the corresponding values obtained when the radical cation is prepared in sulfuric acid. This shift is explained in terms of an electrostatic perturbation of the radical-cation π -electron distribution due to the presence of the counterion. The severe linewidth effects which are observed are accounted for in terms of a modulation of the anisotropic hyperfine and g-tensor interactions. The linewidth variation can be described by a polynomial equation in the nuclear spin quantum number of the equivalent proton groups provided τ_c (correlation time) for the radical-cation motion is chosen to be comparable to that found in solution

(approximately 10^{-9} sec.). Therefore, the radical-cation is relatively unrestricted in its motion and perhaps the counterion (electrophilic agent) is also somewhat unrestricted in its movements on the surface. The results for the anthracene radical-cation generated on a silica-alumina catalyst surface parallel those obtained for perylene on this surface. When the concentration of the aromatic compound is in excess of that required to saturate the radical-forming ability of the catalyst, both chemical and electron-exchange effects are observed. The electron exchange effect is discussed in terms of an electron-transfer mechanism with neutral aromatic molecules. Chemical exchange involves surface protons and occurs after the radical concentration has reached a limiting value. Therefore proton transfer is not involved in radical-cation formation.

Kinell, et al,⁸⁸ have studied the E.S.R. absorption of hexane/silicalgel systems γ -irradiated at low temperatures. Several lines due to defects in the silicagel were observed. One of these lines (at $g = 2.0008$) was accompanied by two satellite lines (separation of 10 gauss) assigned to Si^{29} . Ethyl radicals have been definitely identified as one of the irradiation products. The yields of paramagnetic species in the two phases imply an interaction between the components and the magnitudes of the yields strongly suggest an energy transfer from the silicagel in the formation of free radicals. Chung and Haneman⁸⁹, after crushing silicon crystals in ultrahigh vacuum,

observed an E.S.R. signal at $g = 2.0055$ (with a linewidth of 7.0 gauss) due to a confirmed surface species. This study revealed that the surface structure for both cleaned and annealed clean silicon surfaces involve "dangling bonds", the concentrations being of the order 20% and 2%, respectively. Weeks and Abraham⁹⁰ irradiated a synthetic quartz crystal with 1.7 MeV electrons at $\sim 300^\circ\text{K}$ and then with Co^{60} γ -rays at 80°K . E.S.R. measurements at 80°K revealed the existence of two types of hydrogen atoms. [$|a^{\text{H}}| = 521.3$ G and $|a^{\text{H}}| = 515$ G]. Two satellite lines about the 521.3 gauss hydrogen atom lines with splittings of less than a gauss from the main line have been assigned to the Si^{29} ($I = 1/2$) nucleus. (Natural abundance = 4.7%). The intensity ratio of each of the satellites to the main line is ≈ 0.025 . The calculated intensity ratio of the satellite to the main line, assuming they are due to Si^{29} , is 0.024. The production of atomic hydrogen in silica glass requires only γ -rays (or x-rays) at 78°K without a prior electron irradiation as in the single crystal. In the literature many different values have appeared for $|a^{\text{Si}^{29}}|$. Gardiner⁹¹ adsorbed chlorine gas on the surface of silicagel. A complex E.S.R. spectra resulted on irradiating the sample with a 200-W high-pressure mercury lamp. Lines due to silicagel defects, hydrogen atoms and chlorine atoms were identified. An estimate of 2.7×10^{17} V/cm² was made for the electric-field gradient at the position of the chlorine atom. Noble⁸⁴, et al, have shown that methyl radicals may be stabilized for long periods in zeolites at temperatures below 90°K . These radicals were generated by γ -irradiation of methane sorbed on synthetic zeolite (Linde Type A - $\text{Na}_{12} [(\text{AlO}_2)_{12} (\text{SiO}_2)_{12}] \cdot 27\text{H}_2\text{O}$). Several unidentified species were observed besides the more stable methyl radical. The methyl radical had the following parameters:
 $g = 2.0026$; $|a^{\text{H}}| = 21.9$ gauss; relative intensities 1.0:3.1:2.8:0.9.

Electron spin resonance studies have been made of the defects introduced in porous Vycor glass by γ -irradiation.⁹² As has been mentioned previously, boron occurs as an impurity in porous Vycor glass (p.V.g.). On analysis of the defects, boron is postulated to be trigonally coordinated in p.V.g. in contrast to the tetrahedral coordination observed in other glasses. E.S.R. techniques have been used to study the effects of added gases on the paramagnetic defects introduced in p.V.g. by γ -irradiation.⁹³ Three paramagnetic defects have been identified on γ -irradiation of p.V.g.:⁹² (a) an electron trapped on a silicon atom with at least one oxygen atom missing (Si site), (b) a hole trapped predominantly on an oxygen atom bonded to a trigonally coordinated boron atom (B-O site), and (c) a hole trapped in the S-O network (Si-O site). Defects (b) and (c) are thought to be formed by the removal of a hydrogen atom from a hydroxyl group. On adsorption of hydrogen and deuterium, defects (b) and (c) are removed but defect (a) remains.⁹³ This effect is irreversible which implies that strong chemisorption is occurring, possibly with the formation of SiOH and BOH groups. Adsorbing oxygen, nitric oxide, nitrogen and ammonia did not affect the E.S.R. spectrum of the defects. Since oxygen and nitric oxide have no effect, it may be concluded that the defects are located in the bulk of the solid and are not accessible to oxygen and nitric oxide.

Turkevitch and Fujita⁷⁹ were the first to report methyl radicals stabilized on p.V.g. (Corning Glass No. 7930). The methyl radicals were produced by U.V. photolysis of adsorbed methyl iodide. Deuteromethyl and carbon-13 enriched methyl radicals were also studied. The p.V.g., which had a surface area of $144\text{m}^2/\text{gm}$. (B.E.T. method),

was pretreated in oxygen at 600° - 650°C for flow system experiments and was further treated at 500°C in a vacuum for static experiments. The surface coverage of methyl iodide was estimated to be about 2% of a monolayer for the static experiments. The sample irradiation was carried out with a 500 W low-pressure mercury lamp. A sample of frozen methyl iodide was also irradiated at 77°K, and the E.S.R. parameters of the resulting methyl radicals were measured (Table 2.1).

TABLE 2.1

Characteristics of Methyl and Deuteromethyl Radicals⁷⁹

Condition	Total Spread (g)	HFS(g)	L.W.(g)	Relative Intensities
<u>METHYL RADICAL</u>				
CH ₃ I Matrix at 77°K	68.8	23.2	3.6	1.0:2.8:2.9:1.0
Adsorbed on p.V.g. at Rm.Temp.	67.8	22.7	1.0	1.0:3.0:3.3:1.1
Adsorbed on p.V.g. at 77°K	68.8	22.9	0.8	1.0:3.7:4.1:1.3
<u>DEUTERO METHYL RADICAL</u>				
Adsorbed on p.V.g. at Rm.Temp.	21.2	3.54	1.8	1.0:3.3:6.8:7.8:6.5:3.2: 1.4

From Table 2.1 the ratio $\frac{|a^H|}{|a^D|}$ ($= \frac{22.7}{3.54}$) is 6.41 which is lower than the theoretical ratio of 6.514. The linewidths indicate motion of the methyl radicals on the surface even at 77°K. The measured value of $|a^{C13}|$ was 38.5 gauss. It was found that the methyl radicals were stable for days at room temperature. It was also found that in the static system, prolonged irradiation resulted in a constant concentration of the radical. In the flow system the yield increased linearly with time of irradiation and eventually leveled off. The interaction of the

methyl radicals with several gases was studied. Attempts to produce and stabilize methyl radicals from acetone and dimethyl mercury were unsuccessful.

By studying the linewidths of methyl and deuteromethyl radicals stabilized on silicagel at 77°K, tumbling frequencies of these radicals have been calculated.⁸³ This study will be discussed in detail in Chapter IV. The remainder of this chapter will be devoted to description of work done on methyl radicals stabilized on p.V.g., some of which has already been published.^{80,81} Temperature dependences of the h.f. splittings, linewidths and line asymmetries of methyl radicals stabilized on p.V.g. will be discussed in Chapter III.⁸²

2. Experimental

Each sample of porous Vycor glass (Corning Code No. 7930) was preheated in oxygen (or in air in some cases) to remove organic impurities and then heated in vacuum to dehydrate the surface. The specific values of the temperatures employed and the times of pretreatment will be noted at the appropriate places in the text of this chapter. In this laboratory the surface area of a typical p.V.g. sample was determined, by the Brunauer-Emmett-Teller method, to be 120 m²/gm. In the literature, values for the surface area of p.V.g. range from 120 m²/gm^{80,94} to 342 m²/gm.⁹⁵

Assuming the surface area to be 120-130 m²/gm. and the area of a molecule of methyl iodide to be about 10²⁰ Å² an approximate calculation of the number of molecules required for monolayer coverage is feasible. Two calibrated volumes were installed (one of 4.2 cc and one of 2.0 cc) on the vacuum line used for sample dosing. From the surface area, weight of the p.V.g. sample, and P.V.T. measurements for methyl iodide, it is possible to calculate a percent coverage (Λ). $\Lambda = 1$ for monolayer coverage.

To many of the first samples studied, 2 or 3 cm. of helium was added to prevent (1) sample decomposition due to heating effects on radical recombination (2) sample desorption (to the cell walls) while freezing down to 77°K. It was later shown that methyl iodide adsorbed on p.V.g. does not decompose due to heating (no He in cell) when irradiated with U.V. under the conditions employed in this laboratory. It has also been shown that pressures of helium up to 15.5 cm (at 77°K) do not have any effects on any of the E.S.R. parameters of the methyl radical.

The methyl iodide used was reagent grade supplied by Matheson, Coleman and Bell. It was used without purification after normal degassing procedures. Most samples were irradiated with the full focused arc of a Hanovia S-100 Alpine burner (medium pressure mercury arc). In some cases higher power lamps and filters were employed. These cases will be mentioned as they appear in the text. The published work^{80,81} was carried out on a home made x-band E.S.R. spectrometer.* Most of the remaining work in this chapter was done on a Varian E-3 E.S.R. spectrometer employing 100 KHz modulation.

3. Results

For surface coverages greater than a monolayer, the relative amplitudes of the four methyl radical lines were found to be close to the binomial values of 1:3:3:1 (Fig. 2.1).⁸⁰ The relative amplitudes of the four methyl radical lines deviate from the binomial values on decreasing coverage (or Λ) (Fig. 2.1). The relative amplitudes of the four proton lines have been studied more extensively as a function of Λ and as a function of various surface treatments (see following results as well as Chapters III and IV).

*This spectrometer was built by Dr. M. Fujimoto of the Physics Department, University of Manitoba.

For higher surface coverages the following E.S.R. measurements were made on the methyl radical: Relative amplitudes 1:3:3:1;

$$|a^H| = 23.4 \pm 0.2; g = 2.0024 \pm 0.0001; \text{Linewidth} = 1.5 \text{ gauss.}^{80}$$

For $\Lambda = 1$, the linewidths on increasing H_0 were found to be 1.8, 1.2, 1.1, and 1.0 ± 0.2 .⁸¹ Methyl radical decay (as well as the cascade effect) will be treated in Chapter V.

A. Radical Build-Up Studies

Preliminary studies⁸⁰ showed that upon U.V. radiation of methyl iodide the methyl radical concentration asymptotically approached a saturation value which was independent of Λ if Λ was less than 10. The manner of approach to saturation depended, however, on Λ and the absorbed light intensity. In Fig. 2.2, one can see the build-up of the four methyl radical lines on irradiating a sample ($\Lambda=0.05$) with the full focused arc of a Hanovia S-100 Alpine burner at 77°K. This sample had been preheated in oxygen for 24 hours at 750°C, then heated in vacuum for about 18 hours before adsorbing methyl iodide. Table 2.2 exhibits the relative amplitudes of the above mentioned sample as a function of irradiation time.

TABLE 2.2

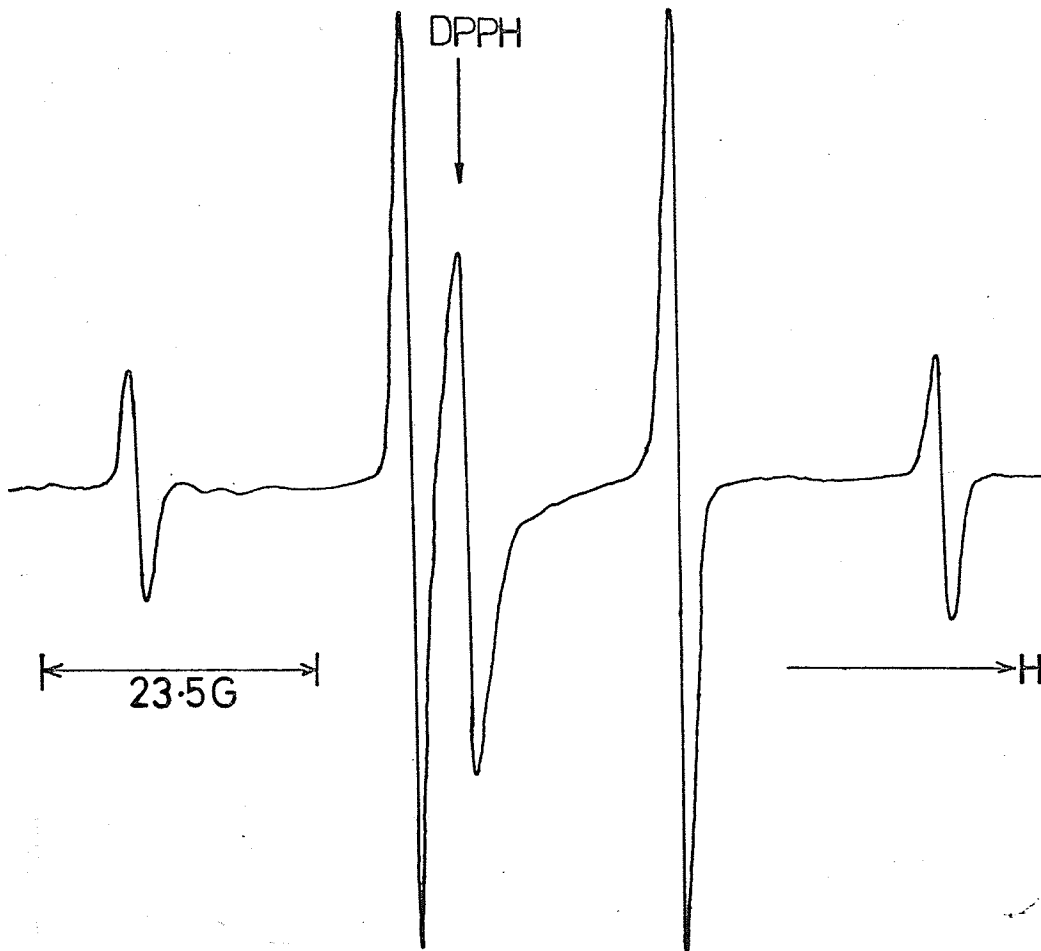
Relative Amplitudes as a Function of Irradiation Time For Methyl Radicals Stabilized on a Dehydrated Surface

<u>IRRADIATION TIME (Min.)</u>	<u>RELATIVE AMPLITUDES</u>
1	1.0:4.59:6.38:1.98
2	1.0:4.37:6.07:1.71
3	1.0:4.54:6.43:1.78
5	1.0:4.78:6.72:1.95
8	1.0:4.53:6.63:1.88
11	1.0:4.66:6.73:1.89
15	1.0:4.74:6.93:1.96
20	1.0:4.64:6.68:1.90
25	1.0:4.63:6.84:1.93
30	1.0:4.60:6.77:1.88
35	1.0:4.68:6.57:1.95
40	1.0:4.67:6.69:1.92
60	1.0:4.71:6.86:1.93
90	1.0:4.61:6.72:1.94

Fig. 2.1

- (a) Spectrum of Methyl Radical at 77°K (high surface coverage)
- (b) Spectrum of Methyl Radical at 77°K (low surface coverage)

(a)



(b)

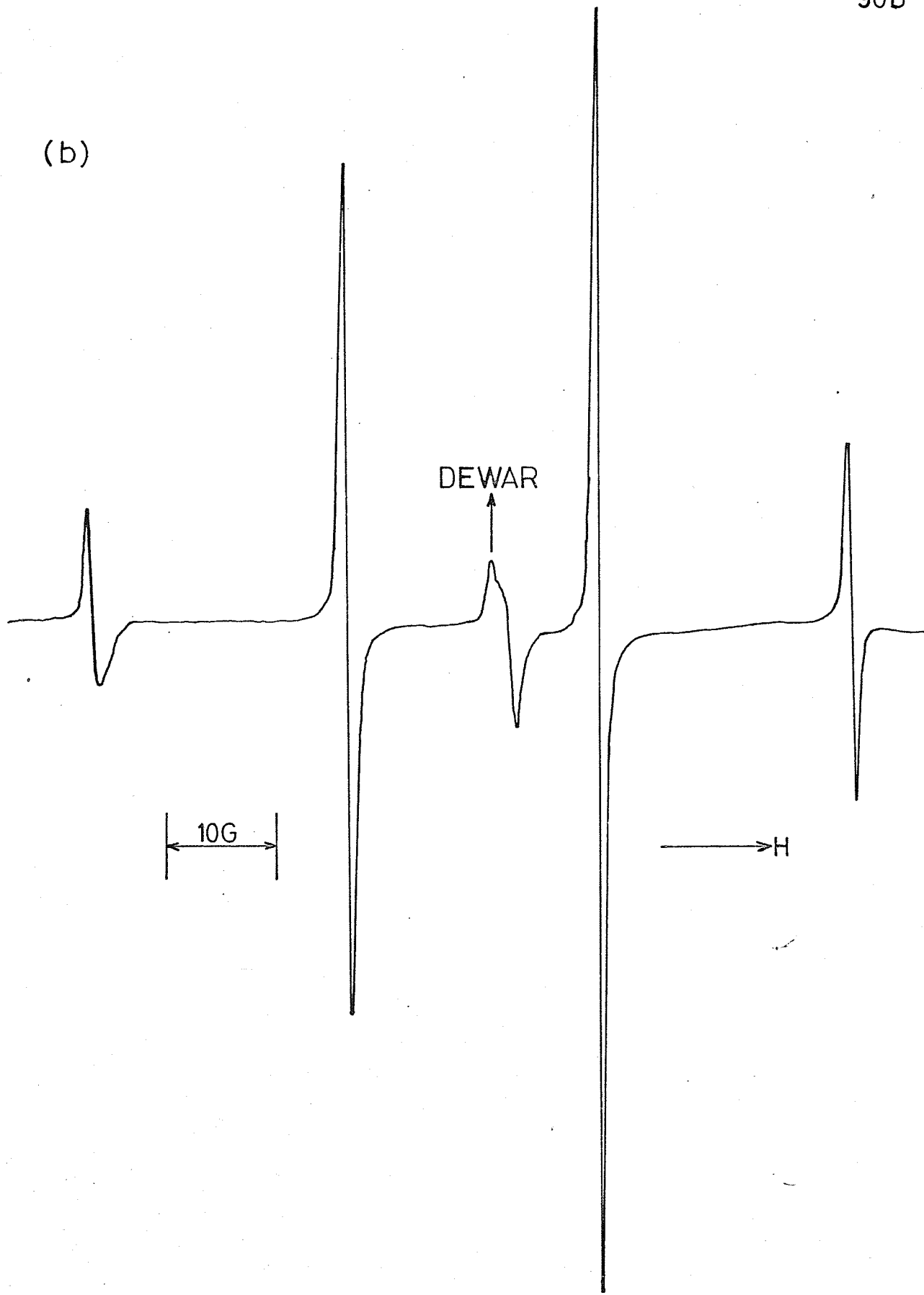
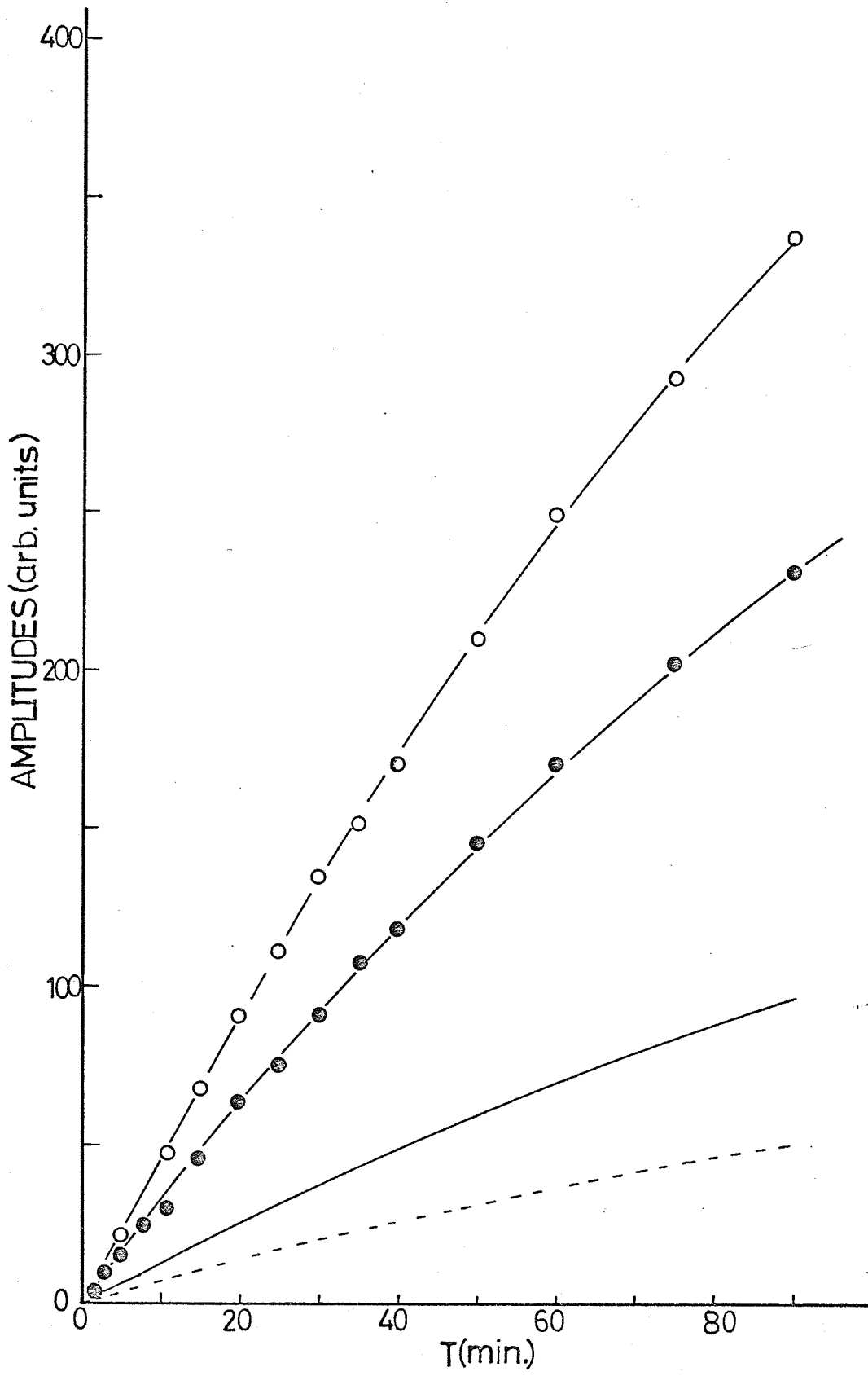


Fig. 2.2

Build-up Study of Methyl Radicals Stabilized on a Regular p.V.g. Surface. The amplitudes of the four lines are Standardized to the Same Gain Setting. The open circles refer to line 3a while the solid circles refer to line 3. The solid line represents the results of studying line 1a while the dashed line represents the results of studying line 1. Lines 1, 3, 3a and 1a are defined on page 102 and exhibited on page 162.



Build-up studies were also performed on a cell containing methyl iodide ($\Lambda=0.06$) adsorbed on a surface which had been chlorinated using carbon tetrachloride as the chlorinating agent.¹⁸ The radical build-up, using the same irradiation set-up as for the previously mentioned build-up study, was much slower due to the fact that much of the adsorbed methyl iodide had been destroyed by discharging the sample (Tesler coil) at an earlier date. The trends, however, are identical to those observable in Fig. 2.2. Table 2.3 shows the relative amplitudes as a function of irradiation time for this chlorinated sample.

TABLE 2.3

Relative Amplitudes vs. Irradiation Time for Methyl
Radicals Stabilized on a Chlorinated Surface (77°K)

<u>IRRADIATION TIME (Min.)</u>	<u>RELATIVE AMPLITUDES</u>
2	1.0:2.3:-:-
4	1.0:3.01:3.49 :1.44
6	1.0:3.71:5.00:1.56
8	1.0:3.35:4.71:1.44
10	1.0:3.82:5.19:1.44
15	1.0:4.23:5.75:1.75
25	1.0:4.23:6.08:1.77
45	1.0:4.50:6.27:1.87
70	1.0:4.34:6.19:1.84
86	1.0:4.61:6.31:1.88

Methyl radical build-up was also noticed on photolysis of methyl bromide and methyl chloride. The methyl radical build-up was slower due to the increased strengths of the carbon-halide bond in these two compounds.

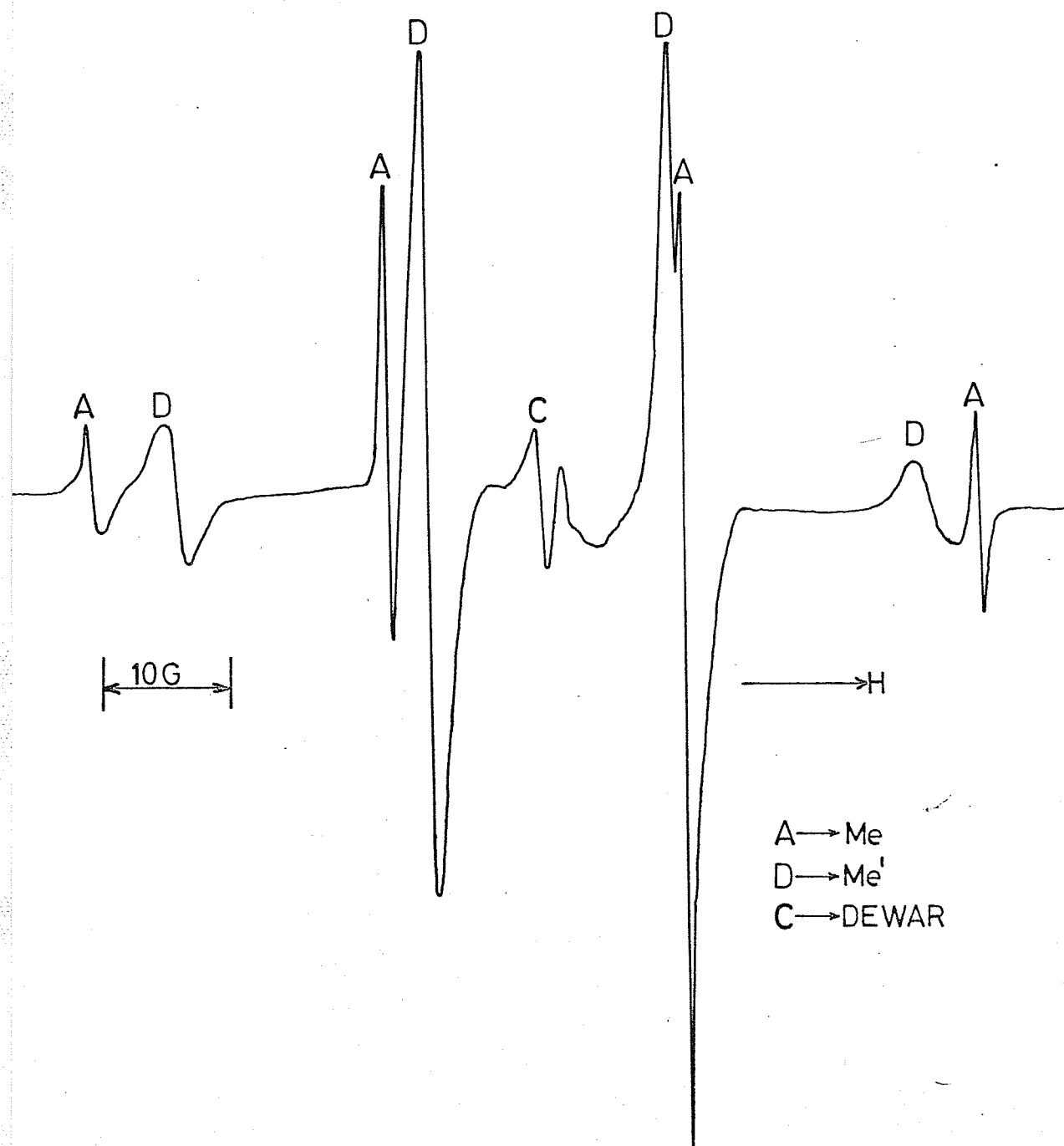
B. A Second Kind of Methyl Radical (denoted Me')

Under certain conditions a second kind of methyl radical was observed on photolysis of methyl iodide at 77°K (Fig. 2.3). This radical was noticeable when the surface coverage of methyl iodide was small ($\Lambda < 1$). Me' has a four line spectrum characterized by the following E.S.R. parameters: $a_{\text{Me}'}^{\text{H}} = 20.2 \pm 0.4$, $g_{\text{Me}'} = 2.0016 \pm 0.0005$.⁸⁰ Me' builds-up faster than Me (normal methyl radical), but decays at liquid nitrogen temperatures. Therefore Me' was noticeable only at early stages of irradiation. It was believed in earlier work that Me' decayed into another radical (x) at liquid nitrogen temperatures.⁸⁰ Later, it was shown neither to decay into the radical x (to be treated in the next section) nor into the normal methyl radical. Therefore Me' must react at liquid nitrogen temperatures and lose its paramagnetic properties. It is interesting to note that Me' increased in concentration on higher and longer preliminary heat treatments of the p.V.g. (700-850°C for longer periods of time than the average). In this case x was not seen to come up as Me' decayed. Does the smaller value of $|a^{\text{H}}|$ for the Me' indicate charge transfer to the surface? This point will be discussed later. If a sample of p.V.g. is suitable, Me' will appear on many reirradiations of the sample.

Further work has been done (using a Varian E-3 spectrometer) in order to elucidate the structure of Me'. Me' appears on irradiation at liquid nitrogen temperatures of samples with high and low power U.V. lamps, high and medium pressure mercury arcs, and with and without

Fig. 2.3

Spectrum of Me and Me' at 77°K. Note that in this case the concentration of Me' is greater than the concentration of Me (coverage is small).



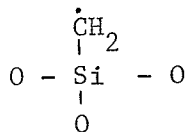
a Vycor filter. Me^{\cdot} occurred also with and without the use of He. All samples studied were pretreated at high temperatures, but not all of these samples yielded Me^{\cdot} . All samples studied did have low methyl iodide surface coverages (1 to 25% of a monolayer). The largest concentration of Me^{\cdot} did occur, however, on a sample pretreated at high temperatures with less than a 1% surface coverage ($\Lambda < .01$) of methyl iodide. Another sample, similarly pretreated, but with twice the coverage, yielded Me^{\cdot} but not nearly to the same extent. Me^{\cdot} was found to decay at liquid nitrogen temperatures, as mentioned before. The proton splitting in Me^{\cdot} has been found to be 19.3 ± 0.05 gauss which is different from the value found in the preliminary work [$|a_{\text{Me}^{\cdot}}^{\text{H}}| = 20.2 \pm 0.4$ gauss].⁸⁰ The linewidths of the Me^{\cdot} lines were found to be larger than those for the normal methyl radical. Both Me^{\cdot} and Me (normal methyl radical) have similar saturation properties. On irradiation of a deuteromethyl iodide sample, a broad seven line spectrum was noticed in addition to the normally obtained deuteromethyl radical. This spectrum was assigned to a deuterio- Me^{\cdot} species, but, because of the smaller splittings and large linewidths no measurements could be made on this radical. A comparison was made of the linewidths of the low-field lines in the Me^{\cdot} and Me spectra.

$$\text{L.W.}_{\text{p-p}} (\text{Me}) = 0.825 \text{ gauss} \quad 77^{\circ}\text{K}$$

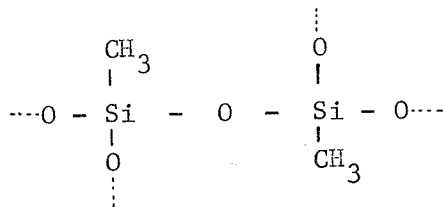
$$\text{L.W.}_{\text{p-p}} (\text{Me}^{\cdot}) = 1.475 \text{ gauss} \quad 77^{\circ}\text{K}$$

An interesting and meaningful experiment has been performed on the sample ($\Lambda < .01$) which had yielded large quantities of Me^{\cdot} . A small quantity of water vapor was added to this sample at room

temperature. After this addition the sample was irradiated at 77°K with and without a Vycor filter. The products included the methyl radical but not Me'. Another interesting experiment should be mentioned at this point. A sample which had previously had methyl iodide adsorbed on it was incompletely oxidized at high temperatures leaving a small impurity on the surface. On U.V. irradiation of this sample at 77°K only Me' was produced. After a long irradiation time a very small concentration of Me appeared. This sample contained hydrogen and mercury as well, since the sample was meant for another purpose. Before photolysis a large central peak was noticed attributed to incomplete oxidation products. On U.V. irradiation, besides the growth of Me', a possible growth in hydrogen atom concentration was noticed as well as the growth of two broad peaks, one on either side of the impurity peak (split from the central impurity peak by 20-21 gauss), which may be part of a 1:2:1 spectrum assignable to the following species.^{7 6}



These two lines, split from a larger central line have also been seen while looking at the U.V. radiation damage of silicone rubber at 77°K. The silicone rubber structure is as follows:



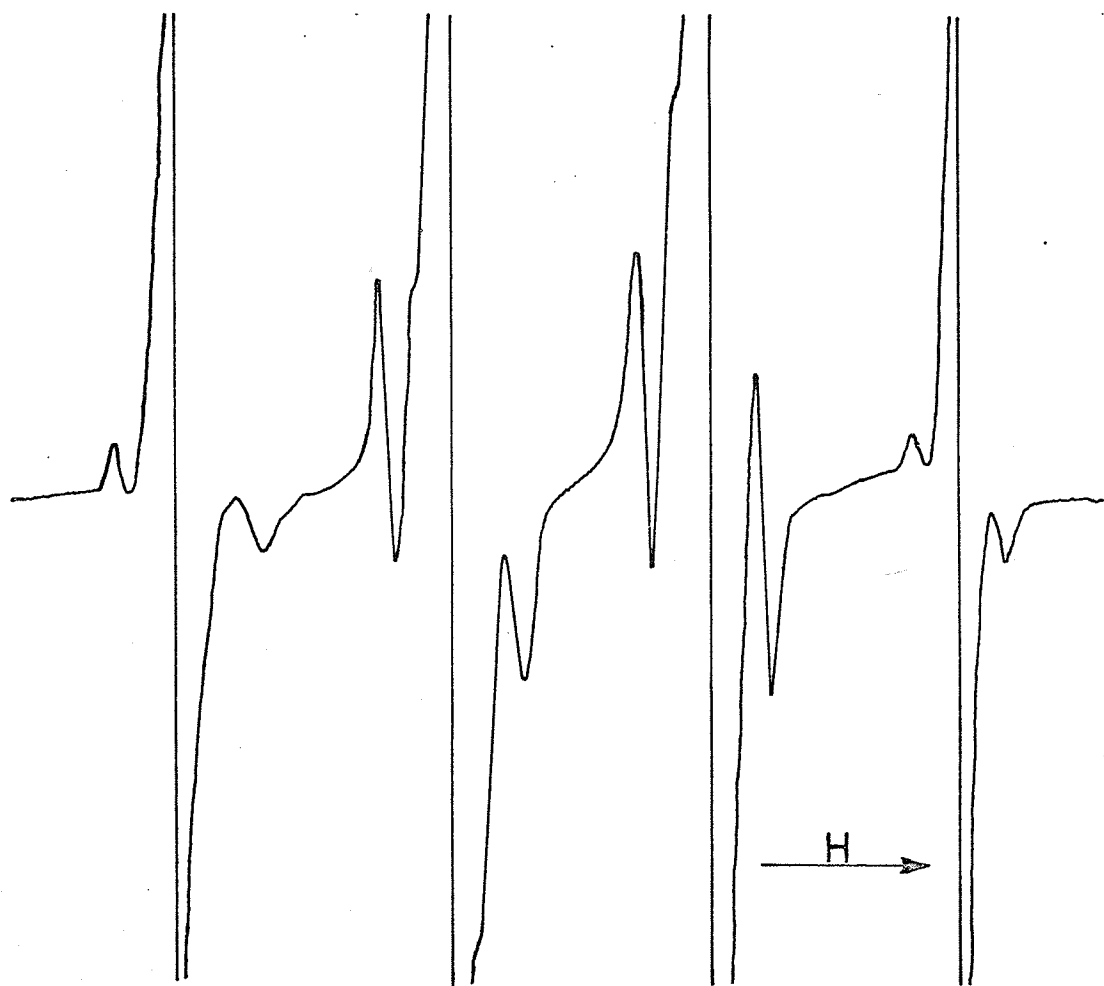
The methyl radical was also observed and probably results from the cleavage of the Si-CH₃ bond. The observed triplet may arise from the abstraction by the methyl radical of a hydrogen atom from the Si-CH₃ group leaving an orientated Si-CH₂ group. A contribution to the central line of the triplet due to the species ≡Si• is also postulated.

C. Satellites of The Four Main Proton Lines of the Methyl Radical

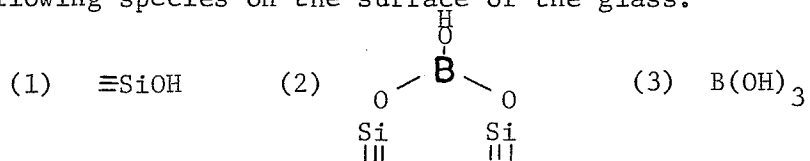
In preliminary work^{80,81} these splittings were observed and were referred to as radical x (see section B of this chapter). This first paragraph will be devoted to presentation of preliminary results obtained on radical x (See Fig. 2.4).^{80,81} It was first thought that Me' decayed into radical x, but on samples pretreated at higher temperatures it was noticed that x did not appear as Me' disappeared. x was found to be prominent on glass samples outgassed at approximately 450°C prior to adsorption, but almost undetectable on samples pretreated at 700°C or above for prolonged periods of time. The intensity ratio ^x/Me decreased as Λ exceeded 10%. In our preliminary work x was interpreted as being due to the methyl radical interacting with a nucleus of spin 3/2 giving four additional lines. At this point it must be noted that Boron-11 has a nuclear spin of 3/2 and a natural abundance of 81.17%. It was argued that boron impurities in p.V.g. may form active sites or inactive boron oxide networks on silicate surfaces, the former being responsible for catalytic activity. The methyl radical at an active boron site may form a weak one-electron bond with boron giving rise to an

Fig. 2.4

Spectrum of Radical $X^{80,81}$ (using home made X-band spectrometer).



additional four-line structure around each proton hyperfine line of the methyl radical. The hyperfine splitting of this methyl radical at a boron site was measured to be 23.1 ± 0.2 gauss. The Boron-11 splitting was measured to be 2.6 ± 0.2 gauss. (See Fig. 2.4). The boron methyl radical proton coupling constant is slightly smaller than the regular methyl radical indicating a shift of a small amount of spin density to the boron-11 nucleus. Quoted as proof for this assignment was the fact that maximum catalytic power is obtained when a surface of silica-alumina is dehydrated at approximately 450°C . In another experiment a sample of p.V.g. was preheated at a high temperature and then exposed to boron trichloride and then water vapor.⁵⁴ The resulting surface was outgassed at 425°C , leaving, presumably, the following species on the surface of the glass.



Adsorbing methyl iodide on this surface and then photolyzing gave only the normal methyl radical. It was therefore assumed that the boron introduced to the surface in this way was of an inactive nature.

Recent work on this topic, as well as reinterpretation of previous work, leads to conclusions which are different from those outlined above. With the Varian E-3 spectrometer better spectra of the radical x have been obtained (Fig. 2.5). A "stick" diagram of the satellites (or radical x) around each proton line in the methyl radical spectrum is presented (Fig. 2.6). From Fig. 2.6 it can be seen that in some cases two other satellites (C and C') have been noticed in addition to the four shown in Figure 2.5.

Fig. 2.5

More recent spectrum of radical X (using Varian
E-3 E.S.R. spectrometer).

100

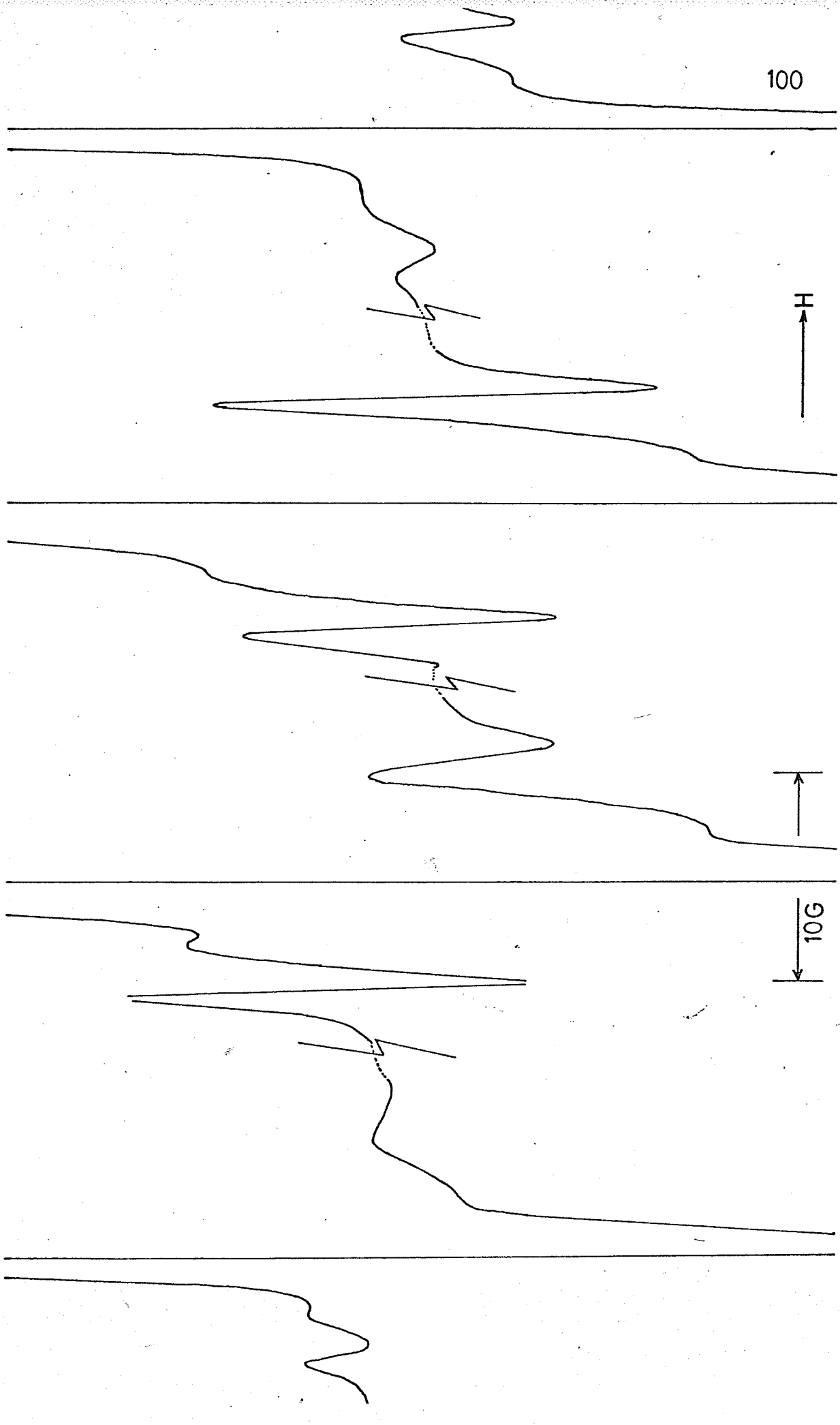
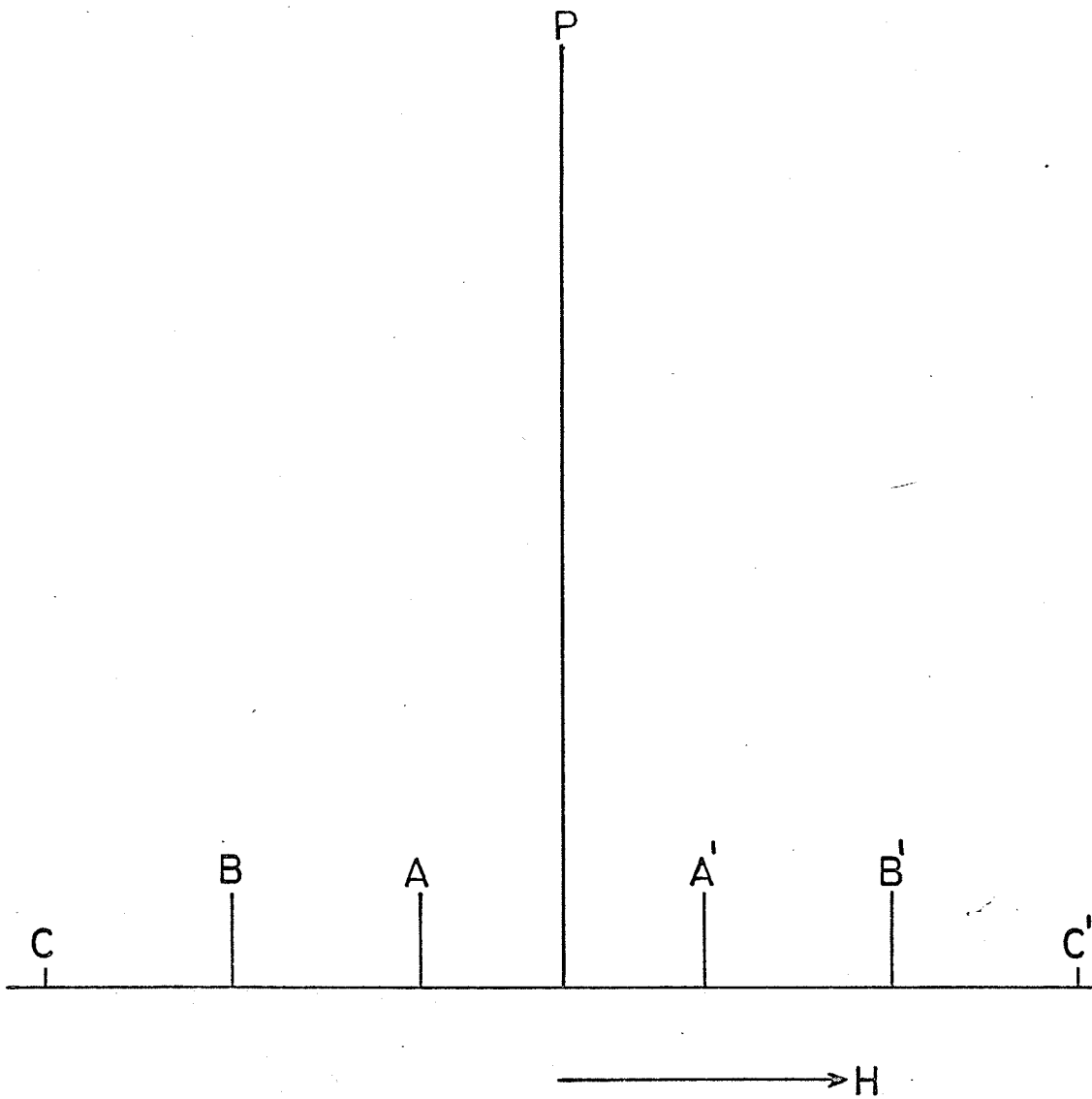


Fig. 2.6

"Stick" diagram of the satellites around one of the four proton lines P.



Two cells (or samples) were oxidized at 750°C to 800°C for 17 hours and then heated in vacuum at the same temperatures for 22 hours. To one sample water vapor was added (in several doses) at 141°C while to the other sample heavy water (99.7 atom %) was added in several doses at the same temperature. Both samples were then heated in vacuum for 11 1/2 hours at 395°C. Methyl iodide was adsorbed on both samples to a concentration of 5% of a monolayer. Both samples were U.V. irradiated for one hour at 77°K with the full focused arc of a Hanovia S-100 Alpine burner. The sample that had been treated with water shows small satellites (four of them) while the sample that had been treated with heavy water shows hardly any evidence of satellites (Fig. 2.7). This fact became obvious after adjusting the gain so that the methyl radical signals from both samples were of comparable magnitudes. The methyl radical lines were found to saturate much easier on these more hydrated surfaces. Some evidence for satellites 10-12 gauss on either side of the main proton lines was observed.

Two further samples were then made. Both were heated in oxygen at 550°C for 17 1/2 hours followed by evacuation at room temperature for 24 hours. One sample was dosed with heavy water several times at 164°C while the other was dosed with light water several times at 164°C. Then they were both heated in vacuum at 425°C for 6 hours. Methyl iodide was then adsorbed on both surfaces to a concentration of 5% of a monolayer. Both samples were then irradiated for one hour at 77°K as were the last two samples. The sample that had been treated with water vapor exhibited large satellites while the sample that had been treated with heavy water showed hardly any satellite structure at all (Fig. 2.8). Let us define the proton lines as 1, 3, 3a, and 1a on increasing H₂O. Line 1 is the low field proton line while

Fig. 2.7

Comparison of Satellites Observed for High Temperature
Degassed Surfaces Followed by Treatment with H_2O and D_2O
at $400^\circ C$.

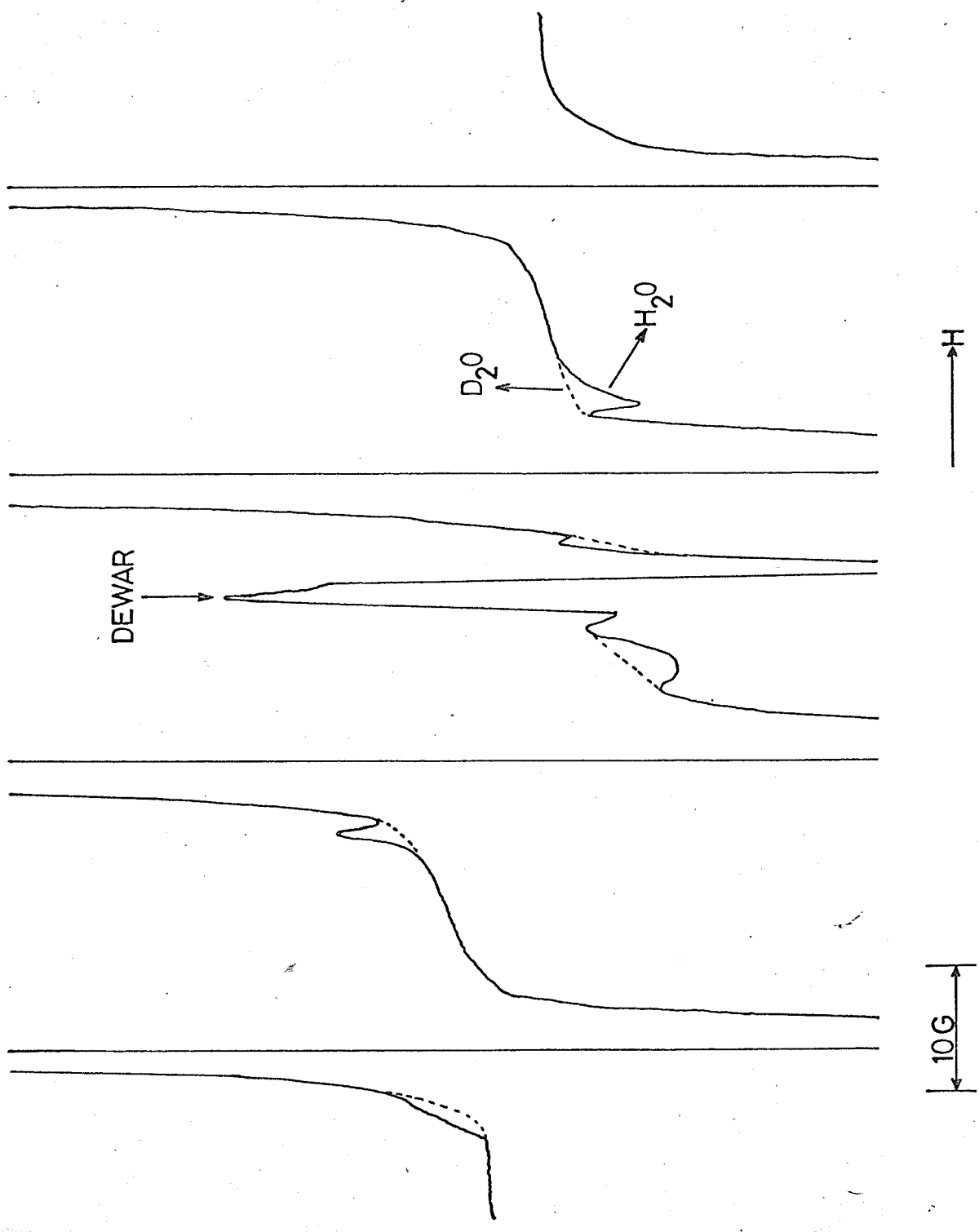
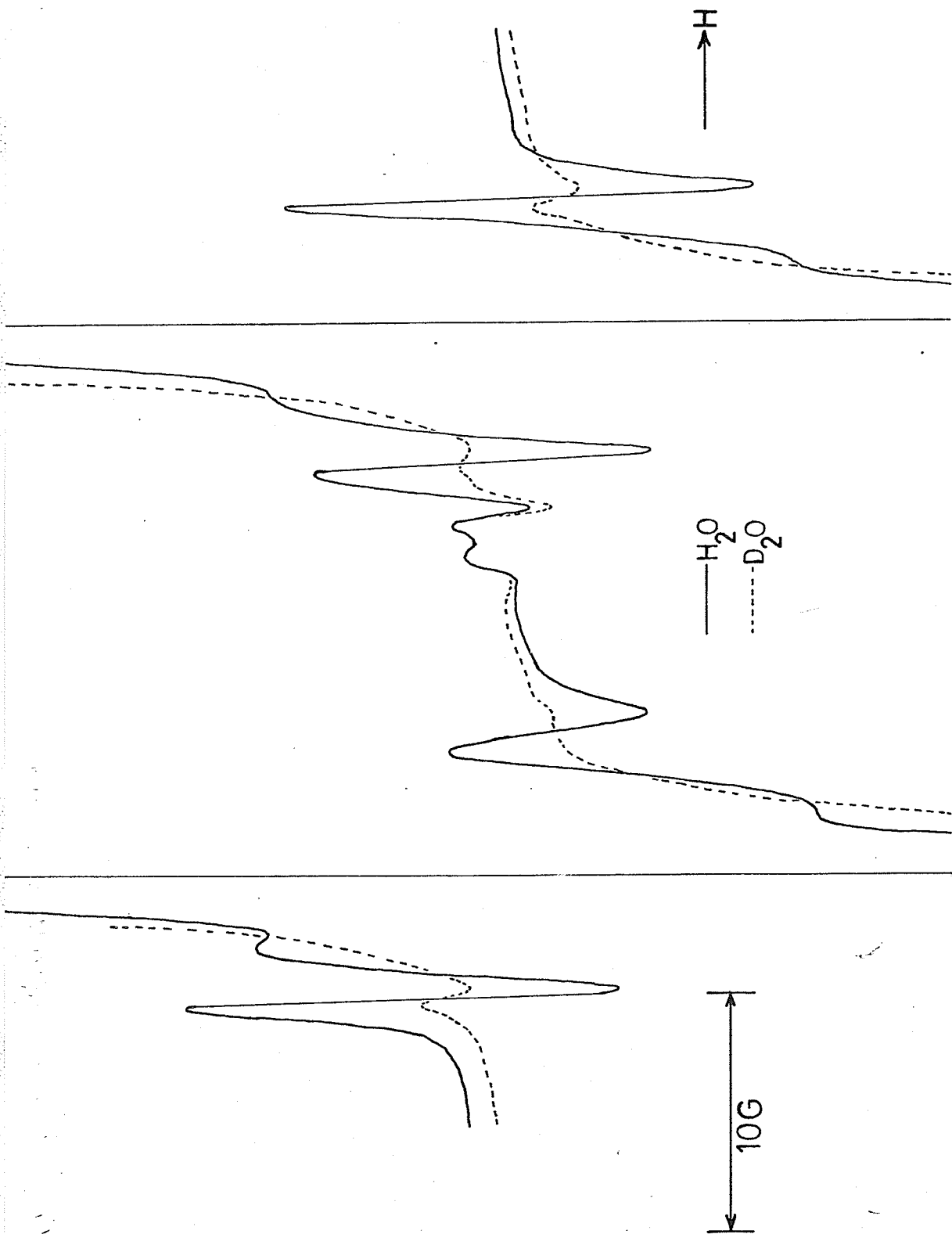


Fig. 2.8

Comparison of Satellites Observed about Proton Lines
3 and 3a for Low Temperature Degassed Surfaces followed
by Treatment with H_2O and D_2O at $400^\circ C$.



line 1a is the high field proton line. In some spectra (very high gain) satellites C and C' were noticed. Satellites C and C' were broader and smaller than B and B' (Fig. 2.9). From Fig. 2.8 one can observe that:

(1) Satellites B and A of line 1 and 3 have larger amplitudes than satellites A' and B'.

(2) Satellites A and B of lines 1a and 3a have smaller amplitudes than A' and B'.

It may also be observed, from some spectra of the methyl radical stabilized on the sample that had been treated with water vapor, that satellites A and A' are broader than B and B'. A and A' are never completely resolved from the proton lines. For any particular proton line the splitting between the satellites and the proton line indicate that satellites A and A' are not related to satellites B and B'. The magnitude of the splittings between C and C' and the proton lines are about twice the magnitude of the splittings between B and B' and the proton lines. When scanning over a larger magnetic field range (i.e. compressing the total spectra), A and A' appear to have slightly larger amplitudes and intensities than B and B'. Satellite B increases in linewidth on increasing field, while B' decreases in linewidth on increasing field. Neither the satellites (looking at B and B') nor the proton lines saturate even at a power level of 270 mw. Both satellites and main proton lines seem to have similar saturation properties. The satellites and the proton lines increased in amplitude up to 8.0 mw and then decreased in amplitude on increasing the power above 8.0 mw. Only general trends on saturation are noted since accurate measurements were not attempted. Average values of the measurable splittings (at 77°K) of the satellites from the main proton lines are shown in Table 2.4.

Fig. 2.9

Spectrum Exhibiting the Satellites C and C' About
Proton Line 3.

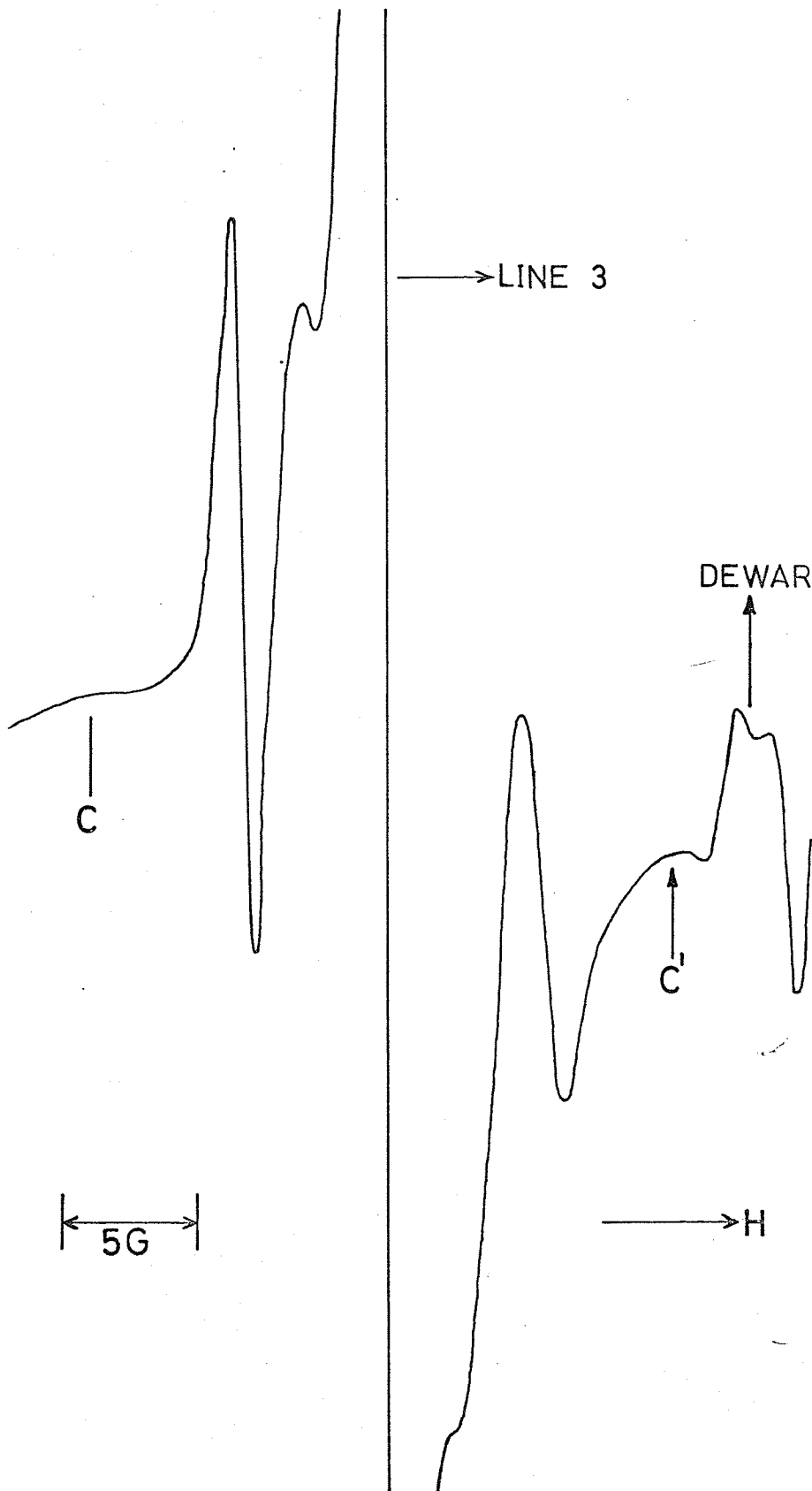


TABLE 2.4

Average Splittings of Satellites From Main
Proton Lines at 77°K.

PROTON LINE	FIELD VALUE (GAUSS)	SPLITTINGS (GAUSS)						
		C	B	A	A' B'	C'	B + B'	
1	3234	-	4.59	2.13	-	6.17	-	10.76
3	3257	10.65	5.12	2.6	-	5.83	11.6	10.95
3a	3280	-	5.78	-	-	5.25	-	11.03
1a	3303	-	6.48	-	-	4.84	-	11.32

Linewidths were only measurable for satellites B and B'. The relative amplitudes of B and B' to the main proton lines were also measured. The averages of the linewidths and relative amplitudes for satellite lines B and B' are shown in Table 2.5.

TABLE 2.5

Average Linewidths And Relative Amplitudes of
B and B' at 77°K. P-P

PROTON LINE	FIELD VALUE (GAUSS)	LINEWIDTHS (G) P-P		RELATIVE AMPLITUDES	
		B	B'	B	B'
1	3234	0.93	2.13	0.036	0.015
3	3257	0.82	1.68	0.038	0.019
3a	3280	0.98	0.90	0.018	0.025
1a	3303	1.40	0.84	0.013	0.027

D. Resolving Proton Lines 3 and 3a.

The temperature dependence studies to be discussed in the next chapter were performed using a modulation of one gauss in order to increase the accessible temperature range. Here, however, a series of experiments were performed in order to see if decreasing the modulation from one gauss would have any effect on the methyl radical lines.

The effect of decreasing the modulation (at 77°K) on the linewidth of line 3a is shown in Table 2.7.

TABLE 2.7

Linewidth of Line 3a as a Function of Modulation

MODULATION (GAUSS)	LINEWIDTH (GAUSS) P-P	SCAN RANGE (GAUSS)
1.000	0.760	±5
0.800	0.667	±5
0.630	0.553	±5
0.500	0.510	±5
0.400	0.482	±5
0.250	0.476	±5
0.160	0.480	±5
0.100	0.485	±5
0.100	0.468	±2.5
0.010	0.453	±2.5
0.005	0.458	±2.5

Below a modulation of 250 mg. line 3a is seen to resolve into two lines. The resolution of line 3a increases as one decreases the modulation from 250 mg to 5 mg (Fig. 2.10). At 5 and 10 mg modulations a shoulder (an unresolved line) is noticeable on line 3 (Fig. 2.10). The linewidths

Fig. 2.10

Spectra of Unresolved Second-Order Splittings of
Lines 3 and 3a (recorded at 77°K).

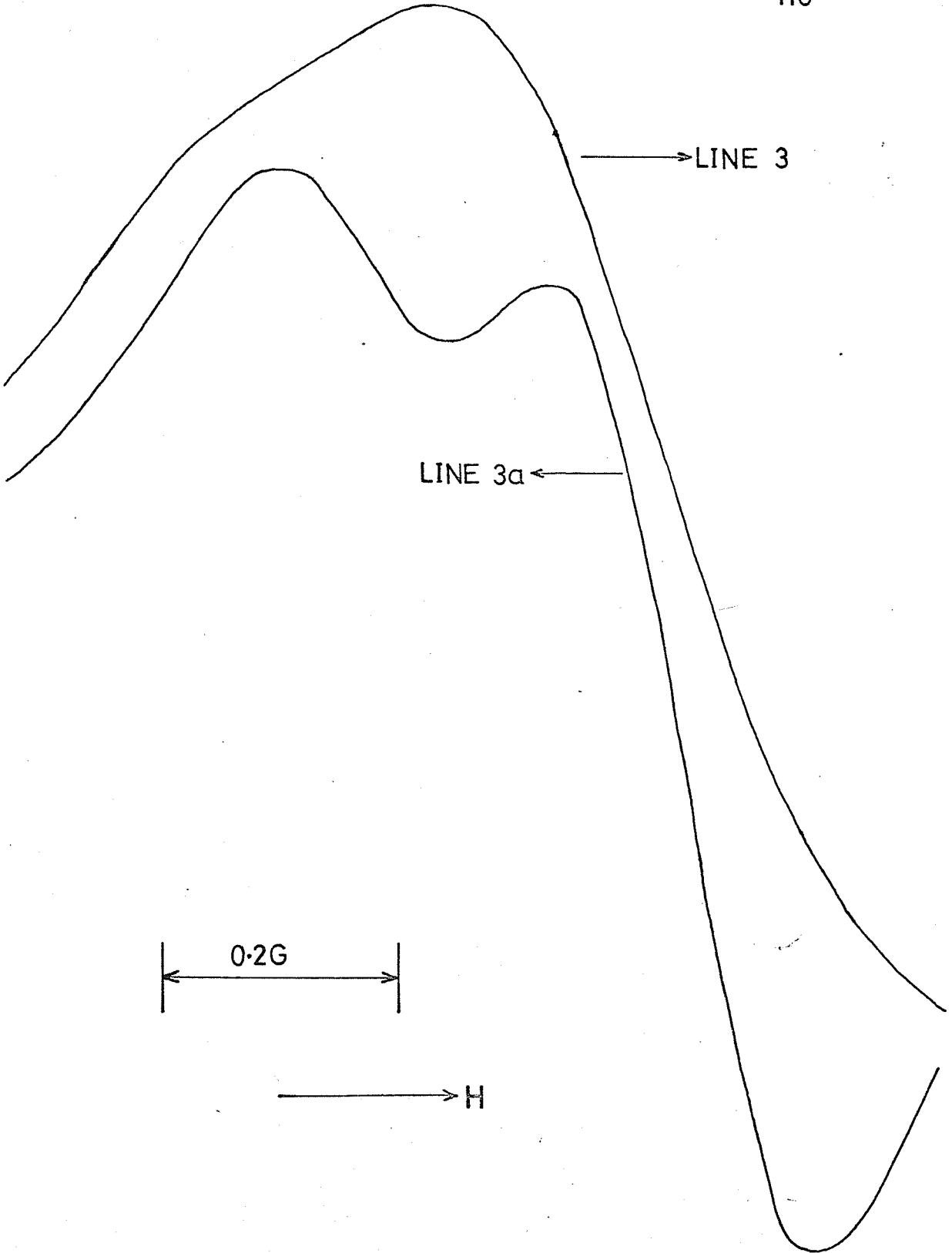
110

LINE 3

LINE 3a

0.2G

H



of the four proton lines at 77°K measured using a modulation of 100 mg and a scan range of ± 5 gauss are:

Line 1	0.825 gauss
Line 3	0.605 gauss
Line 3a	0.485 gauss
Line 1a	0.478 gauss

Three measurements were made at 77°K with a very low modulation (5 mg) on the resolution of line 3a into two component lines. The splitting of these two component lines were 231 mg, 215 mg and 228 mg. The average of these three splittings is 225 mg. The splitting of the two component lines of line 3 is much less accurate because of poor resolution due to the increased linewidth of line 3. This splitting, however, has been measured to be 200 mg and 243 mg. The average of these two values is 221 mg. Shoulders were never noticed on lines 1 and 1a.

E. A Study of the Splitting of the Proton Line
3a and of the Linewidths of 3 and 3a on Warming
and Cooling.

The splittings and linewidths of 3 and 3a were measured at 77°K. The sample (high temperature pretreatment and low Λ) was then warmed up and then recooled. The splittings and the peak-to-peak linewidths were then measured at 77°K. This process was repeated several times on warming to different temperatures and then recooling to 77°K. The results for line 3a are shown in Table 2.8 (measurements made using 100 mg. modulation and small scan ranges).

TABLE 2.8
 Splitting and Linewidth of Line 3a on Warming
 And Cooling Cycles

MEASUREMENT TEMP. (°K)	TEMP. WARMED SAMPLE TO (°K)	COMPONENT SPLITTING AT LOWEST TEMP. (G)	COMPONENT SPLITTING MEASURED (G)	LINEWIDTH LOWEST TEMP. (G)	MEASURED LINEWIDTH (G)
77	77	0.2063	0.2063	0.4569	0.4569
77	132	0.2063	0.2113	0.4569	0.4500
125.5	125.3	0.2063	Poor Resolution	0.4569	0.4556
160.4	160.4	0.2063	Poor Resolution	0.4569	0.4606
77	160.4	0.2063	0.2188	0.4569	0.4425
Sample Stored Overnight at 77°K					
77	160.4	0.2063	0.2265	0.4569	0.4605
77	193	0.2063	0.2200	0.4569	0.4450
77	193	0.2063	0.2265	0.4569	-

The results for line 3 are shown in Table 2.9 (only Linewidth measurements were made due to poor resolution of 2 component lines of line 3).

TABLE 2.9

Linewidth of Line 3 on Warming and Cooling Cycles.

MEASUREMENT TEMP. (°K)	TEMP. WARMED SAMPLE TO (°K)	L.W. AT LOWEST TEMP. (G)	MEASURED L.W. (G)
77	77	0.5694	0.5694
77	132	0.5694	0.5419
125.5	125.5	0.5694	0.5244
77	160.4	0.5694	0.5069
Stored Overnight At 77°K			
77	160.4	0.5694	0.5580
77	193	0.5694	0.4950
77	193	0.5694	0.5113
77	300	0.5694	0.5188
Single Result For Line 1 Below			
77°K	160.4	0.8250*	0.7700
Single Result for Line 1a Below			
77°K	160.4	0.4780*	0.4088

*See Section 3-D of this chapter.

4. Discussion

The relative amplitudes of the four proton lines has been stated to approach the binomial value as the surface coverage of methyl iodide increases (at 77°K). It has also been shown (see chapter V) that as Λ increases, the temperature at which radical decay begins decreases. For large Λ (many monolayers), many of the methyl radicals are not trapped on the surface but are trapped in a methyl iodide matrix which does yield very nearly the binomial relative intensities.⁷⁹ The methyl iodide matrix does not present a wide variety of trapping sites and therefore the relative amplitudes are close to the binomial values. The surface of p.V.g. does present many different trapping sites (potential wells) which leads to asymmetric lines and non-binomial relative amplitudes. The linewidths measured for the methyl radical trapped in a methyl iodide matrix are much larger than for the same radical trapped on the surface of p.V.g.⁷⁹ This means that the radical trapped in a methyl iodide matrix at 77°K is undergoing a stronger but a more symmetric interaction with the matrix than the radical trapped on p.V.g. at 77°K. The trapping sites (or cages) in the methyl iodide matrix disappear very quickly on increasing the temperature. This fact provides a reason for radical decay beginning at lower temperatures when the surface coverage is high.

A. Radical Build-Up Studies

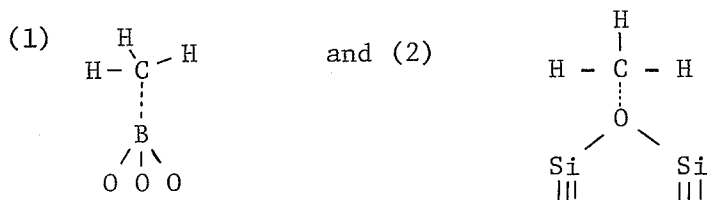
By referring to Fig. 2.2, one can see that the methyl radical concentration does approach a saturation value asymptotically. In the case plotted, the build-up should have been monitored for a much longer period of time in order to show this idea more clearly. The relative amplitudes were monitored on build-up (Table 2.2) with the

intent of showing that they would change on build-up indicating a wide variety of trapping sites. As one can observe this attempt was not successful.

A radical build-up study was also performed on a chlorinated p.V.g. sample with 6% of a monolayer of methyl iodide. This sample had previously been discharged and the radical build-up was found to be very slow. Table 2.3 shows the relative amplitudes as a function of irradiation time. On studying Table 2.3 it is observed that the relative amplitudes do diverge from the binomial values as the irradiation time increases. This is evidence for multiple trapping sites and for the concept that these multiple trapping sites contribute to deviation from the binomial values.

B. The Radical Me^\cdot

Although the conditions necessary for Me^\cdot production are not quite clear there are several consistencies which may be noted and which make plausible assignments for Me^\cdot possible. Two assignments which are possible are:



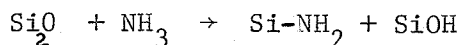
The arguments in favour of these assignments are given below.

Let us first consider assignment (1) [$\equiv\text{B}\cdots\text{CH}_3$]. The Me^\cdot concentration is known to increase on longer and higher temperature sample pretreatments. The diffusion of boron to the surface of p.V.g. occurs only above 600°C .³⁵ Siloxane groups are known to be present

at much lower temperatures. Samples of p.V.g. are known to differ in boron content and therefore Me⁺ may not occur on every sample with similar heat pretreatments. Siloxane bridges do, however, exist on every sample of p.V.g. and every sample with similar temperature pretreatments should yield Me⁺. Low³⁶ has studied the sorption of water on dry p.V.g. He determined that water adsorbs primarily on the surface boron atoms with the formation of $\equiv\text{BOH}$ and $\equiv\text{BOH}_2$ structures. The silica network was found to be hydrophobic. There was, however, a slight reaction of water with the SiO_2 groups to form SiOH groups. Low postulated that the substitution of boron for silicon in the silica network of p.V.g. created strains in the siloxane bridges in the vicinity of the boron atom. Water, therefore, could adsorb on the boron and then migrate to a local strained SiO_2 bridge and react. Boron in p.V.g., however, is three-fold coordinated.^{36,92} Therefore, the substitution of boron should induce minimal strain in the surrounding silica network. Since on high temperature treatments, boron diffuses to the surface, islands of B_2O_3 could be formed. These islands could act as sites for water adsorption. Therefore silanol formation may only occur in the vicinity of these islands. Low³⁸ has also studied I.R. bands assignable to the $\equiv\text{B:NH}_3$ complex. He postulates that this complex may be a precursor to dissociation and a more tightly bound species. With reference to an experiment which was described above i.e.: a sample which had yielded large quantities of Me⁺ was warmed to room temperature and water vapor was added. On reirradiating this sample only Me appeared. Since the siloxane network is hydrophobic and in view of Low's work outlined above [e.g. the reaction of H_2O only with boron surface species] one

could postulate no change in the SiO_2 network while the $\equiv\text{B}$ sites are reacting to form BOH and BOH_2 structures. This work tends to support assignment (1). Also it is known that if a sample, already having yielded Me' , is reirradiated, Me' will reappear. This may mean that the disappearance of Me' is not due to reaction with the adsorption site but due to migration and then reaction or reaction with close proximity parent molecules or other radicals.

Some observation may fit both assignments (1) and (2). For example, Me' is produced in large observable concentrations when Λ is very small. (Best Me' spectra observed when $\Lambda < 1\%$). When Λ is large sites (1) and (2) may be totally occupied or the methyl radical may not be able to reach sites (1) and (2) due to steric hindrance. All infrared and other surface studies agree that the main adsorption sites on p.v.g. are the surface silanol groups (Bronsted sites) and the Lewis acid sites ($\equiv\text{B}$). The only times when the siloxane bridges may be active is when they are strained or when higher temperature adsorption studies are carried out. Normally, however, annealing of strained siloxane groups occurs on high temperature treatment. Also, adsorption studies at elevated temperatures are of the chemisorption, followed by decomposition, variety. For example,



Me' is more highly orientated than Me because: (1) the linewidth of Me' lines are larger than those of Me , (2) the lines are asymmetric and (3) the proton splitting of Me' is smaller than for Me . The fact that $|a_{\text{Me}'}^{\text{H}}| < |a_{\text{Me}}^{\text{H}}|$ indicates unpaired spin

density transfer to the surface site. From adsorption studies the boron Lewis acid site is a known acceptor while the siloxane groups are not known as electron acceptors except under the conditions outlined above (strained or high temperature adsorption).

There was one experiment outlined previously that may favour the following mechanism: Me^\cdot initially adsorbed on the B_2O_3 islands. On migration the Me^\cdot reacts with surrounding strained siloxane bridges giving SiOCH_2^\cdot radicals and SiOH groups. The experiment supporting this mechanism was as follows. An incompletely oxidized sample (which had methyl iodide previously adsorbed on it) was irradiated and yielded Me^\cdot and R-CH_2^\cdot spectra. Only after prolonged irradiation did Me^\cdot appear. In order to believe that the R-CH_2^\cdot spectra is a result of the above mechanism one must ignore the presence in the sample tube of hydrogen, mercury and products of incomplete combustion.

The experiment does show that the methyl radical prefers the Me^\cdot site due to its rapid build-up at the beginning of irradiation. The mechanism of Me^\cdot decay at liquid nitrogen temperatures is not understood.

It is felt that the above arguments show Me^\cdot is most probably at site (1) and not at site (2) as first suggested.⁸⁰ An attempt to see Me^\cdot on pure silica aerogel should be made.

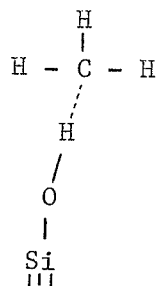
C. Satellites of the Four Main Proton Lines of the Methyl Radical.

Fig. 2.6 shows a "stick" diagram of the satellites around each of the four methyl radical lines. These satellite lines were previously assigned to the interaction of a methyl radical with

After methyl iodide adsorption and photolysis at 77°K the resulting E.S.R. spectrum was studied. The satellite lines did not appear. Two further experiments did show, beyond any doubt, that the boron-11 assignment is not valid and that the splittings are caused by surface protons only. These two experiments are the light and heavy water experiments outlined in section 3-C of this chapter. The satellites were only seen for the samples which had been treated with light water. Also, the sample pretreated at higher temperatures before addition of light water vapor yielded smaller satellites than the sample pretreated at low temperatures before addition of light water vapor. This supports the idea that high temperature dehydroxylation is almost irreversible and that water vapor adsorption occurs mainly at adjacent hydroxyl groups. In actual fact the satellites seen for the heavy water treated sample were more than a factor of 10 smaller than for the sample treated with light water. The fact that the satellites appeared at all on the heavy water treated sample could be due to incomplete deuteration and/or a light water impurity in the heavy water used. Some unresolved splittings were seen about the methyl radical lines on the deuterated samples, particularly about the narrow lines 3a and 1a. These could be due to similar mechanisms responsible for the satellites depicted in Fig. 2.6 but because $\frac{|a^H|}{|a^D|} = 6.514$ they are unresolved.

What types of interactions with the surface protons could lead to these satellites? From splitting measurements and from the temperature dependence studies of these splittings, A and A' do not seem to be related to B, B', C and C'. From adsorption studies, the main adsorption site for lone pair aromatic compounds takes

the form of a hydrogen bond with surface silanol groups. Therefore, splittings A and A' may be due to a small amount of spin delocalization from the π orbital of the methyl radical to the hydrogen atom upon which this radical is stabilized. (a type of hydrogen bond).



This type of adsorption, at low temperatures, would lead to the splitting of each methyl radical line into two lines (A and A'). The size of the splitting would be dependent upon the unpaired spin density transferred. The size of this spin density transfer is small because the splitting between A and A' is about 4 to 6 gauss which would mean a transfer of about 1% of the unpaired spin density originally in the carbon pi orbital of the methyl radical. The reason for the assignment of A and A' to this type of adsorption is due mainly to the fact that on increasing the temperature these splittings seem to disappear (or become unresolvable). This would be consistent with the fact that the strength of this "hydrogen bond" would decrease with increasing temperature.

The splittings B, B' could be reasonably assigned to a weak magnetic dipole-dipole interaction coupling the electron spin to a neighbouring nuclear spin. The satellites would then correspond to

a change in the spin state of a neighbouring nucleus concurrent with the change in spin state of the electron (forbidden Spin-Flip transitions).⁹⁶ In this case B and B' would be interpreted as the occasional concurrent spin flip of the electron and a nearby proton because of a magnetic dipole-dipole coupling. B and B' are not equally spaced from the main line by $g_N \beta_N H$ as would be expected from theory.⁹⁶ A measurement of the relative amplitudes of the satellites to the main line allows a calculation of distance of the proton from the unpaired electron (r_{eff}). If each unpaired electron has n nearby protons at the same distance, this distance would be $\frac{1}{n} \times r_{\text{eff}}$. Since the satellite intensity is proportional to $1/r^6$, it is relatively insensitive to all but the nearest protons. A second set of satellites ($1/r^{12}$ intensity dependence) may be observed corresponding to two neighbouring protons concurrently changing state. A third set of satellites ($1/r^{18}$ intensity dependence) may be observed corresponding to three neighbouring protons concurrently changing state. The calculated values of the satellite separation from the main lines for magnetic field strengths of 3030 and 3390 are 4.6 and 5.2 gauss. One, two and three neighbouring protons concurrently changing state have been observed.^{97,98,99} In most observations of these satellites the measured splittings are larger than those calculated. Rogers and Kispert,⁷⁵ while studying the methyl radical in irradiated single crystals of sodium acetate trihydrate, noticed two satellites spaced 5.6 ± 0.2 gauss on either side of the main methyl radical lines. The low field satellite lines were observed

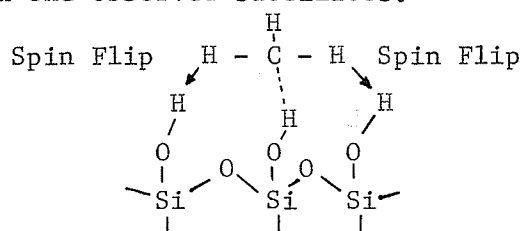
to have larger amplitudes than the high field satellite lines. This trend was noticed previously in another system.⁹⁷ Rogers and Kispert also noticed at high gain a second set of satellite lines, with much lower intensities, spaced 11.2 ± 0.2 gauss from the main lines. They attributed these satellite lines to spin-flip type transitions due to dipole-dipole couplings with protons of the water of crystallization.

Satellites C and C', much smaller and much broader than B and B', are seen only at very high gains. The splitting of satellites C and C' from the main line are about twice the splittings of B and B' from the same main line (See Table 2.4). Therefore satellites C and C' are assigned to spin-flip transitions of two neighbouring protons concurrently.

Let us note some of the differences of our system from the others already mentioned.^{75,97-99} Satellites A and B of lines 1 and 3 have larger amplitude than the high field satellites A' and B' whereas satellites A and B of lines 1a and 3a have smaller amplitude than the high field satellites A' and B'. [There is a change on going from positive M values (low field) to negative M values (high field) where M is the total nuclear spin quantum number]. Satellite B increases in linewidth on increasing H_0 while B' decreases in linewidth on increasing field. Lines B and B' have similar saturation properties as the main methyl radical lines. The saturation properties of spin-flip satellites are not well defined. The splitting of B increases on increasing H_0 (4.59 gauss for line 1 to 6.48 gauss for line 1a). The splitting of B' decreases on increasing H_0 (6.17 gauss for line 1 to 4.84 g for line 1a).

The total splitting ($B + B'$) increases on increasing H_0 (10.76 gauss for line 1 to 11.32 gauss for line 1a). The amplitudes of satellites B and B' relative to the main lines vary from 0.015 to 0.038. The total splitting ($B + B'$) for line 3a decreased from 11.03 gauss to 10.67 gauss on going from 77°K to 201°K. The same trend was noticed for the total splitting ($B + B'$) for line 3. (10.95 gauss at 77°K to 10.65 gauss at 178°K). On increasing temperatures the splitting of B' (line 3) decreased more than the splitting of B (line 3). On increasing temperatures the splitting of B (line 3a) decreased more than the splitting of B' (line 3a). At 201°K the splitting of B was approximately equal to the splitting of B' (line 3a) [Table 2.6]. Some of the above observations may not have been observed in other systems because in those systems the linewidths were generally much larger. Measurements in these systems would not be nearly as accurate. Another possible reason could be that our system presents many more trapping sites than the previous systems studied (i.e. single crystals and low temperature glasses).

Therefore the following two dimensional model may suffice to explain the observed satellites.



Many other models could be imagined in which close proximity protons would be available for concurrent transitions since the surface of p.v.g. is not well defined. The question may be asked: why is A and A' not observable for methyl radicals trapped on high temperature

pretreated glasses? Relative amplitude and linewidth studies indicate that the methyl radical is more strongly bonded to the surface of low temperature treated glass (See chapter IV). Spectra of methyl radicals on dry p.V.g. do show unresolved shoulders which may mean that the "hydrogen bond" between the π -orbital of the methyl radical and the surface free hydroxyl group is not as strong as for wet p.V.g.

D. Resolving Proton Lines 3 and 3a.

Second-order splitting of alkyl radicals in solution has been treated theoretically by Fessenden.¹⁰⁰ Fessenden achieved partial resolution of the second-order splitting (0.23G) of each of the central pair of lines while studying methyl radicals in liquid methane.⁷¹ In this study we have also achieved partial resolution of the second-order splitting of the two central lines. The asymmetry of the whole spectra allowed better resolution of the second-order splitting for the high field 3-intensity line (line 3a) because the linewidth of line 3a is smaller than the linewidth of the low field 3-intensity line (line 3). The measured values for the second-order splitting are:

Line 3a : 0.225G

Line 3 : 0.221G

E. Second-Order Splitting of Line 3a and Linewidths of Lines 3 and 3a on Warming And Cooling.

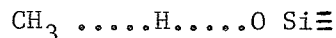
On sample warming the resolution of the second-order splitting for line 3a decreased. But on warming followed by cooling the resolution of the second-order splitting for line 3a increased.

Considering line 3a, it is observed that the linewidth decreased on warming and then recooling to liquid nitrogen temperatures. (Table 2.8). It is also noticed that on storing the sample at 77°K overnight, the linewidth of line 3a increased to the value measured at 77°K before the warming and cooling cycles were begun the day before. These same trends were more noticeable for line 3 (Table 2.9).

The above results mean that much of the linewidth of the methyl radical lines is due to different orientations of the radical on the surface (many different potential wells and therefore many different trapping sites). Also, diffusion of radicals from one potential well to another is possible at liquid nitrogen temperatures (possibly by a quantum mechanical tunnelling mechanism). The contribution of different radical orientations to the linewidths will be discussed in Chapter IV.

5. Conclusions

The radical Me' has been assigned to the model $\equiv B \cdots \cdots CH_3$. The satellites A and A' have been attributed to a "hydrogen bond".



The satellites B and B' are probably due to the simultaneous flipping of the electron and a nearby proton. The satellites C and C' are probably due to the simultaneous flipping of the electron and two nearby protons. It has also been shown that dehydroxylation of p.v.g. at high temperatures is virtually irreversible. The second order splitting of the methyl radical has been observed and measured. Multiple trapping sites (radicals in different orientations and in different potential wells) are believed to contribute greatly to the linewidths. There is evidence for radical diffusion at liquid nitrogen temperatures even though there is no measurable decay.

CHAPTER III
TEMPERATURE DEPENDENCES OF STABILIZED
METHYL RADICALS

1. Introduction

This study was carried out with two purposes in mind. The first being to make a comparison between experimentally obtained temperature dependences of the hyperfine interactions in the methyl radical stabilized on the surface of p.V.g. and the temperature dependences calculated by Schrader¹⁰¹ for methyl radicals free of any interactions with the surroundings.* Schrader's calculated temperature dependences are based on incomplete orbital following in the A_2'' vibrational mode (out-of-plane bending mode) of the methyl radical.¹⁰² DMS suggested that a study of the hyperfine interactions in the methyl radical stabilized on a surface over a wide temperature range (instead of several studies in different media over smaller temperature intervals) would eliminate solvent effects, and lattice interactions, and would therefore lead to consistent temperature coefficients over the whole temperature range. The second purpose of this study was to evaluate the usefulness of some E.S.R. parameters in characterizing the surface of porous Vycor glass (p.V.g.). It is interesting to note that only one other temperature study has been carried out on the hyperfine interactions in the methyl radical.⁷⁴ This was performed in aqueous solution over a temperature range of 60°C (0°C to 60°C). Poor signal-to-noise ratios and large linewidths were reported in that study. The linewidths increased from 0.8 g at high temperatures to 1.1 gauss at lower temperatures. Second-order splittings were not resolved due to the large linewidths. The data was fitted to a straight line relation.

*Reference 101 hereafter referred to as DMS.

$$|a^H| = [22.674 \pm 0.003 - (2.1 \pm 0.2) \times 10^{-3} (t - 25)] \quad (3-1)$$

The temperature coefficient in the room temperature range was found to be

$$\left(\frac{d|a^H|}{dt} \right) = -2.1 \text{ mg}/^\circ\text{C} \quad (3-2)$$

$$= -0.009\%/^\circ\text{C}$$

Fessenden and Schuler⁷² have reported a study of the fluorine hyperfine splitting in the trifluoromethyl radical between -130°C and -200°C . The temperature dependence of the trifluoromethyl radical was found to be $+0.0065\%/^\circ\text{C}$. The fluorine h.f.s., at any particular temperature, was found to depend on the solvent. An outline of the theories pertaining to indirect hyperfine couplings and to the temperature dependences of these couplings will now be presented.

A. Proton Hyperfine Splittings in Aromatic Systems

McConnell^{103,104} has shown that an electron spin polarization associated with an odd electron in a π -molecular orbital in an aromatic free radical can, through an atomic exchange coupling mechanism, produce an appreciable resultant electron spin polarization in the S-atomic orbitals at the aromatic protons. A planar methyl radical can be considered as the simplest example (or prototype) of an aromatic system. In solution, all dipolar hyperfine interactions average to zero due to rapid molecular tumbling. Only the Fermi contact interaction can survive this tumbling. If the odd electron in an aromatic free radical is confined to a π molecular orbital, then there is zero odd-electron density at the in-plane aromatic protons and the contact hyperfine interaction is also zero. The observed couplings with the in-plane aromatic protons must therefore involve some second-order (indirect) process. Before McConnell's¹⁰³ treatment several indirect coupling

mechanisms had been suggested: (1) the out-of-plane zero-point hydrogen vibrations (2) excited electron configurations and (3) a similar mechanism to that responsible for the indirect nuclear spin couplings observed in high resolution N.M.R. McConnell^{103,104} has shown that π -orbital electron-spin polarization could be "transmitted" through a strong atomic exchange coupling mechanism to the σ -bonding electron system and that the resulting electron spin polarization in the σ -bonding system is S-orbital-like in the region of the aromatic protons resulting in contact hyperfine interactions. He also showed that this coupling is proportional to the odd-electron density at the adjacent carbon atom.

$$\Delta\nu(\text{H}_j) = \frac{2}{\sqrt{3}} (\rho_j) (f_j) (1420) \text{ Mc/S} \quad (3-3)$$

where $\Delta\nu$ is the hyperfine splitting due to the protons, ρ_j is the electron density at the carbon atom and f_j is the attenuation factor (a measure of the effective penetration of the "odd-electron" into the σ system). Assuming that the factor f_j is approximately the same for all j , i.e. for all aromatic C-H bonds in an aromatic molecule, the observed hyperfine structure will then permit a determination of the relative (odd electron)-(π electron) densities at different carbon atoms in the aromatic molecule. Further assuming that the f_j values are the same for all aromatic C-H bonds in different aromatic molecules, the absolute π -electron densities might be determined from, say, an empirical value taken from $[\text{C}_6\text{H}_6]^-$. Equation (3-3) may be rewritten:

$$a_i^{\text{H}} = Q_{\text{CH}}^{\text{H}} \rho_i^{\pi} \quad (3-4)$$

where a_i^{H} is the h.f.s. of the aromatic proton at carbon atom i (in gauss), ρ_i^{π} is the odd-electron density in the adjacent carbon atom's π orbital and Q_{CH}^{H} is some constant (-22.5g for C_6H_6^-). Q_{CH}^{H} represents

the proton h.f.s. for a spin density of unity in the carbon π orbital. The superscript refers to the nucleus giving rise to the h.f.s. The subscript closest to Q denotes the atom containing the π spin density which is related to the h.f.s. by the Q-factor. The two subscripts together indicate the σ bond which is being polarized by the π spin density. The negative sign of Q_{CH}^H has been confirmed experimentally and values of Q_{CH}^H ranging from -20 to -30 gauss have been observed. Q_{CH}^H is not a fixed constant and does vary from one molecule to another. Q_{CH}^H should be constant for neutral radicals only. The simplest neutral radicals are the alkyl radicals which have been studied by Fessenden and Schuler.⁷¹ Some of their results are shown in Table 3.1.

TABLE 3.1
Empirical Values of ρ^π , Q_{CH}^H , $Q_{C.CH_3}^H$ For Some
Neutral Radicals.⁷¹

RADICAL	ρ^π	a_α^H	Q_{CH}^H	a_β^H	$Q_{CCH_3}^H$
$\dot{C}H_3$	1.000	23.04g	23.04g	----	-----
$CH_3\dot{C}H_2$	0.919	22.38g	24.35g	26.87g	29.25g
$(CH_3)_2\dot{C}H$	0.844	22.11g	26.20g	24.68g	29.25g
$(CH_3)_3\dot{C}$	0.776	-----	-----	22.72g	29.30 g

The only assumption in obtaining the Q_{CH}^H values in Table 3.1 is that the spin density on the central trigonal carbon atom is given by

$$\rho^\pi = (1-0.081)^n \quad (3-5)$$

where n is the number of methyl groups attached. This assumption is

supported by the following evidence: (1) the values of $Q_{CCH_3}^H$, obtained with spin densities from (3-5) and the experimental values of the methyl h.f. splittings, are nearly constant; (2) the value of ρ^π for the ethyl radical (0.919) agrees very well with the result of an extensive molecular orbital calculation ($\rho^\pi=0.911$).¹⁰⁵ It has been shown, experimentally, that Q_{CH}^H changes slightly according to which atoms or groups are bonded to the central trigonal carbon atom and in some series Q_{CH}^H varies considerably. Table 3.2 shows Q_{CH}^H values for a series of radicals CH_3-CH-X .¹⁰⁶

TABLE 3.2
 Q_{CH}^H values For A Series of Radicals CH_3-CH-X ¹⁰⁶

X	a_α^H	$a_{CH_3}^H$	Q_{CH}^H
CH ₃	21.11g	24.68g	26.2g
H	22.38g	26.87g	24.4g
CO-CH ₂ CH ₃	18.45g	22.59g	23.9g
COOH	20.18g	24.98g	23.7g
OH	15.04g	22.61g	19.5g
O-CHO	14.8 g	23.22g	18.7g
O-CH ₂ CH ₃	13.96g	22.28g	18.3g

A constant value (29.25) was assumed for $Q_{CCH_3}^H$ and the methyl splittings were used to obtain ρ_c^π . Then from the a_α^H values, the Q_{CH}^H 's were computed. The variation in Q_{CH}^H values may be due to the fact that all the radicals are not planar. Considering the experimental evidence, the value of Q_{CH}^H can be fixed at

27.0 \pm 1.0 gauss for neutral hydrocarbon free radicals at positions where two carbon atoms and a hydrogen atom are bonded to the trigonal carbon atom of interest.

As has been stated before, Q_{CH}^H may only be taken as a constant for a restricted group of neutral free radicals. Therefore, McConnell's relationship must be extended to apply to charged radicals. It has been found that Q_{CH}^H varies with excess charge E_i^π .

$$E_i^\pi = (1 - q_i^\pi) \quad (3-6)$$

where

$$q_i^\pi = P(\alpha) + P(\beta) \quad (3-7)$$

q_i^π is the total electron density in the π orbital of carbon i . $P(\alpha)$ is the probability density of α -spin in the π orbital of carbon i and $P(\beta)$ is the probability density of β -spin in the π orbital of carbon i . It has been shown, for positive and negative ions of anthracene, tetracene, and pentacene, that at positions with large h.f. splittings, the positive ion hyperfine splittings are larger than those at the corresponding positions in the negative ion. This difference is due to variations in Q_{CH}^H . An extension to the McConnell relationship has been proposed to account for excess charge effects.¹⁰⁷

$$a_i^H = [Q_{CH}^H(o) + K_{CH}^H E_i^\pi] \rho_i^\pi \quad (3-8)$$

where $Q_{CH}^H(o)$ is the value of Q_{CH}^H appropriate for neutral radicals and K_{CH}^H is a constant. Equation (3-8), with negative values of $Q_{CH}^H(o)$ and K_{CH}^H , accounts for a major part of the variation in the proton h.f. splittings for even alternate hydrocarbons such as

anthracene. Equation (3-8) involves two theoretical quantities, E_i^π and ρ_i^π . Most calculations of spin densities and charge densities for alternant aromatic hydrocarbons indicate that the approximation, $|E_i^\pi| = \rho_i^\pi$, is valid. Making the substitution, equation (3-8) becomes:

$$a_i^H = Q_{CH}^{H(o)} \rho_i^\pi \pm K_{CH}^H [\rho_i^\pi]^2 \quad (3-9)$$

where the + sign is applicable to positive ions and the - sign to negative ions. Assuming that the pairing theorem holds exactly (i.e., that the spin density distribution for the positive and negative ions of the same alternant aromatic hydrocarbon will be identical), the average h.f.s., \bar{a}^H , and the deviation Δa^H can be defined by:

$$\bar{a}^H = \frac{a_+^H + a_-^H}{2} = Q_{CH}^H(o) \rho^\pi \quad (3-10)$$

$$\Delta a^H = \frac{a_+^H - a_-^H}{2} = K_{CH}^H [\rho^\pi]^2 \quad (3-11)$$

Substituting for ρ^π in equation (3-11):

$$\Delta a^H = \frac{K_{CH}^H}{[Q_{CH}^{H(o)}]^2} [\bar{a}^H]^2 \quad (3-12)$$

A plot of Δa^H vs. $[\bar{a}^H]^2$ (both experimental properties) gives a straight line.¹⁰⁸ Using $Q_{CH}^{H(o)} = -27$ gauss, K_{CH}^H is computed to be -12.9 ± 1.1 gauss from the slope of the line in reference 108.

Where radicals or radical ions can be produced or trapped in a diamagnetic single crystal host, anisotropic proton hyperfine splittings can often be detected. McConnell and Strathdee¹⁰⁹ were the first to consider quantitatively the relationship between the anisotropic proton h.f.s. and electron spin densities in planar π -electron radicals.

They showed that the interaction arises primarily through electron-nuclear dipole-dipole coupling. For a C-H fragment, they derived an expression for the complete hyperfine term in the spin Hamiltonian.

$$\mathcal{H}_{\text{H.F.}} = h^{-1} \underline{S} \cdot \underline{A} \cdot \underline{I} \quad (3-13)$$

where \underline{A} is a diagonal hyperfine tensor when defined for the principal axis system of the hyperfine coupling.

$$\underline{A} = \begin{vmatrix} A_{xx} & 0 & 0 \\ 0 & A_{yy} & 0 \\ 0 & 0 & A_{zz} \end{vmatrix} \quad (3-14)$$

The x-axis is taken to be along the C-H bond and the z-axis along the carbon $2P^\pi$ orbital. If A_0 , the isotropic hyperfine coupling, is subtracted from each element of \underline{A} , the anisotropic hyperfine tensor, \underline{T} , is obtained.

$$\underline{T} = \begin{vmatrix} T_{xx} & 0 & 0 \\ 0 & T_{yy} & 0 \\ 0 & 0 & T_{zz} \end{vmatrix} \quad (3-15)$$

Here $(T_{xx} + T_{yy} + T_{zz}) = 0$. McConnell and Strathdee¹⁰⁹ give the following expressions (in MHz) for the elements of \underline{T} .

$$\begin{aligned} T_{xx} &= 43.1 \rho^\pi + 338 \rho^\sigma \\ T_{yy} &= -38.2 \rho^\pi - 152 \rho^\sigma \\ T_{zz} &= -4.9 \rho^\pi - 186 \rho^\sigma \end{aligned} \quad (3-16)$$

where ρ^π is the spin density in the $2P^\pi$ orbital on the carbon atom and ρ^σ is the spin density in the C-H σ molecular orbital. Since the σ spin density is negative near the hydrogen atom and positive near the carbon atom, it is expected that ρ^σ will be small and may be neglected.

However, ρ^σ cannot be neglected for the isotropic h.f.s. In order to use equations (3-16) an estimate of the magnitude of the spin densities must be available.

Both isotropic and anisotropic hyperfine splittings have been observed for protons bonded to nitrogen and oxygen. In the derivation of the McConnell relationship, no assumption was made concerning the particular atom to which the hydrogen was bonded. Therefore,

$$a_{\text{NH}}^{\text{H}} = Q_{\text{NH}}^{\text{H}} \rho_{\text{N}}^{\pi}$$

$$a_{\text{OH}}^{\text{H}} = Q_{\text{OH}}^{\text{H}} \rho_{\text{O}}^{\pi}$$
(3-17)

Reliable values of Q_{NH}^{H} and Q_{OH}^{H} are not known at this time.

Methyl proton splittings can be related to the π -electron spin density on the adjacent carbon atom by the relationship;

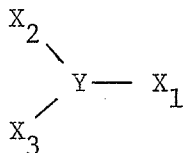
$$a^{\text{H}}(\text{CH}_3) = Q_{\text{CCH}_3}^{\text{H}} \rho_{\text{C}}^{\pi}$$
(3-18)

$Q_{\text{CCH}_3}^{\text{H}}$ has been shown to be constant only for neutral odd-alternant hydrocarbons (this would include the alkyl radicals). For this restricted group of radicals $Q_{\text{CCH}_3}^{\text{H}} = +29.3\text{g}$. For radical ions, $Q_{\text{CCH}_3}^{\text{H}}$ has been given values as low as 18.4g and as high as 38g. The mechanism of h.f. splittings by methyl protons is not completely due to an exchange polarization mechanism. Recent calculations have shown that hyperconjugative electron transfer mechanisms contribute 40% to the proton splitting, the remaining 60% being accounted for by an exchange polarization mechanism. (π - π polarization rather than π - σ polarization for ring proton splittings).¹⁰⁵

B. Hyperfine Splittings From Nuclei Other Than Protons

(1) Isotropic Hyperfine Splitting From Atoms With A Net π -Electron Spin Density.

The treatment and notation of Karplus and Fraenkel will be followed.¹¹⁰ Their calculations, assuming complete orbital following, were developed for carbon-13 hyperfine splittings but the model should be applicable to other nuclei. It has been found, experimentally, that carbon-13 splittings are not correlated in a linear manner with the π -electron spin density on the same carbon atom. Therefore, other contributions besides the single C-H bond contribution considered by McConnell,¹⁰³ must be considered. Let us consider the general case of a four atom fragment from an aromatic system,



where the nucleus of the atom Y is producing an isotropic hyperfine splitting. Let the π -spin density on Y be ρ_Y^π and the π -spin densities on the X_i atoms be $\rho_{X_i}^\pi$ ($i = 1, 2, 3$). One, two or three of the X_i may be hydrogen atoms, in which case $\rho_{X_i}^\pi$ would be zero. First consider the possible π - σ interactions of the π -electrons on Y with the σ electrons around Y. Karplus and Fraenkel show that there will be four such interactions: spin polarization of the 1s electrons on Y, and spin polarization of 2s electrons on the atom Y in the Y- X_1 , Y- X_2 and Y- X_3 σ bonds. For $\rho_Y^\pi = 1$ and $\rho_{X_i}^\pi = 0$,

the contribution to a^Y from the 1s electrons is designated S^Y . The contributions from the 2s electrons are designated $Q_{YX_i}^Y$. There will also be a contribution to a^Y from the π -spin densities on the X_i (in the same sense as the proton splitting in the CH fragment). For $\rho_Y^\pi = \rho_{X_2}^\pi = \rho_{X_3}^\pi = 0$ and $\rho_{X_1}^\pi = 1$, the contribution to a^Y from the 2s electrons on Y will be designated $Q_{X_1Y}^Y$, with similar expressions for $\rho_{X_2}^\pi$ and $\rho_{X_3}^\pi$ equal to unity respectively. Therefore the following expression relating a^Y to the π -electron spin densities may be written.

$$a^Y = [S^Y + \sum_i Q_{YX_i}^Y] \rho_Y^\pi + \sum_i Q_{X_iY}^Y \rho_{X_i}^\pi \quad (3-19)$$

In general, S^Y should be negative, $Q_{YX_i}^Y$ should be positive while, analogous to Q_{CH}^H , the $Q_{X_iY}^Y$ should be negative.

Karplus and Fraenkel¹¹⁰ made quantitative calculations of the spin polarization constants in equation (3-19) for a carbon atom with the X_i being either carbon or hydrogen atoms. Calculations for a planar CHC_2 fragment model yielded $S^C = -12.7g$, $Q_{CH}^C = 19.5g$, $Q_{CC}^C = 14.4g$ and $Q_{C^*C}^C = -13.9g$. Inserting these values into (3-19):

$$a^C = 35.6 \rho_C^\pi - 13.9 \sum_i \rho_{C_i}^\pi \quad (3-20)$$

Sometimes an independent estimate of the ρ^π 's can be obtained from proton hyperfine splittings using equations (3-4) or (3-8). Then a^C may be calculated from (3-20), giving reasonable agreement with experiment.

The sigma-pi interaction parameters (Q 's) depend on bond length, the type of hybridization (including the angles between sigma bonds), and on the nature of the bonding atoms. The proton parameter Q_{CH}^H is somewhat larger in CHC_2 than in CH_3 , which suggests a theoretical justification for some of the variation in the experimental Q_{CH}^H required to fit measured proton splittings. The 1s and 2s contributions are of the same magnitude but opposite in sign. In contrast to the Q values, S^C is relatively independent of the bonds to the carbon atom. S^C does have, though, a quadratic dependence on the ionic character of the bonds. The ionic character of the bonds in hydrocarbons is small and therefore S^C should be nearly constant for these systems.

For the planar methyl radical equation (3-19) reduces to

$$a^C = S^C + 3 Q_{CH}^C \quad (3-21)$$

where $Q_{CH}^C = 18.85g$ and $S^C = -12.7g$. Substituting these numbers into (3-21) we get $a^C = 43.8$ gauss which compares favourably with the experimental measurement of 41 ± 3 gauss made on frozen CH_3 by Cole, et al.⁵⁹ In that investigation, the observed carbon-13 splitting was used as evidence for the planarity of the methyl radical. Karplus and Fraenkel¹¹⁰ also showed that a^C (for the methyl radical) increased by one-half in going 5° from planarity. Therefore the methyl radical must be nearly planar.

(2) Anisotropic Hyperfine Splitting from Atoms with
A Net π -Electron Spin Density.

In contrast to the isotropic hyperfine couplings which usually arise through an indirect π - σ interaction, anisotropic hyperfine couplings result from a dipole-dipole coupling of the nuclear spin

with a non-spherically symmetric electron spin distribution (i.e., an electron in a p,d, orbital). Consider an electron in a p-orbital interacting with the nucleus of the same atom. The dipole-dipole term in the spin Hamiltonian will be:

$$\mathcal{H}_0 = -h^{-1} g_e \beta_e g_N \beta_N \left[\frac{\underline{S} \cdot \underline{I}}{r^3} - \frac{3(\underline{S} \cdot \underline{r})(\underline{I} \cdot \underline{r})}{r^5} \right] \quad (3-22)$$

where \underline{S} and \underline{I} are the spin operators for the electron and nucleus respectively, and \underline{r} is the radius vector between the electron and the nucleus. Equation (3-22) leads to the following anisotropic hyperfine energy ($W_{M_S M_I}^1$);

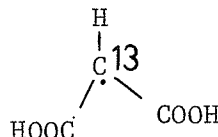
$$W_{M_S M_I}^1 = h^{-1} \frac{g_e \beta_e g_N \beta_N M_S M_I}{2} \left\langle \frac{1-3\cos^2\alpha}{r^3} \right\rangle_{av.} (1-3\cos^2\theta) \text{ MHz} \quad (3-23)$$

where α is the angle between \underline{r} and a principle axis of the anisotropic hyperfine tensor, and θ is the angle between \underline{H}_0 and the same axis (note $\langle 3\cos^2\theta \rangle_{av.} = 1$ when averaged over a sphere). Consider \underline{H}_0 along the Z-axis which we take to be the major axis of the P-orbital, $\theta=0$, so the last term in equation (3-23) will be -2. For a p-orbital, the average value of $\cos^2\alpha$ is 3/5. The anisotropic h.f. energy or coupling with \underline{H}_0 along the Z axis will then be $2\underline{B}_0$, where

$$\underline{B}_0 = \frac{2}{5} h^{-1} g_e \beta_e g_N \beta_N \langle r^{-3} \rangle_{av.} \quad (\text{MHz.}) \quad (3-24)$$

$\langle r^{-3} \rangle_{av.}$ may be calculated from S.C.F. wave functions or from a Slater wave function. As an example of the calculation of a spin density

using this method, consider the malonic acid radical enriched in carbon-13.



The isotropic carbon-13 h.f. coupling is 93 MHz and the anisotropic coupling tensor components are (120, -70, -50) MHz, with the 120 MHz component oriented perpendicular to the radical plane. This anisotropic coupling can thus be identified with the $2B_0$ term in the $2P_z$ atomic anisotropic h.f. coupling tensor. For carbon-13 the value of $2B_0$ is calculated to be 182 MHz. We thus compute $\rho_c^\pi = \frac{120}{182} = 0.66$. This value can be checked from the isotropic proton h.f. coupling (-59 MHz) and $Q_{CH} = -75.6$ MHz, which gives $\rho_c^\pi = 0.78$. This discrepancy may be due to spin density on the carboxyl groups affecting the anisotropic h.f. couplings or to σ -spin density in the bonds or perhaps to an overestimate of $2B_0$ in the atomic carbon $2P^\pi$ orbital.

C. Theoretical Interpretations of the E.S.R. Spectrum of the Methyl Radical.

A valence-bond calculation of the proton isotropic h.f.s. in the methyl radical has been performed by Karplus⁶¹ (assuming complete orbital following). The splitting was computed as a function of the angular configuration of the molecule. For the planar radical a splitting of 27 ± 5 gauss was calculated. Since the calculations are insensitive to angles in the neighbourhood of 90° , a deviation of 10° to 15° from planarity could not be excluded.

Schrader and Karplus¹⁰² have studied incomplete orbital following of the molecular vibrations in the methyl radical through its relationship to the hyperfine splittings observed in the E.S.R. spectrum. Incomplete orbital following, which is a lag of the bonding electron density with respect to the internuclear axis, may occur if the valence-state energy or electron repulsions are decreased by the presence of "bent bonds". In their publication, Schrader and Karplus obtain a semiempirical valence bond estimate of orbital following from the E.S.R. spectrum of certain free radicals. By means of a theoretical interpretation of the hyperfine splittings and their dependence on the molecular vibrations, limits were set on the orbital following in appropriate systems. The methyl radical (planar in equilibrium configuration) and its isotropic analogs were chosen because carbon-13 and proton hyperfine splittings have been shown to have significant dependences on nuclear positions. Let us define ρ as the following parameter. When $\rho = 1$ we have complete following and when $\rho = 0$ we have no following. To determine whether restricted orbital following is necessary for the interpretation of the hyperfine splittings, experimental data^{59,73} was compared with theoretical results (vibrational averages) for complete following (Table 3.3).

TABLE 3.3^a

Comparison Of Experimental and Theoretical Values
($\rho = 1$) of $|a^H|$ and $|a^C|$ For Methyl Radicals.¹⁰²

RADICAL	$ a^H(\text{exptl.}) $	$\langle a^H(\text{th}) \rangle$	$a^C(\text{exptl.})$	$\langle a^C(\text{th}) \rangle$
¹² CH ₃	23.038g	-25.319g	-----	-----
¹³ CH ₃	23.04g	-25.315g	38.34g	70.37g
¹² CD ₃	23.29±0.02g ^b	-25.198g ^b	-----	-----
¹³ CD ₃	23.30g ^b	-25.191g ^b	35.98g	64.79g

a All exptl. values from reference 73.

b These values are obtained by multiplying a^D by $(g^H/g_D) = 6.51437$

The proton results agree reasonably well while the calculated carbon-13 splittings are much too large. In addition, the ratio

$$R_1 = \frac{|a^H| \text{ in } \text{CH}_3}{6.51437 |a^D| \text{ in } \text{CD}_3},$$

which is of interest because of its direct relationship to vibrational effects, has been considered. Theoretically R_1 is slightly greater than one while experimentally R_1 is slightly less than one. Table 3.4 gives values of a^H and a^C for complete orbital following as a function of θ (for planar radical $\theta = 0$) for the radical C^{13}H_3 .

TABLE 3.4
Proton and Carbon-13 Splittings For The Methyl
Radical as a Function of θ ($\rho = 1$)¹⁰²

θ	$a^H(\theta)$	$a^C(\theta)$
0°	-24.90	46.56
5°	-25.11	63.79
10°	-26.09	117.2
15°	-29.09	211.9
20°	-36.58	355.1
25°	-53.11	548.9
30°	-81.90	756.3

The $a^H(\theta)$ and $a^C(\theta)$ values are in reasonable agreement with experimental results. By comparing Tables 3.3 and 3.4 it can

be seen that $a^H(o) \approx \langle a^H \rangle$ while $a^C(o)$ is much different than $\langle a^C \rangle$. $\langle a^C \rangle$ is much larger than $a^C(o)$ because $a^C(\theta)$ increases rapidly with increasing θ . The difference between the θ dependence of $a^C(\theta)$ and $a^H(\theta)$ arises from the form of the carbon hybrid orbitals. Since the zero-point vibrational amplitude is greater in CH_3^* than in CD_3^* , it is expected that $|\langle a^H \rangle|$ in CH_3 would be larger than $6.51437 |\langle a^D \rangle|$ in CD_3 ; that is, $R_1(\text{th}) > 1$.

Schrader and Karplus¹⁰² then considered incomplete orbital following. The results are shown in Table 3.5 for a selection of values of $\rho(o)$ and $\rho(90)$.

TABLE 3.5
 $\langle a^H \rangle$, $\langle a^C \rangle$ and R_1 for Various Values of $\rho(o)$ and $\rho(90)$ ¹⁰²

$\rho(o)$	1	1	0.8	0.8	0.5	0
$\rho(90)$	0.5	0.145	0.425	0.2	0.425	0
$\langle a^H \rangle$	-23.01	-23.05	-23.04	-23.08	-23.04	-24.59
$\langle a^C \rangle$	63.9	56.0	56.0	53.9	56.0	45.81
R_1	1.001	1.001	1.001	1.001	1.001	1.015

$\langle a^H \rangle$ is only slightly affected by incomplete following while $\langle a^C \rangle$ depends strongly on ρ . The ratio R_1 is little changed by variations in ρ and remains greater than one for all choices of $\rho(o)$ and $\rho(90)$. Even zero following [$\rho(o) = 0$, $\rho(90) = 0$], however, leads to a value of $\langle a^C \rangle$ that is somewhat greater than the measured value. Perhaps $\langle a^C \rangle$ can be improved by adjusting other parameters. For instance, an increase in the magnitude of S^C would improve the value of $\langle a^C \rangle$, while leaving $\langle a^H \rangle$ unchanged. Another parameter to which $\langle a^C \rangle$

is sensitive is Δ . A decrease in Δ will result in the desired lowering of $\langle a^C \rangle$. Δ is a function which determines how (π, σ_{CH}) varies with θ . Some results for simultaneous Δ and orbital following variations are given in Table 3.6.

TABLE 3.6
How $\langle a^H \rangle$, $\langle a^C \rangle$ and R_1 Change With Simultaneous Variations
in ρ and Δ Values¹⁰²

$\rho(o)$	$\rho(90)$	$\Delta(eV)$	$\langle a^H \rangle$	$\langle a^C \rangle$	R_1
1	0.5	0	-22.77	63.3	0.9997
		-1	-22.30	62.2	0.9973
		-2	-21.84	61.1	0.9947
1	0.145	0	-22.85	55.5	1.002
		-1	-22.47	54.6	0.995
		-2	-22.09	53.7	0.998
0.8	0.2	0	-22.90	53.5	1.001
		-1	-22.54	52.6	0.999
		-2	-22.18	51.8	0.989
0.5	0.2	0	-23.24	47.7	1.004
		-1	-22.96	47.0	1.003
		-2	-22.68	46.3	1.002

It can be seen that $\langle a^C \rangle$ does decrease as Δ is altered from 0.5 (values used up until now in reference 102) to -2eV. For Δ

sufficiently large and negative, R_1 becomes less than one in agreement with experiment. The value of R_1 is reduced because $a^H(\theta)$ is a decreasing function of θ (for small θ) for appropriate Δ values. Schrader and Karplus concluded that incomplete orbital following is necessary and the degree of orbital following is small. A $\rho(o)$ value somewhat less than unity and a $\rho(90)$ value less than 0.3 seems likely. Only by introducing partial following and thereby decreasing the θ dependence of $a^C(\theta)$ can consistent results be obtained. Possibly other normal modes besides the symmetric bending mode must be used for vibrational averaging. The symmetric and asymmetric stretching modes are expected to have negligible effects on the average h.f. splittings. The other in-plane mode (asymmetric bending) involves significant rehybridization of the carbon sigma orbitals. The alteration of $\langle a^H \rangle$ and $\langle a^C \rangle$ values produced by this vibration is expected to be small as well. Further supporting evidence for incomplete orbital following can be found by looking at $a^C(\text{CH}_3) - a^C(\text{CD}_3)$. For complete following this difference is 5.66g. For reasonable following parameters [$\rho(o)=1$, $\rho(90)=0.145$ or $\rho(o)=0.9$, $\rho(90)=0.192$], the difference is reduced to 2.1 ~ 2.8g. Fessenden⁷³ found this difference, for methyl radicals in liquid methane, to be 2.3 g. A test of Schrader and Karplus¹⁰² results could be obtained by a determination of the temperature dependence of the hyperfine splittings.

D. Theoretical Temperature Dependences Of The Methyl Radical.

Moss,¹¹¹ assuming that the methyl radical is planar with the unpaired electron situated in the P_z orbital, expected that Q (or a^H since $\rho^\pi = 1$) would depend on the amplitude of the out-of-plane vibrations and consequently might be temperature dependent.

He assumed that when the proton moves out of the molecular plane there is a direct spin delocalization into the 1s orbital of the hydrogen atom. The resulting contribution to the Q value will be positive, whereas the major, but indirect, electron spin polarization term is negative. If ϕ is the angle between the nodal plane and the C-H bond, the contribution to Q arising from direct delocalization is expected to vary as $\sin^2\phi$, from symmetry considerations. Therefore,

$$Q = Q_0 + Q^1 \sin^2\phi \quad (3-25)$$

where Q_0 and Q^1 are constants. ϕ varies as the radical vibrates and since the vibrational frequency is much greater than the h.f. frequency we may average over the vibrations to give:

$$Q = Q_0 + Q_1 \langle \sin^2\phi \rangle \quad (3-26)$$

where Q_1 is Q^1 averaged over ϕ . $\langle \sin^2\phi \rangle$ may be estimated if a vibrational analysis of the out-of-plane vibrations is available. Herzberg¹¹² gives the frequency of the out-of-plane vibration in CD_3 as 447 cm^{-1} and the bond lengths in both CH_3 and CD_3 as 1.08 Å. The corresponding frequency in CH_3 is calculated to be 577 cm^{-1} . Using this data equation (3-26) becomes:

$$Q = Q_0 + 0.0104 Q_1 \coth \frac{415}{T} \quad \text{for } \text{CH}_3 \quad (3-27)$$

$$Q = Q_0 + 0.0081 Q_1 \coth \frac{321}{T} \quad \text{for } \text{CD}_3 \quad (3-28)$$

Fessenden and Schuler⁷¹ irradiated liquid CH_4 and CD_4 at 97°K with 2.8 MeV electrons and their results were:

$$Q = -23.038 (\pm 0.01) \text{ gauss for } \text{CH}_3$$

$$Q = -23.295 (\pm 0.02) \text{ gauss for } \text{CD}_3$$

Substituting these values into (3-27) and (3-28) and solving for Q_0 and Q_1 :

$$Q_0 = -24.19 (\pm 0.13) \text{ gauss}$$

$$Q_1 = 111 (\pm 13) \text{ gauss}$$

Zlochower, et al,⁷⁴ studied the methyl radical in aqueous solution and observed an approximate linear dependence of Q upon temperature. The Q values at the extremes of the temperature range studied were (for CH_3 only):

$$Q = -22.726 (\pm 0.01) \text{ gauss at } 273^\circ\text{K}$$

$$Q = -22.601 (\pm 0.01) \text{ gauss at } 333^\circ\text{K}$$

These observations lead to $Q_0 = -24.46 (\pm 0.29)$ gauss and $Q_1 = 152 (\pm 24)$ gauss which agree reasonably with those predicted from Fessenden's results.

DMS developed a theory of the temperature dependence of the hyperfine interactions in the methyl radical based on incomplete orbital following. It was in response to a private communication from D.M. Schrader that the experimental work outlined in this chapter was done. The methyl radical is known to be planar.^{110,61,112-116,73} This work (DMS) refines and extends that work presented in reference 102. Some of the semiempirical parameters have been adjusted so that the calculations reproduce at 97°K the observed splittings due to the proton in C^{12}H_3 , the deuteron in C^{12}D_3 , and carbon-13 in C^{13}H_3 and C^{13}D_3 (Reference 73). As in reference 102 it is assumed that at 97°K only the ground vibrational state is significantly occupied. DMS extends the vibrational averaging of the out-of-plane bending mode (A_2'') to several of the higher states and by doing so calculates the h.f. splittings as a function of temperature. Therefore, by fitting

four observed values at 97°K, the hyperfine interactions are predicted over a wide range of temperatures. The bond length R_{CH} and the A_2'' force constant used were taken from Herzberg's analysis¹¹² of the vacuum U.V. spectra of Herzberg and Shoosmith.¹¹³ Lester, et al,¹¹⁴ and Andrews and Pimentel¹¹⁵ have suggested another force constant (larger by 58.4%) while recently Milligan and Jacox¹¹⁶ observed the A_2'' vibrational mode of the CH_3 radical at a frequency which is only slightly larger than that of Herzberg.¹¹² The differences may arise because of matrix effects present in the low temperature observations of the A_2'' vibrational mode of the methyl radical.¹¹⁴⁻¹¹⁶

Partial orbital following was incorporated into Schrader's calculations in the same manner as in Reference 102. $\rho(o)$ is the limiting value as $\theta \rightarrow 0$ of the ratio $\frac{\theta'}{\theta}$, where θ' is the angle between the axis of the carbon sigma orbital and the plane of the three protons, and θ is the angle between the carbon-hydrogen internuclear axis and the plane of the three protons. $\rho(90)$ is the limiting ratio of the same two angles as $\theta \rightarrow 90^\circ$. The two angles are illustrated in Figure 3.1. It was found that a fit of the data is only possible over a narrow range of values for $\rho(o)$ and $\rho(90)$ [See Fig. 3.2]. The calculations were done for models C and D shown in Fig. 3.2. The shaded area indicates the values of $\rho(o)$ and $\rho(90)$ for which the four experimental results could be fit. All values of $\rho(o)$ and $\rho(90)$ in the shaded area give results between the two extremes (i.e. models C and D). The area above line OA (in Fig. 3.2) represents the non-physical situation in which the relative orbital lag is less for small deviations from molecular planarity than for large.

Fig. 3.1

Illustration of θ and θ^1 . (D.M.S.)

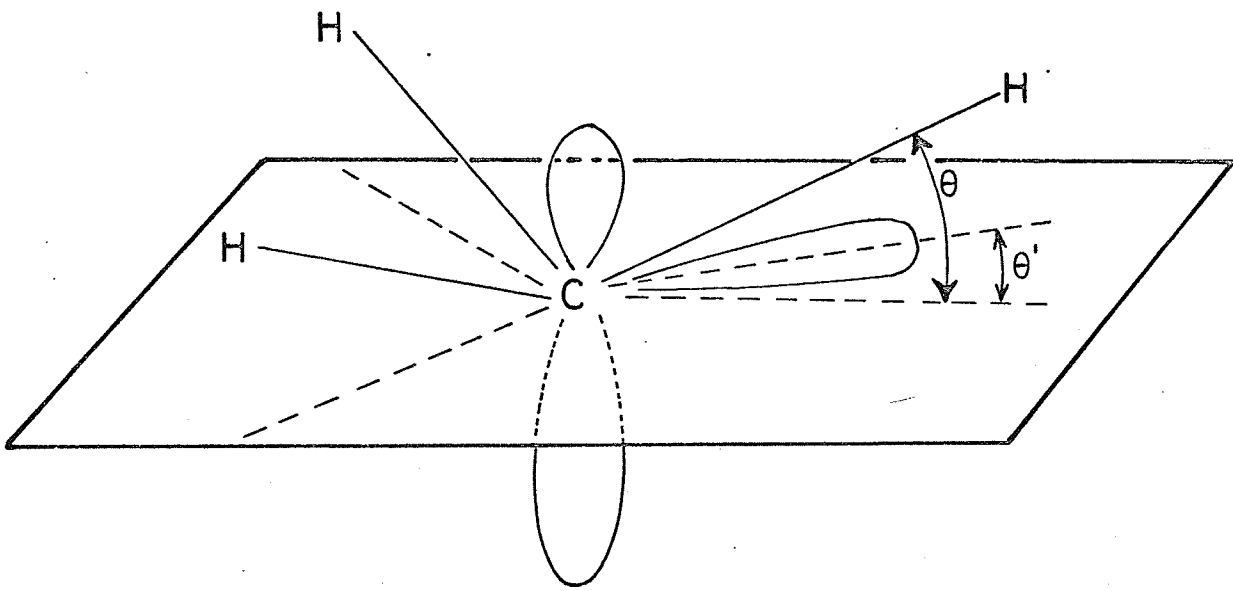
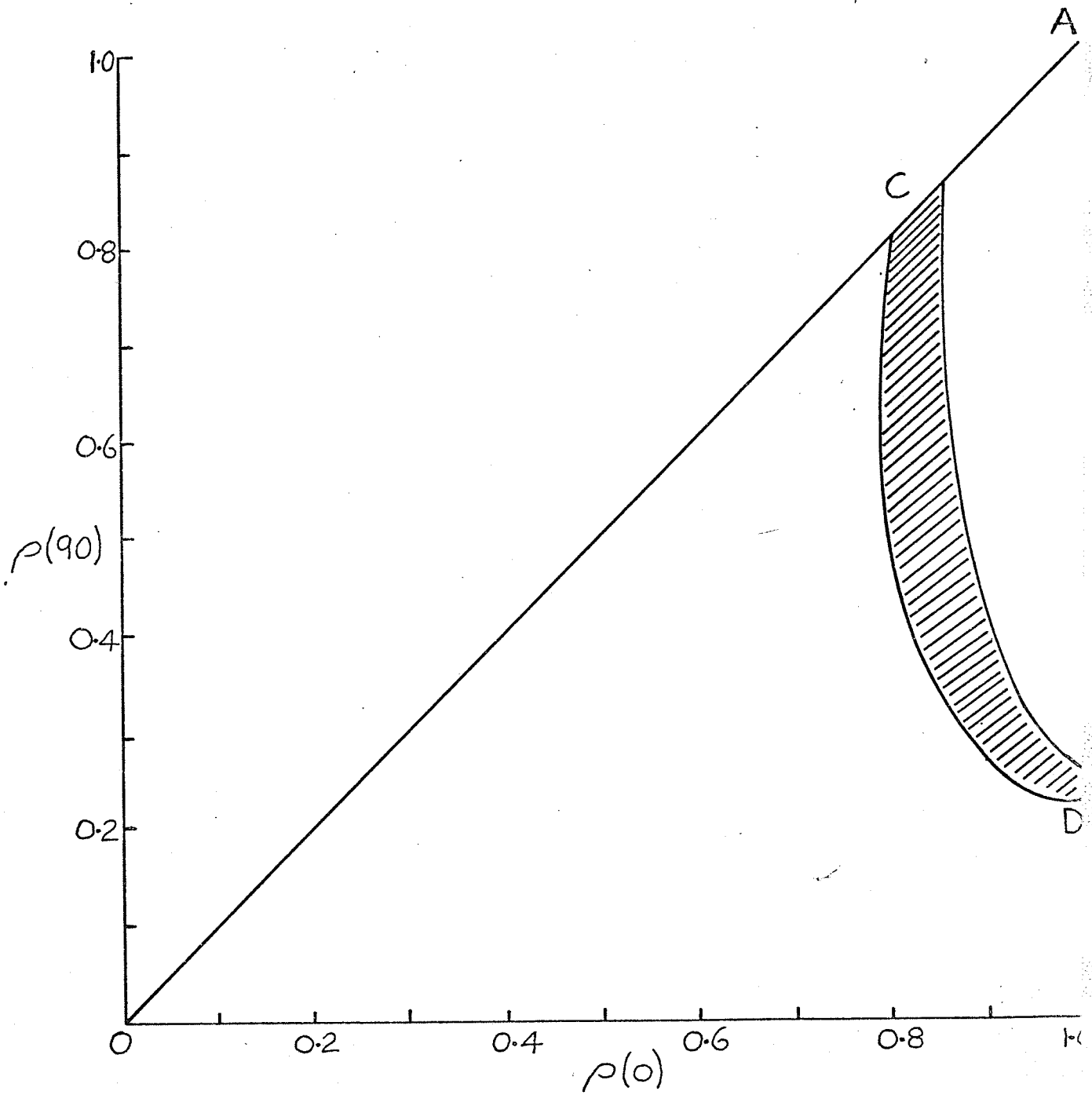


Fig. 3.2

$\rho(90)$ vs. $\rho(0)$. The shaded area indicates useful values of $\rho(90)$ and $\rho(0)$ (D.M.S.).



The splittings calculated by DMS are essentially constant from 0° to 100°K owing to small populations of the excited vibrational states (See Figures 3.3 and 3.4). The calculated dependences for models C [$\rho(0)=0.825$, $\rho(90)=0.825$] and D [$\rho(0)=1.00$, $\rho(90)=0.245$] do not begin to deviate from each other significantly until room temperature. This deviation becomes larger with increasing temperatures (shaded areas in Figures 3.3 and 3.4). The dashed curves in Figures 3.3 and 3.4 are the results obtained when the force constant from references 114 and 115 is used.

Figures 3.5 and 3.6 show the calculated temperature coefficients as a function of temperature for models C. It is evident that since a^C is a sharply increasing function of θ (due mainly to the growth of 2S content of the singly occupied orbital as θ increases [see Table 3.7]), the vibrational average of a^C is greater than a^C at $\theta = 0$.

Fig. 3.3

Calculated values of $|a^H|$ and $6.51437 |a^D|$ for $C^{12}H_3$ and $C^{12}D_3$, respectively, using following models C and D. (DMS). The crosses represent observed values.⁷⁴ The dashed curves are the results obtained when the force constant of Andrews and Pimentel¹¹⁴ was used (DMS).

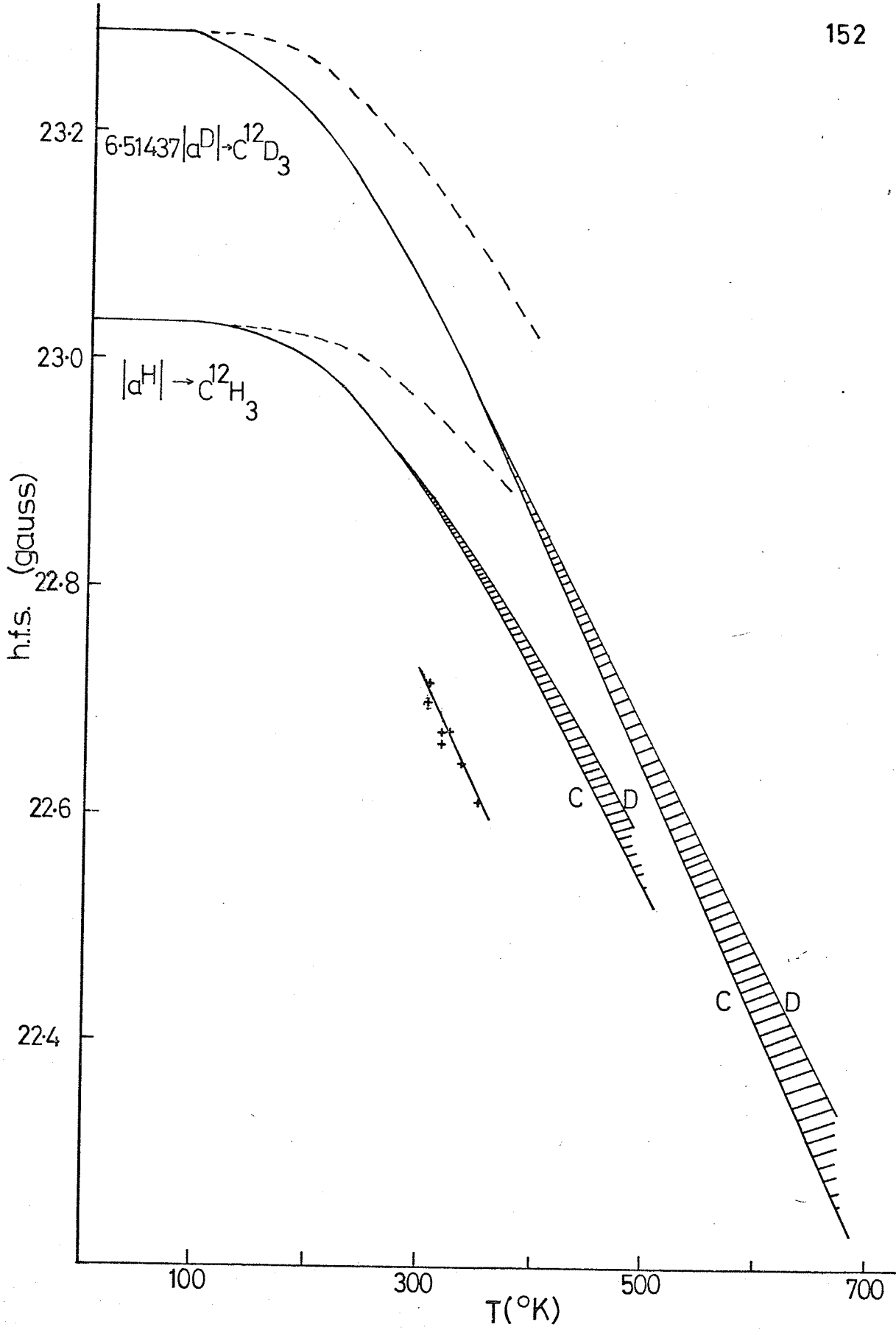


Fig. 3.4

Calculated values of a^c in $C^{13}H_3$ and $C^{13}D_3$ for following models C and D (DMS). The dashed curves are the results obtained when the force constant of Andrews and Pimentel¹⁴ was used (DMS).

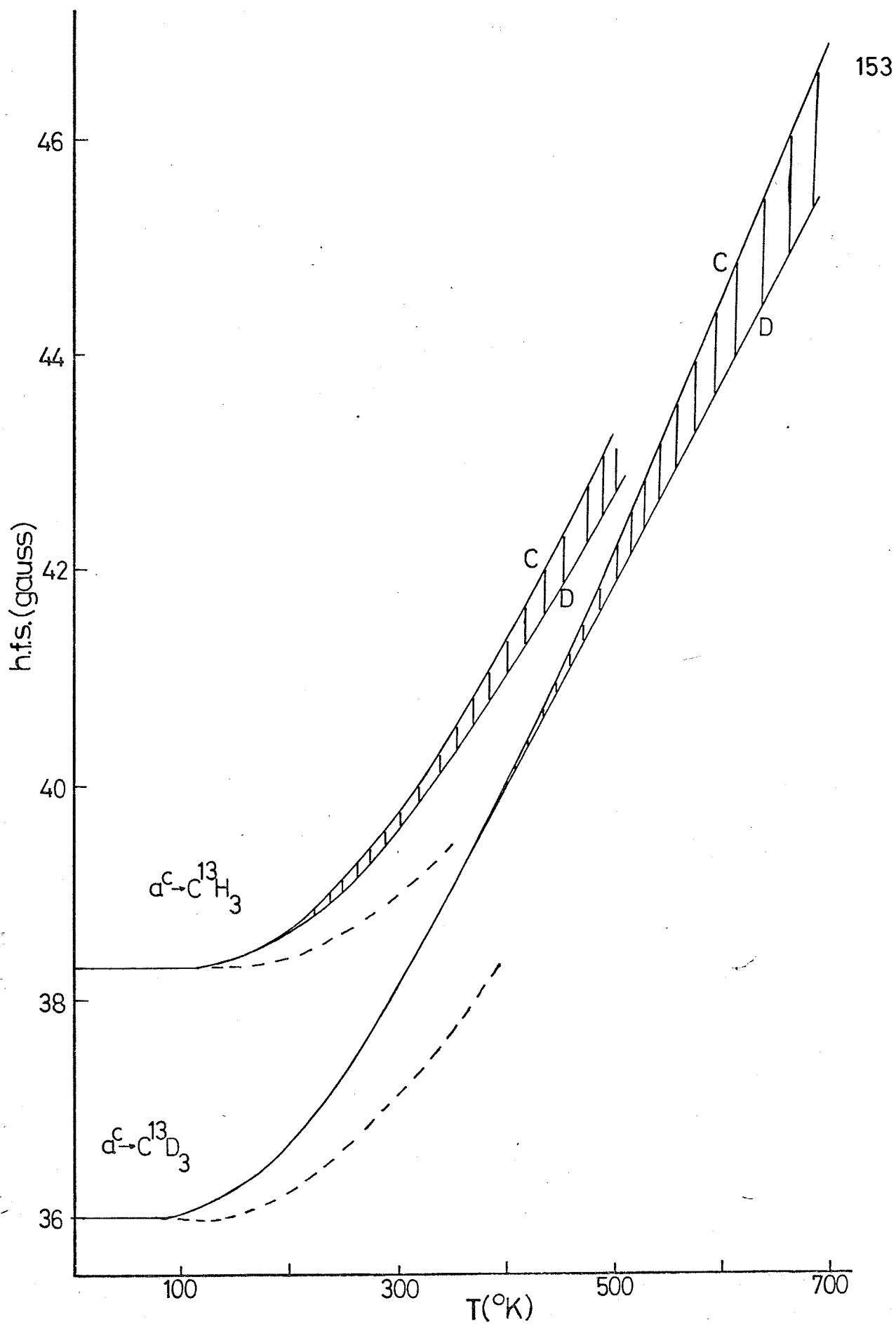


Fig. 3.5

Temperature coefficients of $|a^H|$ and $|a^D|$ for $C^{12}H_3$ and $C^{12}D_3$ as a function of temperature (Following Model C) [DMS].

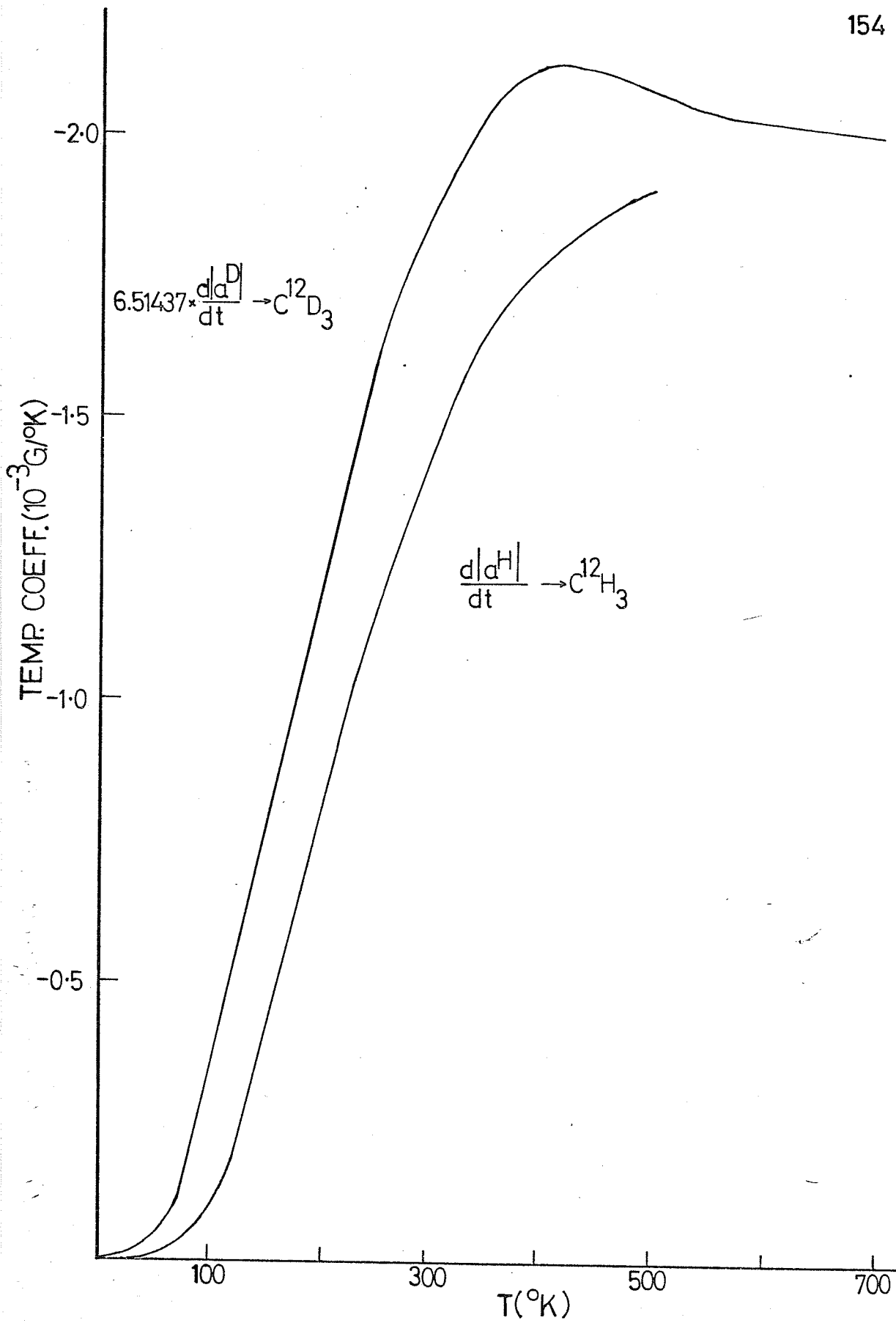


Fig. 3.6

Temperature coefficients of a^c for $C^{13}H_3$ and $C^{13}D_3$ as a function of temperature (Following Model C) [DMS].

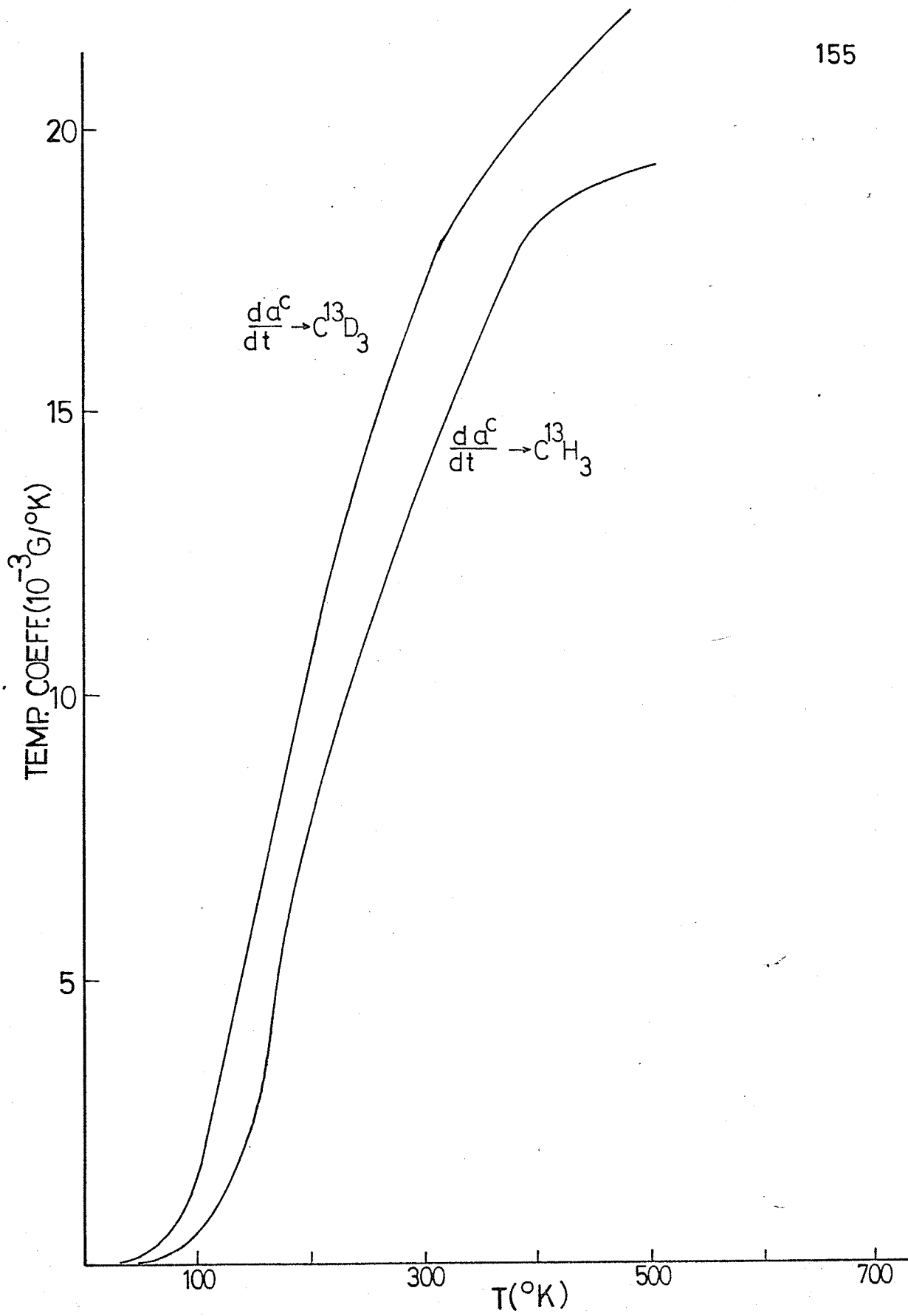


TABLE 3.7

Splittings and Orbital Spin Populations As Functions Of θ (DMS)

θ	θ°	a^H		a^C				Spin Content (Orbital Polarization)			ls_H
		Total	From π_c	Total	From σ_c	From π_c	From ls_c	π_c	σ_c	ls_c	
Following Model C											
0°	0°	-24.24	0.00	28.60	43.33	0.00	-14.73	1-0.0072	0.050	-0.0028	-0.048
5	4.1	-23.31	0.01	35.56	41.15	8.92	-14.51	1-0.0067	0.048	-0.0028	-0.046
10	8.2	-20.66	0.02	57.40	35.11	36.13	-13.84	1-0.0052	0.042	-0.0027	-0.041
15	12.4	-16.87	0.03	97.03	26.84	82.87	-12.68	1-0.0034	0.034	-0.0024	-0.038
20	16.5	-13.44	0.01	159.70	19.37	151.2	-10.96	1-0.0022	0.027	-0.0021	-0.026
25	20.6	-13.86	0.01	252.9	17.38	244.1	- 8.60	1-0.0023	0.028	-0.0017	-0.027
30	24.8	-24.84	0.18	384.4	25.57	364.3	- 5.47	1-0.0076	0.051	-0.0011	-0.049
Following Model D											
0	0	-24.45	0.00	27.05	42.26	0.00	-15.20	1-0.0074	0.051	-0.0030	-0.048
5	4.8	-23.18	0.00	36.40	39.39	11.90	-14.90	1-0.0066	0.048	-0.0029	-0.046
10	8.9	-20.39	0.01	59.95	33.23	40.87	-14.14	1-0.0051	0.042	-0.0027	-0.040
15	12.0	-17.86	0.04	89.54	27.70	75.08	-13.24	1-0.0039	0.036	-0.0026	-0.035
20	14.2	-16.67	0.15	119.6	24.70	107.3	-12.39	1-0.0034	0.034	-0.0024	-0.033
25	15.9	-17.23	0.35	148.0	24.58	135.1	-11.64	1-0.0036	0.035	-0.0022	-0.034
30	17.2	-19.49	0.67	174.2	27.00	158.2	-11.00	1-0.0046	0.040	-0.0021	-0.038

In order to reduce the calculated value of a^C at $\theta = 0$, a reduction of the carbon 2s orbital density at the nucleus was necessary.

" $^{13}\text{CD}_3$ and $^{12}\text{CD}_3$, which have heavier effective masses for the A_2 mode, vibrate with less amplitude than $^{13}\text{CH}_3$ and $^{12}\text{CH}_3$. This has two effects (a) if we have samples of pure CD_3 and of CH_3 in which every molecule occupies the n^{th} vibrational state, a^C will be larger for the CH_3 sample than for CD_3 and also $R_1 < 1.000$, (b) if we allow equilibrium to establish a Boltzmann population of levels, there will be a smaller proportion of molecules in the n^{th} level in the CH_3 sample than in the CD_3 sample. Effect (a) will make the temperature coefficients for CD_3 less than those for CH_3 . Effect (b) will have the opposite result. Effect (a) will be important at low temperatures while effect (b) will dominate at high temperatures.

Looking at Table 3.7 we see a very small contribution to the proton splitting from the π orbital regardless of θ . Therefore predicting a negative value for $\frac{d|a^H|}{dt}$ based upon the direct contact between the proton and the unpaired electron in the π orbital is invalid. The proton temperature dependence is due to the reduction of the spin polarization of the hydrogen 1s orbital as θ increases, which can be achieved only with partial orbital following. Table 3.7 also shows that the polarization of all the orbitals decrease to a little more than half the planar values at $\theta \sim 20^\circ$ to 25° ; and then increase again as θ goes to 30° . Table 3.7 also shows that the carbon-13 splitting for the planar molecule is due to the sigma orbitals, but comes almost completely from the π orbital for large θ .

Table 3.8 lists the contributions of each orbital to the total splitting for several nuclei in the four isotropic variants of CH_3 for models C and D at 0°K . (Zero-point Vibration).

TABLE 3.8
Contributions of Each Orbital to the Total
Splitting for Several Nuclei in Methyl
Radicals (DMS)

MOLECULE	NUCLEUS	ORBITAL	FOLLOWING MODEL	
			C	D
$^{12}\text{CH}_3$	H	$1s_{\text{H}}$	-23.031	-23.031
		σ_{C}	2.239	2.240
		π_{C}	0.008	0.003
$^{12}\text{CD}_3$	D	$1s_{\text{D}}$	-23.287	-23.287
		σ_{C}	2.266	2.266
		π_{C}	0.007	0.001
$^{13}\text{CH}_3$	C	σ_{C}	40.56	39.10
		π_{C}	12.17	14.04
		$1s_{\text{C}}$	-14.43	-14.84
		$1s_{\text{H}}$	- 2.01	- 2.01
$^{13}\text{CD}_3$	C	σ_{C}	41.15	39.68
		π_{C}	9.35	11.24
		$1s_{\text{C}}$	-14.50	-14.91
		$1s_{\text{D}}$	- 2.03	- 2.03

The distinction between the calculations of Moss¹¹¹ and DMS should be made clear. DMS assumes a definite quantum-mechanical model and calculates contributions to the splittings from each orbital in the molecule. Moss empirically fits the parameters Q_0 and Q_1 . Moss's equation introduces inaccuracies in a^H , but enables him to extend the vibrational averaging to an infinite number of states. DMS averages only to the fourth excited state for CH_3 and to the sixth excited state for CD_3 .

2. Experimental

Methyl radicals were produced on the surface of porous Vycor glass by the U.V. photolysis at liquid nitrogen temperatures of adsorbed methyl iodide. The methyl iodide was reagent grade obtained from Matheson, Coleman and Bell. The deuterated methyl iodide (minimum isotopic purity of 99 atom % D) and the carbon-13 enriched methyl iodide (57.1 atom % carbon-13) were obtained from Merck, Sharpe and Dohme of Canada, Limited (Montreal). Other than normal degassing procedures, these compounds were used without any further purification. The porous Vycor glass (Corning Code No. 7930) samples were pretreated by heating in oxygen (750°C-900°C) for 6-8 hours to oxidize all organic matter on the surface followed by heating in vacuum (10^{-4} - 10^{-5} mm Hg) at the same temperatures for a further 16-24 hours to dehydrate the surface. The methyl iodides were then adsorbed at room temperature giving surface concentrations between 5% and 25% of a monolayer. The samples were then immersed in liquid nitrogen and photolysed for one hour using the full focused arc of a Hanovia S-100 alpine burner.

The samples were then transferred quickly into a normal E.S.R. quartz dewar where several spectra were recorded at liquid nitrogen temperatures. The samples were again transferred into the cavity insert of a standard variable temperature assembly. The temperature was monitored with a thermocouple placed in the cavity insert just above the cavity. The temperature was controlled to $\pm 2^\circ$. Several spectra were recorded at the lowest temperature attainable by the variable temperature assembly. The temperature was then raised and sufficient time was allotted for thermal equilibrium to be established. Several spectra were recorded at this temperature. This procedure was continued to higher temperatures until the signal to noise ratio became too small for further measurements to be made. The procedure outlined above will be referred to hereafter as a temperature run. Each temperature run was completed in 6-8 hours.

Two temperature runs were performed on methyl radicals stabilized on a chlorinated¹⁸ p.V.g. surface. In this case the p.V.g. was heated in oxygen at 650°C for 21 1/2 hours and then in vacuum at 675°C for 26 hours. The surface was then reacted several times with carbon tetrachloride at $425\text{--}475^\circ\text{C}$. After each reaction (or dose of carbon tetrachloride) the products were pumped off at $425\text{--}475^\circ\text{C}$. Each dose of carbon tetrachloride was allowed to interact with the surface for about 45 minutes before pumping off the products. A specific amount of methyl iodide was then allowed to adsorb on the chlorinated surface resulting in a surface coverage of approximately 10% of a monolayer. Two temperature runs, as outlined above, were

carried out on this sample. These temperature runs were slightly different, in that, on reaching a reasonably high temperature and still maintaining a good signal-to-noise ratio, the process was reversed and measurements were made as the sample was cooled.

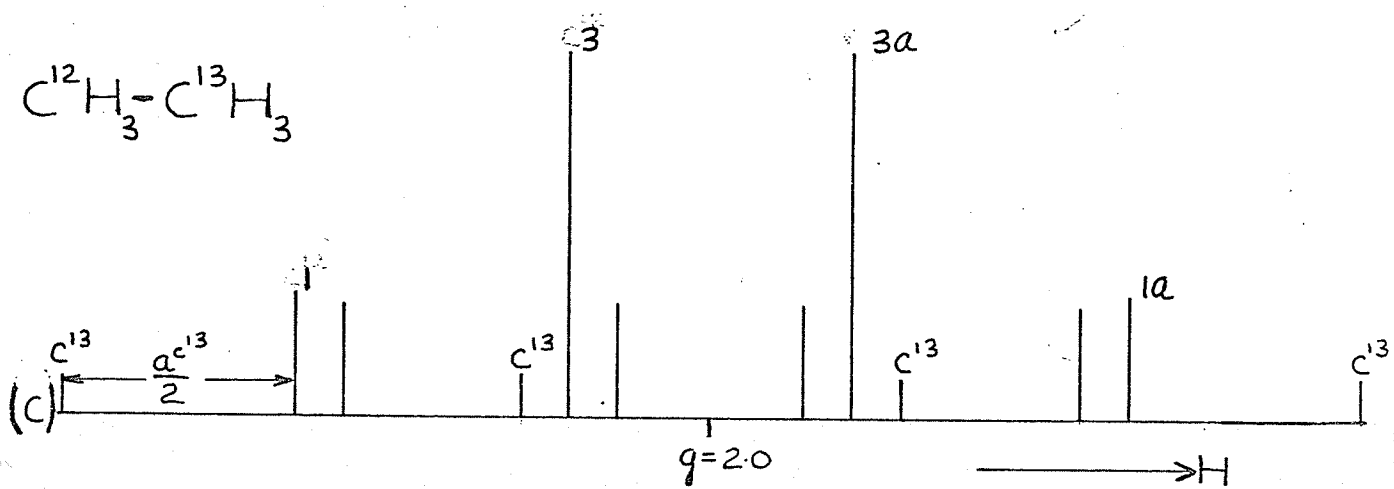
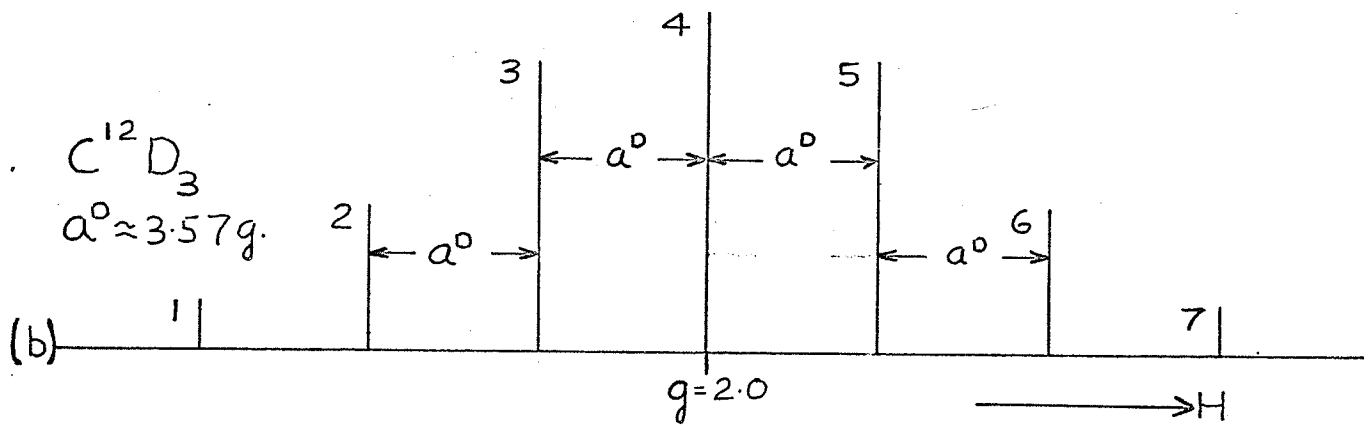
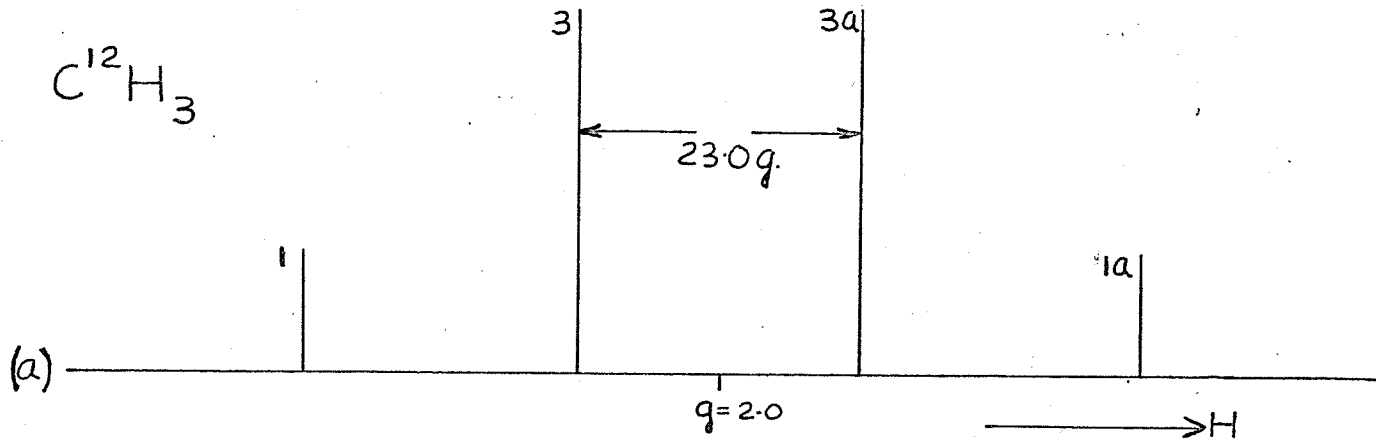
A Varian E-3 E.S.R. spectrometer employing 100 KHz modulation was used. The measurements were made using the Fieldial control included in the spectrometer. A large number of measurements were made in order to compensate for any instabilities in the instrument. The signal-to-noise ratio was extremely good until the highest temperatures were reached.

3. Methods of Measurement of E.S.R. Parameters

The four lines in the methyl radical spectrum are labelled 1, 3, 3a and 1a in going from low to high field (see Figure 3.7(a)). The proton splitting measured was that between lines 3 and 3a since this would allow measurements to be made over the largest temperature range (77°K-400°K). Within one temperature run 3 to 6 spectra were recorded at each temperature. A total of seven temperature runs were made. Therefore the proton splitting recorded at any single temperature is an average of 21 to 42 measurements. Within one temperature run the average deviation at any one temperature (calculated from the scatter of values) is ± 0.025 gauss. Two temperature runs could be displaced from the average by a maximum of ± 0.040 gauss. The reason for the displacement between runs is believed to be due to the spectrometer (perhaps changes in the temperature of the magnet cooling water). In order to obtain the temperature coefficients as a function of temperature the average values of the proton h.f. splittings are plotted on a much expanded

Fig. 3.7

"Stick" diagram of $C^{12}H_3$ (a), $C^{12}D_3$ (b) and
 $C^{12}H_3-C^{13}H_3$ (c) indicating measurements made.



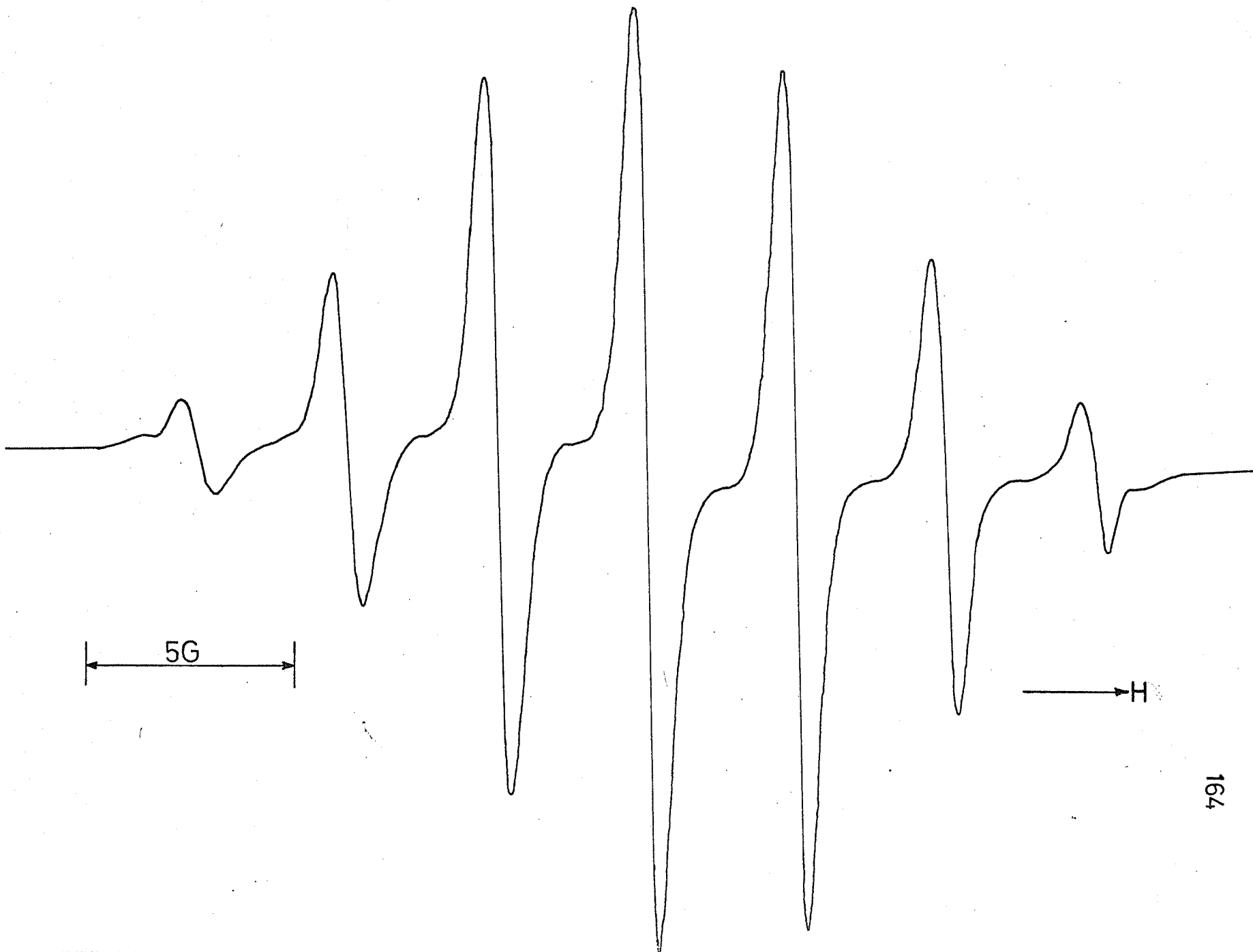
temperature scale and the slopes are recorded for 25° intervals. The slopes ($\Delta|a^H|/\Delta T$) are then plotted as a function of the mid-points of the temperature intervals.

The line widths of the proton lines are measured directly from the first derivative lines (magnetic field difference between upper and lower maxima). The asymmetry of the proton lines is also plotted as a function of temperature. The asymmetry of a first derivative line was estimated by dividing the amplitude of the lower half of the line by the total amplitude of the line. The intensity (area measured by making use of a planimeter) of line 3 divided by the total intensity of line 3 and 3a is also plotted as a function of temperature. The relative intensities (areas) of all four proton lines are plotted as a function of temperature as well.

Only preliminary results concerning the temperature dependence of $|a^D|$ can be presented. A typical CD_3 spectrum at 77°K is seen in Fig. 3.8. The deuterated methyl radical lines are numbered 1 to 7 on going from low to high field (See. Fig. 3.7(b)). The deuterium splittings between lines 2 and 3, 3 and 4, 4 and 5, 5 and 6, and 2 and 6 divided by 4 are averaged and plotted as a function of temperature. The splitting between lines 1 and 7 was avoided since the attainable temperature range would have been decreased due to the low intensity of these lines. Only three temperature runs were made and a relatively large spread in results was obtained due to the small value of $|a^D|$ and the small change of $|a^D|$ with temperature. It is nevertheless possible to make some useful comments from the results. Further measurements should be made on this radical in order to study the ratio R_1 (isotope effects) over a large temperature range.

Fig. 3.8

Spectrum of the Deuteromethyl Radical at 98.7°K



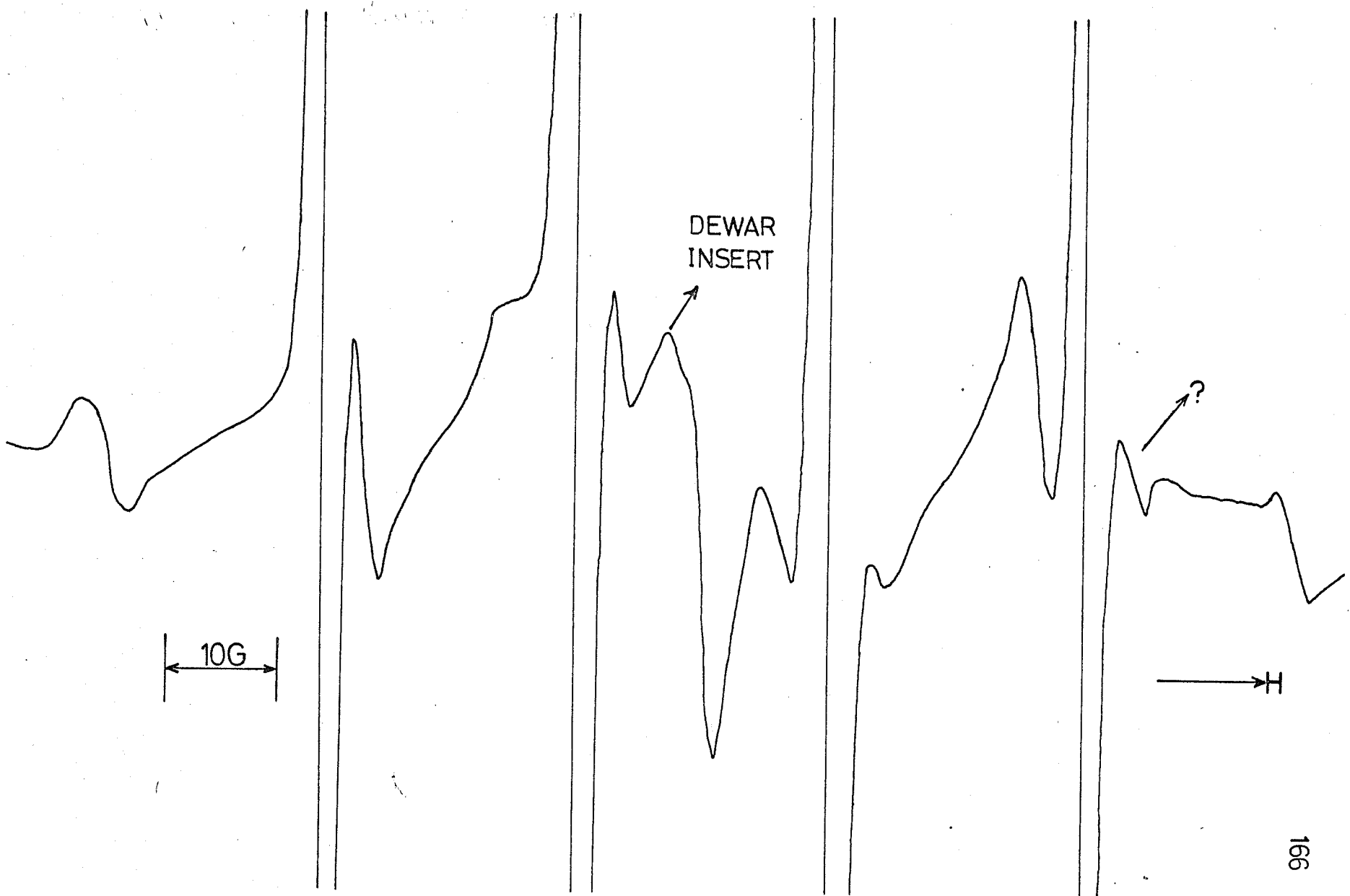
A typical spectrum of the $\text{CH}_3^{12} - \text{CH}_3^{13}$ mixture is seen in Fig. 3.9. The carbon-13 splitting measurements were made between the lowest field carbon-13 line and line 1 of the proton spectrum (See Fig. 3.7(c)). This value was multiplied by a factor 2 to obtain $|a^{\text{C}^{13}}|$. A total of three temperature runs have been made. This was sufficient since the change in $|a^{\text{C}^{13}}|$ with temperature is very large compared to the change in $|a^{\text{H}}|$ and $|a^{\text{D}}|$ with temperature. The validity of the method used to measure $|a^{\text{C}^{13}}|$ was checked by carrying out a temperature run where the carbon-13 splitting was measured in a different way^{59,79} (subtracting the separation between lines 1 and 1a from the separation between the outermost carbon-13 lines). The agreement between the two methods was found to be excellent. The temperature coefficients of the carbon-13 splittings are plotted as a function of temperature as was done for the proton splittings (see above).

Two temperature runs were made on methyl radicals stabilized on a chlorinated surface. The proton splittings were measured as described above (also see Fig. 3.7(a)). The asymmetry function, defined above, was also plotted as a function of temperature for this system. The line width and intensity studies were not performed.

The accuracy of the values for the proton and carbon-13 splittings was estimated by calibrating the Fieldial using aqueous peroxyamine disulfonate solutions.¹¹⁷ The values for the proton splittings are within ± 0.06 gauss of the values plotted (Fig. 3.10). The carbon-13 h.f. splittings between 125°K and 325°K are within ± 1.0 gauss of the values on the curve shown in Fig. 3.14. Between 77°K and 125°K the error in the carbon-13 splittings is ± 2.0 gauss. Not enough experimental work has been done to calculate the accuracy of the deuterium h.f. splittings.

Fig. 3.9

Spectrum of a Mixture of $C^{12}H_3$ and $C^{13}H_3$ Radicals
At 192°K.



RESULTS

A. Proton Hyperfine Splittings

The proton hyperfine splitting measured between 77°K and 400°K is shown in Fig. 3.10.* The general shape of the temperature dependence is comparable to that calculated by DMS (indicated by ellipses in Figure 3.10). The errors involved in plotting this curve were estimated in section 3. In a number of runs (5 out of 7) a plateau was obtained between 250°K and 300°K. This plateau is not obvious in Figure 3.10 since the values plotted are averages of all seven runs some of which were displaced from one another. Figure 3.11 has been included to emphasize the presence of this plateau and the displacement between runs. In Figure 3.11 the average values of the proton h.f.s. for three typical temperature runs are plotted. It is believed that this plateau is real and is indicative of a surface effect which becomes stronger as the temperature is lowered. Another interesting feature observed in Figure 3.11 is a slight maximum in $|a^H|$ at 135°K. This feature was observable to a greater extent in many of the temperature runs, but did not appear in the average plot (Figure 3.10). These features will be discussed further in section 5 of this chapter.

Let us now examine the temperature coefficients of the averaged proton hyperfine splittings (Figure 3.10) as a function of temperature (see Table 3.9). The values of $[\Delta|a^H| / \Delta T] \times 10^3$ are plotted as a function of the midpoints of the temperature intervals in which they were measured (Figure 3.12). Comparisons of our observed values with other experimental⁷⁴ and calculated^{101,111} values can be seen in Table 3.10.

*Raw data of the seven proton h.f.s. runs may be seen in Appendix I, page 249.

Fig. 3.10

Temperature dependence of the proton hyperfine splitting. Ellipses represent the values calculated by Schrader (DMS) for model C ($\rho(90) = \rho(0) = 0.8$). Solid line is the temperature dependence found experimentally by Zlochower et al.⁷⁴ Error line shows the maximum displacement of different temperature runs from the average value. Distance between bars on the error line indicate the average deviation for one temperature run.

TEMPERATURE DEPENDENCE
OF THE PROTON HYPERFINE
SPLITTING

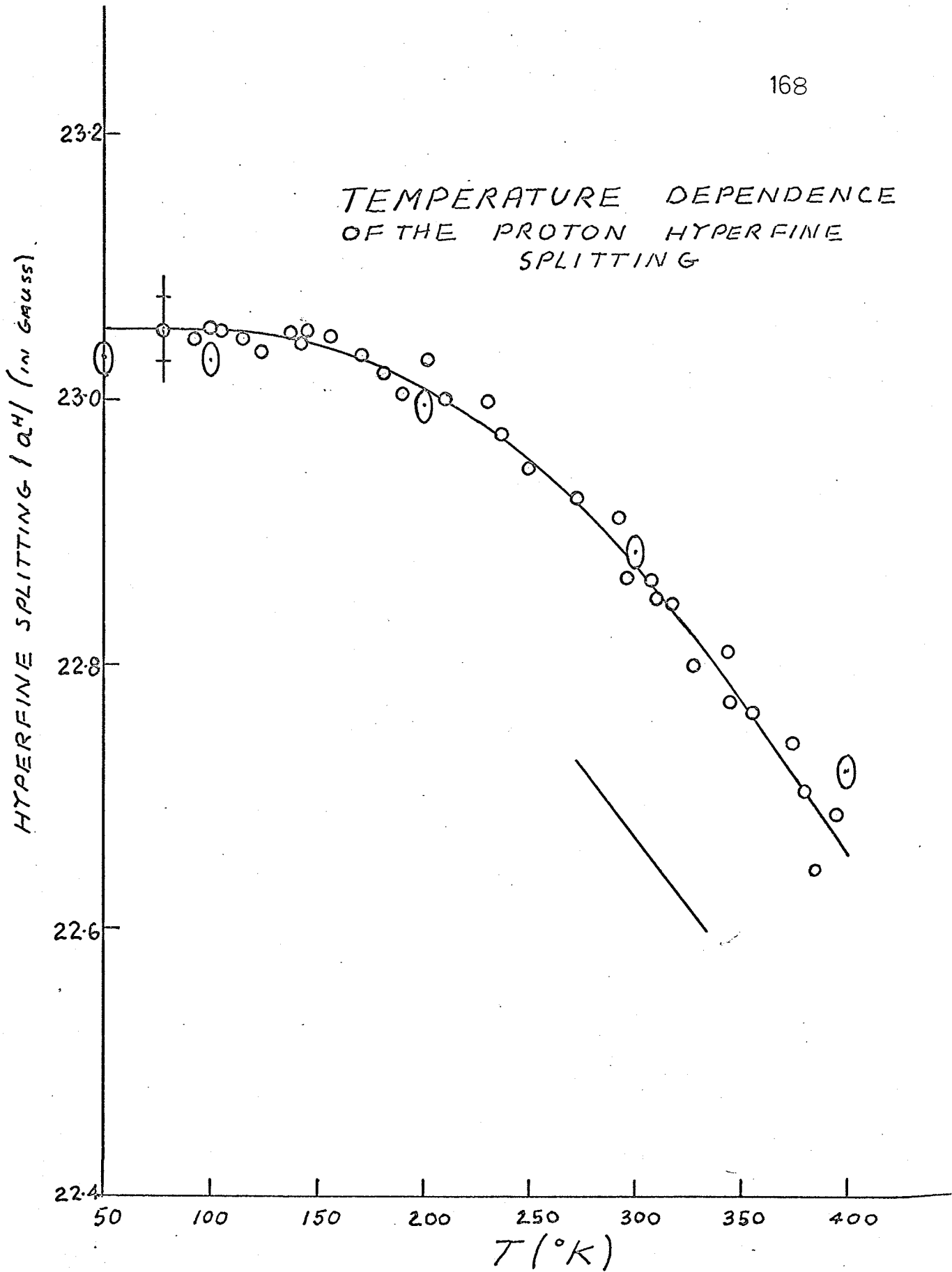


Fig. 3.11

Temperature dependence of the proton hyperfine splitting. Values plotted are from three temperature runs. Notice the displacement and the plateau at 250°-300°K.

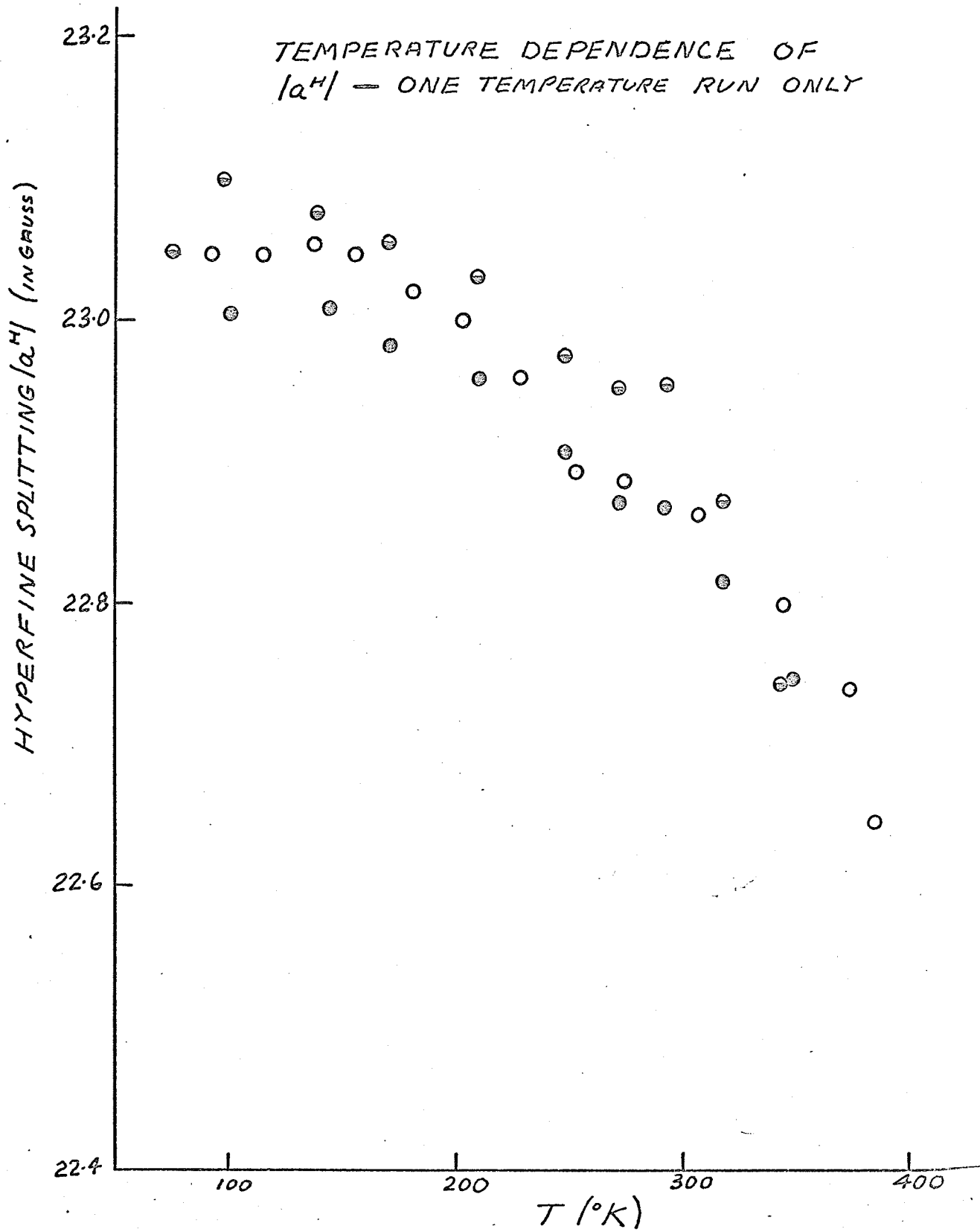


TABLE 3.9

Temperature Coefficients of Proton and Carbon-13
Splittings

$ a^H $		$ a^{C^{13}} $	
$T_2(^{\circ}K) - T_1(^{\circ}K)$	$\frac{\Delta a^H }{\Delta T} \times 10^3$ (gauss/ $^{\circ}K$)	$T_2(^{\circ}K) - T_1(^{\circ}K)$	$\frac{\Delta a^{C^{13}} }{\Delta T}$ (gauss/ $^{\circ}K$)
25-0*	0	87.5-75	0.206
50-25*	0	100-87.5	0.218
75-50*	0.03	112.5-100	0.206
100-75	0.08	125-112.5	0.090
125-100	0.19	137.5-125	0.037
150-125	0.35	150-137.5	0.023
175-150	0.55	167.5-150	0.016
200-175	0.75	175-167.5	0.014
225-200	0.89	187.5-175	0.012
250-225	1.09	200-187.5	0.012
275-250	1.40	225-200	0.012
300-275	1.60	250-225	0.013
325-300	1.90	275-250	0.013
350-325	2.13	300-275	0.014
375-350	2.48	325-300	0.015
400-375	2.96		

extrapolated values

Fig. 3.12

Temperature dependence of the temperature coefficients
of the proton splitting. Average deviation is indicated.

TEMPERATURE COEFFICIENTS OF
PROTON SPLITTING

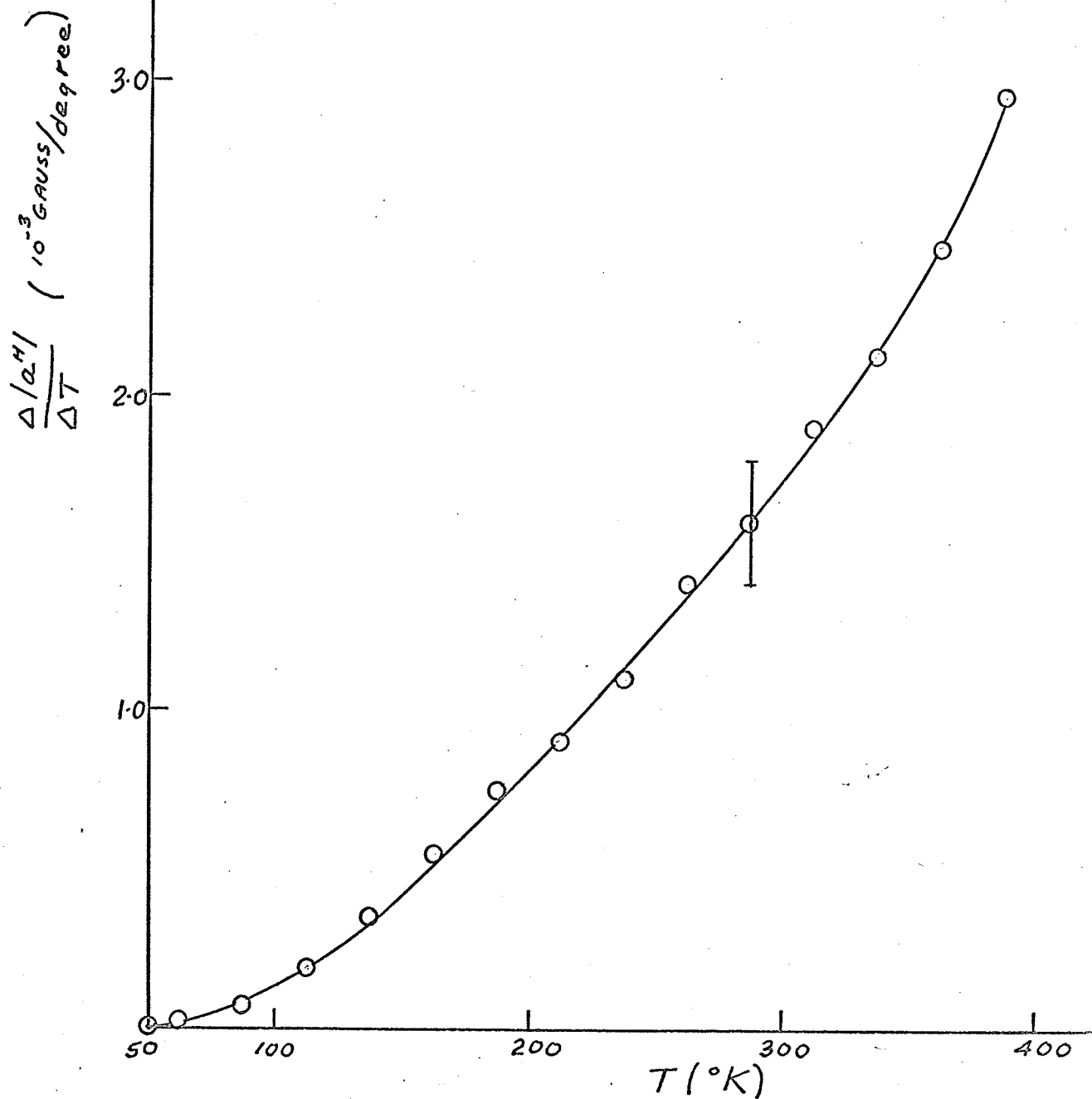


TABLE 3.10

Comparisons of Temperature Coefficients

$$\frac{d|a^H|}{dT} \times 10^3 \text{ (gauss/}^\circ\text{K)}$$

T(°K)	Observed ^a	Calculated ^b	Calculated ^c	Observed ^f
273	2.1±0.2	1.33±0.20	1.21±0.03	1.50±0.20
298	2.1±0.2	1.48±0.20	1.35±0.03	1.75±0.20
333	2.1±0.2	1.67±0.20	1.55±0.05	2.05±0.20

$$\frac{d|a^{C13}|}{dT} \text{ (gauss/}^\circ\text{K)}$$

T(°K)	Calculated ^c	Observed ^g
273	0.0116±0.0007	0.0135±0.0025
298	0.0129±0.0008	0.0145±0.0025
333	0.0146±0.0008	0.0160±0.0025*

a reference 74

b calculated from relations given in reference 111 by DMS

c calculated by DMS

f this work - from Figure 3.12

g this work - from Figure 3.15 (only observed values)

* extrapolated from Figure 3.15

B. Deuterium Hyperfine Splittings

Preliminary results of the measurement of $|a^D|$ as a function of temperature were included to demonstrate a general difference between the results of this work and those calculated by DMS. It can be seen in Fig. 3.13 that although there is a large scatter in results the absolute values of the temperature coefficients are larger than those predicted. The results indicate that the temperature coefficient measured in the temperature interval 200 to 300°K is approximately 2.3×10^{-3} gauss/°K which is much larger than the calculated values of $1.67 \pm 0.02 \times 10^{-3}$ gauss/°K, $1.79 \pm 0.03 \times 10^{-3}$ gauss/°K and $1.91 \pm 0.06 \times 10^{-3}$ gauss/°K, for the temperatures 273°K, 298°K and 333°K respectively (DMS). The measurements of $|a^D|$ were only performed over the temperature interval 77°K to 315°K because the deuteromethyl radical lines are less intense than the methyl radical lines. Incidentally, the temperature coefficients of the CD_3 radical appear to be larger than the corresponding temperature coefficients of the CH_3 radical, as predicted by theory (DMS).

C. Carbon-13 Splittings

The temperature dependence of the carbon-13 h.f.s. is shown in Fig. 3.14. Notice is to be made of the decrease in the absolute value of the carbon-13 splitting which begins at 145°K and which becomes extreme at approximately 120°K. The values plotted in Figure 3.14 are averages of three temperature runs. In two of the three runs a slight increase was observed in the absolute value of the carbon-13 h.f.s. in the temperature interval 150°K-125°K which would make the

Fig. 3.13

Temperature dependence of the deuterium hyperfine splitting. Have plotted $6.51437 |a^D|$ vs. $T(^{\circ}\text{K})$ where 6.51437 is the ratio of the g-factors of the proton and deuteron. Schrader's calculated results are shown by ellipses (DMS). Average deviation is ± 0.09 gauss (indicated).

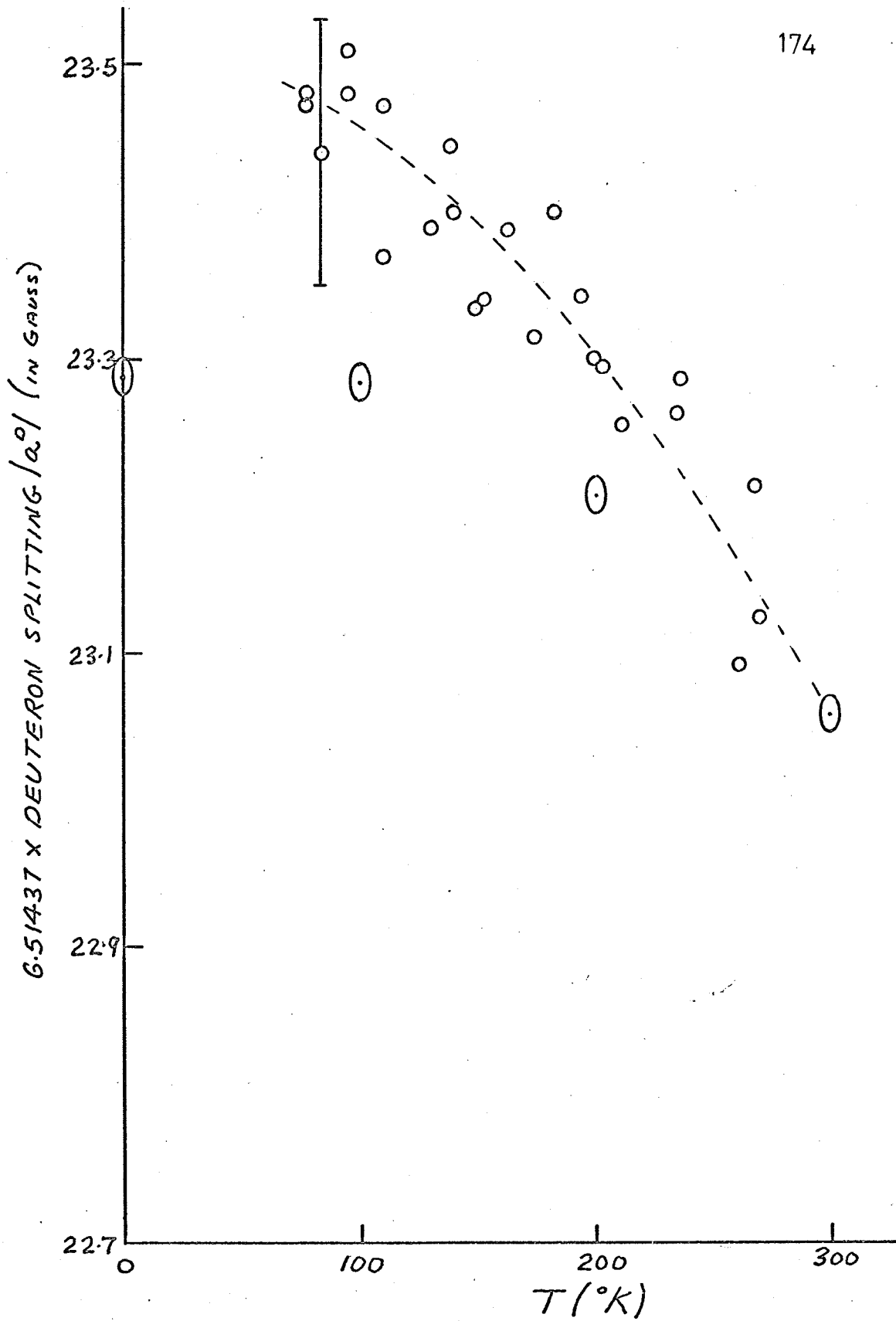
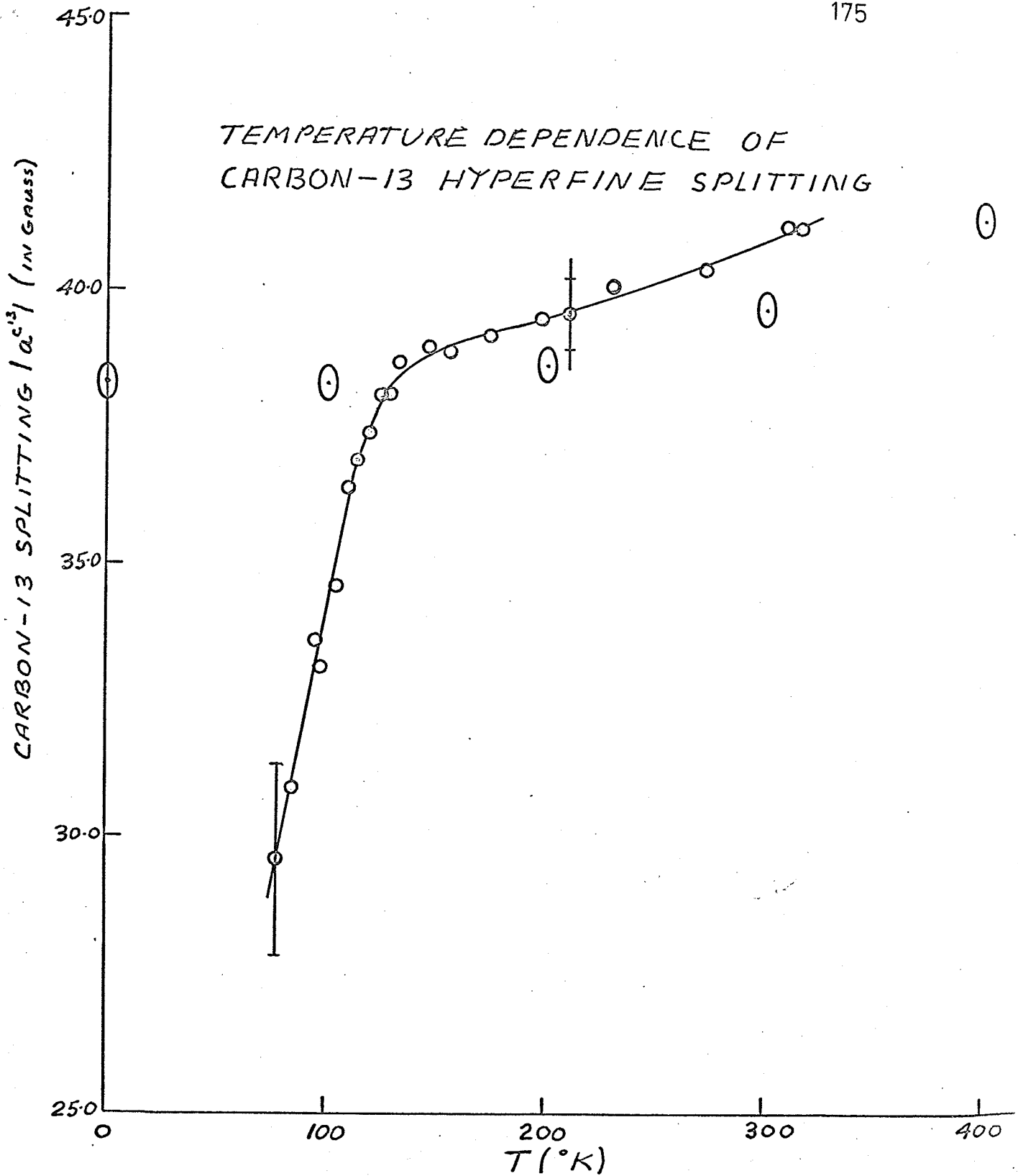


Fig. 3.14

Temperature dependence of carbon-13 splitting. Ellipses are the calculated values (DMS). Errors are indicated. Error line represents displacement between runs while bars indicate average deviation within one run.

TEMPERATURE DEPENDENCE OF
CARBON-13 HYPERFINE SPLITTING



decrease in the carbon-13 h.f.s. on going to lower temperatures even more pronounced. This slight increase can be seen in Fig. 3.14. In the temperature range 125°K to 325°K a displacement was obtained between temperature runs as was found in the study of the proton h.f.s. The maximum value of the displacement (in the temperature range 125°K to 325°K) was calculated to be ± 1.00 gauss with respect to the averages plotted in Figure 3.14. The scatter in values within one temperature run was largest at very low temperatures because at these temperatures the C^{13} lines were broadened considerably. Between 120°K and 310°K, the average deviation from the mean, within one temperature run, was calculated to be ± 0.65 gauss. Between 77°K and 120°K, the average deviation from the mean, within one temperature run, was calculated to be ± 1.75 gauss and the displacement was not larger than the scatter of points within one temperature run.

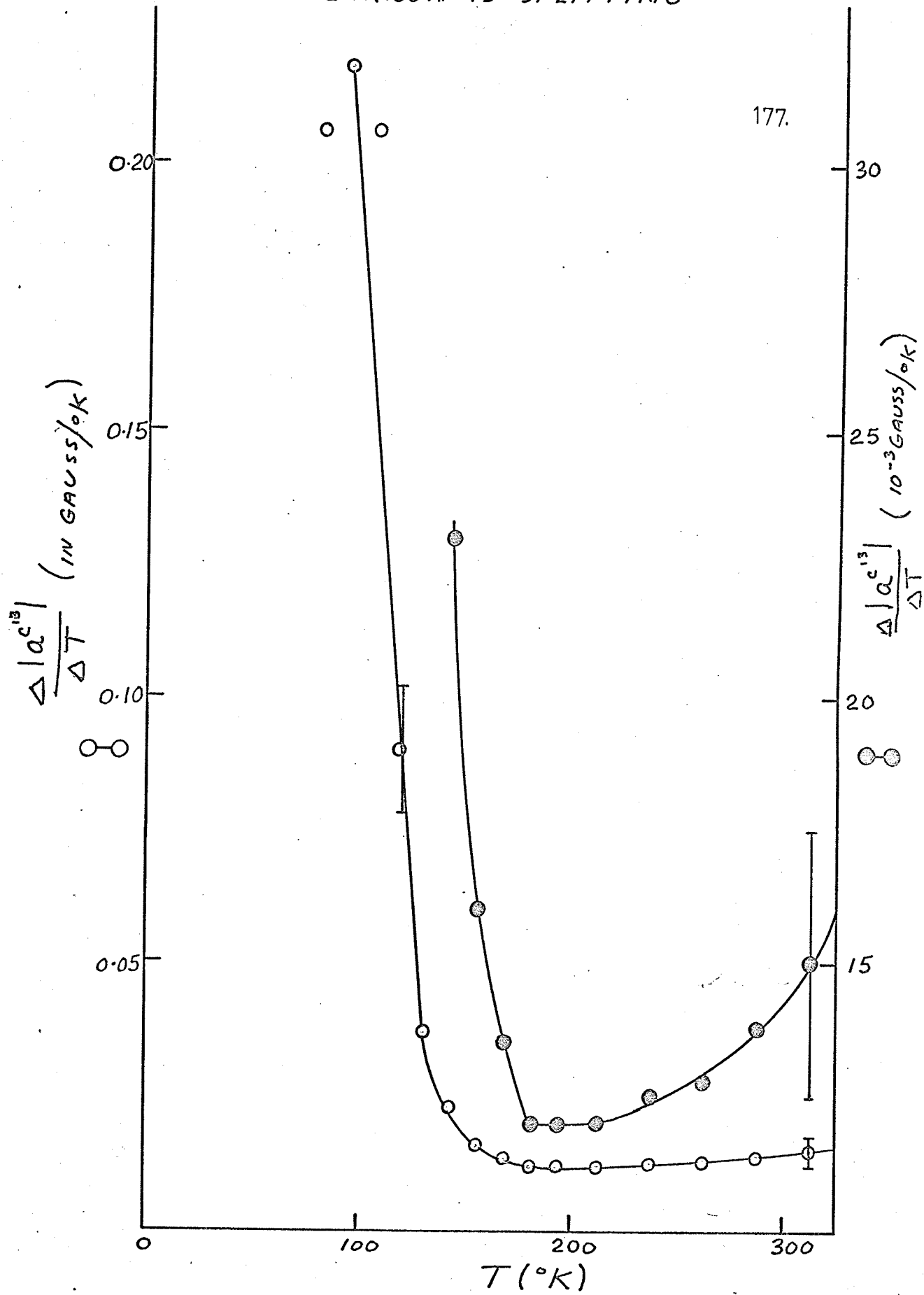
The curve showing the temperature dependence of the carbon-13 h.f.s. was extrapolated and led to a value of 10.6 ± 2.5 gauss for $|aC^{13}|$ at $T = 0^\circ K$. What is required, of course, is a measurement of $|aC^{13}|$ at some temperature considerably below 77°K. This measurement may not be feasible due to increased anisotropy of the carbon-13 lines at lower temperatures.

The temperature coefficients of the carbon-13 h.f. splittings have been examined as a function of temperature as was done for the proton splittings (Table 3.9). The average deviation of $\Delta|aC^{13}| / \Delta T$ between 75°K and 125°K has been estimated at ± 0.012 gauss/°K, and between 125°K and 325°K the average deviation has been estimated to be ± 0.0025 gauss/°K. A comparison of the observed values with values calculated by DMS are given in Table 3.10. The temperature coefficients of the averaged carbon-13 splittings are plotted as a function of temperature (Fig. 3.15) as in the case of the proton h.f.s. Two ordinate scales are employed to amplify the change in $\Delta|aC^{13}| / \Delta T$ at either end of the temperature range.

Fig. 3.15

Temperature dependence of carbon-13 temperature coefficients. Solid circles correspond to right hand scale while open circles correspond to left hand scale. Average deviations in different temperature ranges are indicated.

TEMPERATURE COEFFICIENTS OF
CARBON-13 SPLITTING



It is worth noting that, at higher temperatures where the proton lines tend to the binomial distribution, the amplitude of the low field carbon-13 line appeared to be larger than the amplitude of the high field carbon-13 line. This would mean that aC^{13} is positive in sign.¹¹⁸

D. Line Width, Asymmetry, And Intensity Studies Of The Proton Lines

In Figure 3.16 the linewidths of lines 3 and 3a are shown as a function of temperature. The linewidth of 3 reaches a minimum at $200 \pm 25^\circ K$. The linewidth of 3a does not increase nearly so much at low temperatures but does have a similar dependence at temperatures above $225^\circ K$. The linewidth of 3a is smaller than the linewidth of 3. The error in these measurements is estimated to be ± 0.04 gauss. The linewidths of the four proton lines decrease on going to higher values of the magnetic field. For instance, at $99^\circ K$, the following measurements were made.

Line 1	ΔH_{pp}	= 1.05g
Line 3	ΔH_{pp}	= 0.95g
Line 3a	ΔH_{pp}	= 0.83g
Line 1a	ΔH_{pp}	= 0.78g

The four lines are presumably still of unequal width at $350^\circ K$, but to a lesser extent. Much more will be said about the proton linewidths in the following chapter.

The asymmetry of the proton lines 3 and 3a decrease as the temperature is increased (Fig. 3.17). Lines 1 and 1a exhibit similar dependences as lines 3 and 3a. Lines 1a and 3a are not nearly as asymmetric as lines 1 and 3. At any one temperature the asymmetry of the proton lines decreases with increasing field values. This feature has been noticed in this laboratory for many different radicals stabilized on the surface of p.V.g. The asymmetry of lines 1a and 3a is opposite

Fig. 3.16

Temperature dependence of linewidths of proton lines
3 and 3a. Average deviations are shown.

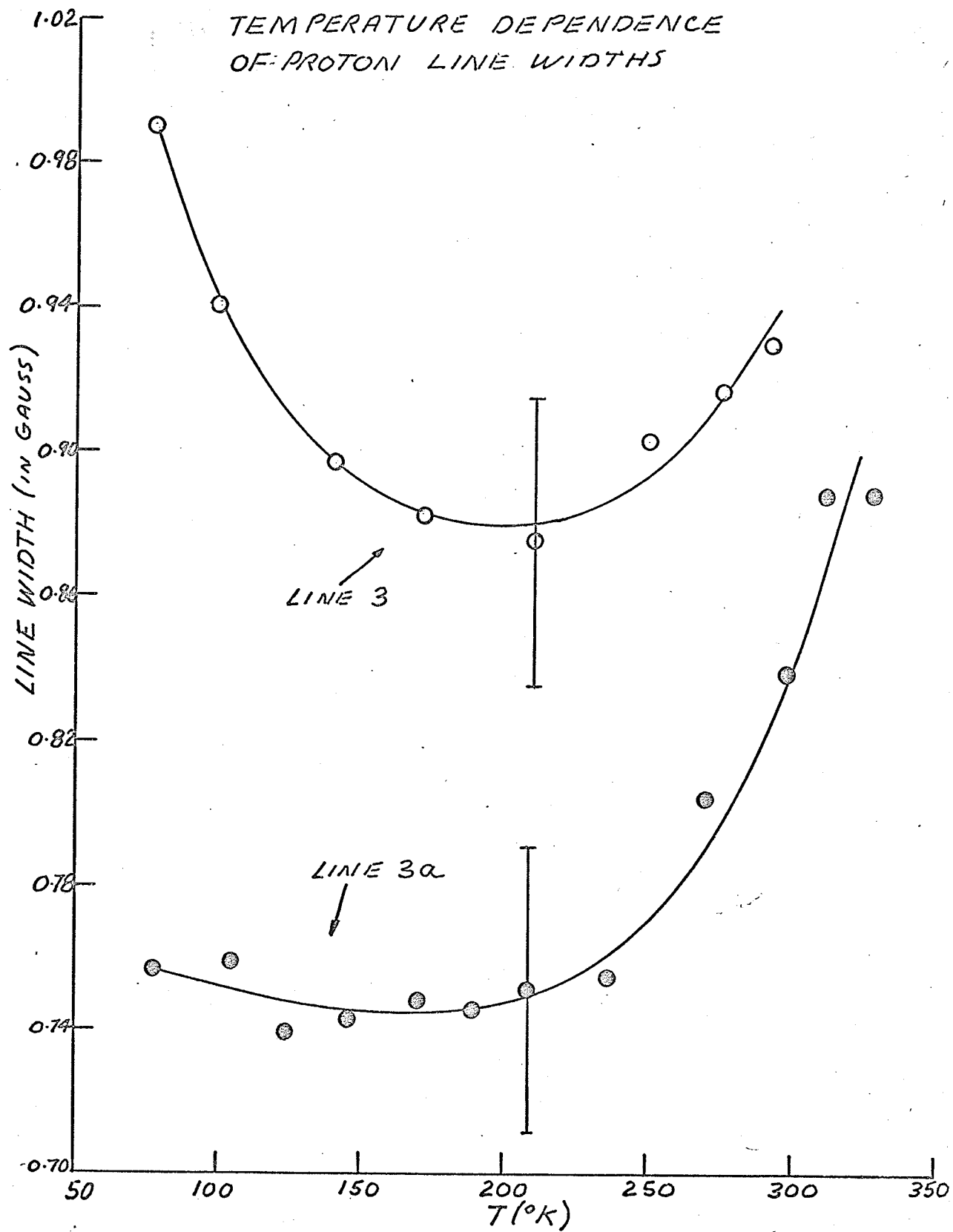
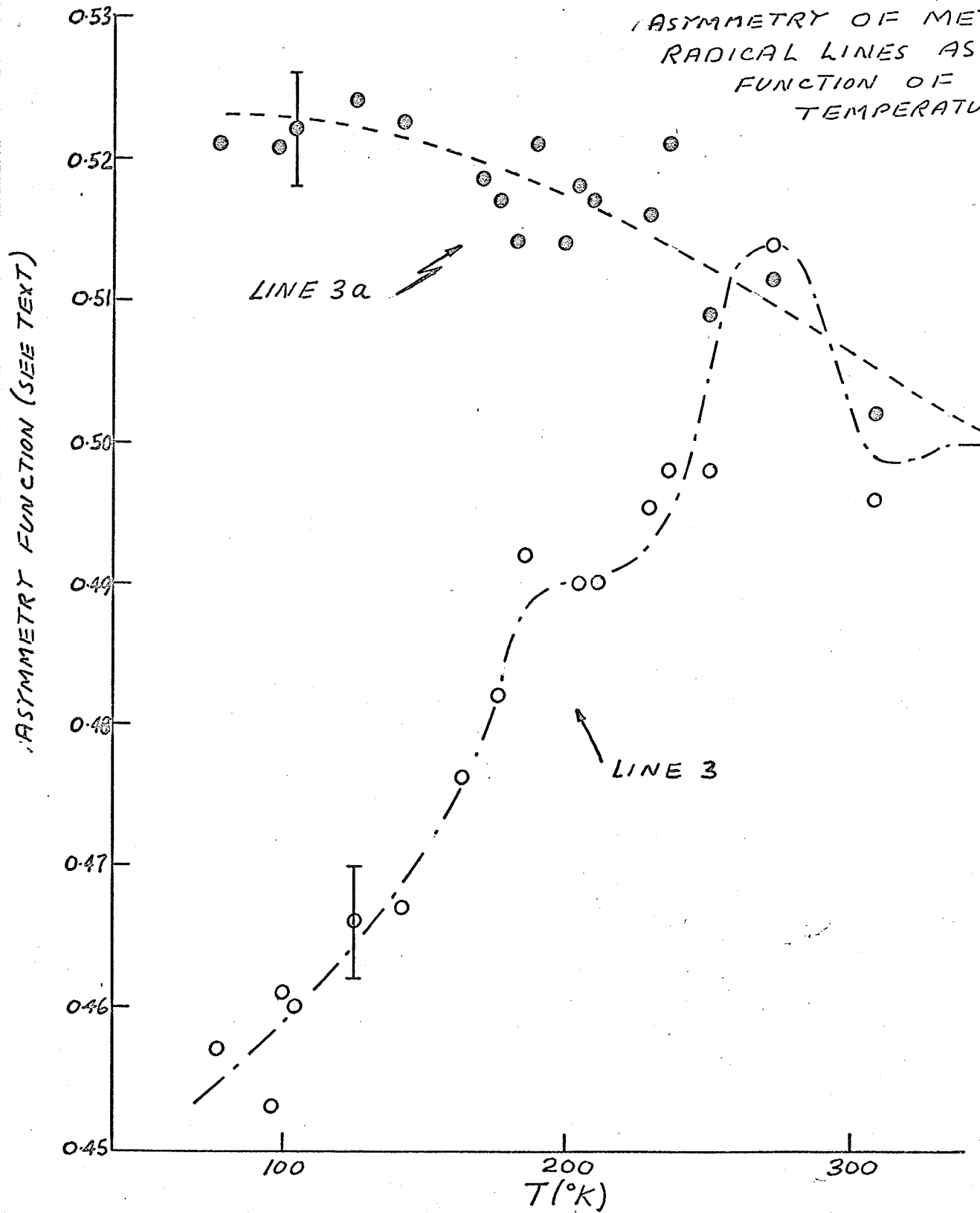
TEMPERATURE DEPENDENCE
OF PROTON LINE WIDTHS

Fig. 3.17

Asymmetry of lines 3 and 3a as a function of temperature.
Average deviations are shown (± 0.004).

ASYMMETRY OF METHYL
RADICAL LINES AS A
FUNCTION OF
TEMPERATURE

to that of lines 1 and 3. There are two features to note in Fig. 3.17 regarding line 3. In all asymmetry curves plotted for line 3, a plateau was noticed at approximately 200°K as well as a peculiar maximum at 275°K. The slope of the curve seems to decrease on approaching 77°K.

The area of line 3 divided by the total area of lines 3 and 3a has been measured as a function of temperature. The resulting curve can be seen in Figure 3.18. The resemblance between this curve and the asymmetry curve for line 3 in Fig. 3.17 is remarkable. The plateau occurs between 175°K and 200°K and the peculiar maximum occurs at 265°K. The approach of this ratio to a value of 0.5 is taken to be an indication of the approach of the relative intensities of the four proton lines to the binomial value of 1:3:3:1. To check this the relative intensities of the four lines were measured as a function of temperature and then plotted (Figure 3.19). Figure 3.19 shows that the relative intensities do approach the binomial values as the temperature is increased (at 300°K the observed relative intensities are 1.0:3.3:3.3:0.9).

A study was carried out to determine if the four proton lines are symmetrical with respect to the areas above and below the baseline (Fig. 3.20). The lines were found to be symmetric within experimental error over the temperature range 77°K to 300°K. Note that the experimental error will be largest for the two smaller lines (i.e. lines 1 and 1a). It could not be shown that the three proton hyperfine splittings were of unequal value.

E. Methyl Radicals on a Chlorinated Surface

The proton hyperfine splitting was measured on increasing the temperature and then on decreasing the temperature. Two runs of this nature were performed and the results (averages of the two runs) are shown in Figure 3.21. Also plotted in Figure 3.21 are the calculated values of DMS and the experimental values from Figure 3.10.

Fig. 3.18

Area of line 3 divided by total area of lines 3 and 3a
as a function of temperature. Average deviation is indicated
(± 0.004).

$\left(\frac{\text{AREA OF LINE 3}}{\text{AREA OF LINES 3+3a}} \right)$ AS A FUNCTION
OF TEMPERATURE

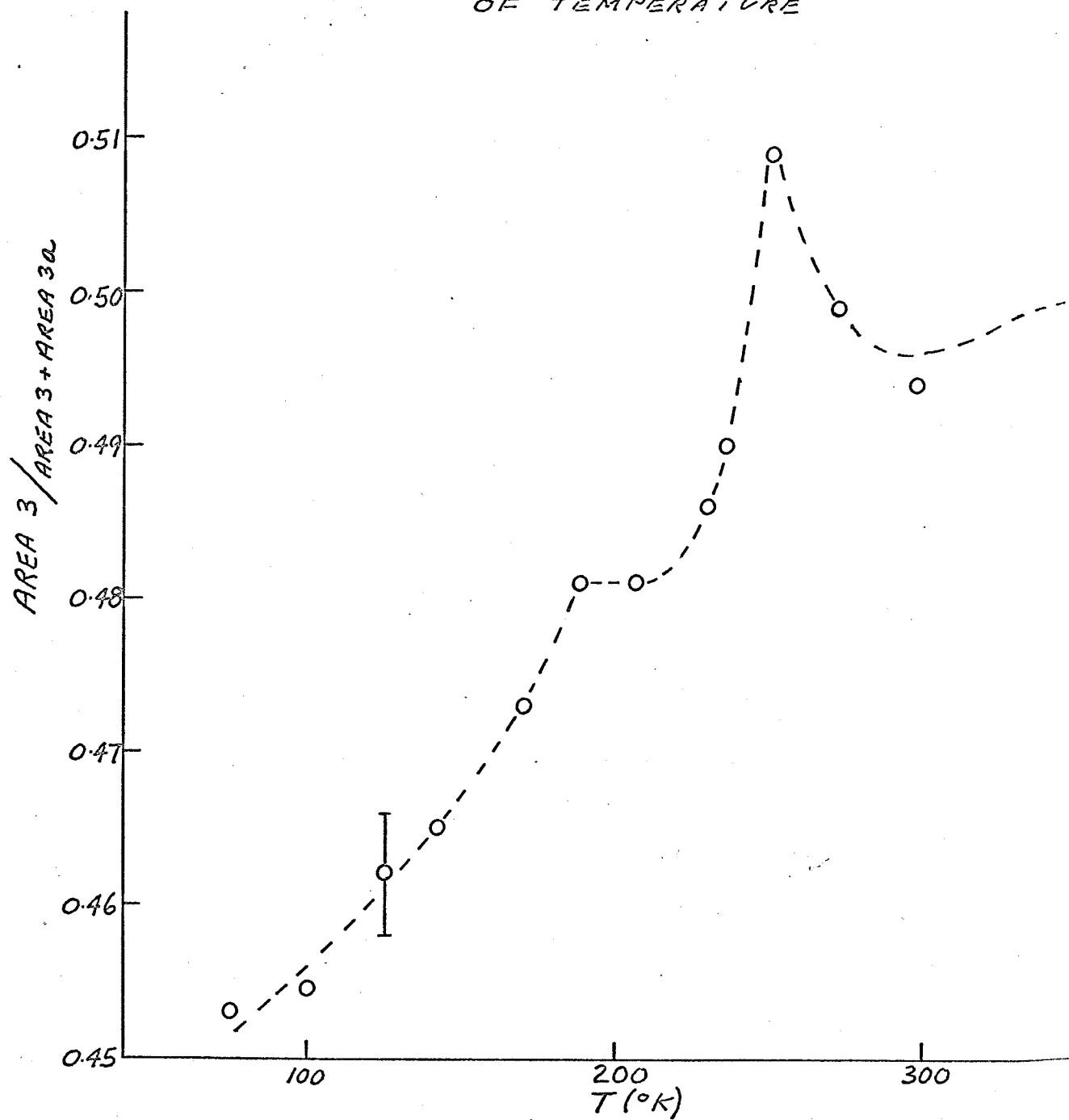


Fig. 3.19

Relative intensities of the four methyl radical lines as a function of temperature. Values are obtained by setting the intensity of line 1 = 1.

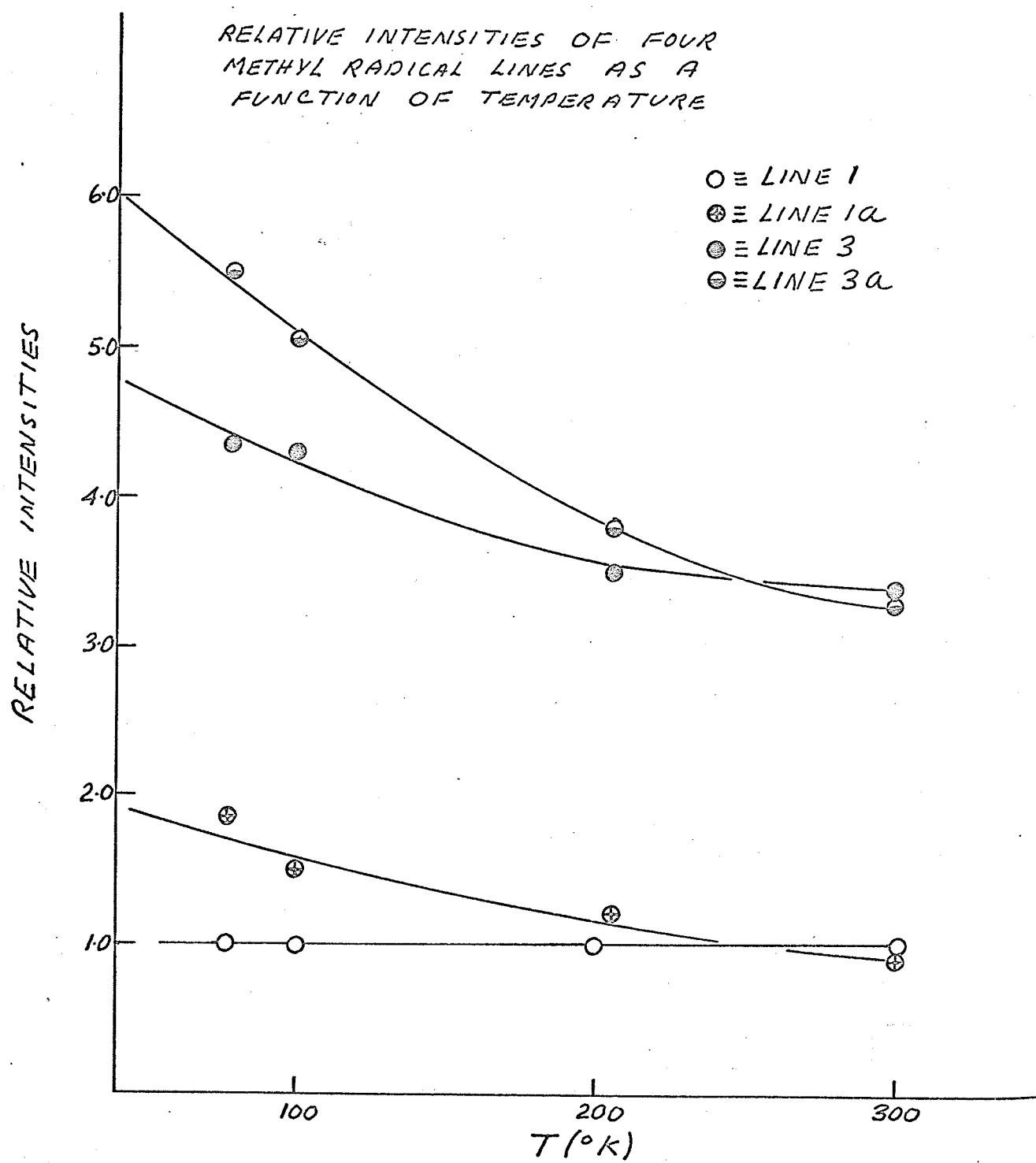


Fig. 3.20

Area of proton lines below baseline divided by total area of lines as a function of temperature.

$\left(\frac{\text{AREA OF LOWER HALF OF LINE}}{\text{TOTAL AREA OF LINE}} \right)$ AS A

FUNCTION OF TEMPERATURE

AREA RELATION (SEE TEXT AS WELL AS ABOVE)

● ≡ LINE 1a
○ ≡ LINE 3a

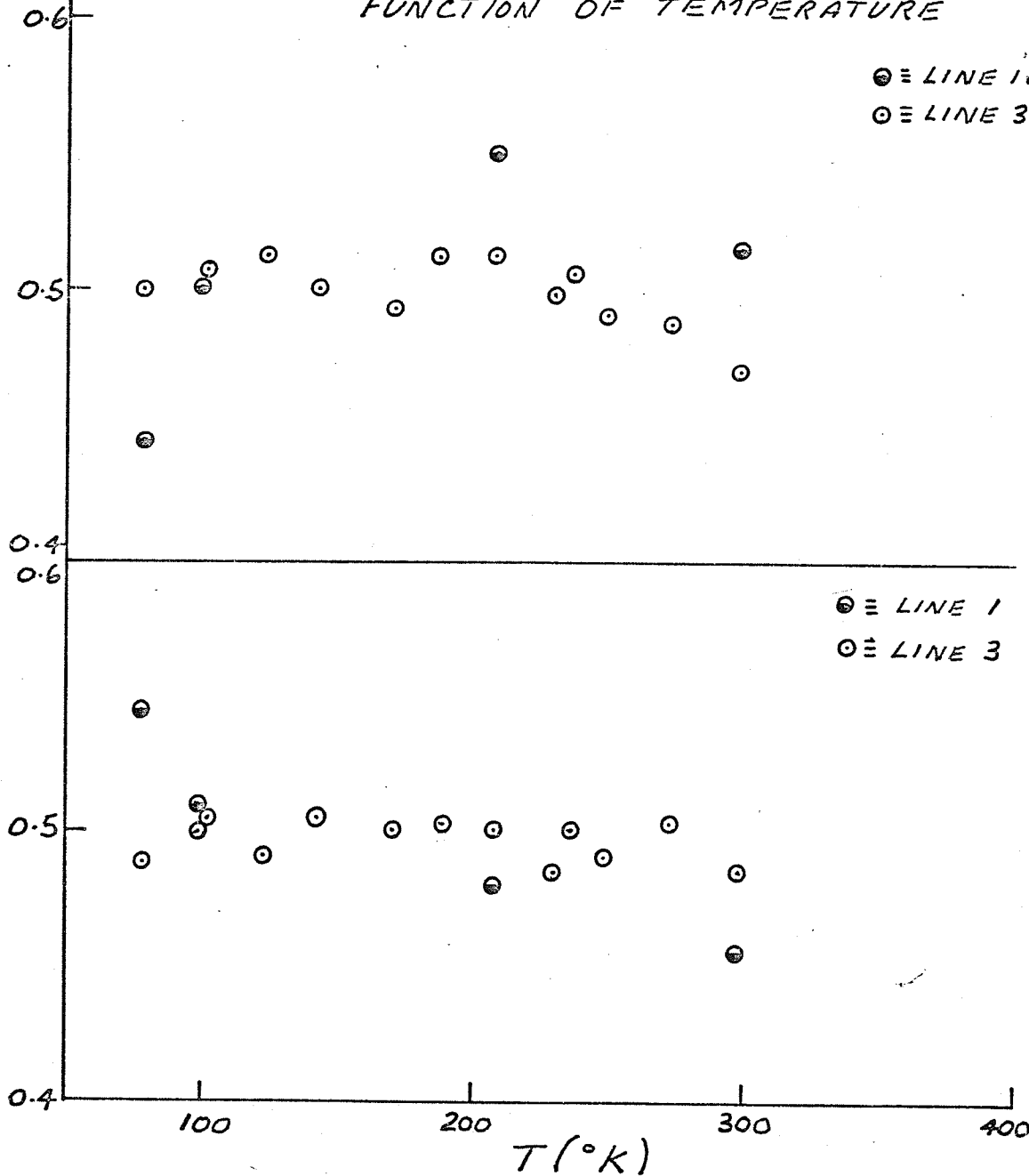
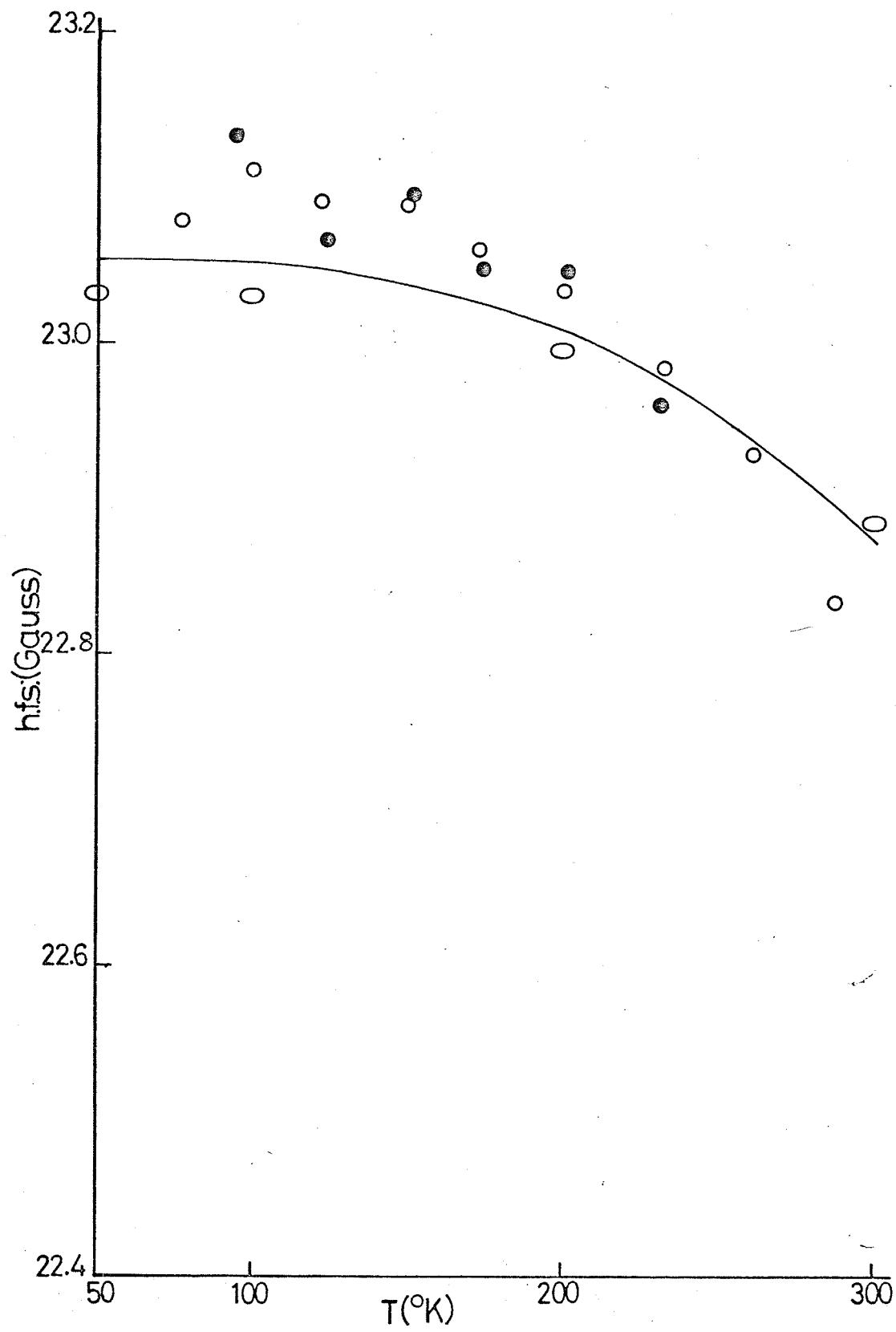


Fig. 3.21

Temperature dependence of the proton splitting of methyl radicals stabilized on chlorinated p.V.g. Calculated values are indicated by the ellipses (DMS). The solid line is the experimental values obtained on a regular p.V.g. surface (Fig.3). The open circles represent results obtained on warming while the solid circles are the results obtained on cooling.



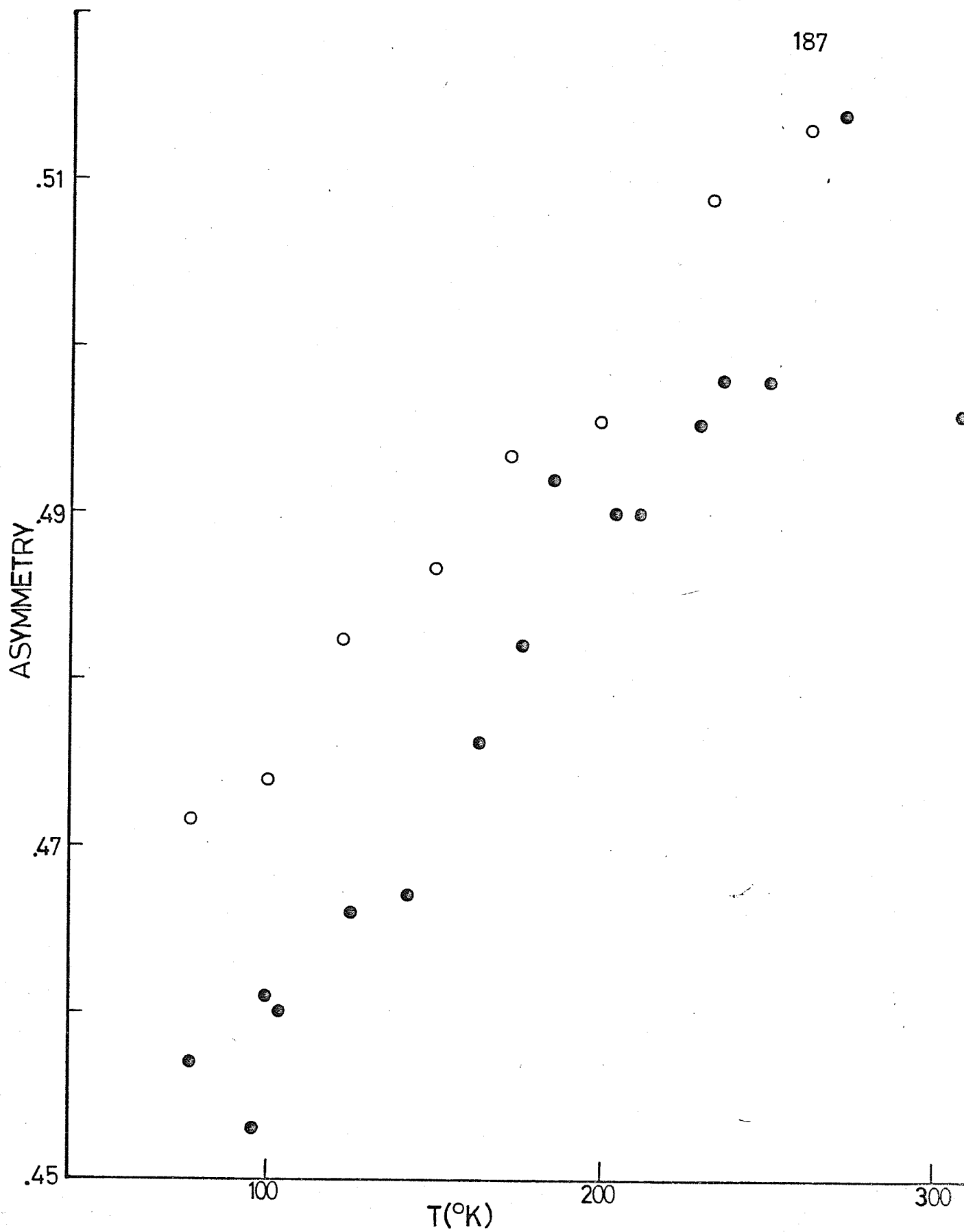
The asymmetry function (defined in section 3 of this chapter) has been plotted as a function of temperature for this system as well (Fig.3.22). For comparison, the asymmetry values for line 3 from Fig. 3.17 have been included in Fig. 3.22.

5. Discussion of Results

Experimentally, the temperature dependence theory of Schrader (DMS) has been generally substantiated. The shapes of the temperature dependences as well as the directions of change of $a^{C^{13}}$, a^H and a^D with temperature have been predicted successfully. The absolute values of the temperature coefficients have been determined experimentally to be larger in the case of a^H and a^D than predicted. This observation substantiates the choice of Herzberg's¹¹² force constant by DMS. This may be due to the fact that DMS only evaluated the effect of the A_2'' vibrational mode on the spin polarization at the protons and deuterons. Other factors such as matrix effects (or surface effects), particularly at low temperatures, may be involved. At any one temperature the temperature coefficient of $|a^D|$ was found to be greater than the temperature coefficient of $|a^H|$ as was predicted (DMS). The temperature dependence of $a^{C^{13}}$ agrees with theory at high temperatures but disagrees with theory below 200°K. This disagreement at low temperatures is attributed to surface interactions, which will be discussed later. Very little change from the predicted temperature dependence of a^H is noticed in the temperature range where the carbon-13 exhibits the anomalous behaviour. This fact must indicate that the surface is interacting with or is responsible indirectly for a change in a parameter on which $a^{C^{13}}$ depends heavily. In the same sense a^H must be almost independent of this parameter. The proton splitting is almost independent

Fig. 3.22

Asymmetry of line 3 for methyl radicals stabilized on chlorinated p.V.g. as a function of temperature (open circles). Solid circles represent the results obtained on a regular p.V.g. surface (Fig. 3.17).



of the σ_c and π_c orbitals while the carbon-13 splitting depends heavily on these two orbitals. For low values of θ and θ' , the proton splitting depends predominantly on the $1s_H$ orbital and the carbon-13 splitting depends almost exclusively on the σ_c and the $1s_c$ orbitals. Further discussion of possible interactions and parameters will be presented later.

The results obtained may be discussed in terms of physical changes of the system in different temperature ranges. At approximately 275°K a plateau is noticed in the plot of the temperature dependence of the proton h.f.s. (Figures 3.10, 3.11). Also, at this temperature, the symmetry of the proton lines is restored and the relative intensity of the proton lines approach the binomial values very closely. It is therefore postulated that above 275°K the tumbling and translational motions of the methyl radical are almost independent of surface effects. Below 275°K the protons begin to interact with the surface but no interaction of the surface with the C-13 nucleus is noticeable from the results obtained (i.e. carbon-13 h.f.s.). Carbon-13 linewidth studies may prove that an interaction does begin in this temperature range. Below 275°K the tumbling and translational motions of the methyl radical have been altered so that there is an average interaction between the protons and the surface. At still lower temperatures this interaction increases in magnitude causing a decrease in the frequency of the tumbling motion as well as a decrease in the translational motion. Some radicals are becoming localized at specific surface sites below 275°K. If the plateau noticed in the plot of the proton h.f.s. (Fig. 3.11) versus temperature is real the surface interaction may be explained as a perturbation of the A_2'' vibrational mode which increases the value of

θ (decreases $|a^H|$) as a function of temperature from those values predicted (DMS). The changes in a^H with temperature are attributed to a reduction of the spin polarization of the hydrogen 1s orbital as θ increases which can only occur if incomplete orbital following is included (DMS). The plateau may be explained as the temperature region in which θ due to the normal predicted temperature effect becomes equal to θ due to the perturbation. At temperatures above this plateau the normal trend of $|a^H|$ again predominates. At temperatures just below the plateau $|a^H|$ (or θ) due to the perturbation predominates. The effect of the surface on the protons is not considered to be excessive since the observed linewidths over the whole temperature range studied are comparable to those measured for methyl radicals in aqueous solution.⁷⁴ The observed line widths are much smaller than those measured in most matrices.^{72,79,58} It will be shown in the next chapter that the actual line widths are almost the same as those observed for the methyl radical in liquid methane.⁷¹

A plateau is noticed in the temperature dependence of the carbon-13 h.f.s. at 200°K. Above 200°K the line widths of the proton lines increase in a somewhat parallel manner and below 200°K the linewidth of 3 increases much more rapidly than 3a. At 200°K a plateau is seen in the asymmetry plot of line 3 and in the intensity ratio plot for line 3. These phenomena may be explained by proposing that the proportion of radicals localized at specific sites is constant in the temperature range around 200°K (say 200°±25°K). This would mean that an equilibrium exists between mobile and localized radicals on the surface and that $\frac{\partial \Delta G}{\partial T}$ for this equilibrium is fortuitously zero at this temperature.

Thus it is believed that at 200°K the translational motion of the radicals is beginning to freeze out. This means that the tumbling motions of many of the radicals have become reorientations at specific

surface sites. Therefore the line broadening below 200°K can be due to the orientation of radicals at surface sites (anisotropic). Other evidence in favour of this mechanism has been presented - Tables 2.8 and 2.9. Radicals localized at different sites are responsible for proton line asymmetry as well. Each trapping site is a little different from the others and therefore the spectra recorded are due to the superposition of many spectra with slightly different hyperfine interactions and line widths. The line broadening above 200°K is mainly due to the translational motions of the radicals (isotropic). This isotropic line broadening may be due to slow electron exchange between the radical and the parent compound or between like radicals, or due to radical exchange between potential wells of different energies.

At 145°K the absolute value of the carbon-13 h.f.s begins to drop. This decrease becomes very rapid at 125°K. It may be interesting to note at this point that the decay kinetics of methyl radicals on p.V.g. was determined to be first order between 103°K and 143°K.⁸⁰ This was interpreted in terms of a low stationary state concentration of mobile methyl radicals on the surface. The results presented here would seem to predict a higher mobility of methyl radicals at temperatures above 145°K and therefore the radical decay should become second order above this temperature. It must be noted at this point that the surface coverages in Reference 80 were above a monolayer while the surface coverages in this work are between 5% and 25% of a monolayer. In all samples studied in this work, including the work carried out on chlorinated surfaces, radical decay did not become noticeable until the temperature range 110°K-125°K was reached. One could say, therefore, that the translational motion (or diffusion) of the radicals across the surface is lost below this temperature range, leaving only radical

reorientation at specific surface sites. Results in Chapter II, however, indicate diffusion of radicals even at liquid nitrogen temperatures. As the temperature is lowered from 125°K the reorientation of the radical about its three-fold symmetry axis becomes more significant. At some low temperature the radical will become fixed (with pi orbital directed towards the surface site) and will only exhibit a rotation about its three-fold axis or will not rotate at all.

The large decrease in the absolute value of the carbon-13 h.f.s. below 145°K can be explained in several ways assuming the above physical model to be valid. If it is assumed that the decrease in $|a^{C^{13}}|$ continues below 77°K and since there is no evidence from Fig. 3.14 to the contrary, the decrease in the C-13 h.f.s. could be due to the slow cancellation of the isotropic splitting by an anisotropic term which becomes prominent when the motion of the methyl radical becomes primarily a rotation about its three-fold axis. Based on an experiment by Adam and Weissman on the anisotropic splitting in the triphenyl methyl radical,¹¹⁹ and assuming the methyl radical is planar and undergoes reorientation only about its symmetry axis or not at all, Cole et al⁵⁹ predicted $|a^{C^{13}}|$ to be 60-66 gauss or 4-10 gauss. The observed extrapolated value for $|a^{C^{13}}|$ at 0°K is 10.6 ± 2.5 gauss which agrees with the lower predicted value calculated by assuming the anisotropic splitting to be opposite in sign to the isotropic splitting value. If the two signs are the same the predicted value is 60-66 gauss. The observed results indicate that the anisotropic term is negative since the isotropic term is known to be positive. In contrast to our results, McConnell and Fessenden,¹²⁰ assuming that the

isotropic part of the C-13 h.f.s. for the malonic acid radical is positive and equal in value to that of the methyl radical⁵⁹ ($a^{C13} = +41 \pm 3g$), estimated that the anisotropic C-13 h.f.s. to be of the same sign as the isotropic part and equal to about 46 gauss.

The decrease observed for the C-13 h.f.s. may also be explained in terms of a transfer of unpaired electron spin density from the carbon pi orbital to the surface site. A significant decrease in the absolute value of the proton h.f.s. would be expected to accompany this transfer. In several temperature runs a slight decrease in the absolute value of the proton h.f.s. was noticed on lowering the temperature from 135°K to 77°K. A measurement of the proton h.f.s. is needed below 77°K in order to clarify this. Both anisotropic cancellation and transfer of unpaired electron spin density may be occurring simultaneously.

Other explanations may be offered for the C-13 decrease. DMS has shown that as θ and $\theta^1 \rightarrow 0$ the C-13 h.f.s. approaches its lowest positive value and the proton h.f.s. approaches its highest negative value (+28.6 and -24.24 respectively for model C). From experimental results many values of a^{C13} have been calculated for $\theta = 0$, some of which are lower than the values given above. There exists in the literature numerous conflicting experimental results as to the relationship between the proton h.f.s. and the carbon-13 h.f.s.⁷³ It is imagineable that perturbations of the A_2'' vibrational mode and/or the carbon σ orbitals at low values of θ due to surface effects could be responsible for the observed low temperature decrease in the C-13 h.f.s.

All results discussed above were obtained for methyl radicals stabilized on porous glass surfaces which have been dehydroxylated at high temperatures (leaving only "free" hydroxyl groups on the surface).

Methyl radicals were studied on a chlorinated surface in order to determine: (1) if any of the E.S.R. parameters mentioned previously would change significantly on changing surface groups (2) if the temperature dependences would be altered due to surface alteration. ($\equiv\text{SiOH} \rightarrow \equiv\text{SiCl}$). Only the proton h.f.s. and the asymmetry function were studied on the chlorinated surface. Linewidths and relative intensities have been studied more rigorously as a function of chemical composition of the surface. The results of these studies will be treated in the next chapter. The proton h.f.s. has been studied as a function of increasing temperature and then as a function of decreasing temperature (Fig. 3.21). On increasing the temperature the results are:

1) At low temperatures, $|a^{\text{H}}|$ on the chlorinated surface may be slightly larger than $|a^{\text{H}}|$ on the dehydroxylated surface (or regular surface).

2) The temperature coefficients $\left(\frac{\Delta |a^{\text{H}}|}{\Delta T}\right)$ on the chlorinated surface may be slightly larger than the temperature coefficients at corresponding temperatures on the dehydroxylated surface.

3) For equivalent initial concentrations, the proton h.f. splittings may be measured over a much larger temperature range for the regular surface. This fact did not allow us to obtain a high enough temperature to observe a plateau as had been seen for the regular surface. Therefore the interaction between the methyl radical and the chlorinated surface is not as large as the interaction between the methyl radical and the regular surface. The methyl radical decays much faster at high temperatures on the chlorinated surface.

On decreasing the temperature one finds that $|a^{\text{H}}|$ follows the same path as it did on increasing the temperature (see Fig. 3.21). The error involved in the study of a^{H} as a function of decreasing temperature is a little larger because of the smaller initial concentration of methyl radicals.

An examination of Fig. 3.22 reveals that the asymmetry of the proton lines at all temperatures is slightly less for the chlorinated surface. This also indicates that the interaction between the methyl radical and the chlorinated surface is smaller than the interaction between the methyl radical and the regular surface. This observation also indicates that many of the available trapping sites may have been destroyed on chlorination. Other than the differences mentioned above the asymmetry and proton h.f.s. plots resembled closely those for the regular surface. The accuracy of the measurements are not as good as for regular surface studies since only two temperature runs were performed.

6. Conclusions

The theory of Schrader (DMS) was developed assuming the methyl radical to be planar and completely free of any surface or matrix interactions. The general trends observed in this study substantiate the theory. Most of the deviations from theory mentioned in sections 4 and 5 of this chapter can be explained in terms of surface interactions except those noticed at higher temperatures. It is probable that matrix effects are of some importance and, therefore, they may have to be included in the development of a theory regarding temperature dependences of hyperfine splittings. The studies carried out on the chlorinated surface indicates smaller interactions between the radical and this surface. Further work on the effects of varying the chemical composition of the surface will be discussed in the next chapter.

It will be shown in the next chapter that linewidths are more sensitive to the interaction of the surface with the methyl radical than any other E.S.R. parameter.

Isotope effects (i.e. ratio of $\frac{a^H}{a^D}$) are not understood. The departures of this ratio from the theoretical value are not easily explained. Possible sources of the deviation of this ratio from the theoretical value are: 1) in-plane vibrations 2) a slight breakdown of the assumption of small vibrational amplitudes 3) matrix effects which perturb the form of the out-of-plane vibration. I feel that much information could be gained about this ratio as well as surface effects by carefully studying the ratio of $\frac{a^H}{a^D}$ as a function of temperature using the radicals CH_3 , CH_2D , CD_2H , and CD_3 as well as their carbon-13 analogs. Also, changes in the amount of orbital following could be obtained by studying the difference [$a^{\text{C}13}(\text{CH}_3) - a^{\text{C}13}(\text{CD}_3)$] as a function of temperature. Much work can be done on isotope effects using radicals stabilized on p.V.g.

CHAPTER IV

FURTHER STUDIES OF LINEWIDTHS

1. Introduction

Kivelson¹²¹ has theoretically treated E.S.R. linewidths of free radicals (microcrystalline model). This theory is only valid for substances in which the magnetic anisotropy is small and for which the orbital magnetism has been essentially quenched. The theory is restricted to high (room) temperatures, strong applied fields, small anisotropy, weak exchange, and no relaxation through chemical reactions. Spin-orbit interactions as a mechanism of relaxation were not discussed. It was assumed that the principal mechanism for nuclear relaxation is the interaction of the nucleus with the unpaired electrons. Kivelson¹²¹ applied the theory to liquids considering weak exchange. The results obtained could be combined into a relation:

$$\text{Linewidth} = T_2^{-1}(M) = \alpha + \beta M + EM^2 + KM^4 \quad (4-1)$$

where α , β , E , and K are parameters independent of the nuclear quantum number M . This result was obtained after making the following assumptions:

$$\begin{aligned} T_2^{-1} \tau_c &\ll 1 \\ a^2 &\ll \gamma^2 B^2 \\ T_2^{-1} &\ll |\gamma B| \\ (\Delta\gamma/\gamma)^2 &\ll 1 \end{aligned} \quad (4-2)$$

where B is the applied field, γ is the gyromagnetic ratio, a is the hyperfine splitting and $\Delta\gamma$ is the anisotropy in the gyromagnetic ratio.

$$\Delta\gamma = \gamma_{\parallel} - \gamma_{\perp} = (\beta/\hbar) (g_{\parallel} - g_{\perp}) \quad (4-3)$$

If $T_2^{-1}(M)$ is subtracted from $T_2^{-1}(-M)$ the following relation is obtained:

$$\Delta T_2^{-1}(M) = -2 \beta M \quad (4-4)$$

If the conditions of equation (4-2) hold, the line shape is nearly Lorentzian. Equation (4-1) holds for free radicals with $S = 1/2$ and one group of equivalent interacting nuclei. On applying equation (4-1) to linewidth variations in the system vanadyl etioporphyrin in benzene solution, K, the quadrupole contribution to the linewidth, was assumed to be negligible.^{121,122} Kivelson¹²¹ considering previous work on vanadyl etioporphyrin, decided that other relaxation mechanisms such as spin-orbit interactions would contribute to α but probably not to β and E. Therefore, α , could be written as $\alpha^1 + \alpha^{11}$ where α^{11} is the contribution from unspecified sources. The experimental data for the vanadyl system could not be fitted exactly with Lorentzian shaped curves; in fact, the "apparent" intensity, peak height times line width squared, is not the same for all lines. Second-order frequency shifts were included in the theory and were found to have little effect.

Rogers and Pake¹²² studied the paramagnetic relaxation in solutions of VO^{++} . The results supported Kivelson's theoretical work.¹²¹ The experimental linewidths were determined by measuring the width of one of the component lines directly and then determining the relative width of the rest of the components from their derivative heights by use of the equality

(derivative height) x (derivative width)² = constant
for lines of equal intensity. The validity of this assumption was checked and the assumption was found to give adequate results. The disagreement of experiment with theory arises from two factors.

- (1) the line components do overlap
- (2) the line shapes are not purely Lorentzian

No attempt was made to correct for these factors. Two features of the vanadyl spectrum still remain unexplained quantitatively although qualitatively at least one of these is explainable by the microcrystalline model. These two features are:

(1) the magnitude of the hyperfine constant varies with the solvent used.

(2) the individual component lines are asymmetric with respect to the baseline (as found for methyl radicals stabilized on p.V.g.). The first effect can be qualitatively explained by the change in solvents causing a change in the structure of the microcrystallite thereby perturbing the electronic wave function and hence the hyperfine interaction.

The second effect could be due to incomplete motional averaging of the anisotropic g-tensor or hyperfine tensor. This view is supported by greater component symmetry at lower viscosities and higher temperatures and by increased component symmetry at lower values of the resonant frequency. For contributions to arise from such terms, one would expect the symmetry to vary with m_I , since $bm_I \geq \Delta\gamma B_0$ where b is the hyperfine anisotropy. The asymmetry in the methyl radical components has been found to vary with m_I (see chapter III) whereas in the spectrum of VO^{++122} the asymmetry is independent of m_I .

Wilson and Kivelson¹²³ studied the linewidths of the hyperfine components of the E.S.R. spectra of vanadyl acetylacetonate in liquid toluene as a function of concentration, temperature, and applied field. A residual linewidth, independent of nuclear quantum number and applied field, was studied and found to vary as T/η , where η is the viscosity. This residual linewidth was ascribed to a spin-rotational interaction.

The peak-to-peak linewidth ΔH may be fitted to the expression¹²¹

$$\Delta H = \alpha^1 + \alpha^{11} + \beta M + \gamma M^2 + EM^4 \quad (4-5)$$

where all the parameters may depend upon temperature. γ arises from the modulation of the anisotropic hyperfine tensor, α^1 from the modulation of both the anisotropic hyperfine tensor and the anisotropic g tensor, β from a cross correlation between the two, E from quadrupolar relaxation, and α^{11} from other unspecified mechanisms. Wilson and Kivelson¹²³ decided that E was too small to be considered and that a small negative cubic (correction) term must be included. Therefore, the data was fitted to the equation

$$\Delta H = \alpha + \beta M + \gamma M^2 + \delta M^3 \quad (4-6)$$

α^{11} arises via the modulation of rotational angular momentum and the interaction of this momentum (electrons do not rigidly follow the movement of the nuclear framework generating a magnetic moment) to the spin by means of spin-rotational coupling. The values of ΔH , calculated with the α , β , γ , and δ values obtained by a least-squares fit agree, within experimental error, with the measured values, except for the $M = -1/2$ line. Wilson and Kivelson¹²⁴ studied deuterated vanadyl acetylacetonate in carbon disulfide. Their results indicated that neither intermolecular dipolar interactions nor unresolved proton extrahyperfine splittings contributed appreciably to the linewidth. Wilson and Kivelson¹²⁵ have also studied the anisotropic and spin-rotational effects in copper complexes.

The linewidth theory of Kivelson,¹²¹ and more recently by Wilson and Kivelson,¹²³ has been generalized and extended by Freed and Fraenkel to include several sets of equivalent nuclei.¹²⁶

This more general theory predicts the alternating linewidth phenomenon. The theory of Freed and Fraenkel¹²⁶ has been extended and exemplified.¹²⁷⁻¹³⁰

Adrian, et al,¹³¹ studied the E.S.R. spectrum of the formyl radical (HCO) and the deuterated radical (DCO) in solid carbon monoxide over the temperature range 4.2° to 30°K. The observed line shapes were temperature dependent. The lines were broad and unsymmetrical with the linewidth varying from one hyperfine component to the next. It was shown that the line shapes were due to the combination of a pronounced anisotropy in the g-factor with a small anisotropy in the proton h.f. interaction. Adrian, et al, decided that the variation in line width and shape between various hyperfine components is due to the fact that the broadening effects of the anisotropic proton h.f.s. and the g-factor anisotropy are added for one hyperfine component and subtracted for the other. The change in the E.S.R. spectrum between 4.2°K and 11°K is interesting. The change is basically a sharpening of the individual peaks of the spectrum while the overall width of the lines remains constant. This seemed to rule out a change in the rotational freedom of the radical, since an increase in the rotational freedom of the radical would partially average out the magnetic anisotropies and thus decrease the total line width. Local disorder in the matrix at 4.2°K could add to the "natural linewidth" (i.e. linewidth if the magnetic anisotropies were not present) by causing random shifts in the hyperfine splitting and/or the g-factor. Warm up would anneal out the disorder and a well resolved spectrum would result. The cause of the line broadening and loss of resolution which occurs on warming the sample above 16°K is not definitely known. This might be due to an incipient rotation or reorientation of the radicals within the matrix. Since the g-factor anisotropy makes the electron-spin

energy levels orientation dependent, the electron spin is thereby coupled to the rotational motion. This coupling could provide an efficient relaxation mechanism which would shorten the electron spin lattice relaxation time sufficiently to broaden the lines. Also, in a polycrystalline sample, the resultant line shape will be a superposition of frequencies corresponding to all possible orientations of the magnetic field. A discrepancy was found in this study in the ratio of the anisotropic hyperfine interactions in HCO and DCO. Here the observed ratio is roughly 5:1 so that the h.f. anisotropy in DCO is proportionally larger than it is in HCO. It is possible that the HCO radical is executing torsional oscillations of a magnitude large enough to partially average out the magnetic anisotropies. The amplitude of such torsional oscillations would be larger for the lighter HCO radical, and thus the magnetic anisotropy would be reduced somewhat more in HCO than it would in DCO. The complex electron spin resonance spectrum of NO_2 in polycrystalline argon at 4.2°K^{58} appears to be the result of line broadening by a marked anisotropy in both the g-factor and the nitrogen hyperfine splitting. When the magnetic anisotropies are axially symmetric and small compared to the corresponding isotropic terms, the following formula¹³² gives the frequency of the hyperfine lines:

$$h\nu(M_N) = \frac{(1/3 g_{\parallel} + 2/3 g_{\perp}) \beta H + A_N M_N}{(3 \cos^2 \theta_H - 1)} + [1/3 (g_{\parallel} - g_{\perp}) \beta H + 1/2 B_N M_N] \quad (4-7)$$

where: g_{\parallel} and g_{\perp} are the g-factors parallel and perpendicular to the symmetry axis.

A_N is the isotropic nitrogen hyperfine splitting constant

B_N is the anisotropic nitrogen hyperfine splitting constant

θ_H is the angle between the magnetic field and the symmetry axis.

For the methyl radical, assuming the direction parallel to the 3-fold symmetry axis and the two directions perpendicular to it as the principal axes of the g and h.f. tensors, equation (4-7) becomes

$$h\nu(M_I) = g \cdot \beta H + A M_I + [1/3 (g_{\parallel} - g_{\perp}) \beta H + 1/2 B M_I] (3\cos^2\theta - 1) \quad (4-8)$$

$$\text{where } g = 1/3 (g_{\parallel} + 2 g_{\perp})$$

$$A = 1/3 (A_{\parallel} + 2 A_{\perp})$$

$$B = \text{anisotropic h.f.s.} = f(\theta)$$

$$\theta = \text{angle between } H_0 \text{ and the 3-fold axis.}$$

Fiat, et al,⁴⁰ studied the N.M.R. relaxation mechanisms of CH_3OH , CD_3OH and CH_3OD adsorbed on p.V.g. T_1 was measured to be one to three orders of magnitude longer than T_2 . Both T_1 and T_2 were strongly dependent on the coverage Λ . This dependence was explained by the existence of a distribution of correlation times characteristic of molecular motions. It was shown that dipolar interactions between the adsorbed molecules and the surface OH groups contribute significantly to the longitudinal relaxation T_1 . On deuteration of the p.V.g. surface using D_2O it was found that 10% of the surface remained undeuterated.⁴⁰ This value agrees very well with the percentage of the surface remaining undeuterated discussed in chapter II. (satellite studies). Lower T_1^{-1} values for CH_3OH adsorbed on a methylated surface were attributed to larger distances between the adsorbate and the surface protons.

Fiat, et al, plotted the correlation times as a function of

$$\begin{aligned} V(\text{cc/gm at S.T.P.}) & \quad \text{For } \Lambda = 1.00 \tau_c \approx 10^{-10} \text{ sec.} \\ & \quad \text{For } \Lambda = 0.30 \tau_c \approx 10^{-9} \text{ sec.} \\ & \quad \text{For } \Lambda = 0.10 \tau_c \approx 10^{-8} \text{ sec.} \\ & \quad \text{For } \Lambda = 0.05 \tau_c \approx 10^{-7} \text{ sec.} \end{aligned}$$

Motional processes having correlation times of 10^{-10} to 10^{-7} sec. are associated with surface diffusion. Rotational motion have characteristic times of $\approx 10^{-11}$ sec. It was also found that lateral interactions began at $\Lambda = 0.5$. Woessner²⁶ studied N.M.R. phenomena of benzene adsorbed on silica gel ($\Lambda = 0.75$). He found that benzene molecules rotate rapidly about their hexagonal axis even at 77°K. There was a broad distribution of temperature dependent correlation times for this motion. There were three apparent transverse relaxation states which were characterized by different temperature dependent reorientation rates of the molecular axis, and by different orientation distribution functions of this axis. Transitions occurred between these states with changing temperature. He found the term $\langle 3\cos^2 \theta - 1 \rangle$ to be non-zero. In all states the molecules were rotating rapidly. Reuben, et al,³⁹ studied the N.M.R. relaxation times of ammonia adsorbed on p.V.g. T_1 and T_2 of the adsorbate strongly depended on Λ (coverage). They found a broad distribution of correlation times and evidence for two main adsorbate sites ($\equiv\text{SiOH:NH}_3$ and $\equiv\text{B:NH}_3$). For $\Lambda = 1.00$ τ_c is approximately 10^{-9} sec. For very low Λ , τ_c was found to be about 10^{-7} sec. Many relaxation mechanisms were considered but 2-dimensional surface diffusion was most strongly supported. Two dimensional surface diffusion can be represented by the equation

$$\tau = \tau_0 \exp. \left(\frac{\Delta Q}{RT} \right) \quad (4-9)$$

where $\tau_0 \cong 10^{-13}$ - 10^{-14} and ΔQ is the difference between the heat of adsorption and the lowest value of the heat of adsorption during diffusion to the next site.

The work to be described in the remaining sections of this chapter began after a study by Gardiner and Casey appeared.⁸³ Their work will be discussed in reasonable detail. They reported

that the E.S.R. spectra of methyl and deuterio-methyl radicals adsorbed on a silica gel surface at 77°K were characterized by a marked dependence of the line width on the nuclear spin quantum number. The silical gel had been degassed at ~ 300°C for several hours at a pressure less than 10^{-4} mm. Less than a monolayer of the methyl iodides were adsorbed. The samples were U.V. irradiated at 77°K with an unfiltered GE-UAZ mercury lamp. The line widths were determined, by measuring the width of one of the lines, and determining the widths of the other lines using the expression

$$(\text{derivative height}) \times (\text{derivative width})^2 = \text{constant}$$

Gardiner and Casey argued that the asymmetry (or linewidth variation) of the CH_3 and CD_3 lines is not due to incomplete averaging of the g-tensor anisotropy. They fitted their linewidth data to an equation similar to equation (4-1) (omitting the quadrupole term) using curvilinear regression analysis.

$$(\tau_2)^{-1} = a_0 + a_1 M + a_2 M^2 \quad (4-10)$$

where

$$\begin{aligned} a_0 &= \frac{4}{45} (\Delta\gamma B)^2 \tau_c + K \\ a_1 &= \frac{4}{15} b \Delta\gamma B \tau_c \\ a_2 &= \frac{b^2}{5} \tau_c \end{aligned} \quad (4-11)$$

where:

- τ_c = correlation time
- b = hyperfine anisotropy = $2/3 (A_{\parallel} - A_{\perp})$
- $\Delta\gamma$ = g-tensor anisotropy = $g_{\parallel} - g_{\perp}$
- K = unspecified contributions to the line width independent of M
- B = applied field H_0

In the formulation (4-11) b does not appear in a_0 . Equations (4-11) should enable a determination of τ_c if b or $\Delta\gamma$ is known. Heller¹³³ obtained a value for b for the CH_3 group in the radical $\text{CH}_3\text{C}(\text{COOH})_2$. This value of b ($=4.5 \times 10^6 \text{ s}^{-1}$) was used by Gardiner and Casey as an estimate of b in the methyl radical. From the ratio a_1/a_2 they determined $\Delta\gamma$ to be 1.20×10^{-3} for the methyl radical. They estimated b for the CD_3 radical to be $\frac{4.5 \times 10^6 \text{ s}^{-1}}{0.69} = 0.69 \times 10^6 \text{ s}^{-1}$. The ratio of a_1/a_2 gave $\Delta\gamma = 9.5 \times 10^{-4}$ for the $\left(\frac{a^{\text{H}}}{a^{\text{D}}}\right)$ CD_3 radical. The average value of $\Delta\gamma$ is $\frac{9.5 \times 10^{-4} + 1.20 \times 10^{-3}}{2} = 1.08 \times 10^{-3}$. Using this value and the appropriate values of b , the correlation times were calculated from a_1 .

$$\tau_c (\text{CH}_3) = 5.0 \times 10^{-8} \text{ sec.}$$

$$\tau_c (\text{CD}_3) = 7.9 \times 10^{-8} \text{ sec.}$$

These correlation times led to tumbling frequencies of $2.0 \times 10^7 \text{ s}^{-1}$ (CH_3) and $1.3 \times 10^7 \text{ s}^{-1}$ (CD_3). "Free" rotational frequencies are usually an order of 10^3 greater, therefore these frequencies indicate some hindrance to the rotation by the surface and the exact nature of this "tumbling" remains somewhat obscure.

2. Experimental

A. Nature of the Samples Studied

The nature of the samples studied will be mentioned first, followed by a description of the experiments carried out on these samples.

Sample <u>1</u>	$\text{C}^{13}\text{H}_3\text{I}$ on high temperature (800° - 950°C) degassed surface $\Lambda = 0.07$
Sample <u>2</u>	CD_3I on high temperature (800° - 950°) degassed surface $\Lambda = 0.07$
Sample <u>3</u>	CD_3I on high temperature (800° - 950°C) degassed surface $\Lambda = 0.28$

- Sample 4 CH_3I on high temperature (700°-800°C) degassed surface
 $\Lambda = 0.05$
- Sample 5 $\text{C}^{13}\text{H}_3\text{I}$ on 600-700°C degassed surface. Surface reacted
 with CCl_4 at 400°-450°C.¹⁸
 $\Lambda = 0.07$
- Sample 6 CH_3I on 800°C degassed surface. Several doses of H_2O
 at 141°C followed by degassing at 400°C.
 $\Lambda = 0.05$
- Sample 7 CH_3I on 710°C degassed surface. Several doses of D_2O
 at 149°C followed by degassing at 400°C.
 $\Lambda = 0.05$
- Sample 8 CD_3I on 700-800°C degassed surface. Reacted with CCl_4
 at 400-500°C.¹⁸
 $\Lambda = 0.075$
- Sample 9 CH_3I on 650°-700°C degassed surface. Reacted with CCl_4
 at 550°-600°C.¹⁸
 $\Lambda = 0.05$
- Sample 10 CH_3I on 500°C degassed surface. Added H_2O at 164°C
 several times followed by outgassing at 425°C.
 $\Lambda = 0.05$
- Sample 11 CH_3I on 500°C degassed surface. Added D_2O at 164°C
 several times followed by outgassing at 425°C.
 $\Lambda = 0.05$

In each case, the temperature pretreatment included oxidation using O_2 followed by degassing at the same temperatures. After treatments with CCl_4 outgassing followed at reaction temperatures. The samples were all irradiated at 77°K using the full focused arc of a Hanovia S-100 Alpine burner in order to produce the necessary concentration of methyl

or deuterio-methyl radicals. Some samples were studied more than once and therefore underwent more than one low temperature U.V. irradiation.

B. Linewidths

It is appropriate to discuss the indirect measurement of linewidths. An example will follow the discussion. For lines of a particular shape, the amplitudes of the derivative signal are inversely-proportional to the square of the width, and the amplitudes are therefore more sensitive to linewidth differences among the hyperfine components than the widths themselves. For (unsaturated) Lorentzian lines, the half-width at half-maximum intensity Δ_i of a line of degeneracy D_i can be determined from the peak-to-peak amplitude of the first derivative of the line, A_i , by the relation $\Delta_i = (SD_i/A_i)^{1/2}$, where S is a measure of the sensitivity of the spectrometer. The full width between derivative extrema is given by $\delta_i = (2/\sqrt{3})\Delta_i$, and the transverse relaxation time T_{2i} by $[|\gamma_S|T_{2i}]^{-1} = \Delta_i$, where γ_S is the effective magnetogyric ratio of the electron in the free radical.

Linewidth theory shows that, in general, a degenerate hyperfine line is a superposition of Lorentzian shaped lines rather than a single Lorentzian line, and there is thus no simple analytical relation between the linewidths and the amplitudes. Nevertheless, departures of observed line shapes from a Lorentzian form, at least in the central portion of the line, are small. It is therefore convenient to define an experimental relative - width parameter W_i for the i th hyperfine line with respect to some reference line r (usually the central line of the spectrum) by the relation

$$W_i = [(D_i/A_i) (A_r/D_r)]^{1/2} \quad (4-12)$$

The true relative widths Δ_i/Δ_r or δ_i/δ_r will not be given by W_i unless the departures from the Lorentzian shape are small.

Let us suppose the peak-to-peak linewidth (δ) for line 3a is 0.470 gauss. Assume the relative amplitudes to be 5.15|25.00|38.50|10.10. Let us calculate δ_3 .

$$W_3 = \left[\left(\frac{3}{25}\right) \left(\frac{38.5}{3}\right) \right]^{1/2} = 1.241$$

$$\therefore \delta_3 = 0.470 (1.241) = 0.584 \text{ gauss.}$$

$\delta_3 = (\sqrt{2}/\sqrt{3}) \Delta_i$ where Δ_i is the half-width at half-maximum intensity.

$$\Delta_i = \frac{\sqrt{3}}{2} \delta_3$$

$$\therefore \Delta_3 = \frac{1.732}{2} (\delta_3) = .866 (0.584) = 0.506 \text{ gauss}$$

$$2\Delta_3 \text{ (full width at half-maximum intensity)} = 2(.506) = 1.012\text{g.}$$

$$2\Delta_3 \text{ (Mc/S)} = 1.012 \times 2.803 = 2.835 \text{ Mc/S}$$

C. Linewidth Studies Performed

The linewidth studies which have been performed will now be outlined. For CH_3 radicals a 100 mgauss modulation was used with a scan range of ± 2.5 gauss. At any one temperature, the linewidth (δ) recorded for any component line is an average of 7-12 measurements. For CD_3 radicals a similar procedure was followed except that the modulation used was 125 mgauss. The relative amplitudes were measured in all cases. The relationships of Gardiner and Casey⁸³ (equations 4-10 and 4-11) were applied here. The studies performed were:

1. Sample 1: Compared measured and calculated linewidths at 77°K.
2. Samples 2 and 3: Determined correlation times and tumbling frequencies at 77°K using measured linewidths and the b value used by Gardiner and Casey.⁸³
3. Sample 3: Determined the tumbling frequency from 77°K to 151°K using only measured linewidths.

4. Sample 4: Compared the tumbling frequencies obtained from measured and calculated linewidths (77°K).
5. Sample 4: Determined the tumbling frequency from 77°K to 199°K using only measured linewidths.
6. Sample 5: Determined the tumbling frequency at 77°K on two separate occasions from measured linewidths. (To compare parameters and estimate the error of the method).
7. Samples 6 and 7: Determined the tumbling frequencies from measured linewidths at 77°K.
8. Sample 8: Determined the tumbling frequency from 77°K to 154°K using only measured linewidths.
9. Sample 9: Determined the tumbling frequency from 77°K to 183°K using only measured linewidths.
10. Samples 10 and 11: Determined the tumbling frequency at 77°K using only measured linewidths.

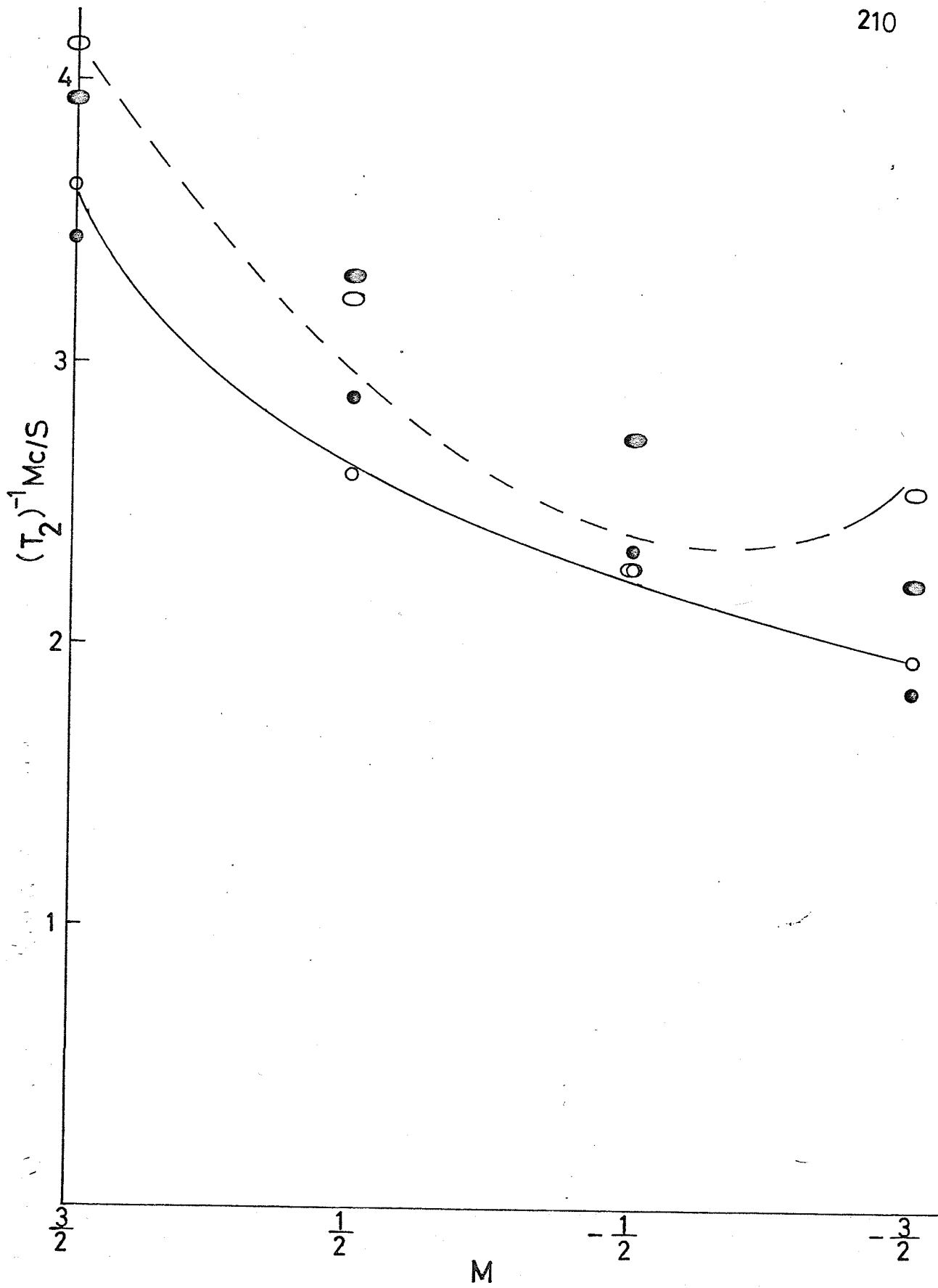
3. Results

The line shape of the methyl radical lines was found to be neither Gaussian nor Lorentzian by a method outlined on page 806 of Reference 10. The lines were much closer to being Lorentzian than Gaussian. Each methyl radical line deviated from the two principle line shapes by a different degree.

The linewidths of methyl radicals stabilized on sample 4 at 77°K were measured and plotted (Fig. 4.1). Also plotted in Fig. 4.1 is the calculated linewidths (using the method outlined in Chapter IV, Section 2B) using the measured linewidth of line 3a. Both the measured and calculated

Fig. 4.1

Measured and calculated linewidths as a function of nuclear quantum number M (spectra recorded at 77°K). The open circles are the measured linewidths. (solid line). These measured linewidths have been curve fitted (solid circles). The open ellipses (dashed line) are the calculated linewidths which have been curve fitted (solid ellipses). Notice greater curvature of calculated linewidths.



linewidths were then fitted to the relation $(T_2)^{-1} = a_0 + a_1 M + a_2 M^2$ using curvilinear regression analysis. The fitted curves are also shown in Figure 4.1. The measured linewidths gave the relation

$$\frac{1}{T_2} = 2.603 + 0.535M + 0.016 M^2 \quad (4-13)$$

from which the tumbling frequency of $2.6 \times 10^8 \text{ sec.}^{-1}$ was calculated (using $b = 4.5 \times 10^6 \text{ S}^{-1}$). The calculated linewidths gave the relation

$$\frac{1}{T_2} = 3.017 + 0.567M + 0.026M^2 \quad (4-14)$$

which leads to a tumbling frequency of $1.58 \times 10^8 \text{ S}^{-1}$. It is to be noticed that the tumbling frequency from the calculated values is lower than the tumbling frequency from the measured values. Also both these tumbling frequencies are higher than those calculated by Gardiner and Casey.⁸³ The difference may be due to a higher OH concentration present on Gardiner and Casey's samples.

Table 4.1 gives the measured values of the linewidths of all samples studied at 77°K. The error in the measurements of the methyl radical linewidths varied from $\pm 45\%$ to $\pm 1.5\%$ on going from line 1 to line 1a. These were estimated from the scatter in measured values of the peak-to-peak linewidths. It is not known how the non Lorentzian shapes of the lines affect the error in converting the linewidths from peak-to-peak to half-intensity values. The deuteromethyl radical linewidths were in error by $\pm 4\%$ to $\pm 1\%$ on going from line 1 to line 7. (estimated from the scatter). The abbreviation Reg. means a normal high temperature pretreated surface. The abbreviation Cl. means the surface has been chlorinated. The surfaces which have been treated with light and heavy water are noted H_2O and D_2O . Table 4.2 shows the measured linewidths as a function of temperature. Table 4.3 exhibits the parameters derived from curvilinear regression analysis applied to

the linewidths measured at 77°K. Table 4.4 presents the same parameters as Table 4.3 as a function of temperature. Table 4.5 shows the relative amplitudes for some samples and for one temperature run. The trends visible in Tables 4.1 to 4.5 will be discussed in the next section.

Many of the trends in the above mentioned Tables may best be exemplified by plotting the data.

TABLE 4.1

Measured Peak-to-Peak and One-Half Intensity Linewidths at 77°K

Sample	Linewidths _{p-p} (gauss)				Linewidths _{1/2 int.} (Mc/s)			
	1	3	3a	1a	1	3	3a	1a
1 (Reg.)	0.825	0.568	0.470	0.453	4.010	2.760	2.282	2.200
4 (Reg.)	0.747	0.538	0.469	0.403	3.633	2.612	2.282	1.962
	0.743	0.560	0.478	0.427	3.609	2.712	2.322	2.070
5 (Cl)	0.769	0.575	0.472	0.447	3.730	2.790	2.290	2.170
	0.773	0.582	0.475	0.450	3.752	2.823	2.307	2.185
9 (Cl)	0.849	0.634	0.506	0.466	4.121	3.077	2.457	2.262
6 (H ₂ O)	0.913	0.688	0.487	0.521	4.430	3.339	2.364	2.531
7 (D ₂ O)	0.792	0.573	0.479	0.440	3.844	2.780	2.326	2.137
10 (H ₂ O)	0.905	0.677	0.496	0.509	4.391	3.286	2.410	2.472
11 (D ₂ O)	0.907	0.616	0.476	0.468	4.405	2.989	2.313	2.273

CD₃ RADICALS

	1	2	3	4	5	6	7	1	2	3	4	5	6	7
2 (Reg.)	0.618	0.579	0.515	0.455	-	0.355	0.310	3.000	2.809	2.502	2.211	-	1.725	1.506
3 (Reg.)	0.644	0.615	0.550	0.469	0.428	0.361	0.328	3.124	2.988	2.670	2.374	2.078	1.753	1.593
8 (Cl)	0.524	0.488	0.443	0.394	0.341	0.299	0.266	2.542	2.370	2.151	1.912	1.657	1.451	1.292

TABLE 4.2

Linewidths As A function of Temperature

Sample	Radical-Surface	T(°K)	LINEWIDTH _{p-p} (GAUSS)				LINEWIDTH _{1/2} INT. (Mc/S)									
			1	3	3a	1a	1	3	3a	1a						
4	CH ₃ -Reg.	77	0.747	0.538	0.469	0.403	3.630	2.612	2.282	1.962						
"	"	77	0.743	0.560	0.478	0.427	3.609	2.712	2.322	2.070						
"	"	109	0.666	0.508	0.453	0.386	3.233	2.466	2.199	1.874						
"	"	140	0.646	0.528	0.468	0.406	3.136	2.564	2.270	1.969						
"	"	167	0.644	0.555	0.465	0.433	3.127	2.696	2.256	2.103						
"	"	113	0.653	0.505	0.456	0.386	3.171	2.453	2.212	1.874						
"	"	199	0.674	0.564	0.467	0.422	3.274	2.738	2.265	2.050						
9	CH ₃ -Cl	77	0.849	0.634	0.506	0.466	4.121	3.077	2.457	2.262						
"	"	110	0.688	0.529	0.458	0.399	3.342	2.569	2.221	1.938						
"	"	155	0.674	0.547	0.461	0.424	3.271	2.657	2.236	2.056						
"	"	183	0.667	0.569	0.465	0.425	3.238	2.761	2.256	2.065						
CD ₃ RADICALS																
			1	2	3	4	5	6	7	1	2	3	4	5	6	7
8	CD ₃ -Cl	77	0.524	.488	.443	.394	.341	.299	.266	2.542	2.370	2.151	1.912	1.657	1.451	1.292
8	"	98	0.469	.421	.389	.349	.305	.273	.230	2.278	2.044	1.889	1.692	1.482	1.324	1.114
8	"	112	0.423	.386	.373	.336	.303	.273	.239	2.054	1.872	1.809	1.631	1.470	1.325	1.159
8	"	154	0.463	.395	.373	.341	.307	.277	.253	2.245	1.918	1.812	1.657	1.492	1.344	1.230
3	CD ₃ -Reg.	77	0.644	.615	.550	.489	.428	.361	.328	3.124	2.988	2.670	2.374	2.078	1.753	1.593
"	"	102	0.545	.518	.485	.427	.371	.329	.287	2.643	2.513	2.353	2.073	1.802	1.598	1.394
"	"	127	0.513	.468	.442	.398	.355	.323	.277	2.488	2.274	2.148	1.933	1.725	1.570	1.345
"	"	151	-	.458	.421	.391	.348	.314	.283	-	2.220	2.040	1.800	1.690	1.522	1.372

TABLE 4.3

Parameters Derived From Curvilinear Regression Analysis
Applied to Measured Linewidths At 77°K

Sample	Radical-Surface	a_0	a_1	a_2	$b(S-1)$	$\Delta\gamma$	τ_c (s)	$\frac{1}{\tau_c}$ (Tumbling Freq.) (sec. ⁻¹)
4	CH ₃ -Reg.	2.603	0.535	0.016	4.5x10 ⁶ (a)	12.59x10 ⁻³	3.82x10 ⁻⁹	2.60x10 ⁸
"	"	2.662	0.501	0.014	"	12.97x10 ⁻³	3.51x10 ⁻⁹	2.85x10 ⁸
5	CH ₃ -Cl	2.724	0.578	0.017	"	12.38x10 ⁻³	4.25x10 ⁻⁹	2.35x10 ⁸
"	"	2.744	0.522	0.018	"	10.72x10 ⁻³	4.43x10 ⁻⁹	2.26x10 ⁸
9	"	2.956	0.620	0.019	"	12.10x10 ⁻³	4.66x10 ⁻⁹	2.15x10 ⁸
6	CH ₃ -H ₂ O	3.131	0.667	0.028	"	8.79 x10 ⁻³	6.90x10 ⁻⁹	1.45x10 ⁸
7	CH ₃ -D ₂ O	2.748	0.558	0.019	"	10.57x10 ⁻³	4.80x10 ⁻⁹	2.08x10 ⁸
10	CH ₃ -H ₂ O	3.107	0.663	0.026	"	9.41 x10 ⁻³	6.41x10 ⁻⁹	1.56x10 ⁸
11	CH ₃ -D ₂ O	2.957	0.707	0.031	"	8.52 x10 ⁻³	7.55x10 ⁻⁹	1.33x10 ⁸
2	CD ₃ -Reg.	2.237	0.256	0.003	0.69x10 ⁶ (b)	5.21 x10 ⁻³	2.91x10 ⁻⁸	3.44x10 ⁷
3	"	2.376	0.273	negative	"	-	-	-
8	CD ₃ -Cl	1.906	0.217	0.001	"	10.63x10 ⁻³	1.21x10 ⁻⁸	8.27x10 ⁷

(a) ≡ Reference 133

(b) ≡ Reference 83

TABLE 4.4

Parameters Derived From Curvilinear Regression Analysis
As A Function Of Temperature

Sample	Radical-Surface	T(°K)	a ₀	a ₁	a ₂	b(S ⁻¹)	Δγ	τ _c (s)	$\frac{1}{\tau_c}$ (S ⁻¹)
4	CH ₃ -Reg.	77	2.603	0.535	0.016	4.5x10 ⁶ (a)	12.59x10 ⁻³	3.82x10 ⁻⁹	2.60x10 ⁸
"	"	77	2.662	0.501	0.014	"	12.97x10 ⁻³	3.51x10 ⁻⁹	2.85x10 ⁸
"	"	109	2.431	0.435	0.010	"	16.11x10 ⁻³	2.42x10 ⁻⁹	4.13x10 ⁸
"	"	140	2.477	0.380	0.006	"	22.94x10 ⁻³	1.49x10 ⁻⁹	6.73x10 ⁸
"	"	167	2.538	0.351	0.006	"	20.73x10 ⁻³	1.52x10 ⁻⁹	6.58x10 ⁸
"	"	113	2.426	0.431	0.008	"	17.85x10 ⁻³	2.08x10 ⁻⁹	4.81x10 ⁸
"	"	199	2.419	0.414	0.007	"	21.14x10 ⁻³	1.76x10 ⁻⁹	5.68x10 ⁸
9	CH ₃ -Cl	77	2.957	0.620	0.019	"	12.10x10 ⁻³	4.66x10 ⁻⁹	2.15x10 ⁸
"	"	110	2.504	0.456	0.011	"	15.26x10 ⁻³	2.68x10 ⁻⁹	3.73x10 ⁸
"	"	155	2.543	0.407	0.010	"	15.33x10 ⁻³	2.38x10 ⁻⁹	4.20x10 ⁸
"	"	183	2.570	0.402	0.006	"	20.07x10 ⁻³	1.57x10 ⁻⁹	6.39x10 ⁸
3	CD ₃ -Reg.	77	2.376	0.273	negative	0.69x10 ⁶ (b)	-	-	-
"	"	102	not calculated	0.219	"	"	-	-	-
"	"	127	"	0.188	"	"	-	-	-
8	CD ₃ -Cl	77	1.906	0.217	0.0012	"	10.63x10 ⁻³	1.21x10 ⁻⁸	8.27x10 ⁷
"	"	98	1.685	0.191	0.0010	"	10.75x10 ⁻³	1.04x10 ⁻⁸	9.64x10 ⁷
"	"	112	-	0.147	negative	-	-	-	-
"	"	154	1.631	0.161	0.010	"	9.07x10 ⁻⁴	1.04x10 ⁻⁷	9.62x10 ⁶

(a) ≡ Reference 133

(b) ≡ Reference 83

TABLE 4.5

Relative Amplitudes for Some Samples
And For One Temperature Run

Sample	Radical-Surface	T(°K)	Rel. Amplitudes
5	CH ₃ -Cl	77	1.00 4.73 7.47 2.12
4	CH ₃ -Reg.	77	1.00 4.97 8.81 2.45
"	"	109	1.00 4.49 6.72 2.08
"	"	140	1.00 4.22 6.07 1.92
"	"	167	1.00 3.95 5.46 1.72
"	"	113	1.00 4.36 6.56 2.09
"	"	199	1.00 3.64 4.82 1.53
6	CH ₃ -H ₂ O	77	1.00 4.85 8.18 2.14
7	CH ₃ -D ₂ O	77	1.00 4.89 8.12 2.26
10	CH ₃ -H ₂ O	77	1.00 4.98 8.27 2.14
11	CH ₃ -D ₂ O	77	1.00 5.04 8.35 2.10
2	CD ₃ -Reg.	77	1.00 3.10 6.84 9.09 10.40 5.17 1.93
3	CD ₃ -Reg.	77	1.00 3.36 7.58 10.18 10.25 5.59 2.06
8	CD ₃ -Cl	77	1.00 3.57 8.23 11.14 11.11 6.38 2.38
8	CD ₃ -Cl	98	1.00 3.52 8.04 10.89 10.80 6.26 2.35

Figure 4.2 shows the measured linewidths for sample 4 (CH₃-Reg.) as a function of nuclear spin quantum numbers (M) at various temperatures. Figure 4.3 shows the tumbling frequencies of the methyl radical on samples 4 (Reg.) and 9 (Cl) as a function of temperature.

Fig. 4.2

Measured linewidths (at 1/2 total intensity) as a function of M
at various temperatures (sample 4).

Curve 1: 77°K (open circles and solid line)

Curve 2: 109°K (open circles and solid line)

Curve 3: 140°K (solid circles and solid line)

Curve 4: 199°K (semi-solid circles and dashed line)

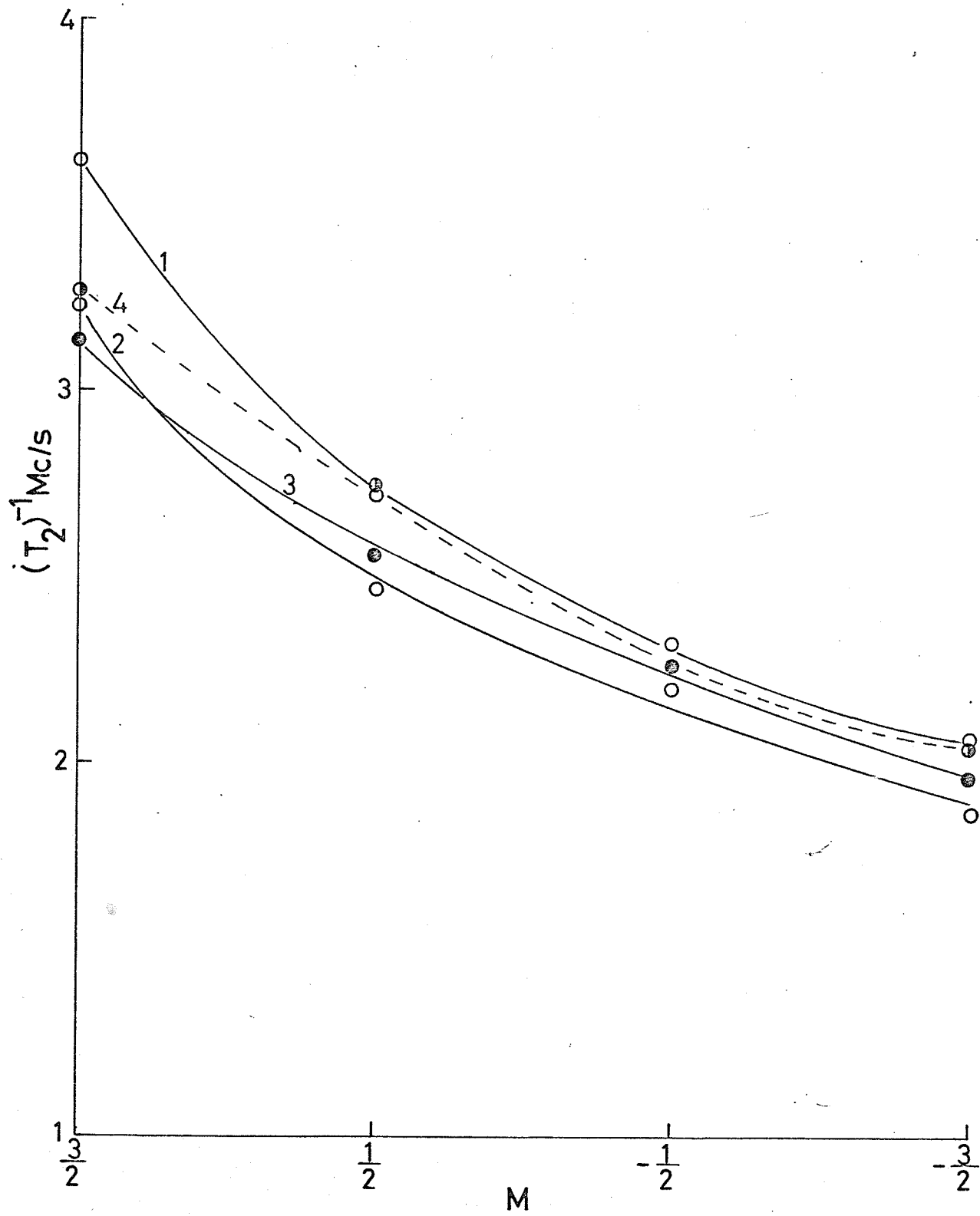


Fig. 4.3

Tumbling frequencies (from measured linewidths)
as a function of temperature. Sample 4 - open
circles and solid line. Sample 9 - solid circles
and dashed line.

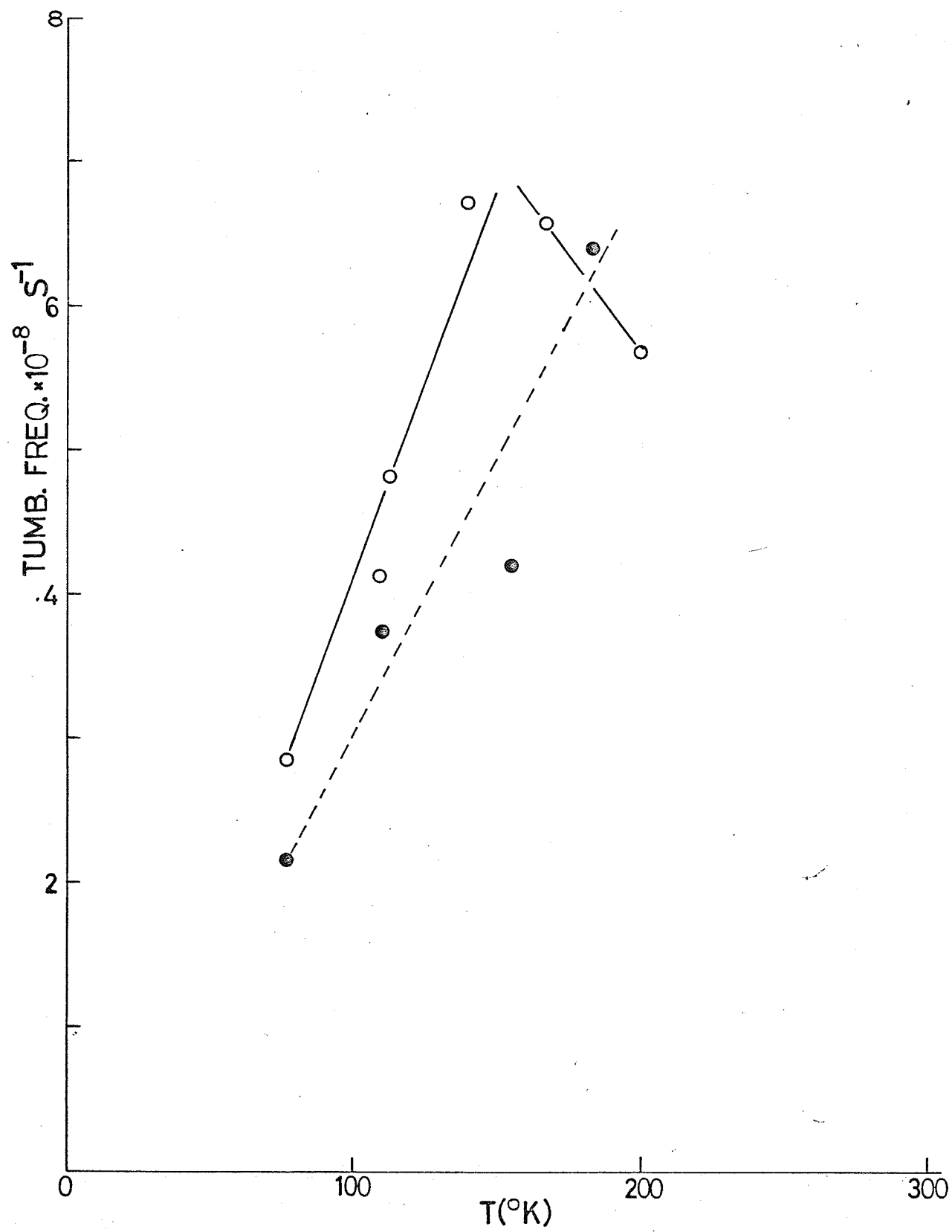


Figure 4.4, a plot of the log of the tumbling frequencies for samples 4 and 9 versus $(T^\circ\text{K})^{-1}$, led to the following activation energies for "tumbling".

$$E_A(\text{CH}_3, \text{Sample 4, Reg.}) \approx 292 \text{ cal/mole}$$

$$E_A(\text{CH}_3, \text{Sample 9, Cl}) \approx 282 \text{ cal/mole}$$

The linewidths of the CD_3 radical (sample 8-Cl) have been plotted at various temperatures as a function of M (Fig. 4.5). Fig. 4.6 shows the same features for the CD_3 radical adsorbed on sample 3 (Reg. Surface). The effects of sample chlorination on the dependence of linewidths on M (at 77°K) are shown in Fig. 4.7. In the same sense, the effects of treating samples with light and heavy water are also shown in Fig. 4.7 (77°K). Figure 4.8 shows a plot of the linewidths of lines 1 and 3 versus temperature (samples 4 and 9). Included in Fig. 4.8 are results on linewidth as a function of warming and cooling cycles (Chapter II).

Gardiner and Casey,⁸³ as mentioned before, used a value for b obtained by Heller¹³³ while studying the radical $\text{CH}_3\text{C}(\text{COOH})_2$. Using this value for b a value of $2.85 \times 10^8 \text{ s}^{-1}$ can be calculated, using measured linewidths, for the tumbling frequency of a methyl radical at 77°K on p.v.g. From the results of Rogers and Kispert,⁷⁵ studying the methyl radical in a single crystal of sodium acetate trihydrate at 77°K another value of b is available ($b = 1.3 \times 10^6 \text{ s}^{-1}$). Using this value a smaller value of the tumbling frequency is calculated for the same example cited above (i.e. $\frac{1}{\tau_c} = \text{tumbling frequency} = 2.38 \times 10^7 \text{ s}^{-1}$). This value is about a factor of ten smaller than the one obtained above. If Gardiner and Casey⁸³ had used this value of b ($1.3 \times 10^6 \text{ s}^{-1}$) and their

Fig. 4.4

Logarithms of the tumbling frequencies vs. T^{-1} .
The open circles and solid line refer to sample
4 while the solid circles and dashed line refer
to sample 9.

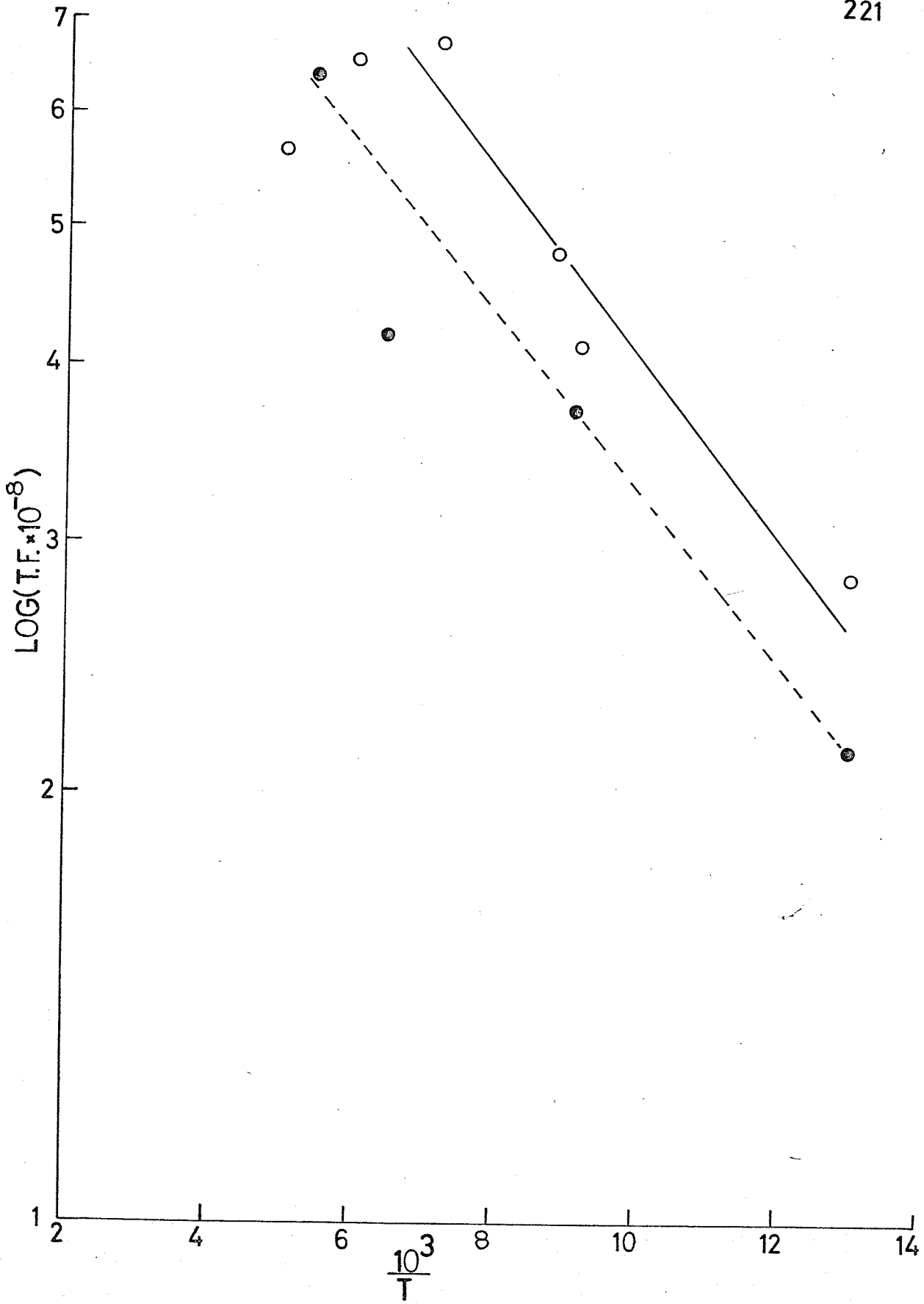


Fig. 4.5

Measured linewidths (sample 8) vs. M at various temperatures.

- Curve 1: $T = 77^{\circ}\text{K}$ (open circles and solid line)
- Curve 2: $T = 98^{\circ}\text{K}$ (solid circles and solid line)
- Curve 3: $T = 112^{\circ}\text{K}$ (semi-solid circles and solid line)
- Curve 4: $T = 154^{\circ}\text{K}$ (open ellipses and dashed line)

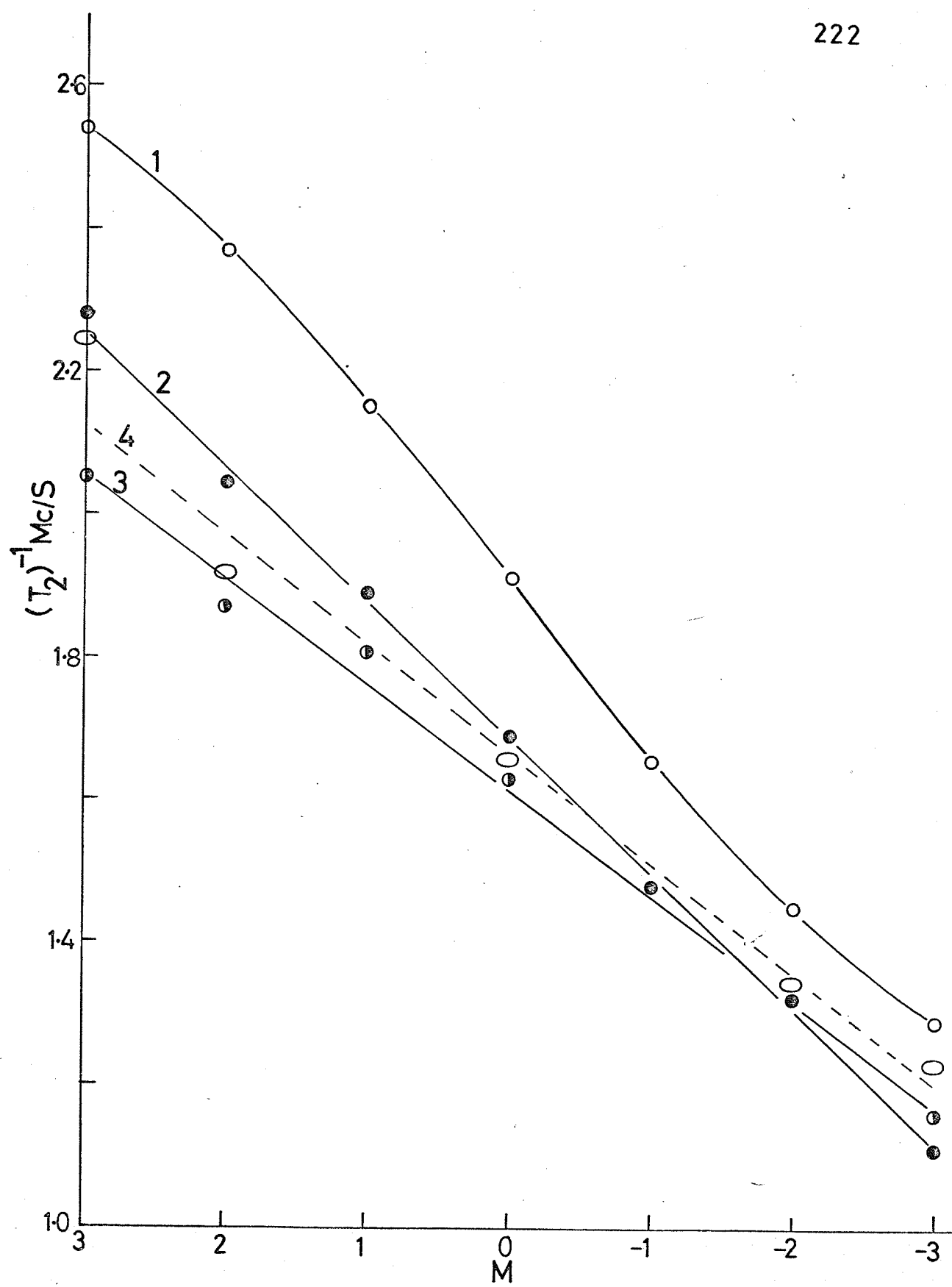


Fig. 4.6

Measured linewidths (sample 3) vs. M at various temperatures.

Curve 1: $T = 77^\circ\text{K}$ (open circles and solid line)

Curve 2: $T = 102^\circ\text{K}$ (solid circles and solid line)

Curve 3: $T = 127^\circ\text{K}$ (semi-solid circles and solid line)

Curve 4: $T = 151^\circ\text{K}$ (open ellipses and dashed line)

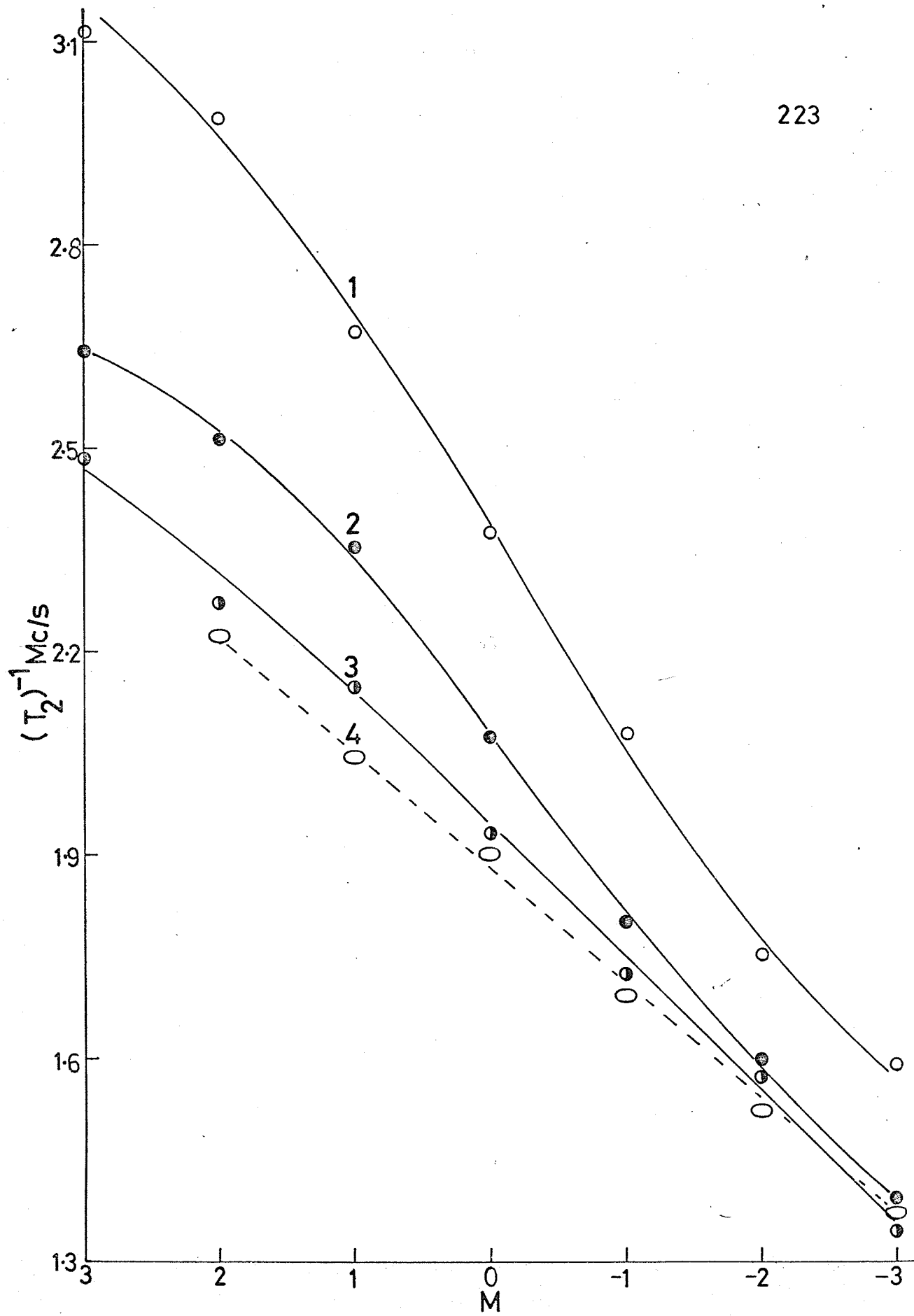


Fig. 4.7

Measured linewidths as a function of M for different samples at 77°K. All measured linewidths for $M = -1/2$ lie between the two bars indicated.

Curve 1: Sample 4
Curve 2: Sample 5
Curve 3: Sample 6
Curve 4: Sample 7
Curve 5: Sample 10
Curve 6: Sample 11

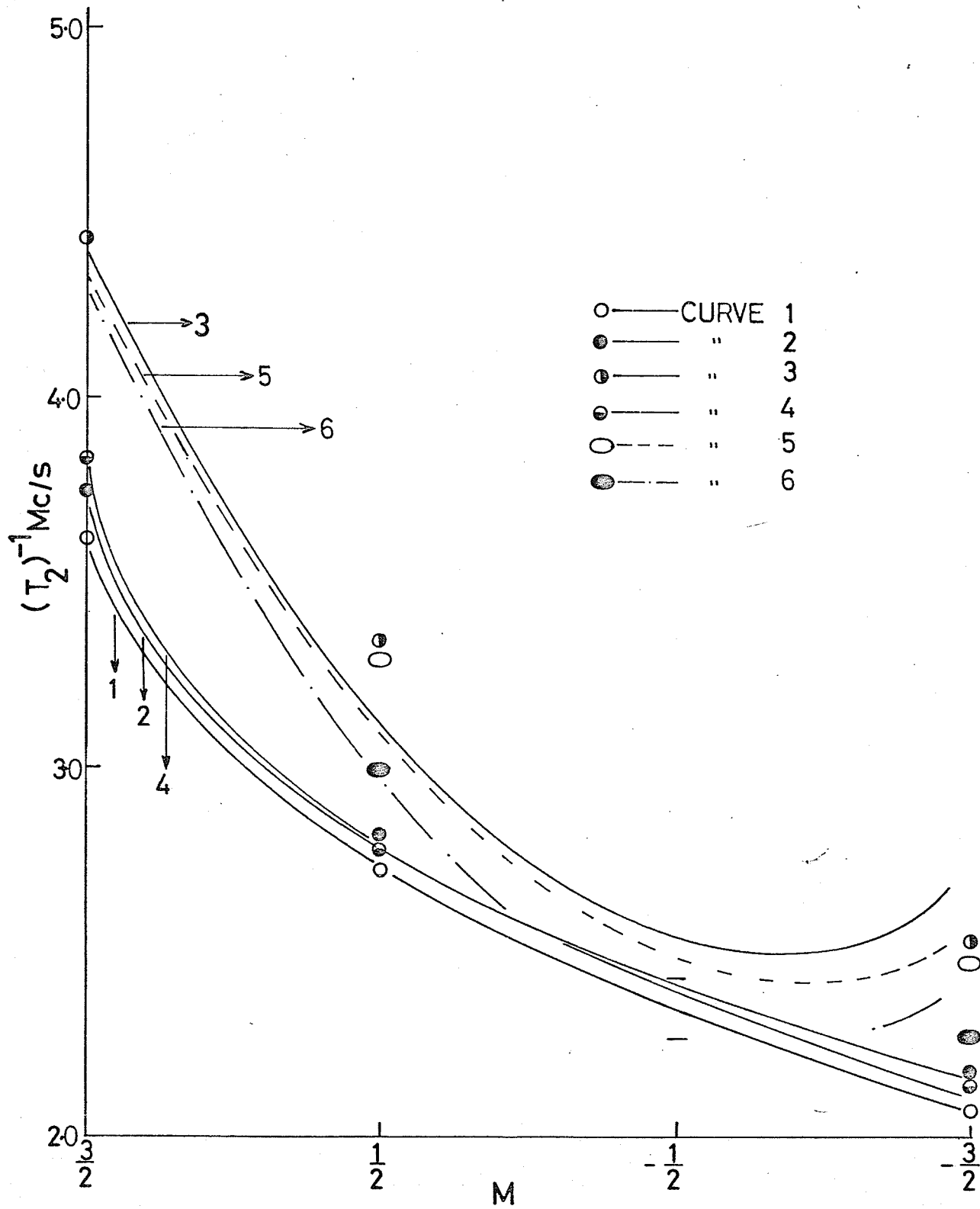
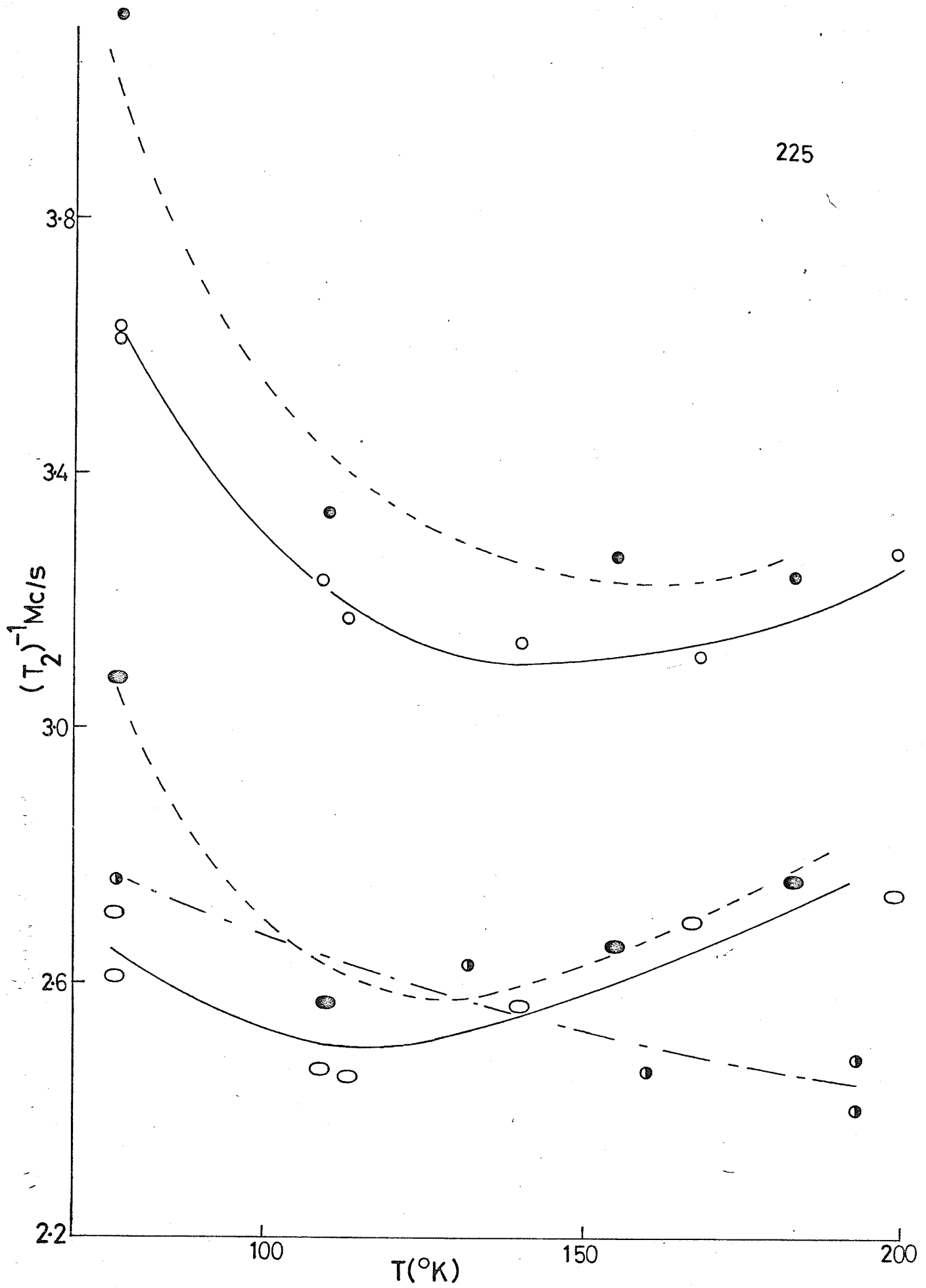


Fig. 4.8

Measured linewidths (lines 1 and 3) as a function of temperature.

Open circles	(solid line) - line 1	Sample 4
Solid circles	(dashed line) - line 1	Sample 9
Open ellipses	(solid line) - line 3	Sample 4
Solid ellipses	(dashed line) - line 3	Sample 9
Semi-solid circles	(dashed line) - line 3	Warming and Cooling S Table 2.9



calculated linewidth values, tumbling frequencies of the order of 10^6 would have been obtained for the methyl and deuteromethyl radical stabilized at 77°K on the 300°C temperature pretreated silica gel surface used.

4. Discussion

As mentioned before, the line shapes were neither Lorentzian nor Gaussian. Each proton line differed by a different degree from the two main line shapes. Equation (4-4) was used as well to test the line shapes. The value of β (or a_1) from equation (4-4) did not equal that found by curvilinear regression analysis. Therefore the line shapes are definitely not Lorentzian. Another explanation may be another linewidth contributing factor present in a_0 which is dependent on temperature. For the lines $M = +1$ and $M = -1$ (sample 4) the value of a_1 calculated from equation (4-4) was approximately 200-250 mgauss greater at 77°K than that found by curve fitting. Contrary results were obtained for lines $M = \pm 1/2$. The calculated results (equation 4-4) were approximately 200 mgauss smaller than those from equation 4-10. The deviation of a_1 [from equation (4-4)] from the value found by curve fitting changed as a function of temperature. The deviation decreased for lines $M = \pm 3/2$ on increasing the temperature to 167°K and then began increasing again on approaching 200°K. The reason for the higher temperature increase is not understood. The reason for the lines being neither Lorentzian nor Gaussian at low temperatures may be rationalized in terms of orientation effects or incomplete averaging of the g-tensor. These concepts will be discussed later in this discussion.

A comparison of the results obtained in this work to those of Gardiner and Casey⁸³ will now be discussed. Gardiner and Casey measured one linewidth and calculated the remainder making use of the relation

$$(\text{derivative height}) \times (\text{derivate width})^2 = \text{constant}$$

which holds for lines of equal intensity. They then, using the calculated values, fitted their calculated linewidths to equation (4-10). A comparison of the calculated linewidths to measured linewidths is shown in Fig. 4.1. The method of Gardiner and Casey leads to a value for the line $M = -3/2$ which is larger than the linewidth of line $M = -1/2$. The measured values show a decrease in linewidth on increasing H_0 . Also, the calculated linewidths are larger than the measured values. The difference in these two methods is due to the irregular amplitudes and relative intensities of the four lines. The method of Gardiner and Casey overestimates the term in M^2 which means an overestimation in the hyperfine anisotropy. The calculated linewidths also lead to larger a_0 and a_1 terms as well as a smaller value for the tumbling frequency (approximately twice as small). As mentioned previously, a value of b , calculated from the results of Rogers and Kispert,⁷⁵ would lower the tumbling frequencies of Gardiner and Casey as well as those calculated in this work, from the measured linewidths, by a factor of approximately 10. There is also a question about the term a_2 used in the publication by Gardiner and Casey. It is believed that a_2 should be equal to $\frac{b^2}{8} \tau_c$ instead of $\frac{b^2}{5} \tau_c$. There are many differences between the surface employed by Gardiner and Casey and the surface used in this study. In this work high temperature degassed p.V.g. was used, whereas, Gardiner and Casey used low temperature pretreated silica gel. The surface coverages used in the studies described in the last section are much

lower than those of Gardiner and Casey. The linewidths were measured in this study and not calculated from one measured linewidth. Therefore the surface and the methods employed were quite different.

Let us now focus our attention on Table 4.1 and Fig. 4.7. The measured linewidths for the methyl radical stabilized on a chlorinated surface appear to be larger than the linewidths for the same radical stabilized on a regular surface. This may be due to unresolved splittings due to stronger adsorption to the chlorinated surface or due to a large electric field present on the chlorinated surface. The linewidths on hydrated surfaces (designated H_2O) are larger than those for chlorinated or regular surfaces. The linewidths found on surfaces treated with H_2O are larger than for surfaces treated with D_2O . This is direct evidence for unresolved proton splittings. But even this observation seems to be complicated by an apparent dependence on M. The linewidths observed for the deuterio-methyl radical are smaller than those for the methyl radical. In opposition to the first observation mentioned in this paragraph the linewidths for the deuteromethyl radical on the chlorinated surface appear to be smaller than the measured linewidths for the deuteromethyl radical stabilized on a regular surface.

The variation of the measured linewidths with increasing temperature (Table 4.2, Fig. 4.2, Fig. 4.5 and 4.6) will now be examined. Considering sample 4, line 1 decreases to 140-167°K and then increases. Line 3 decreases to 115°K then increases. Lines 3a and 1a decrease to 115°K and then remain almost constant up to 199°K. Line 1 [sample 9 (Cl)] decreases up to 183°K. Line 3 decreases to 115°K and then increases while lines 3a and 1a decrease to about 115°K and remain constant up to 183°K. Comparisons of these studies with the results of the previous chapter are not possible because the maximum temperature attainable with the low modulations

used here is 200°K. General trends seem to compare with those studies performed in Chapter III but, for example, it is not possible to say if line 3a increases above 200°K as was shown previously. It does appear that lines 1 and 3 have linewidth dependences which are different than lines 3a and 1a. The two halves of the spectrum differed with respect to satellites (H_2O surfaces) as well. A decrease in the modulation seems to have shifted the observed minimum for line 3 to lower temperatures. Lines 1 and 2 (sample 8) decrease up to 112°K and then increase. Line 3 decreases to 112°K and then remains almost constant. Line 4 decreases to 112°K and then increases slightly. Lines 5 and 6 decrease to 98°K-112°K and then increase slightly. Line 7 decreases to 98°K and then increases. Considering sample 9 the following observations were made. Lines 1-6 decreased to 127°-151°K. Line 7 decreased to 127°K and then increased slightly. Figures 4.5 and 4.6 reveal almost a straight line dependence for linewidth vs. M which means a very small hyperfine anisotropy contribution.

Consideration will now be given to a_0 , a_1 , a_2 , $\Delta\gamma$ and the tumbling frequencies at 77°K (Table 4.3). In previous work outlined in the introduction to this Chapter the "constant" a_0 was resolved into two terms. One of these terms depended on modulations of the anisotropic hyperfine and g-tensor while the other was due to unspecified or unidentifiable contributions. It is worth noting that Gardiner and Casey⁸³ have written this term down as a function of modulations in the g-tensor plus a constant (equation 4-11). The term a_0 for $CH_3(Cl)$ is greater than for $CH_3(Reg.)$. The value of a_0 for $CH_3(H_2O, D_2O)$ is much greater than for $CH_3(Reg.Cl)$ while a_0 for $CH_3(H_2O)$ is greater than that for $CH_3(D_2O)$. These observations may be explained by increased interaction

with the surface on going through the series $\text{CH}_3(\text{Reg})$, $\text{CH}_3(\text{Cl})$, $\text{CH}_3(\text{D}_2\text{O})$, $\text{CH}_3(\text{H}_2\text{O})$ although the difference between a_0 for $\text{CH}_3(\text{H}_2\text{O})$ and $\text{CH}_3(\text{D}_2\text{O})$ is most probably due to unresolved splittings. It is interesting to note that $a_0(\text{CD}_3) \approx \frac{a_0(\text{CH}_3)}{1 \text{ to } 1.5}$.

This observation may be explained in terms of a much smaller value for the h.f. anisotropy in the deuteromethyl radical. Again we find a contrary result: $a_0(\text{CD}_3, \text{Reg})$ is greater than $a_0(\text{CD}_3, \text{Cl})$. These contradictory results may be due to the fact that the deuterium atom has a quadrupole moment. Therefore, the very nearly linear dependence of linewidth on M (Fig. 4.5, 4.6) may be due to a much smaller hyperfine anisotropy or a negative quadrupole term in equation 4-10. The results for the parameter a_1 almost parallels those for a_0 except for the two following observations: $a_1(\text{CH}_3, \text{H}_2\text{O})$ is approximately equal to $a_1(\text{CH}_3\text{D}_2\text{O})$ and $a_1(\text{CD}_3) \cong \frac{a_1(\text{CH}_3)}{2}$. The results for a_2 are the same as for a_1 except that $a_2(\text{CD}_3) \cong \frac{\text{CH}_3}{10}$. a_2 depends on b^2 which reveals why there is such a large difference between $a_2(\text{CD}_3)$ and $a_2(\text{CH}_3)$. The coefficient a_2 for CD_3 runs turned out to be negative many times since the hyperfine anisotropy is so small for this radical. This fact made calculations of $\Delta\gamma$ and the tumbling frequencies very unreliable for CD_3 systems. The results for $\Delta\gamma$ at 77°K are opposite to those for a_0 , a_1 and a_2 :

$$\begin{aligned} \Delta\gamma(\text{CH}_3, \text{Cl}) &< \Delta\gamma(\text{CH}_3, \text{Reg}) \\ \Delta\gamma(\text{CH}_3, \text{H}_2\text{O} \text{ or } \text{D}_2\text{O}) &\ll \Delta\gamma(\text{CH}_3, \text{Reg}, \text{Cl}) \\ \Delta\gamma(\text{CH}_3, \text{H}_2\text{O}) &\cong \Delta\gamma(\text{CH}_3, \text{D}_2\text{O}) \\ \Delta\gamma(\text{CD}_3, \text{Reg}) &< \Delta\gamma(\text{CD}_3, \text{Cl}) \\ \Delta\gamma(\text{CD}_3, \text{Reg}) &\cong \frac{\Delta\gamma(\text{CH}_3, \text{Reg})}{2} \\ \Delta\gamma(\text{CD}_3, \text{Cl}) &\cong \Delta\gamma(\text{CH}_3, \text{Cl}) \end{aligned}$$

The last two observations do not appear to be consistent. The calculated tumbling frequencies (T.F.) yield the same relations as the $\Delta\gamma$ results except the last two observations are not quite the same as for $\Delta\gamma$.

$$\begin{aligned} \text{T.F. (CD}_3, \text{Reg)} &\approx \frac{\text{T.F. (CH}_3, \text{Reg)}}{8} \\ \text{T.F. (CD}_3, \text{Cl)} &= \frac{\text{T.F. (CH}_3, \text{Cl)}}{3} \end{aligned}$$

Observations were also made of the tumbling frequencies, a_0 , a_1 , a_2 and $\Delta\gamma$ as a function of temperature (Table 4.4, Fig. 4.3, Fig. 4.4). The coefficient a_0 ($\text{CH}_3, \text{Reg.}$) decreases in value to about 120°K, increases again to approximately 170°K, and then decreases to 200°K (highest temperature attained for these studies). a_0 (CH_3, Cl) decreases to 120°K at which point it begins to increase again and still is increasing at 185°K. a_0 (CD_3, Cl) decreases to 154°K which is the highest temperature attainable for this system. This trend is most likely due to the fact that the CD_3 radical remains orientated at particular sites until much higher temperatures because of its greater mass. The parameter a_1 (CH_3, Reg) decreases up to 170°K and then begins to increase in magnitude. a_1 (CH_3, Cl) decreases to 183°K while a_1 (CD_3, Reg) is observed to decrease up to 127°K. a_1 (CD_3, Cl) decreases to about 115°K where it increases again up to 154°K. a_2 (CH_3, Reg) decreases to about 140°K where it begins to increase slightly whereas a_2 (CH_3, Cl) decreases up to 183°K. $\Delta\gamma$ and T.F. have the same temperature dependences. T.F. (CH_3, Reg) increases up to 140°K where it decreases again to 200°K. T.F. (CH_3, Cl) increases up to 183°K. Only two measurements were made for the system (CD_3, Cl) while none above 77°K are available for the system (CD_3, Reg) due to negative a_2 values. The above mentioned results indicate a stronger interaction between

the methyl radical and a chlorinated surface. The tumbling frequency is plotted as a function of temperature ($^{\circ}\text{K}$) for sample 4 in Fig. 4.3. The maximum at approximately 140°K corresponds with the temperature at which the carbon-13 splitting began to decrease (Chapter III). Above 140°K orientation of the radical may not be very important while below 140°K radical orientation may be of prime importance. In Fig. 4.3 the tumbling frequency is plotted as a function of temperature for sample 9 (CH_3Cl). For sample 9 the tumbling frequency is seen to increase up to 185°K which may mean the radical is orientated to greater temperatures for a chlorinated surface. It is not known how b and $\Delta\gamma$ are changing with temperature. In order to calculate the tumbling frequencies the same value of b is used for all temperatures studied. How this is affecting the calculations of the "a" values and $\Delta\gamma$ as a function of temperature is not understood. Are tumbling frequencies actually being calculated above 77°K ? Above 77°K both b and $\Delta\gamma$ should become more completely averaged due to more rapid radical motions. Fig. 4.4 exhibits a plot of the log of the tumbling frequencies as a function of $\frac{1}{T}$. For this Arrhenius plot activation energies of "tumbling" have been calculated for samples 4 and 9. The activation energies calculated are within 10 cal/mole of one another and are of the right order of magnitude for transitions or exchange energies between different conformations of the radical (at different sites) on the surface (increased movement or tumbling).

Figure 4.8 shows the linewidths (lines 1 and 3) of samples 4 and 9 as a function of temperature. In each case the linewidths decrease on increasing temperature indicating increased movement on the surface. (For example, loss of unresolved splitting due to the radical movement away from the interacting atom). In almost all cases the linewidths increase again indicating diffusion or movement which results in an uncertainty in the energy of the transition under consideration. Also included in Fig. 4.8 are the values of the

linewidth of line 3 from Chapter II (decrease in linewidth on warming and cooling). This decrease also indicates the release of the radicals from specific sites and the return to these sites via slow diffusion at liquid nitrogen temperatures.

Table 4.5 gives the relative amplitudes of some of the samples at 77°K and also the results of one temperature run. The binomial distribution is approached on increasing the temperature. At 77°K the relative amplitudes are not binomial for any of the samples. The relative amplitudes for the different systems is similar at 77°K, and therefore one can conclude that these measurements are insensitive to surface characteristics but are reasonably sensitive to increases in temperature.

It may be worth mentioning that in systems where the linewidths are larger, the second-order splitting is more poorly resolved. For example, the second order splitting is almost not detectable for the intentionally hydrated surfaces where the linewidths are largest.

5. Conclusions

The methyl radical lineshapes are not Lorentzian or Gaussian. Each line has a different shape. Studying the linewidths as a function of temperature lead to the following conclusions:

(1) The initial linewidth decrease is due to the disappearance of unresolved splittings due to radical movement, a spin-rotational interaction, a decrease in b and $\Delta\gamma$ on increasing the temperature, or a mixture of many of these factors.

(2) The linewidth broadening which occurs at higher temperatures is due to an uncertainty in the energy levels possibly because of diffusion between potential wells.

(3) Each line has a different temperature dependence.

The linewidths calculated by Gardiner and Casey⁸³ are larger than the measured values because of the non-binomial relative amplitudes and intensities. This same reason leads to an over-estimation of b and a smaller tumbling frequency. If the value of b calculated from Roger's and Kispert's⁷⁵ work is employed the resulting tumbling frequencies are about a factor of 10 smaller.

Linewidth studies at liquid nitrogen temperatures revealed that: L.W. (CH₃,Reg) < L.W. (CH₃,Cl) < L.W. (CH₃,D₂O) < L.W. (CH₃,H₂O). These studies also revealed an unresolvable proton splitting for the system (CH₃,H₂O) which was dependent on M (the nuclear spin quantum number). The linewidths for CD₃ radicals are smaller than the linewidths of the CH₃ systems. In contrast to the results above the L.W. (CD₃,Cl) was found to be less than the L.W. of the system (CD₃,Reg.). The tumbling frequencies at 77°K were observed to vary as: T.F. (CH₃,H₂O or D₂O) << T.F. (CH₃,Cl) < T.F. (CH₃,Reg.). The tumbling frequencies on the H₂O and D₂O surface are the same within experimental error. It was also shown that T.F. (CD₃,Reg) < T.F. (CD₃,Cl) and that:

$$T.F. (CD_3,Reg) \approx \frac{T.F. (CH_3,Reg)}{8}$$

$$T.F. (CD_3,Cl) \approx \frac{T.F. (CH_3,Cl)}{3}$$

The hyperfine anisotropy has been shown to be very small for both CH₃ and CD₃ at liquid nitrogen temperatures. The small value of b indicates some reorientations even at 77°K.

It has been shown for the system (CH₃,Reg) that the tumbling frequency increases up to about 140°K and then decreases. For the system (CH₃,Cl) the tumbling frequency has been shown to still be increasing at 185°K. The temperature at which the maximum in the

system (CH_3, Reg) occurs corresponds with the temperature at which the C-13 h.f.s. begins to decrease. Above 77°K one can still ask if the calculations for tumbling frequencies are real and meaningful or are they yielding some other entity dependent upon changes in linewidth, b and $\Delta\gamma$. The resulting activation energies are very small (about 300 cal/mole) and may be associated with oscillations of the adsorbed molecule between different available surface sites.

The decrease in the linewidths with temperature are most likely due to the same process as that for the linewidth changes seen in Chapter II on warming and cooling of the sample. This mechanism is most likely the release of the radical from particular surface sites. The asymmetry and non-binomial relative amplitudes are most likely due to incomplete motional averaging of the g -tensor and hyperfine tensor or to radicals taking up particular orientations with respect to the applied magnetic field. Because of the many indications for motion of the radicals at liquid nitrogen temperatures the first reason is believed to be the correct one. Very small effects upon asymmetry are expected due to incomplete motional averaging of the hyperfine tensor because of the small magnitude of b . It is interesting to note that the tumbling frequencies are small for rotation but are of the right order of magnitude for diffusion.

CHAPTER V

DECAY KINETICS

1. Introduction

Preliminary work⁸⁰ established that on raising the temperature from 77°K, the methyl radical signal amplitude gradually diminished and approached a final value which depended on temperature and surface coverage. A cascade was noticed as the temperature was changed stepwise (Fig. 5.1). The decay was observed to begin at lower temperatures as the surface coverage of methyl iodide was increased. For each coverage Λ , there is a critical temperature at which radical decay commenced.

The presence of the cascade phenomenon implies that the radicals are trapped in sites with a large range (or continuum) of activation energies. The presence of a critical temperature indicates a minimum depth for this continuous distribution of binding energies. The radicals on low coverage surfaces are stabilized at sites on the surface of p.V.g., whereas when Λ is large many of the radicals are trapped in the layers of adsorbate molecules where the binding energy for the methyl radical may be somewhat less than on the surface of p.V.g.

The decay was attributed⁸⁰ to surface diffusion of desorbed radicals, followed by recombination to form ethane. Gas-chromatographic analysis revealed that both methane and ethane were present in the recombination products. The ratio of ethane to methane was large when the surface coverage was low. It was postulated that the methane was formed during photolysis by hydrogen abstraction by activated (hot) methyl radicals. The decay was shown to follow first-order kinetics (Fig. 5.2) and the rate constant was dependent on surface coverage.

Fig. 5.1

Proton Line Amplitude vs. Decay Time (in minutes) at
Various Temperatures.⁸⁰ Note stepwise decay.

Surface coverages: a - 1 layer, b - 7 layers

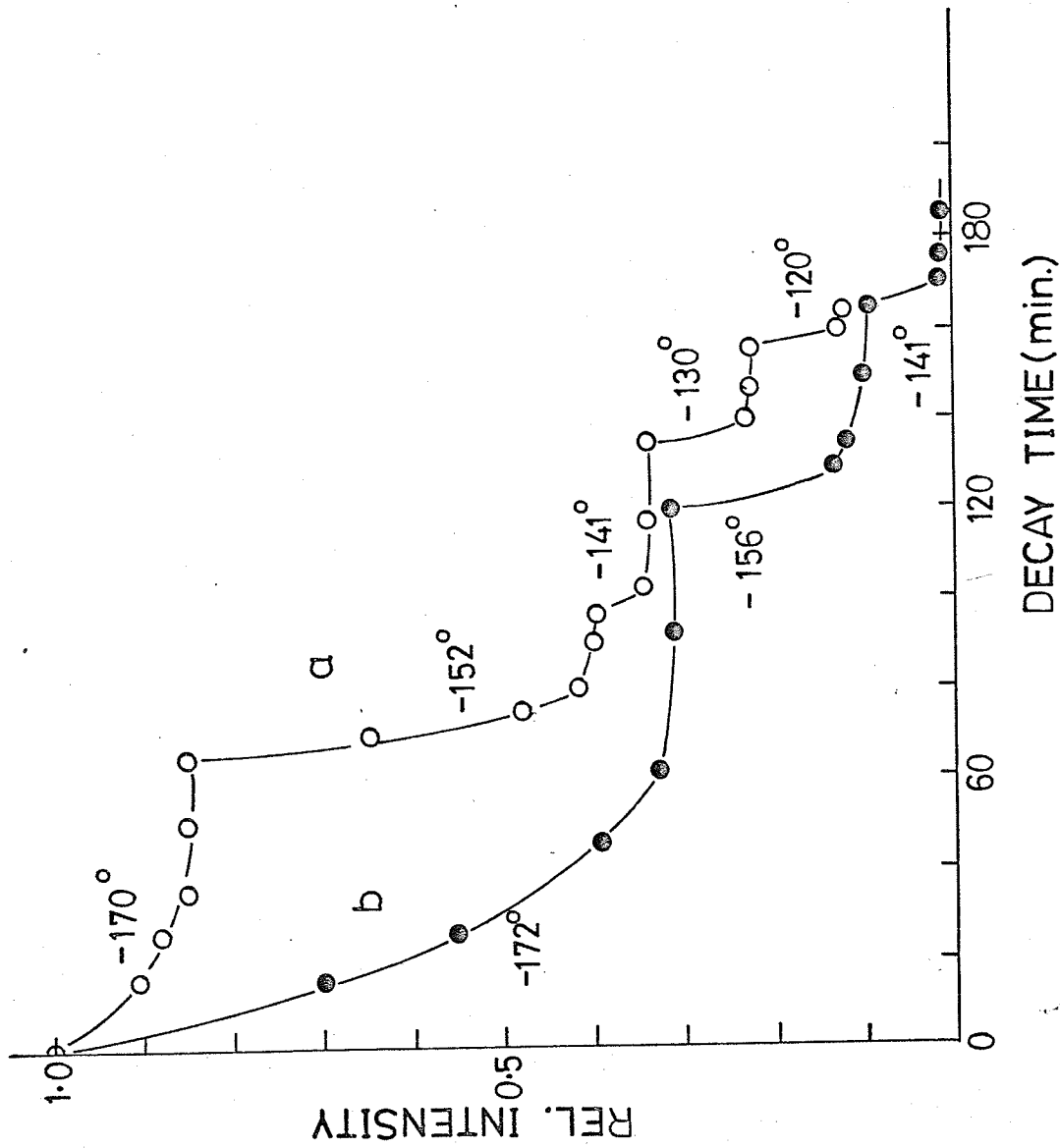
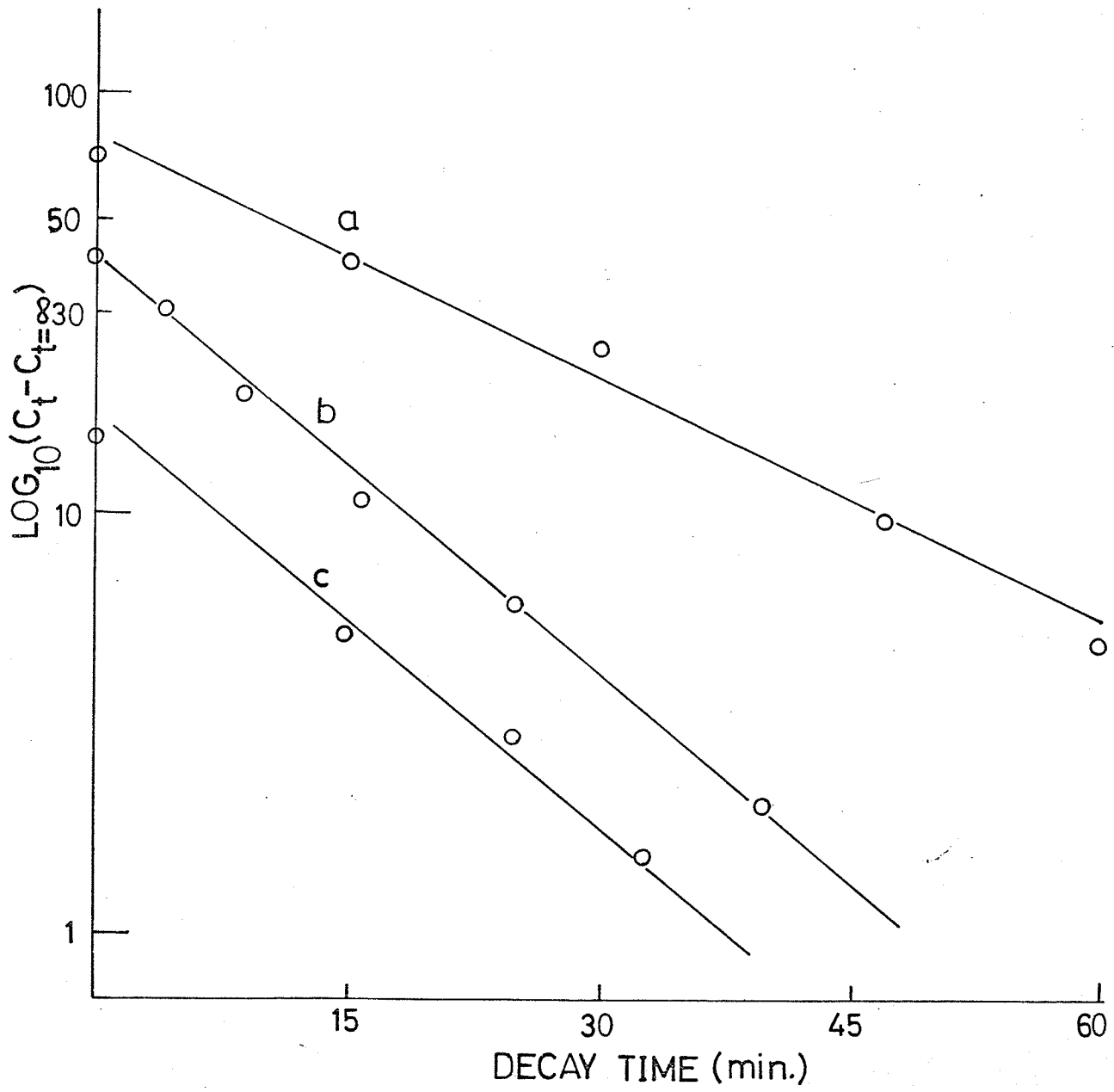


Fig. 5.2

Decay of methyl radicals at -170°C as the logarithm of the change in the E.P.R. spectrum is plotted against time, indicating first-order kinetics, with the rate constant $k = (1 \sim 0.4) \times 10^{-1} \text{ min.}^{-1}$.⁸⁰ Coverages: a - 7 layers, b - 5 layers, and c - 1 layer.



This was interpreted by assuming that the rate is determined by the release of the radical from the surface site, and that subsequent diffusion on the surface is fast and results in a low stationary concentration of mobile radicals. Recent work on the decay kinetics of methyl radicals, to be discussed below, confuses parts of the picture presented above (Ref. 80). However, it must be pointed out that the surface treatments, the surface coverage and the spectrometer used in the more recent studies are significantly different than those used in the preliminary work.

2. Experimental

The sample employed for kinetic studies was heated in oxygen at 700°-800°C and then degassed at these temperatures for many hours. The methyl iodide was then adsorbed at room temperature giving $\Lambda = 0.04-0.05$. The methyl radicals were produced at 77°K using the full focused arc of a Hanovia S-100 Alpine burner (medium pressure mercury lamp). The sample was then transferred to the cavity insert of a normal variable temperature assembly. The temperature was monitored with a thermocouple placed in the insert just above the cavity. The temperature was controlled to $\pm 1^\circ\text{K}$. A Varian E-3 E.S.R. spectrometer was used.

The temperature was raised from near 77°K (using a flow system) to a value where decay occurred. Lines 3 and 3a were scanned many times in both directions (upfield and downfield) during the first few minutes of decay. After these first few minutes the two lines were scanned in both directions less frequently until 60 or 70 minutes had elapsed. The temperature was then raised to another value and the same procedure was performed. The process of raising the temperature and watching the decay was repeated until the signal-to-noise ratio became

too small. The same sample was regenerated at 77°K using the same mercury lamp. The procedure outlined above was then repeated. Decay data for lines 3 and 3a (in both directions) was accumulated at the following temperatures: 110°K, 130°K, 145°K, 152°K, 173°K, 220°K, 233°K, 260°K, 292°K, and 298°K. No decay was noticed up to 100°K. The results presented and discussed are for line 3a in the forward (upfield) direction. All other measurements gave comparable results.

A typical decay curve is shown in Fig. 5.3 (amplitude of line 3a versus time in minutes). All measurements made during radical decay at a particular temperature were standardized to one gain setting on the spectrometer by multiplying the measured amplitudes by the appropriate factor. In fact, for consistency, all measurements made at all temperatures listed above were standardized to one appropriate gain setting. This became a necessity when second-order kinetics was considered. In order to fit the decay curves to rate equations the amplitude of the line at $t = \infty$ must be measured or estimated. The amplitude at $t = \infty$ is designated in Fig. 5.3 as S.S. (steady-state).

3. Results and Discussion

At every temperature where decay was studied it was found that the decrease in concentration of methyl radicals is very sensitive to small changes in temperature. This effect was studied after the initial decay had occurred (i.e. after the first 20 minutes of radical decay). It was shown that a small decrease in temperature will stop decay while a small increase in temperature will increase the decay rate. This seems to be direct evidence for a continuum of trapping potentials (sites) with a continuum of activation energies. Each decay plotted appeared to have small plateaux or a cascade effect (see Fig. 5.3).

Fig. 5.3

Decay of line 3a at 152°K. The value of $C_{t=\infty}$ (=S.S.) is estimated by extrapolation.

AMPLITUDES (STANDARDIZED)

80

70

60

0

20

40

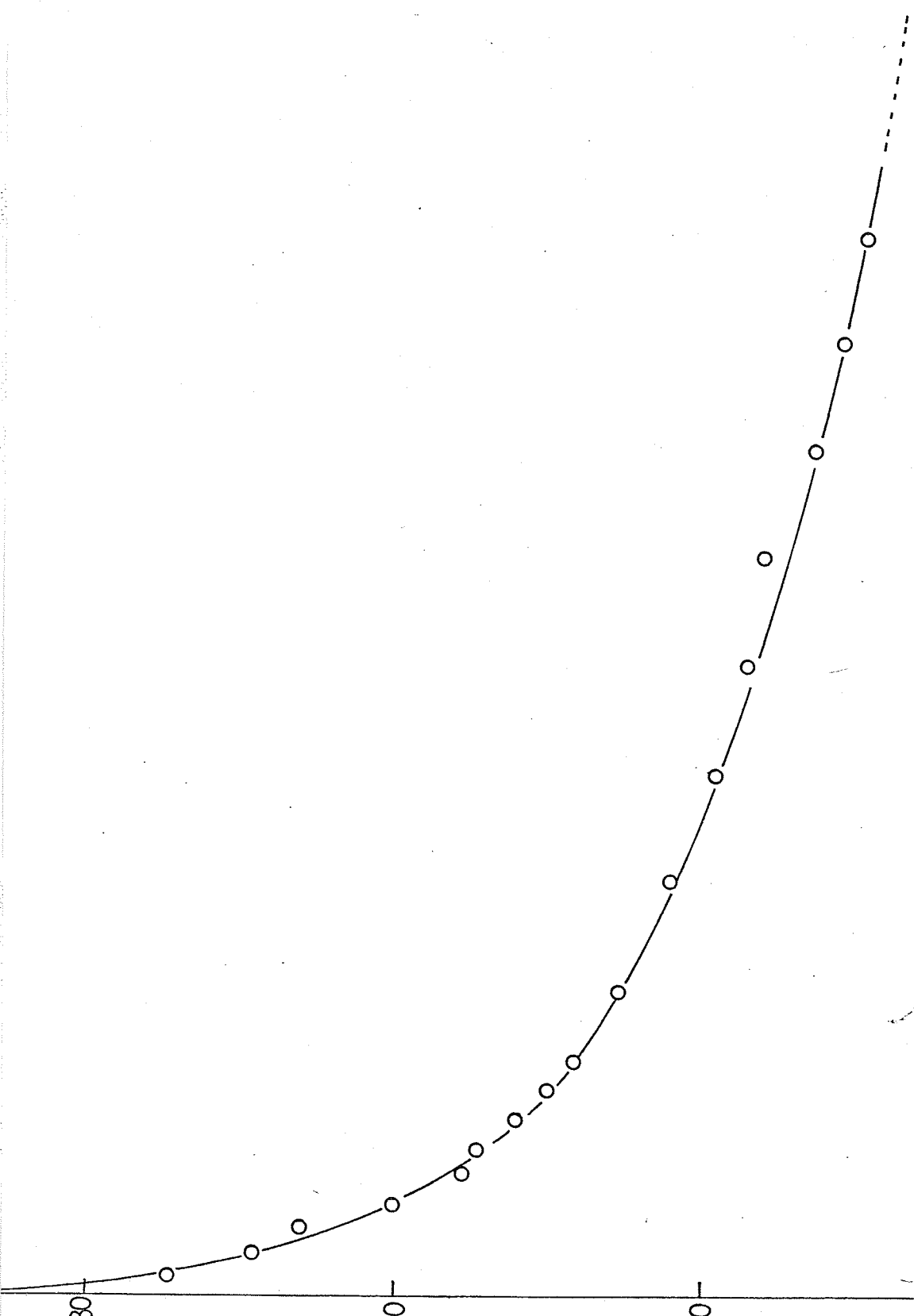
60

80

241

$C_{T=85}$

T(min.)



$C_{T=85}$

This may be due to small fluctuations in temperature in the variable temperature assembly or to the presence of sites which differ from one another by only a small amount of energy (i.e. activation energy). This would mean that radicals trapped at sites with smaller activation energies are decaying first leaving predominantly radicals trapped at sites with larger activation energies. These radicals then decay leaving predominantly radicals trapped at sites with larger activation energies still, and so on. The energy difference between these levels would be very small. Small fluctuations in temperature in the variable temperature assembly may also give rise to a similar effect.

An attempt was made to fit the decay data to the integrated forms of first, second and three-halves order rate equations. The first-order ($n = 1$) rate equation may be written as

$$\log \frac{C_0}{C} = \frac{k}{2.303} t, \quad (5-1)$$

where k is the rate constant, t is the time, C_0 is the initial concentration ($t = 0$), and C is the concentration at any time t . For example, C_0 is the initial amplitude of line 3a minus the amplitude of 3a at $t = \infty$ (S.S.). The variable, C , is the amplitude of line 3a at time t minus S.S. The integrated forms of the rate equations where $n = 3/2$ and $n = 2$ are given below.

$$n = 2: \left(\frac{1}{C} - \frac{1}{C_0} \right) = kt \quad (5-2)$$

$$n = 3/2: 2 \left(\frac{1}{C^{1/2}} - \frac{1}{C_0^{1/2}} \right) = kt \quad (5-3)$$

It was found that at all temperatures studied the methyl radical is decaying rapidly enough after 60 or 70 minutes to make the estimate of the S.S. concentration difficult. A recommendation may be made

here for further studies on this topic. The decay was monitored in this work for a maximum of 70 minutes. It is recommended that in further work on this topic the decay be monitored until an accurate estimate of S.S. is possible. It was found that equation (5-2) could be fitted to all data making use of reasonable values of S.S. An effort was made to fit the first order rate equation (equation 5-1) to the accumulated results for decay runs at 110°, 130° and 145°K. In order to make equation 5-1 fit a large value for S.S. had to be assumed. This would mean that the decay is stopping faster than the measured decay curves indicated. It was concluded that second-order kinetics fitted the results at all temperatures better than any other rate law. It is worth mentioning that $t^{1/2}$ (time at which one-half the original concentration is reached) relationships may have been useful in determining the order of the decay if the decay had been monitored for longer periods of time.

The general rate equation is

$$-\frac{dc}{dt} = k c^n \quad (5-4)$$

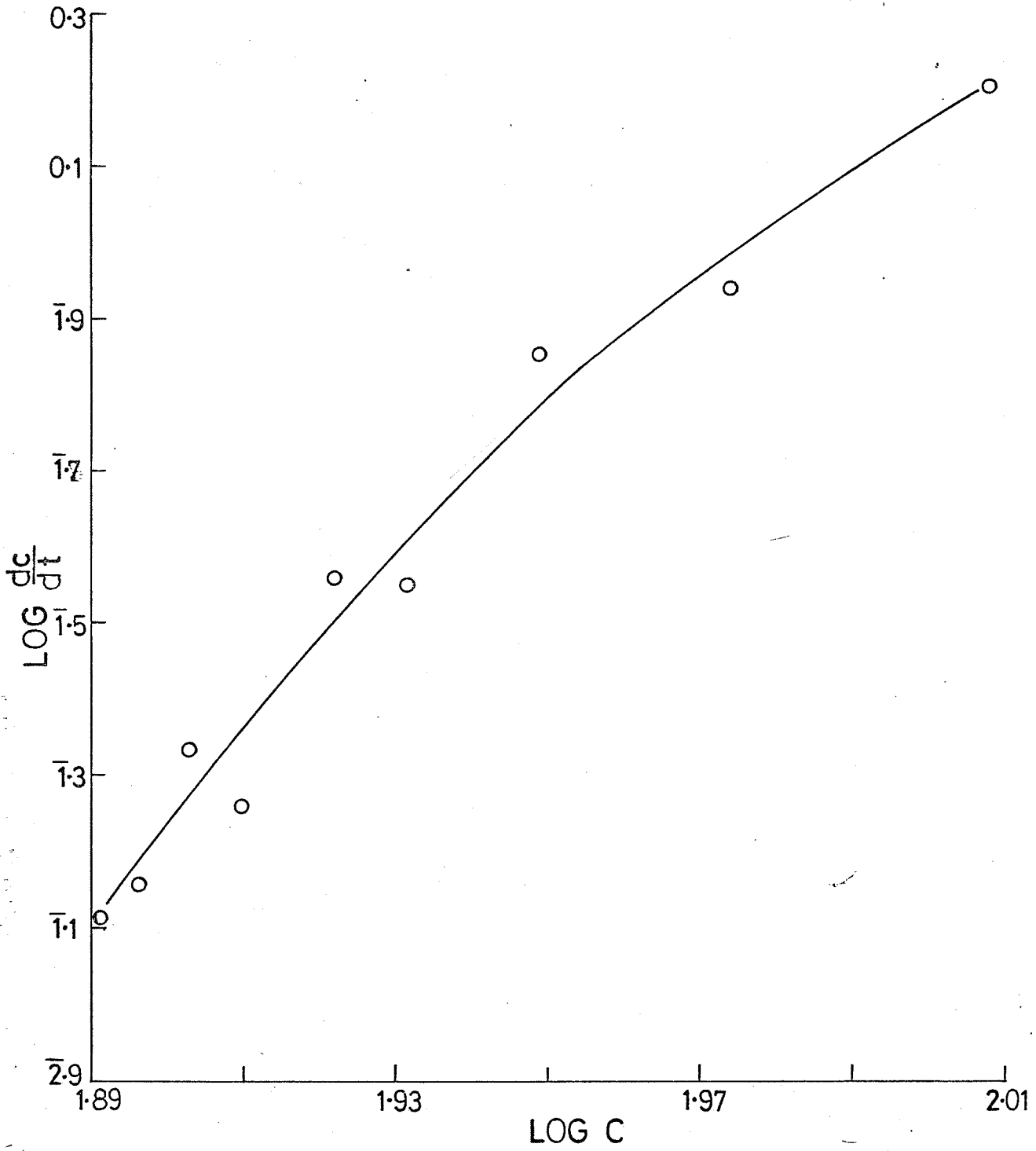
This relationship becomes, on taking logarithms of both sides,

$$-\log \frac{dc}{dt} = \log k + n \log c \quad (5-5)$$

If one plots $\log \frac{dc}{dt}$ vs. $\log c$, the slope, n , allows the calculation of $\log k$. This relationship was plotted for the results at 110°K for line 3a (Fig. 5.4). The plot shows slight curvature. The average value of n obtained from this plot is 1.0. From this procedure one obtains the order with respect to time n_t . This order is not the true order and may be found to be larger than the true order n .

Fig. 5.4

$\text{Log } \frac{dc}{dt}$ as a function of $\text{Log } C$ (sample at 110°K).
The slope of this curve is n_t and the intercept is $\log k$. Note the curvature.

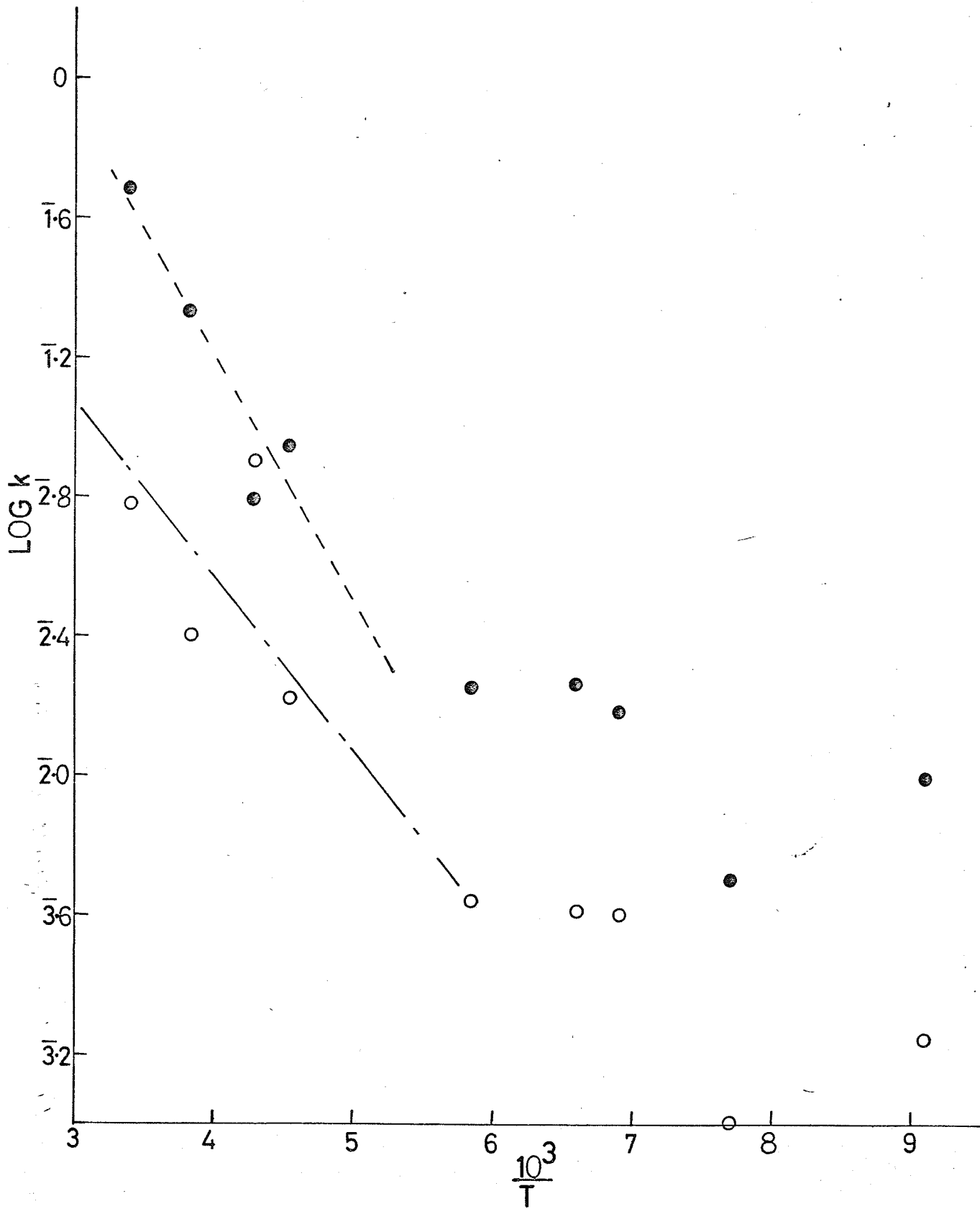


The fact that n_t is greater than n (order with respect to concentration) means that, as the decay proceeds, the rate falls off more rapidly than it would do if the true order applied to the time course of the reaction. This abnormally large falling off has been classically interpreted to mean that some intermediate or product in the reaction is acting as an inhibitor. Similar results have been obtained on plotting equation (5-5) for hydrogen atom decay.¹³⁴ Normally, in order to obtain the true order n , initial reaction velocities are plotted against initial concentrations at some temperature T (using equation 5-5 again). This procedure of dealing with initial velocities avoids possible complications due to interference by products. This procedure should be carried out on the system under discussion.

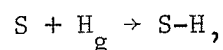
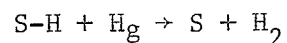
Assuming we are correct in assigning $n = 2$ to the decay, a plot of $\log k$ versus $1/T$ has been done (Fig. 5.5). One set of data, standardized to two different gain settings, is plotted in Fig. 5.5. The scatter in results within each curve is most probably due to the fact that the decay was not followed long enough to yield accurate values for S.S. The Arrhenius plot shows a small activation energy or none at all below 173°K ($\frac{1}{T} \times 10^3 = 5.8$). Above this temperature the activation energy is between 2.0 and 3.2 Kcal/mole. An activation energy of this magnitude indicates a diffusion controlled reaction. There is a definite curvature in the Arrhenius plot. This can result if there are two competing reactions with different activation energies and is often observed where the same reaction may occur both homogeneously and heterogeneously. The homogeneous reaction usually has a higher activation energy and so it is favored at high temperatures, whereas the heterogeneous reaction predominates at lower temperatures.

Fig. 5.5

Log k vs. $1/T$ (Arrhenius plot). One set of data standardized to two gain settings and worked out independently. Note curvature in this plot.



Another explanation for this curvature might be tendered.¹³⁵ This explanation results from a study by Schuler and Laidler¹³⁵ of the heterogeneous recombination of hydrogen atoms on surfaces. It was proposed that hydrogen atom recombination on clean glass (i.e. not poisoned by water) surfaces occurs by the following reactions,



where S-H is the surface stabilized hydrogen atom and H_g is the hydrogen atom in the gas phase. The symbol S represents the surface site. The recombination reaction is first order in hydrogen atoms up to 250°C where it becomes second order. The temperature 250°C is the desorption temperature. The activation energy for the recombination was found to be zero between -180°C and -80°C. The activation energy between -80°C and 250°C was observed to be 0.9 Kcal/mole. These results were explained by suggesting that the hydrogen atoms are van der Waals adsorbed to the glass in the low temperature region and chemisorbed at the higher temperatures. Small amounts of curvature in the Arrhenius plot may also be attributed to the existence of more than one mechanism of diffusion.¹³⁶

4. Conclusions

The methyl radical decay kinetics are not as simple as originally thought.⁸⁰ In fact, the decay probably goes by second-order and not by first order as originally concluded.⁸⁰ Radical decay is very sensitive to small variations in temperature indicating a continuum of sites with a continuum of activation energies. A critical temperature at which decay begins was noticed. The fact that $n_t > n$ indicates, classically,

inhibition to reaction by reaction products. The Arrhenius plot is bent. Below 173°K the activation energy is small or zero. Above 173°K the activation energy is 2.0 - 3.2 Kcal/mole indicating a diffusion controlled decay. Three possible reasons for the curvature in the Arrhenius plot have been suggested. The curvature in the Arrhenius plot occurs in the same temperature region as the minimum in the plot of linewidth vs. temperature (Fig. 3.16).

APPENDIX I

PROTON HYPERFINE SPLITTING AS A FUNCTION OF TEMPERATURE
(RAW DATA)

RUN NUMBER	TEMPERATURE (°K)	$ a^H $ IN GAUSS
1	92.1	23.046
	114.9	23.046
	137.7	23.054
	156.5	23.047
	181.9	23.021
	203.7	23.000
	228.7	22.959
	252.2	22.894
	274.4	22.887
	307.0	22.864
	344.0	22.800
	373.5	22.739
	384.7	22.643
2	101.2	23.005
	144.7	23.009
	171.4	22.982
	211.2	22.960
	247.8	22.908
	272.0	22.871
	292.3	22.868
	317.5	22.817
	348.5	22.746
	3	77.0
98.7		23.102
139.5		23.075
171.4		23.055
210.4		23.032
248.7		22.976
272.2		22.954
293.5		22.956
318.0		22.876
343.5		22.742

RUN NUMBER	TEMPERATURE (°K)	$ a^H $ IN GAUSS
4	77.0	23.060
	104.2	23.052
	123.8	23.035
	146.2	23.050
	169.6	23.025
	188.7	23.005
	208.2	22.989
	236.4	22.974
	269.7	22.950
	297.2	22.813
	311.8	22.828
	327.0	22.804
	358.2	22.784
379.0	22.698	
5	77.0	23.051
	98.7	23.146
	139.6	23.087
	171.4	23.073
	210.4	23.024
	248.4	22.975
	271.8	22.909
	293.5	22.916
	318.1	22.838
	345.2	22.792
6	167.8	23.126
	198.6	23.060
	229.2	23.038
	271.8	22.988
	309.2	22.870
	354.0	22.745
	395.7	22.686
7	271.8	22.955
	316.4	22.856
	344.2	22.830
	379.0	22.709

BIBLIOGRAPHY

1. A. Carrington and A.D. McLachlan, Introduction to Magnetic Resonance, (New York: Harper and Row, 1967).
2. P.B. Ayscough, Electron Spin Resonance in Chemistry, (London: Methuen, 1967).
3. M. Bersohn and J.C. Baird, An Introduction to Electron Paramagnetic Resonance, (New York: W.A. Benjamin Inc., 1966).
4. D.J.E. Ingram, Spectroscopy at Radio and Microwave Frequencies, Second Edition, (London: Butterworths, 1967).
5. Free Radicals in Biological Systems, ed. M.S. Blois et al, (New York: Academic Press, 1961).
6. R.H. Sands, An Introduction to E.P.R., (Varian Associates, 10th Annual E.P.R. Workshop, Palo Alto, 1966).
7. G.E. Uhlenbeck and S. Goudsmit, Nature 117, 264 (1926).
8. W.A. Anderson, Classical versus Quantum Mechanical Description of Electron Spin Resonance, (Varian Associates, Ninth Annual NMR-E.P.R. Workshop, Palo Alto, 1965).
9. L. Petrakis, J. Chem. Educ. 44, 432 (1967).
10. C.P. Poole, Jr., Electron Spin Resonance, Chapter 20, (New York: Interscience, 1967).
11. A. Carrington and A.D. McLachlan, Introduction to Magnetic Resonance, Appendix I, (New York: Harper and Row, 1967).
12. M.L. Hair, Infrared Spectroscopy in Surface Chemistry, (New York: Marcel Dekker, Inc., 1967).
13. L.H. Little, Infrared Spectra of Adsorbed Species, (London: Academic Press, 1966).
14. R.S. McDonald, J. Phys. Chem. 62, 1168 (1958).

15. F.H. Hambleton, J.A. Hockey, and J.A.G. Taylor, *Nature* 208, 138 (1965)
16. J.B. Peri, *J. Phys. Chem.* 69, 211 (1965); 70, 2937 (1966).
17. N.W. Cant and L.H. Little, *Can. J. Chem.* 42, 802 (1964).
18. J.B. Peri, *J. Phys. Chem.* 70, 2937 (1966).
19. H.A. Benesi and A.C. Jones, *J. Phys. Chem.* 63, 179 (1959).
20. V.Y. Davydov, A.V. Kiselev and L.T. Zhuravlev, *Trans. Faraday Soc.* 60, 2254 (1964).
21. F.H. Hambleton, J.A. Hockey and J.A.G. Taylor, *Trans. Faraday Soc.* 62, 801 (1966).
22. G.J. Young, *J. Colloid Sci.*, 13, 67 (1958).
23. R.S. McDonald, *J. Amer. Chem. Soc.*, 79, 850 (1957).
24. G.J.C. Frohnsdorff and G.L. Kington, *Trans. Faraday Soc.*, 55, 1173 (1959).
25. M.R. Basila, *J. Chem. Phys.*, 35, 1151 (1961).
26. D.E. Woessner, *J. Phys. Chem.*, 70, 1217 (1966).
27. T. Yoshino, *J. Chem. Phys.*, 23, 1564 (1955).
28. N.W. Cant and L.H. Little, *Can. J. Chem.*, 43, 1252 (1965).
29. I.D. Chapman and M.L. Hair, *Trans. Faraday Soc.*, 61, 1507 (1965).
30. P.J. Hendra and E.J. Loader, *Nature*, 216, 789 (1967).
31. M.L. Hair and I.D. Chapman, *J. Amer. Ceram. Soc.*, 49, 651 (1966).
32. A.N. Sidorov, *Opt. Spectry. U.S.S.R. English Transl.*, 8, 424 (1960).

33. M.J.D. Low and N. Ramasubramanian, Chem. Commun. 20, 499 (1965).
M.J.D. Low and N. Ramasubramanian, J. Phys. Chem., 70, 2740 (1966).
34. M.J.D. Low and P. Ramamurthy, Chem. Commun., 609, (1967).
35. M.J.D. Low and N. Ramasubramanian, J. Phys. Chem., 71, 730 (1967).
36. N. Ramasubramanian and M.J.D. Low, J. Phys. Chem., 71, 3077 (1967).
37. M. Folman and D.J.C. Yates, Proc. Roy. Soc. (London), A246,
32, (1958).
M. Folman and D.J.C. Yates, Trans. Faraday Soc., 54, 1684 (1958).
38. M.J.D. Low, N. Ramasubramanian, V.V. Subba Rao, Preprint.
39. J. Reuben, D. Fiat, and M. Folman, J. Chem. Phys., 45, 311 (1966).
40. D. Fiat, J. Reuben, and M. Folman, J. Chem. Phys., 46, 4453 (1967).
41. N. Sheppard, N.V. Mathieu, and D.J.C. Yates, Z. Electrochem.,
64, 734 (1960).
42. N. Sheppard and D.J.C. Yates, Proc. Roy. Soc. (London), A238,
69 (1956).
43. M. Baverez and J. Bastick, Bull. Soc. Chim. Fr., 1965, 3662
44. C. Morterra and M.J.D. Low, Chem. Commun., 1968, 203
45. T.H. Elmer, I.D. Chapman and M.E. Nordberg, J. Phys. Chem.,
67, 2219 (1963).
46. I.D. Chapman and M.L. Hair, J. Catal., 2, 145 (1963).
47. M. Folman, Trans. Faraday Soc., 57, 2000 (1961).
48. M. Baverez and J. Bastick, Bull. Soc. Chim., Fr., 1964, 3226
49. M.V. Mathieu and B. Imelik, J. Chim. Phys., 59, 1189 (1962).

50. J.J. Fripiat and M. Van Tongelen, *J. Catal.*, 5, 158 (1966).
51. J.A. Hockey and B.A. Pethica, *Trans. Faraday Soc.*, 57, 2247 (1961).
52. J.A. Hockey, *Chem. Ind. (London)*, 1965, 57.
53. L.R. Snyder and J.W. Ward, *J. Phys. Chem.*, 70, 3941 (1966).
54. F.H. Hambleton and J.A. Hockey, *Trans. Faraday Soc.*, 62, 1694 (1966).
55. W. Gordy and C.G. McCormick, *J. Amer. Chem. Soc.*, 78, 3243 (1956).
56. H.N. Rexroad and W. Gordy, *Bull. Amer. Phys. Soc. [II]* 2, 227 (1957).
57. B. Smaller and M.S. Matheson, *J. Chem. Phys.*, 28, 1169 (1958).
58. C.K. Jen, S.N. Foner, E.L. Cochran and V.A. Bowers, *Phys. Rev.*, 112, 1169 (1958).
59. T. Cole, H.O. Pritchard, N.R. Davidson and H.M. McConnell, *Mol. Phys.*, 1, 406 (1958).
60. L.A. Wall, D.W. Brown and R.E. Florin, *J. Phys. Chem.*, 63, 1762 (1959).
61. M. Karplus, *J. Chem. Phys.*, 30, 15 (1959).
62. E.L. Cochran, Paper D-1, Proc. of Fourth Int. Symp. on Free Radical Stabilization, (Nat. Bur. of Stand., Wash., D.C., 1959).
63. P.B. Ayscough and C. Thomson, *Trans. Faraday Soc.*, 58, 1477 (1962).
64. P.B. Ayscough, K.J. Ivin and J.H. O'Donnell, *Trans. Faraday Soc.*, 61, 1110 (1965).
65. P.B. Ayscough, B.R. Brooks and H.E. Evans, *J. Phys. Chem.*, 68, 3889 (1964).

66. P.B. Ayscough, R.G. Collins and F.S. Dainton, *Nature*, 205, 965 (1965).
67. W.V. Bouldin, R.A. Patten and W. Gordy, *Phys. Rev. Letters*, 9, 98 (1962).
68. W.V. Bouldin and W. Gordy, *Phys. Rev.*, 135, A806 (1964).
69. W. Gordy and R. Morehouse, *Phys. Rev.*, 151, 207 (1966).
70. R.L. Morehouse, J.J. Christiansen, and W. Gordy, *J. Chem. Phys.*, 45, 1751 (1966).
71. R.W. Fessenden and R.H. Schuler, *J. Chem. Phys.*, 39, 2147 (1963).
72. R.W. Fessenden and R.H. Schuler, *J. Chem. Phys.*, 43, 2704 (1965).
73. R.W. Fessenden, *J. Phys.Chem.*, 71, 74 (1967).
74. I.A. Zlochower, W.R. Miller Jr., and G.K. Fraenkel, *J. Chem. Physics*, 42 3339 (1965).
75. M.T. Rogers and L.D. Kispert, *J. Chem. Phys.*, 46, 221 (1967).
76. S. Siegel and H. Judeikis, *J. Chem. Phys.*, 43, 343 (1965).
77. G.B. Pariiskii, G.M. Zhidomirov and V.B. Kazanskii, *Zhurnal Strukturnoi Khimii-English Translation*, 4, 364 (1963).
78. V.B. Kazanskii and G.B. Pariiskii, *Proc. 3rd Int. Cong. Catalysis*, 1964, 367.
79. J. Turkevich and Y. Fujita, *Science* 152, 1619 (1966).
80. M. Fujimoto, H.D. Gesser, B. Garbutt and A. Cohen, *Science* 154, 381 (1966).

81. M. Fujimoto, H.D. Gesser, B. Garbutt and M. Shimizu, *Science* 156, 1105 (1967).
82. G.B. Garbutt, H.D. Gesser and M. Fujimoto, *J. Chem. Phys.*, (in press).
83. C.L. Gardiner and E.J. Casey, *Can. J. Chem.*, 46, 207 (1968).
84. G.A. Noble, R.A. Serway, A. O'Donnell and E.S. Freeman, *J. Phys. Chem.*, 71, 4326 (1967).
85. V.B. Kazanskii and G.B. Pariiskii, *Kinetika i Kataliz - English Translation* 2, 507 (1961).
86. G.B. Pariiskii and V.B. Kazanskii, *Kinetika i Kataliz - English Translation* 5, 96 (1964).
87. G.M. Muha, *J. Phys. Chem.*, 71, 633 (1967); 71, 640 (1967).
88. Per-Olof Kinell, A. Lund and T. Vänng Ård, *Acta Chemica Scandinavica* 19, 2113 (1965).
89. M.F. Chung and D. Haneman, *J. App. Phys.* 37, 1879 (1966).
90. R.A. Weeks and M. Abraham, *J. Chem. Phys.*, 42, 68 (1965).
91. C.L. Gardiner, *J. Chem. Phys.*, 46, 2991 (1967).
92. G.M. Muha, *J. Phys. Chem.*, 70, 1390 (1966).
93. G.M. Muha and D.J.C. Yates, *J. Phys. Chem.*, 70, 1399 (1966).
94. P.H. Emmett and T.W. DeWitt, *J. Amer. Chem. Soc.*, 65, 1253 (1943).
95. F.A. Schwertz, *J. Amer. Ceram. Soc.*, 32, 390 (1949).
96. G.T. Trammell, H. Zeldes, and R. Livingston, *Phys. Rev.*, 110, 630 (1958).

97. H. Zeldes and R. Livingston, Phys. Review, 96, 1702 (1954).
98. W. Snipes and W. Bernhard, J. Chem. Phys., 43, 2921 (1965).
99. W. Köhnlein and J.H. Venable, Jr., Nature 215, 618 (1967).
100. R.W. Fessenden, J. Chem. Phys., 37, 747 (1962).
101. D.M. Schrader, J. Chem. Phys., 46, 3895 (1967)
hereafter referred to as DMS
102. D.M. Schrader and M. Karplus, J. Chem. Phys., 40, 1593 (1964).
103. H.M. McConnell, J. Chem. Phys., 24, 764 (1956).
104. H.M. McConnell and D.B. Chesnut, J. Chem. Phys., 28, 107 (1958).
105. D. Lazdins and M. Karplus, J. Chem. Phys., 44, 1600 (1966).
106. H. Fischer, Z. Naturforschg. 20A, 428 (1965).
107. J.P. Colpa and J.R. Bolton, Mol. Phys., 6, 273 (1963).
108. J.R. Bolton, J. Phys. Chem., 71, 3702 (1967).
109. H.M. McConnell and J. Strathdee, Mol. Phys., 2, 129 (1959).
110. M. Karplus and G.K. Fraenkel, J. Chem. Phys., 35, 1312 (1961).
111. R.E. Moss, Mol. Phys., 10, 339 (1965).
112. G. Herzberg, Proc. Roy. Soc., A262, 291 (1961).
113. G. Herzberg and J. Shoosmith, Can. J. Phys., 34, 523 (1956).

114. W. Lester, S. Andrews and G.C. Pimentel, J. Chem. Phys., 44, 2527 (1966).
115. L. Andrews and G.C. Pimentel, J. Chem. Phys., 47, 3637 (1967).
116. D.E. Milligan and M.E. Jacox, J. Chem. Phys., 47, 5146 (1967).
117. H.A. Kuska and M.T. Rogers, J. Chem. Phys., 40, 910 (1964).
118. E. deBoer and E.L. Mackor, J. Chem. Phys., 38, 1450 (1963).
119. F.C. Adam and S.I. Weissman, J. Amer. Chem. Soc., 80, 2057 (1958).
120. H.M. McConnell and R.W. Fessenden, J. Chem. Phys., 31, 1688 (1959).
121. D. Kivelson, J. Chem. Phys., 33, 1094 (1960).
122. R.N. Rogers and G.E. Pake, J. Chem. Phys., 33, 1107(1960).
123. R. Wilson and D. Kivelson, J. Chem. Phys., 44, 154 (1966).
124. R. Wilson and D. Kivelson, J. Chem. Phys., 44, 4440 (1966).
125. R. Wilson and D. Kivelson, J. Chem. Phys., 44, 4445 (1966).
126. J.H. Freed and G.K. Fraenkel, J. Chem. Phys., 39, 326 (1963).
127. J.H. Freed and G.K. Fraenkel, J. Chem. Phys., 40, 1815 (1964).
128. J.H. Freed and G.K. Fraenkel, J. Chem. Phys., 41, 699 (1964).
129. J.H. Freed and G.K. Fraenkel, J. Amer. Chem. Soc., 86, 3477 (1964).
130. J.H. Freed, J. Chem. Phys., 41, 2077 (1964).
131. F.J. Adrian, E.L. Cochran and V.A. Bowers, J. Chem. Phys., 36, 1661 (1962).
132. F.J. Adrian, J. Chem. Phys., 36, 1692 (1962).

133. C. Heller, J. Chem. Phys., 36, 175 (1962).
134. L. Bader, private communication.
135. K.E. Schuler and K.J. Laidler, J. Chem. Phys., 17, 1212 (1949).
136. A.S. Nowick and G.J. Dienes, Phys. Stat. Sol., 24, 461 (1967).